

**Effect of Process Parameters and Die Design on the Orientation of
Reinforcement Fibers in Extruded Polymer Composite**

**By
Amirreza Khorsand**

**A Thesis submitted to the Faculty of Graduate Studies of the
University of Manitoba in partial fulfillment of the requirements of the
degree of**

DOCTOR OF PHILOSOPHY

Department of Mechanical and Manufacturing Engineering
University of Manitoba
Winnipeg, Manitoba, Canada

Copyright © 2017 by Amirreza Khorsand

ABSTRACT

Three micro-structural parameters that influence the mechanical properties of discontinuous fiber thermoplastic composites are Fiber Orientation Distribution (FOD), Fiber Length Distribution (FLD) and fiber volume fraction (V_f). During manufacturing FOD in a composite would change due to fiber rotation caused by shear flow, extensional flow or a combination of both. Previous studies on flow-induced orientation is limited only to injection molding, capillary and parallel plate rheometers. Knowledge on the combined effect of die design and process variables on fiber orientation during extrusion of composites using a twin screw extruder is currently not available. Developing this knowledge is the goal of this thesis. HDPE (High Density Polyethylene) fibers and HDPE composite fibers consisting of the each of the following reinforcements (micron-sized glass fibers (aspect ratio of 27), glass spheres (aspect ratio of 1), and carbon nano tubes (CNT) were extruded by varying die design (9 dies), screw speed, and reinforcement volume fraction in the feed. The FOD) and V_f in the composite melt, determined using X-ray tomography of the frozen samples, was found to vary along the extrusion line as well as with the variables identified above. Hence, the viscosity of the melt, determined using Cogswell approach and verified independently using rheometer measurements and modeled using modified Ausias' model, also varied. The change in FOD in the melt within the die due to imposed extensional and shear strains was successfully modeled using Dihn-Armstrong model. The change in the viscosity of the melt within the die due to changes in FOD together with pressure gradient across the die, which develops concurrently, determined the mass flow rate (i.e volumetric flow rate) of composite melt out of the die. This demand on mass flow rate imposed by the die was met by the extruder by varying the amount of melt coming out of the reservoir (at the end of the screws). Simulation suggests that shear strain results in better orientation than extensional strain..

The die with least cone angle (30°) resulted in maximum fiber orientation and output mass flow rate at least die pressure, when compared to other dies for the same feed rate and screw speed.

TABLE OF CONTENTS

| | |
|--|-----|
| LIST OF FIGURES | VII |
| LIST OF TABLES | XI |
| LIST OF SYMBOLS | XIV |
| CHAPTER 1. INTRODUCTION..... | 1 |
| 1.1 BACKGROUND..... | 1 |
| 1.2 OBJECTIVE OF THESIS..... | 5 |
| 1.3 THESIS SCOPE..... | 7 |
| 1.4 ORGANIZATION OF THESIS..... | 8 |
| CHAPTER 2. LITERATURE REVIEW..... | 9 |
| 2.1 BACKGROUND INFORMATION..... | 9 |
| 2.1.1 <i>Fiber Rotation in Moving Fluid</i> | 10 |
| 2.1.2 <i>Flow Regimes</i> | 10 |
| 2.1.2.1 <i>Extensional Flow</i> | 10 |
| 2.1.2.2 <i>Shear Flow</i> | 11 |
| 2.1.3 <i>Dynamics of Fiber Rotation During Polymer Processing</i> | 11 |
| 2.1.3.1 <i>Fiber Rotation in Shear Flow</i> | 14 |
| 2.1.3.2 <i>Dynamics of Fiber Rotation in Extensional Flow</i> | 16 |
| 2.1.4 <i>Influence of Channel Geometry on Melt Flows and Fiber Orientation</i> | 17 |
| 2.1.5 <i>Influence of Post-Extrusion Drawing</i> | 21 |
| 2.1.6 <i>Injection Molding of Thermoplastics</i> | 21 |
| 2.1.7 <i>Extrusion of Thermoplastics</i> | 23 |
| 2.1.8 <i>Composite Micro-Structural Parameters</i> | 25 |
| 2.1.9 <i>Fiber Orientation and Its Distribution</i> | 25 |
| 2.1.9.1 <i>Orientation Tensor</i> | 27 |
| 2.1.9.2 <i>Orientation Factor</i> | 29 |
| 2.1.10 <i>Measurement of FOD of Micro-Sized Fibers</i> | 29 |
| 2.2 PROCESSING-MICROSTRUCTURE RELATIONSHIPS..... | 31 |
| 2.2.1 <i>Micron-Sized Fiber Reinforced Composites</i> | 32 |
| 2.2.1.1 <i>Studies Involving Shear Flow –Induced Fiber Orientation</i> | 32 |
| 2.2.1.2 <i>Studies Involving Elongational Flow-Induced Fiber Orientation</i> | 35 |
| 2.2.2 <i>Nano-sized Fiber reinforced composites</i> | 36 |
| 2.2.2.1 <i>Studies involving shear flow –induced nanofiber orientation</i> | 36 |

| | |
|---|----|
| 2.2.2.2 <i>Studies Involving Elongational Flow-Induced Nano Fiber Orientation</i> | 39 |
| 2.2.3 <i>Effect of Die Parameters</i> | 43 |
| 2.3 NUMERICAL STUDIES PREDICTION OF FLOW-INDUCED ORIENTATATION | 43 |
| 2.4 ANALYTICAL STUDIES ON FLOW INDUCED ORIENTATION | 45 |
| 2.5 RHEOLOGY OF POLYMER COMPOSITE | 46 |
| 2.6 SUMMARY OF LITERATURE REVIEW | 47 |
| | |
| CHAPTER 3. EXPERIMENTAL DETAILS | 52 |
| 3.1 INTRODUCTION | 52 |
| 3.2 MATERIALS | 52 |
| 3.3 FIBER SPINNING | 52 |
| 3.3.1 <i>Extruder</i> | 52 |
| 3.4 EXPERIMENTAL DESIGN | 59 |
| 3.4.1 <i>HDPE Fibers</i> | 59 |
| 3.4.2 <i>HDPE-Glass Composite Fibers</i> | 59 |
| 3.4.2.1 <i>Material Parameters</i> | 59 |
| 3.4.2.2 <i>Die Hole Geometry</i> | 61 |
| 3.4.2.3 <i>Process Parameters</i> | 61 |
| 3.4.3 <i>HDPE-Spherical-Glass Composite Fibers</i> | 62 |
| 3.4.4 <i>HDPE-CNT Fibers</i> | 62 |
| 3.4.4.1 <i>Material and Extrusion Parameter</i> | 62 |
| 3.4.4.2 <i>Die Hole Geometry</i> | 62 |
| 3.5 CHARACTERIZATION OF MELT-SPUN FIBERS | 67 |
| 3.5.1 <i>Fiber Volume Fraction Measurement</i> | 67 |
| 3.5.2 <i>Reinforcement Fiber Orientation Distribution (FOD)</i> | 67 |
| 3.5.2.1 <i>HDPE-Glass Composite Fiber</i> | 67 |
| 3.5.3 <i>Repeatability and reproducibility</i> | 73 |
| 3.5.4 <i>Rheology measurement</i> | 73 |
| 3.5.5 <i>Electrical conductivity measurement</i> | 78 |

| | |
|---|-----|
| CHAPTER 4. RESULT AND DISCUSSION | 82 |
| 4.1 INTRODUCTION | 81 |
| <i>4.1.1 Experimental Results of Micron-Sized Fiber Reinforced PE Composite</i> | 81 |
| <i>4.1.2 Confirmation of Vf and OF measurements through Mechanical Properties</i> | 82 |
| 4.2 MICRON-SIZED FIBER REINFORCED HDPE COMPOSITE | 86 |
| <i>4.2.1 Effect of manufacturing variables on the orientation factor</i> | 96 |
| <i>4.2.2 Combined effect of OF and VF microstructure of flow</i> | 100 |
| <i>4.2.2.1 Viscosity measurement using rheometer</i> | 100 |
| <i>4.2.2.2 Viscosity measurement inside extruder</i> | 110 |
| <i>4.2.2.3 Fiber orientation modeling</i> | 123 |
| 4.3 NANOCOMPOSITE FIBER ORIENTATION | 146 |
| <i>4.3.1 HDPE/CNT composite fiber</i> | 149 |
| 4.4 DISCUSSION | 151 |
| CHAPTER 5. CONCLUSION | 162 |
| 5.1 SUMMARY OF TASKS AND RESULTS | 162 |
| 5.2 CONCLUSIONS | 164 |
| 5.3 GUIDELINES FOR DIE DESIGN | 167 |
| 5.3 ORIGINAL CONTRIBUTIONS | 167 |
| 5.4 LIMITATION OF THIS WORK AND RECOMMENDATIONS FOR THE FUTURE WORK | 168 |
| REFERENCE | 169 |
| APPENDIX A | 179 |
| APPENDIX B | 195 |
| APPENDIX C | 201 |
| APPENDIX D | 207 |

LIST OF FIGURES

| | |
|--|----|
| Figure 1.1. Classification of polymer matrix composites..... | 3 |
| Figure 1.2. Variables affecting orientation and V_{Out} in extruded composite fiber | 6 |
| Figure 2.1. Schematic of uniaxial rheometer..... | 12 |
| Figure 2.2. Sample of Uniaxial elongation with constant extension rate at constant $\dot{\epsilon}$ | 12 |
| Figure 2.3. Shear flow..... | 13 |
| Figure 2.4. Velocity gradient..... | 13 |
| Figure 2.5. Linear shear Stress distribution..... | 13 |
| Figure 2.6. High aspect ratio fiber in shear low..... | 15 |
| Figure 2.7. Rotation of fiber perpendicular to flow direction..... | 15 |
| Figure 2.8. Fiber rotation in shear flow | 18 |
| Figure 2.9. Fiber alignment in extensional flow. | 19 |
| Figure 2.10. Converging and diverging channels..... | 20 |
| Figure 2.11. Schematic of the fiber spinning die..... | 20 |
| Figure 2.12. Post processing of fibers..... | 22 |
| Figure 2.13. The principal components of an injection molding machine..... | 22 |
| Figure 2.14. Typical extrusion line showing major equipment. | 24 |
| Figure 2.15. Coordinate system used in determination of fiber spatial orientation..... | 26 |
| Figure 2.16. Collection of glass fiber in polyethylene composite fiber..... | 28 |
| Figure 2.17. Cross section of fiber. | 30 |
| Figure 3.1. Leistritz extruder Micro-18mm..... | 54 |
| Figure 3.2. Schematic of Extruder..... | 55 |
| Figure 3.3. Pressure profile (a) and temperature profile (b) during collection of sample..... | 56 |
| Figure 3.4. Die assembly and die plate, grey area corresponds to polymer melt flow. | 58 |
| Figure 3.5. PE fiber, PE-CNT fiber, PE-glass fiber, PE-CAB-nanoclay fiber, from left to right respectively..... | 58 |
| Figure 3.6. Fiber spinning dies..... | 63 |
| Figure 3.7. X-radia's Micro X-ray CT..... | 70 |
| Figure 3.8. Computed tomography image of composite fiber..... | 70 |
| Figure 3.9. JPEG images exported by X-ray and ready to be analyzed by AVIZO Fire 7..... | 71 |

| | |
|---|-----|
| Figure 3.10. X-ray image reconstructed using Avizo Fire® software..... | 71 |
| Figure 3.11. Coordinate reference system..... | 72 |
| Figure 3.12. Pressure steady state condition after 30 minutes for HDPE extruded fiber. | 74 |
| Figure 3.13. AR2000 rheometer (TA Instruments) | 77 |
| Figure 3.14. Parallel plate schematics..... | 77 |
| Figure 3.15. Prob station and semiconductor | 79 |
| Figure 3.16. Current versus voltage measurement using semiconductor..... | 79 |
| Figure 3.17. XRD intensity pattern..... | 91 |
| Figure 4.1. Volume fraction measurement verification with pycnometer and image analysis..... | 83 |
| Figure 4.2. Fiber orientation distribution for 60-3mm die with volume fraction in feed from 3.6 to 25%..... | 83 |
| Figure 4.3. Fiber length distribution..... | 84 |
| Figure 4.4. Composite Modulus versus experimental V_{Out} | 87 |
| Figure 4.5. Composite Modulus versus experimental $V_{Out} * a_{3333}$ | 87 |
| Figure 4.6. Flow chart of combined effect on V_{Out} and OF | 90 |
| Figure 4.7. Measurements along extruder..... | 90 |
| Figure 4.8. HDPE viscosity measured using Rheometer | 102 |
| Figure 4.9. Experimental viscosity of HDPE-Spherical glass composite with a $V_F=4.6\%$ | 102 |
| Figure 4.10. Experimental viscosity of HDPE-Spherical glass composite with a $V_F=5.9\%$ | 103 |
| Figure 4.11. Experimental viscosity of HDPE-Spherical glass composite with a $V_F=17.8\%$ | 103 |
| Figure 4.12. Volume fraction factor of HDPE-Spherical glass composite | 104 |
| Figure 4.13. Experimental viscosity as function time of HDPE-fiber glass composite with V_F of 7.4%, 14%, and 19% at constant strain rate of 0.1 (1/s)..... | 106 |
| Figure 4.14. Volume fraction of factor of HDPE-fiber glass composite..... | 107 |
| Figure 4.15. Experimental viscosity of HDPE-fiber glass composite as a function of time with V_F of 7.4%, 14%, and 19% at constant strain rate of 0.1 (1/s). | 108 |
| Figure 4.16. In plane orientation factor (a_{1313}) of HDPE-fiber glass composite | 108 |
| Figure 4.17. Effect of V_F on normalized viscosity at constant a_{1313} | 109 |
| Figure 4.18. Effect of a_{1313} on normalized viscosity at constant V_F | 109 |
| Figure 4.19. Pressure variation along the length of a die hole | 113 |

| | |
|---|-----|
| Figure 4.20. Comparison of shear viscosity measured using extruder with shear viscosity measured using Rheometer for HDPE | 113 |
| Figure 4.21. Comparison of shear viscosity measured using extruder with shear viscosity measured using Rheometer for HDPE Spherical glass | 114 |
| Figure 4.22. Comparison of experimental measured flow rate using extruder with that calculated using modified Ausias model for HDPE Spherical glass composite with $V_F= 4.6, 5.9,$ and 17.8% | 129 |
| Figure 4.23. Location 1, 2, and 3 where viscosity was calculated with die assembly. | 118 |
| Figure 4.24. Comparison of shear viscosity measured using extruder is location 1 with shear viscosity calculated using modified Ausias Rheometer developed model for HDPE glass fiber composite with $V_F=9.1, 14, 20,$ and 27 | 118 |
| Figure 4.25. Comparison of shear viscosity measured using extruder in location 2 with shear viscosity measured using modified Ausias Rheometer developed model for HDPE glass fiber composite with $V_F=9.1\%, 14\%, 20\%,$ and 27% | 119 |
| Figure 4.26. Comparison of experimental measured flow rate in location 2 with that flow rate calculated using modified Ausias model for HDPE fiber glass composite with $V_F=9.1\%, 14\%, 20\%,$ and 27% | 120 |
| Figure 4.27. Comparison of shear viscosity measured using extruder in location 3 with shear viscosity calculated using modified Ausias Rheometer developed model for HDPE glass fiber composite with $V_F=9.1\%, 14\%, 20\%,$ and 27% | 121 |
| Figure 4.28. Comparison of experimental measured flow rate in location 3 with that flow rate calculated using modified Ausias model for HDPE fiber glass composite with $V_F=9.1\%, 14\%, 20\%,$ and 27% | 122 |
| Figure 4.29. Elongation viscosity calculated as function of elongation rate calculated using Cogswell model in location 2 for HDPE glass fiber composite with $V_F=9.1\%, 14\%, 20\%,$ and 27% | 124 |
| Figure 4.30 Location for measurement of initial fiber orientation..... | 129 |
| Figure 4.31. Comparison of fiber orientations inside the die and in the final fiber composite. (a) ϕ with respect to extrusion direction (Z) and (b) is in plane (XY) orientation angle of θ with respect to X axis. | 130 |
| Figure 4.32. Fiber rotation model..... | 131 |
| Figure 4.33. Initial fiber orientation distribution at die cone entry for $30^\circ, 60^\circ,$ and 90° die | 132 |

| | |
|--|-----|
| Figure 4.34. Armstrong model prediction of a_{3333} for composite ($V_{in}= 25\%$) manufactured using 30, 60, 90 degree die..... | 132 |
| Figure 4.35. Armstrong model prediction of a_{1313} for composite ($V_{in}= 25\%$) manufactured using 30, 60, 90 degree die. | 133 |
| Figure 4.36. Armstrong model a_{3333} prediction vs changes in elongational strain for 30, 60, and 90 degree die at volume fraction of $V_{in}= 25\%$ | 134 |
| Figure 4.37. Armstrong model prediction of a_{3333} for composite ($V_{in}= 18\%$) manufactured using 30, 60, 90 degree die..... | 135 |
| Figure 4.38. Armstrong model prediction of a_{1313} for composite ($V_{in}= 18\%$) manufactured using 30, 60, 90 degree die. | 136 |
| Figure 4.39. Armstrong model prediction of a_{3333} for composite ($V_{in}= 18\%$) manufactured using 30, 60, 90 degree die. | 137 |
| Figure 4.40. Armstrong model prediction of a_{3333} for composite ($V_{in}= 12\%$) manufactured using 30, 60, 90 degree die. | 138 |
| Figure 4.41. Armstrong model prediction of a_{1313} for composite ($V_{in}= 12\%$) manufactured using 30, 60, 90 degree die. | 139 |
| Figure 4.42. Armstrong model prediction of a_{3333} for composite ($V_{in}= 12\%$) manufactured using 30, 60, 90 degree die. | 140 |
| Figure 4.43. Armstrong model prediction of a_{3333} for composite ($V_{in}= 9.1\%$) manufactured using 30, 60, 90 degree die..... | 141 |
| Figure 4.44. Armstrong model prediction of a_{1313} for composite ($V_{in}= 9.1\%$) manufactured using 30, 60, 90 degree die..... | 142 |
| Figure 4.45. Armstrong model prediction of a_{3333} for composite ($V_{in}= 9\%$) manufactured using 30, 60, 90 degree die. | 143 |
| Figure 4.46. Initial fiber orientation distribution for fiber composite in the cone region of 30° die for various die. | 144 |
| Figure 4.47. Effect of imposed shear strain of 0.5 imposed on fiber rotation in a composite with two different initial a_{3333} with V_{in} of 9.1%. | 147 |
| Figure 4.48. Effect of imposed elongation strain of 2.2 imposed on fiber rotation in a composite with two different initial a_{3333} with V_{in} of 9.1%. | 148 |
| Figure 4.49. Measured longitudinal electrical conductivity for HDPE-CNT composite | 152 |

| | |
|--|-----|
| Figure 4.50. Longitudinal electrical conductivity network..... | 152 |
| Figure 4.51. Transverse and longitudinal electrical conductivity (line between points are connected for illustration purpose and it is not fitted curve) | 153 |
| Figure 4.52. Comparison of experimental measured flow rate with that calculated using modified. | 155 |
| Figure 4.53. Buffer zone at extruder end identified by arrow | 155 |
| Figure 4.54. Comparison of experimental measured mass flow rate with programmed mass flow rate 90 degree die at constant screw speed of 40 rpm. | 156 |
| Figure 4.55. Comparison of experimental measured mass flow rate with programmed mass flow rate 90 degree die at constant screw speed of 40 rpm. | 159 |
| Figure 4.56. Shear and elongation strain in die... .. | 161 |

LIST OF TABLES

| | |
|--|----|
| Table 2.1. Summary of Inference on the influence of parameters on FOD during extrusion of polymer composite with discontinuous reinforcement fibers in elongational flow | 50 |
| Table 2.2. Summary of Inference on the influence of parameters on FOD during extrusion of polymer composite with discontinuous reinforcement fibers in shear flow. | 50 |
| Table 2.3. Summary of Inference on influence of parameters on FOD during extrusion of polymer composite with discontinuous reinforcement fibers..... | 51 |
| Table 3.1. List of materials and their suppliers | 54 |
| Table 3.2. Temperature profile of heating barrel for HDPE matrix..... | 55 |
| Table 3.3. Die parameters used to manufacture Pure HDPE..... | 60 |
| Table 3.4. Designed experiments of PE Fibers with screw speed of 40 (rpm), die entry angle of 180° , die diameter of 3 (mm), and with same temperature profile (Table 3.1) for all 9 specimens..... | 60 |
| Table 3.5. Die-Hole Geometry..... | 63 |
| Table 3.6. Designed experiments for second set of experiment to study effect of the geometry of the die hole on the orientation of the glass fiber with in PE-Glass composite fibers with screw speed of 40 (rpm), die land length of 2.7 (mm), die diameter of 3 (mm), and same temperature profile (Table 3.1) for all 18 specimens..... | 64 |
| Table 3.7. Designed experiments of the geometry of the die hole on the flow rate at various screw speed of the glass fiber with in PE-Glass Composite Fibers, die angle of 60°, die land length of 2.7 (mm), die diameter of 3 (mm), and with the same temperature profile (Table 3.1) for all 10 specimens..... | 65 |
| Table 3.8. Designed experiments of the PE-Spherical Glass Composite Fibers, die land length of 2.7 (mm), die diameter of 3 (mm), and with the same temperature profile (Table 3.1) for all 6 specimens. | 65 |
| Table 3.9. Designed experiments of the die hole geometry effect on the orientation of the CNT with in PE-CNT Composite Fibers, die land length of 2.7 (mm), die diameter of 3 (mm), and with the same temperature profile (Table 3.1) for all 14 specimens. | 66 |

| | |
|--|-----|
| Table 3.10. Die-Hole Geometry for CNT spinning | 66 |
| Table 3.11. Designed experiments of mass flow rate and Pressure reparability | 74 |
| Table 3.12. Designed experiments of the shear viscosity measurement of already extruded HDPE, HDPE-Spherical Glass, and HDPE-Glass fibers at a temperature of 200 (c) for all 7 specimens. Shear rate changes between 2.5×10^{-5} (s^{-1}) and 82 (s^{-1}) for specimen 1-4 and it was kept constant 0.1 (s^{-1}) for specimen 5-7..... | 76 |
| Table 3.13. Designed experiments of HDPE-CNT Composite Fibers longitudinal conductivity measurement of already extruded fibers. | 80 |
| Table 3.14. Designed experiments of HDPE-CNT Composite Fibers transverse conductivity measurement of already extruded fibers. | 80 |
| Table 4.1. Changes in volume fraction along extruder at different location..... | 91 |
| Table 4.2. Effect of V_{out} resulted from change in screw speed at constant feed rate | 91 |
| Table 4.3. Effect of pressure resulted from change in volume fraction in feed at 40 rpm screw speed. | 92 |
| Table 4.4. Effect of pressure on % V_{Out} in composite at 40 rpm screw speed..... | 93 |
| Table 4.5. Effect of Flow rate (m^3/s) on % V_{Out} in composite at 40 rpm screw speed..... | 94 |
| Table 4.6. Effect of volume fraction in the feed on volume fraction in composite for die entry angles of 60° , die hole diameter of 3 mm, with two L/D ratios. | 95 |
| Table 4.7. Changes in Orientation along the extruder at different locations..... | 97 |
| Table 4.8. Effect of orientation change resulted from change in pressure in feed at 40 rpm screw speed..... | 98 |
| Table 4.9. Effect of orientation change resulted from change in pressure in feed at 40 rpm screw speed..... | 99 |
| Table 4.10. Fiber orientation before and after shear viscosity test using Rheometer | 107 |
| Table 4.12. Comparison of experimental measured a_{3333} for samples tested for shear viscosity using Rheometer with a_{333} predicted using Dinh-Armstrong model. | 148 |
| Table 4.13. Dinh-Armstrong model a_{1313} confirmation with rheometer | 148 |
| Table 4.14. Longitudinal conductivity test..... | 152 |
| Table 4.15. Tensile testing of HDPE-CNT extruded composite with weight fraction of 15%. | 153 |
| Table 4.16 Reservoir degree of fill for $V_{IN}=25\%$ for different dies. | 161 |

LIST OF SYMBOLS AND ABBREVIATION

HDPE: High Density Polyethylene

CNT: Carbon Nano Tube

V_{In} : Fiber volume fraction in the feed

V_F : Fiber volume fraction in the melt

V_{Out} : Fiber volume fraction in the extruded composite.

E_C : Composite fiber modulus

E_m : Polymer matrix modulus

E_f : Polymer matrix modulus

V_m : Polymer matrix volume fraction

χ : effect of aspect ratio (reinforcing efficiency).

FOD: fiber orientation distribution

η : shear viscosity

η_0 : neat HDPE shear viscosity

α : aspect ratio and volume fraction factor

$\dot{\gamma}$: shear rate

P_0 : melt pressure at the entrance to the conical section of the die

P_1 : melt pressure at the end of the conical section.

ΔP_{Cone} : pressure changes across cone section of the die

$\Delta P_{Cone,E}$: elongational pressure drop across cone section of the die

$\Delta P_{Cone,S}$: shear pressure drop across cone section of the die

σ : applied normal stress in melt flow,

λ : extensional viscosity

$\dot{\epsilon}$: extensional rate, and

n : power law constant

δ : die angle,

Q : is the flow rate,

r_0 : entry diameter of the cone

r_1 : exit diameter of the cone.

τ : applied shear stress in flow

γ : is the total shear strain measured from start of the flow. The initial fiber orientation is given by

θ_0 : initial fiber orientation with respect to extrusion axis

φ_0 : initial in-plane fiber orientation

ϵ : elongation strain

CHAPTER 1. Introduction

Composite materials consist of two or more materials and have properties superior to any of their constituent components. Advanced composite materials have been used for engineering structures for over 60 years. The use of composite materials in structural applications has been steadily increasing, due to their highly specific properties and their greater resistance to corrosion when compared to metals. A polymer composite is a polymer matrix reinforced with high strength, high modulus fibers. There are a large number of available choices in fibers, for example the type of resin, the fiber orientation/architecture within the resin, and the manufacturing method employed. This has made these composites very attractive for use in a variety of engineering applications across a range of fields including applications in the military, aerospace, automotive and wind energy industries, as well as applications in civil infrastructure, and building materials.

This chapter presents a brief overview of other published research on composites along with the rationale and synopsis of this study. A detailed literature review is presented in Chapter 2, and Chapter 3 presents details on this study's materials and experimental procedure. Results are discussed in Chapter 4, while conclusions and recommendations based on these results are presented in Chapter 5.

1.1 Background

Fiber reinforcements are available in a wide variety of forms, as shown in Figure 1.1. Polymer composites come in three types and are classified as particulate, discontinuous, or continuous fibers composites, based on the geometry of reinforcement. Randomly dispersed reinforcements (L/D where L is the fiber length and D is the fiber diameter) with an aspect ratio of 1 to 20 result in particulate composite. Discontinuous fiber composites contain short fibers with

an aspect ratio of 20 to 1000. Continuous fiber composites contain fibers with aspect ratios greater than 1000. Continuous fiber composites are used in structural applications in the aerospace industry, where the desired mechanical performance outweighs the relatively higher cost of these fibers. Continuous fiber composites are subdivided into two categories based on the fiber architecture. They may be either a non-woven tape composite, or a woven textile composite.

Over the past four decades, the properties of polymer composites have been tailored at three size scales: millimetre (laminate level), micrometer (lamina level), and sub-micron (fiber level). Fibers with diameters in the micrometer range have been used in continuous fiber composites. Recent discoveries in the field of polymer composites have ignited interest in tailoring the structure of composites at a fourth size scale, namely the nano-scale. The discovery of carbon nano-tubes with a diameter in the range of 10 – 50 nm ($1 \text{ nm} = 10^{-9}\text{m}$), a length of few microns, a modulus of 1000 times, and strength of 100 times of steel makes the development of composites at this size scale possible.

A number of nano-reinforcements, such as carbon, steel, and nano-clay, are currently used in manufacturing composites, and these nano-reinforcements may have the structure of fibers, platelets or particles. While most of the current research involving nano-reinforcements is focused on improving functional properties—such as diffusional resistance, electrical conductivity, and thermal conductivity—significant attention has also been paid to improving structural properties and developing structural composites with desired functional properties. However, the full potential of nano-fibers for improving structural properties (i.e. strength and stiffness) has yet to be realized. As with the case of micrometer-sized discontinuous fibers, a lack of control over their orientation is one of the reasons for poor structural properties of composites with nano-fibers.

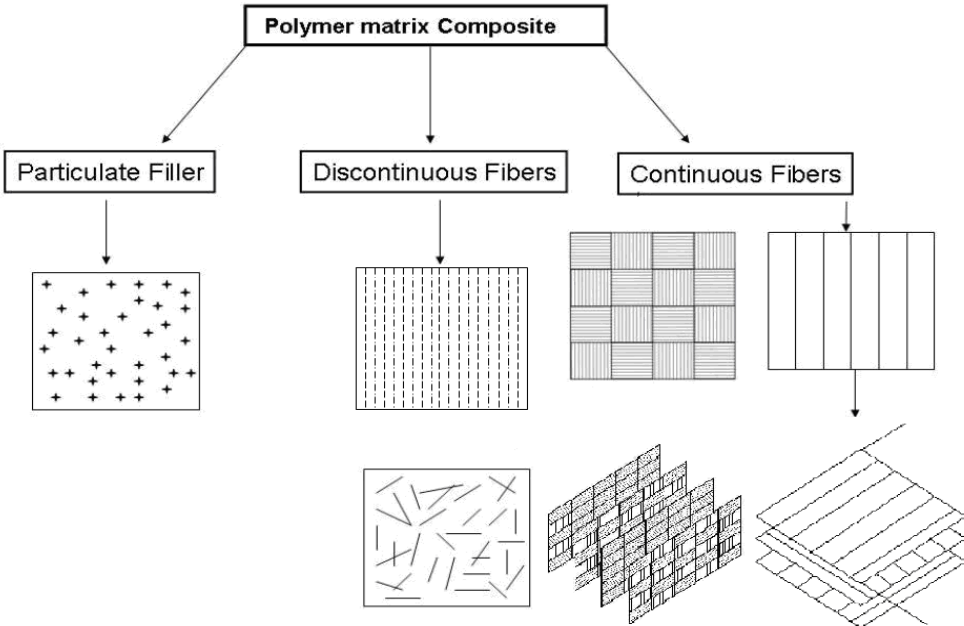


Figure 1.1. Classification of polymer matrix composites.

Flow-induced orientation of discontinuous fibers in Newtonian and non-Newtonian fluids have been extensively studied in the past as per article by [1-25]. Most of these studies focus on micron-sized fibers and are usually concerned with shear flow-induced orientation in injection molding, capillary and parallel plate rheometers, or extensional flow-induced fiber orientation in ram extrusion and fiber drawing in a tensile tester. Also, these studies have mainly focused on the effect of shear rate/ draw ratio and fiber volume fraction on fiber orientation, but none are related to twin-screw extrusion. Despite offering insight into the role of shear and extensional flows on fiber orientation, they do not offer any insight into the role of die design. There are also no published experimental studies on the combined effect of die design and process variables (such as feed rate, fiber volume fraction in feed, and die temperature) on fiber orientation.

Knowledge of this effect is necessary to control the fiber orientation in, and properties of, composites extruded using a twin-screw extruder. Published theoretical studies include Jeffery's analytical model [26] for rotation of a ellipsoidal particle in a Newtonian shear flow, Batchelor's extended Jeffery's model for arbitrary shape in Newtonian shear flow[27], Dihn and Armstrong's analytical model [28] for predicting fiber rotation in both extensional and shear flow with dilute fiber concentration, and Molden [29]. Nevertheless, studies involving twin-screw extruders, wherein both extensional and shear flows are encountered within the dies, are rare. However, twin-screw extruders are increasingly used to directly manufacture profiles (such as sheets, films, tubes, rods, and fibers) and parts.

Moreover, the flow of polymer melt during twin screw extrusion is simple and in steady state when compared to complex and non-steady state flow encountered in injection molding. For concentrated melt flows, numerical methods have been developed. These determine changes in the orientation tensor iteratively and require as input an accurate model for rheology of filled polymer

melts. Pioneering work done by Prof. Charles Tucker and his team has resulted in commercial software (Autodesk ® Moldflow) for predicting fiber orientation during injection molding, but while there are commercially available software codes for predicting extrusion of polymers (Ludovic® - Twin screw simulation software), none of them can predict the fiber orientation.

Hence, the focus of this thesis is flow-induced fiber orientation during twin-screw extrusion of composites. Nevertheless, additional study is required to understand the combined effect of die design and processing variables on the micron-sized discontinuous fiber orientation in composites extruded using a twin screw extruder. Similar conclusions can be drawn for nano-sized fibers based in the review presented in Chapter 2.

1.2 Objectives of the thesis

In view of the knowledge gaps highlighted in the previous section, the objectives of this thesis are as follows:

1. Study experimentally and delineate the combined effect of die design and extrusion variables on the orientation of the micro-sized fibers in composites extruded using a twin-screw extruder;
2. Generate guidelines for optimal die design to maximize fiber orientation;
3. Extend the results of objectives 1 and 2 to understand the extrusion conditions that can maximize the orientation of nano-fibers in composites made with a twin-screw extruder.

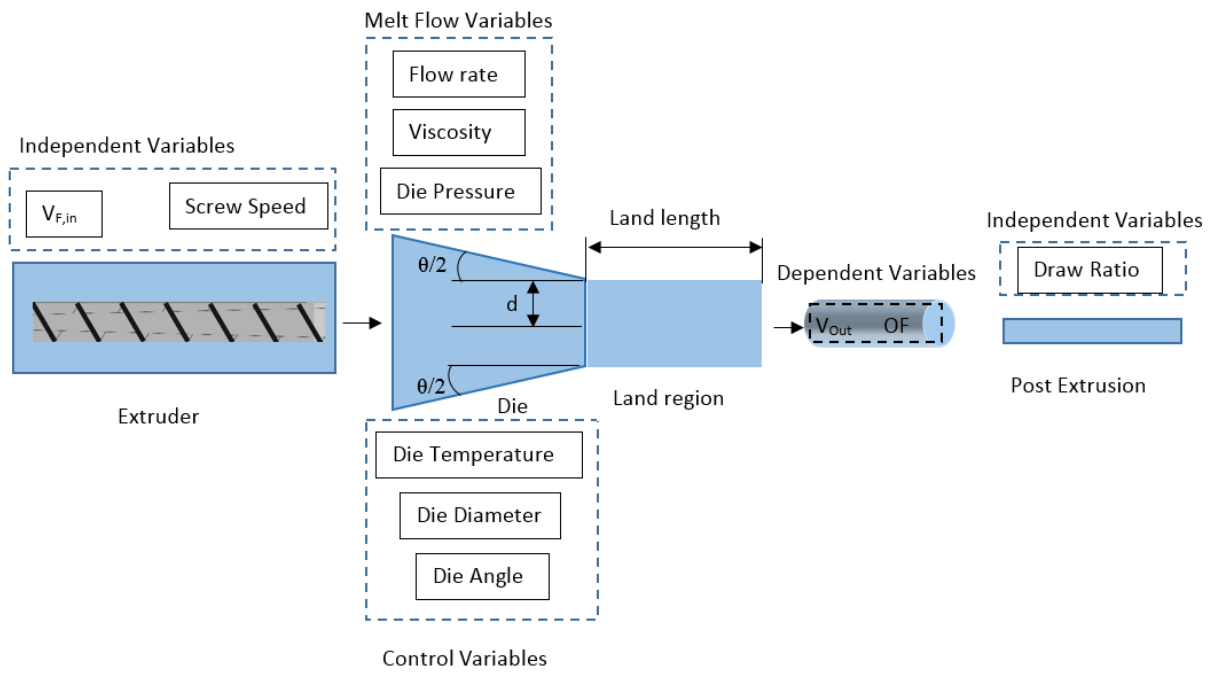


Figure 1.2. Variables affecting orientation and V_{Out} in extruded composite fiber.

1.3. Thesis Scope

1. This study is limited to extruded composite fibers; hence, the design of conical dies was considered. The die design parameters, identified in the schematic in Figure 1.2, are $d_{\text{exit}}/d_{\text{inlet}}$, cone angle, and land length. Die angle was varied from 30° , 45° , 60° , 60° (longer land length), 90° , and 180° while keeping the extrusion ratio (i.e. $d_{\text{exit}}/d_{\text{inlet}}$) constant at 0.32, resulting in six dies.

Composite fibers, made up of HDPE and micron-sized glass fibers (aspect ratio of 27), were extruded using each of these six dies. Independent variables identified in Figure 1.2 were different for each die; for example, extrusion was done at a screw speed of 40 RPM while the fiber weight fraction varied (10%, 20%, 30%, 40%, and 50%). In order to aid in the analysis, additional extrusion runs were completed by extruding pure HDPE as well as HDPE filled with glass spheres (aspect ratio of 1). In order to study the effect of screw speed, additional experiments were completed using the 60° die at 40, 60, 100, 150, and 250 (rpm). All extrusions were completed at a constant die temperature of 200 (c) and corresponding control variables are identified in Figure 1.2.

During each run, the pressure, the fiber orientation distribution (FOD), the fiber volume fraction (V_f), and the flow rate were measured at various locations along the extrusion line as indicated in Figure 1.2, after steady state had been reached. The pressure was measured at the end of the extruder and at the entry to the die. Using frozen samples, the FOD and the V_f were measured non-destructively, using 3-D images generated using X-ray Micro CT, at the extruder end, at the die entry and at the die exit. These measurements of fiber orientation and V_f were independently confirmed using tensile test and helium pycnometer, respectively.

Using the measured flow rate and pressure, the extensional and shear viscosity inside the cone and the land regions of the die were determined following the Cogswell approach [30]. Shear viscosity was independently measured using a rheometer and modeled to establish the effect of fiber aspect ratio, fiber volume fraction, and fiber orientation. Using this model and the measured fiber orientation and V_f in the land region, shear viscosity in the land region was simulated and compared with the values determined using the Cogswell approach. The viscosity results allowed interpretation of the variation in the measured pressure and flow rate during various extrusions in terms of changing FOD along the extrusion line.

Finally, using the FOD at the die entry, the extensional and shear strains imposed by the die design, and the Dihn-Armstrong model, the fiber rotation (and this changes in FOD) within the die was predicted and analyzed. This analysis then allowed for delineation of the combined effect of die design and extrusion variables on the fiber orientation in the extruded composites. Based on these results, recommendations were made on optimal die design.

Similar experiments and analyses were performed using HDPE and carbon nano-tubes to understand the combined effect of die design and extrusion variables on orientation of nano- fibers in extruded composites. Electrical conductivity measurements were used to study the orientation indirectly.

1.4 Organization of the Thesis

While an overview of published literature is presented in this chapter, a detailed review is presented in Chapter 2. Chapter 3 presents details on materials and experimental procedure. Results are presented and discussed in Chapter 4. Conclusions and recommendations based on the results are presented in Chapter 5.

CHAPTER 2. Literature Review

This chapter provides a comprehensive review of the current published literature on flow induced orientation in polymer composites. The objective is to identify the knowledge gaps in the area of flow-induced orientation in support of the scope and the proposed objectives for this thesis.

First, background information on flow-induced fiber orientation is provided briefly. Subsequently, past research in this area is presented and discussed critically. Based on this discussion, knowledge gaps in this area are identified and used to support the motivation and proposed objectives of this particular study.

2.1 Background Information

Alignment of short and high-aspect ratio fibers during thermoplastic polymer composite processing occurs because fibers tend to align themselves naturally in the direction of flow. Fibers suspended in a moving fluid rotate and orient themselves under the action of the velocity gradient in the melt flow. Even at low concentrations, the orientational dynamics of fiber and the rheology of the suspension influence one another. A number of researchers have studied this in polymer composites manufactured using processes such as injection molding [31], extrusion [32], compression molding [33]. Some studies have evaluated the effect on fiber alignment of electric [34] and magnetic fields [35] superposed on the melt flow within a polymer matrix. Next the mechanism of fiber rotation in flow regimes is introduced.

2.1.1 Fiber Rotation in Moving Fluid

Fiber rotation in moving fluid has been studied by many researchers, and Petrie [31] has reviewed those articles. Two different flow regimes can be observed during processing of thermoplastics (both are observed during extrusion). These are explained below, followed by a discussion on the dynamics of single fiber rotation.

2.1.2 Flow Regimes

2.1.2.1 Extensional Flow

The fluid flow in response to an extensional (i.e. tension) force is known as extensional flow. Consider the case of a thermoplastic polymer subjected to a tensile test at a constant strain rate and at a temperature higher than its melting temperature, as shown in Figure 2.1. The strain on the polymer melt and the stress required to achieve that strain would increase, as shown in Figure 2.2, indicating that steady-state flow conditions had been achieved.

The extensional viscosity is defined by Equation (2.1)

$$\lambda = \frac{\sigma}{\dot{\epsilon}} \quad (2.1)$$

$\dot{\epsilon}$ is extension rate and σ is the stress on the thermoplastic polymer.

$$\sigma = \frac{F}{A}, \quad \dot{\epsilon} = \frac{1}{L} \frac{dL}{dt} \quad (2.2)$$

F is applied force, A in cross section area, L is the length and t is time.

In a pure extensional flow there would not be any shear. Such extensional flow would also be observed in fluid flow through converging and diverging sections, which will be discussed later in section 2.1.3.2.

2.1.2.2 Shear Flow

The fluid flow in response to a shear force is known as shear flow. Consider a polymer melt flow through a cylindrical channel, as shown in Figure 2.3. The fluid velocity at the wall will be lower than the fluid velocity at the center of the channel due to interaction between the wall and the polymer melt. This velocity gradient, illustrated in Figure 2.4, results in shearing of the polymer melt and the shear stress in the polymer varies from zero at the center to a maximum at the wall. For Newtonian flow (i.e. viscosity is independent of shearing rate), the distribution in shear stress is linear as shown.

This shear flow results in pressure drop across the channel length and is related to the maximum wall shear stress by

$$\tau_w = \frac{\Delta p \cdot r}{2L} \quad (2.3)$$

The shear viscosity of the polymer melt is defined as

$$\eta = \frac{\Delta p \cdot r}{2L\dot{\gamma}} \quad (2.4)$$

Where the shear rate is related to the flow rate by

$$\dot{\gamma} = -\frac{dU(r)}{dr} \quad (2.5)$$

Δp corresponds to pressure drop, L is the length of cylindrical channel, R is radius of channel, $U(r)$ is the velocity profile, and τ_w corresponds to shear stress.

2.1.3 Dynamics of Fiber Rotation during Polymer Processing

The tendency of suspended high-aspect-ratio fibers to align themselves along the streamlines of a given flow is easily understood on intuitive grounds. Consider a high-aspect-ratio fiber aligned in a shear flow as in shown in Figure 2.6.

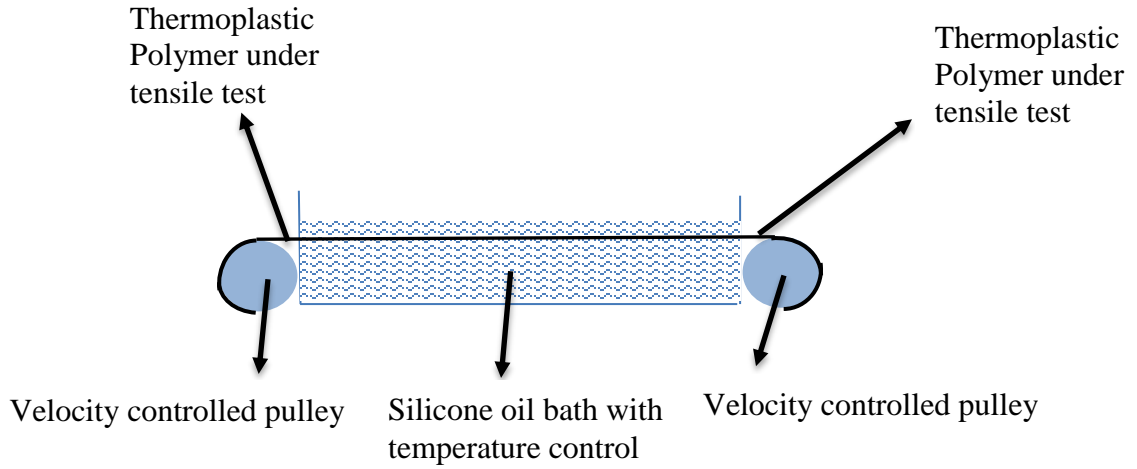


Figure 2.1. Schematic of uniaxial rheometer.

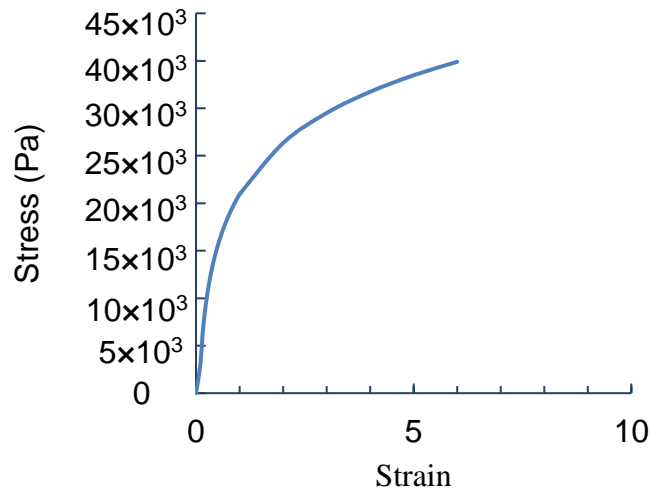


Figure 2.2. Sample of Uniaxial elongation with constant extension rate at constant $\dot{\epsilon}$.

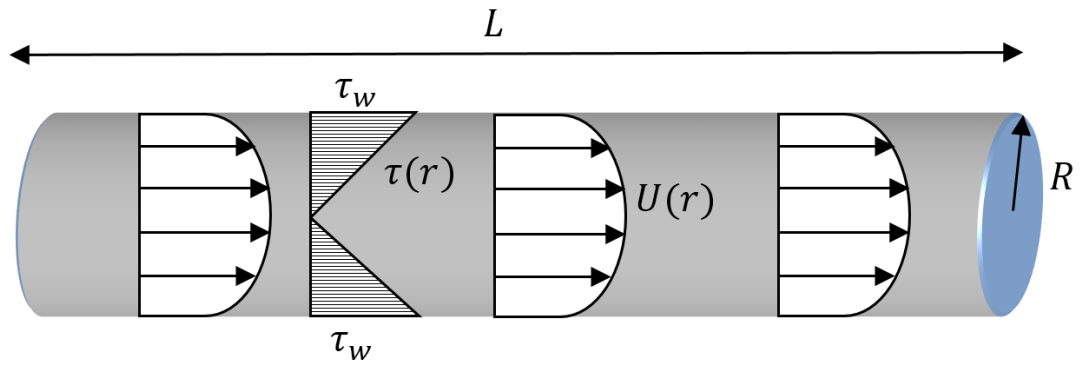


Figure. 2.3 Shear flow.

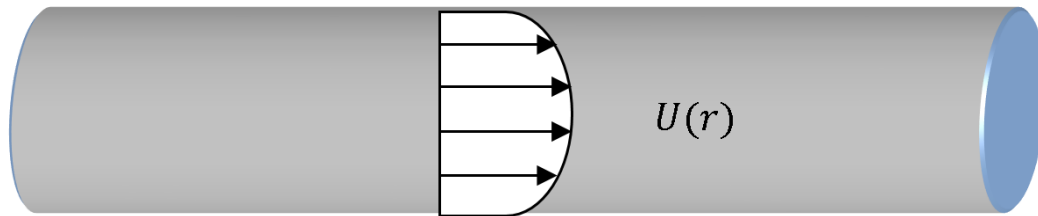


Figure 2.4. Velocity gradient .

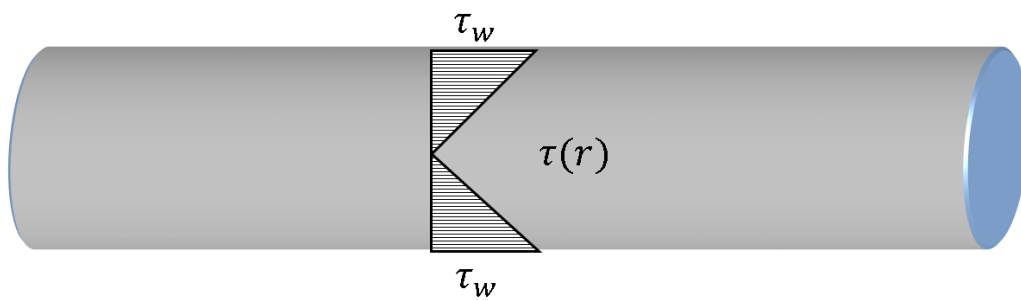


Figure 2.5. Linear shear stress distribution.

The variation in the velocity of the fluid acting across the length of the fiber would be minimal and hence, the rotation would be minimal. However, when a fiber is oriented with its long axis perpendicular to the streamlines, the velocity gradient across the length of the fiber length would be maximum resulting in maximum rotation. The fiber rotates with the fluid, regardless of the fiber's diameter, as shown in Figure 2.7.

Thus, a high-aspect-ratio fiber is slow to leave an aligned orientation and quick to realign itself once it is out of alignment. Therefore, high-aspect-ratio fibers spend a large fraction of the time aligned with the flow, with most of the fibers aligning themselves along streamlines. In shear flow, the fibers rotate periodically because no stable equilibrium orientation exists, whereas in pure extensional flow such an equilibrium orientation is available, with fibers approaching that orientation with time. Even during the processing of unreinforced polymers, Tate's [32] study indicates the effect of elongation and shear strain act to stretch and align polymer molecules.

2.1.3.1 Fiber Rotation in Shear Flow

Let us consider the rotation of a single fiber in a shearing flow of a polymer melt through a capillary of length L and radius R_0 . Figure 2.8 shows a fiber in simple shearing flow and defines the coordinate system and angles which describe the particle's motion. If the fiber is aligned so that its axis is making φ angle with flow direction, the fiber rotates. The orientation of the fiber is given by φ at position (a) in Figure 2.8 which is equal to zero when the fiber axis is parallel to the velocity gradient points along the z -axis in Figure 2.8. As the fiber moves along the cone with flow to position (b), imposed shear stress would rotate the fiber to orientation of φ' .

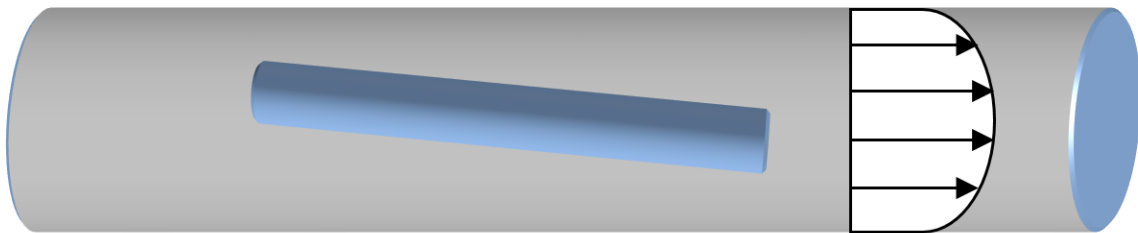


Figure 2.6. High aspect ratio fiber in shear flow.

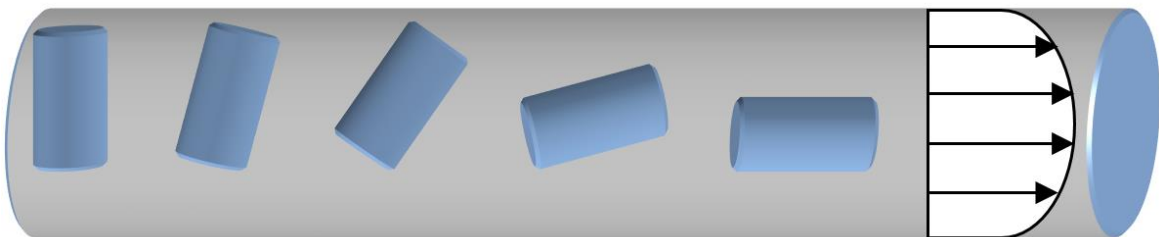


Figure 2.7. Rotation of fiber in shear flow.

Due to the variation of fluid velocity acting along its length, the fiber rotates. Jeffery [26], in his classic theoretical study, solved the equations governing viscous (creeping) flow around a spheroidal particle in unbounded shear flow and determined the rotation of a spheroidal particle in a dilute, shearing suspension. Brenner [36] showed that any particle with an axis of symmetry can be treated as an equivalent spheroid with the aspect ratio $e = a/b$, where a is the length of the fiber and b is the diameter of the fiber. For simple shearing flow, the tumbling rate is given by:

$$\dot{\varphi} = \dot{\gamma} \frac{1}{e+1} (e^2 \cos^2 \varphi + \sin^2 \varphi) \quad (2.6)$$

where φ is the angle between the fiber x-axis, e is the fiber aspect ratio, and $\dot{\gamma}$ is the shear rate. Dihn and Armstrong [28] further extended Equation (2.6) to calculate the final orientation of the fiber in steady shear flow by:

$$\tan \varphi = \tan \varphi_0 [\gamma^2 + 1]^{1/2} \quad (2.7)$$

where γ is the total shear strain imposed on fiber as it passes through a cone.

2.1.3.2 Dynamics of Fiber Rotation in Extensional Flow

Extensional flow causes the rotation of a single fiber in polymer melt through a capillary of length L and radius R_0 . Dihn and Armstrong [28] determined the orientation of fibers in steady elongation flow. Figure 2.9 shows a fiber in simple elongation flow and defines the coordinate system and angles which describe the particle's motion. As the fiber moves along the cone with the flow to from position (a) to position (b) just after entering the capillary section, the illustrated representative volume will elongate as shown in location (b). This elongated representative volume imposes alignment to fiber which would rotate the fiber to an orientation of φ' . The motion of fiber with orientation of φ_0 at $t = 0$ is given by:

$$\tan \varphi = e^{-\left(\frac{3}{2}\right)\varepsilon} \tan \varphi_0 \quad (2.8)$$

where $\varepsilon = \dot{\varepsilon}t$ is the Hencky strain between t and $t = 0$. Therefore, having the strain value ε , the θ for the fiber can be calculated. The rate of rotation has an exponential relation to strain; therefore, the fibers rotate faster in extensional flow than in shear.

2.1.4 Influence of Channel Geometry on Melt Flows and Fiber Orientation

Dies used during polymer composite processing are not just cylindrical (as discussed above) and may have converging and diverging geometries, as shown in Figure 2.10. For example, a schematic of the fiber-spinning die used in this study is shown in Figure 2.11. θ is the cone angle, L_1 is the cone length, R_0 and R_1 are entry and exit diameters of the cone, and L_2 is the land length, as illustrated in Figure 2.11. While the shear flow would be predominant along the land length, both the shear and extensional flows would be encountered in the cone region. The magnitude of the shear flow with respect to the extensional flow depends on the cone angle and the ratio of the entry to exit diameters. Cogswell [30] and Binding [37] have developed methodologies to delineate the extensional and shear components of viscosity within the cone, using the experimentally measured pressure drop across the cone. However extensional and shear components of viscosity effect on fiber orientation has not been studied before. These studies has extended exciting viscosity calculation methodology to determine the extensional and shear viscosities within the conical section of the fiber-spinning die. As a result, these viscosities help to delineate the orientation of reinforcing fibers during the extrusion of composite fibers.

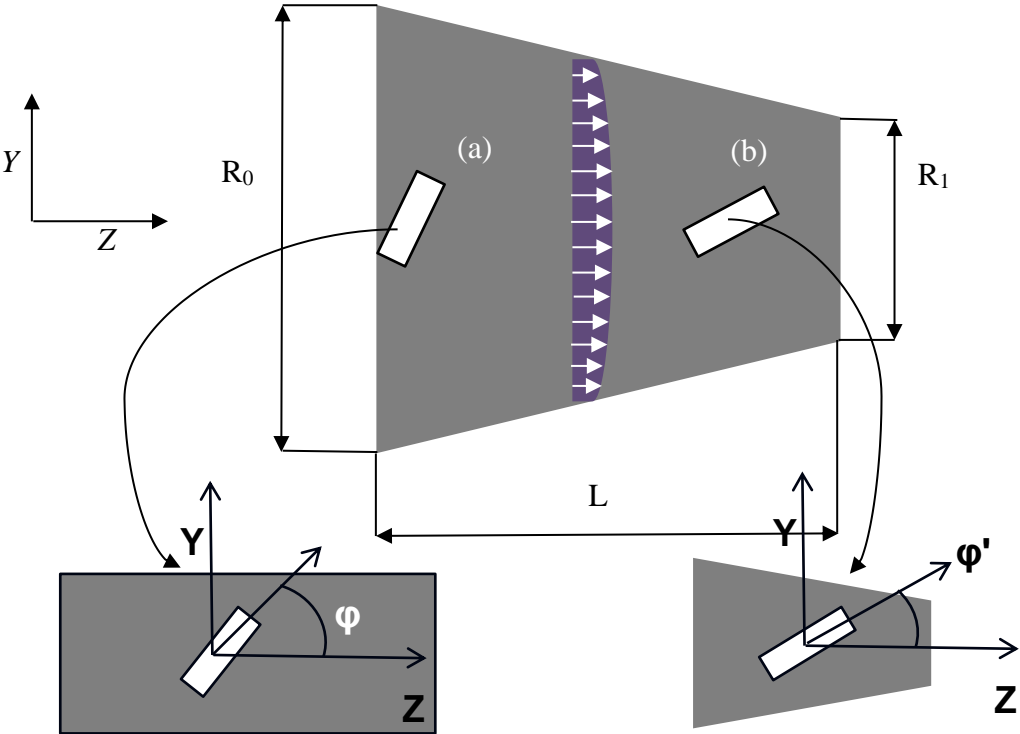


Figure 2.8. Fiber rotation in shear flow.

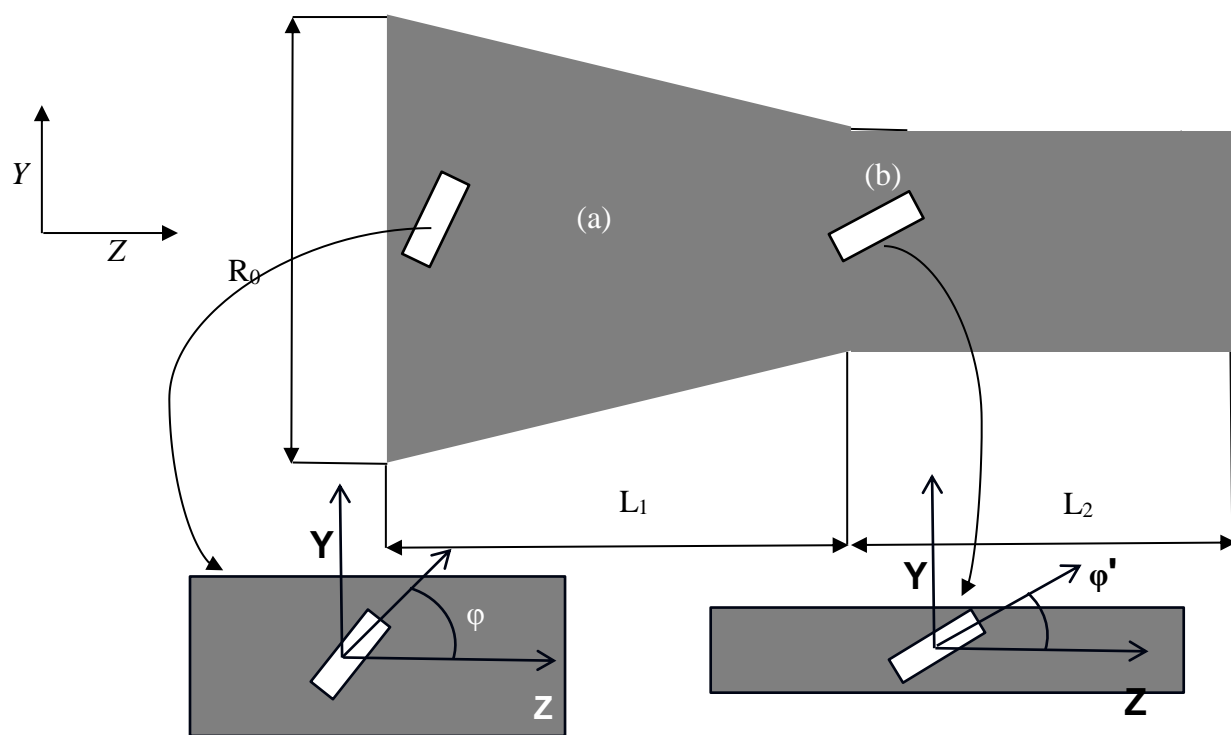


Figure 2.9. Fiber alignment in extensional flow.

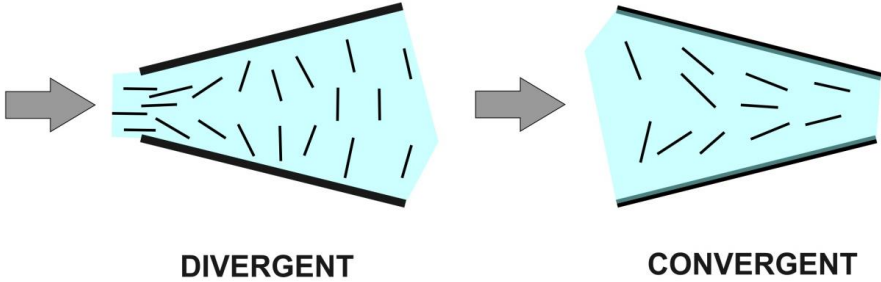


Figure 2.10. Converging and diverging channels.

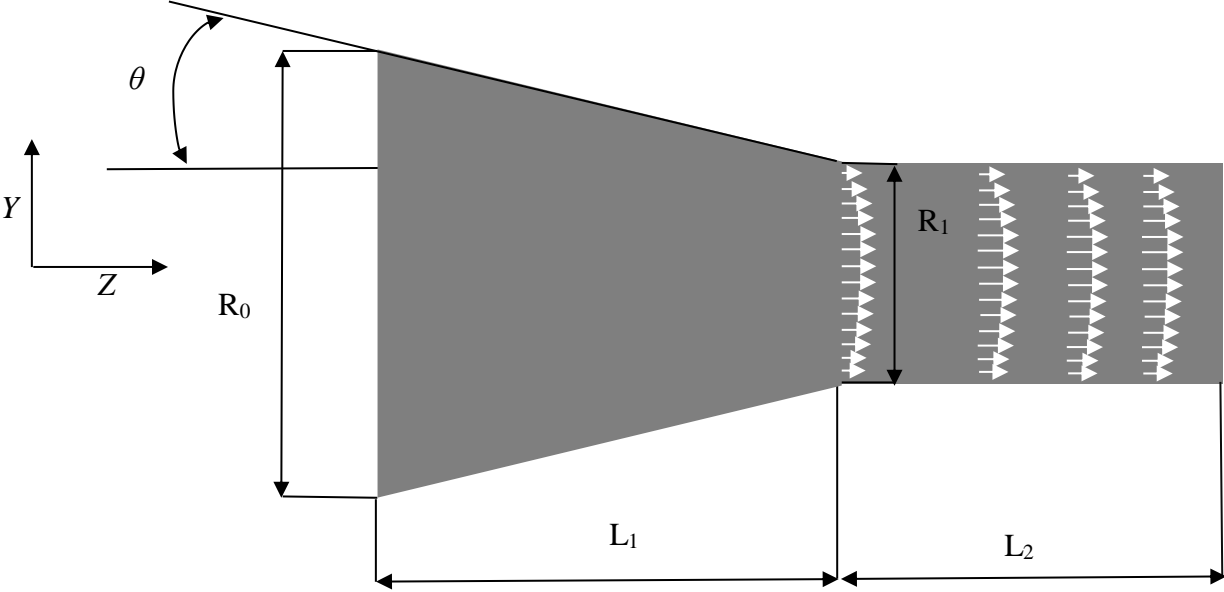


Figure 2.11. Schematic of the fiber spinning die.

2.1.5 Influence of Post-Extrusion Drawing

Sometimes, a composite fiber extruded through a fiber-spinning die may be drawn in the melt state, during which the diameter of the composite fiber reduces further. Extension flow is encountered during this step and is the reason for any orientation of the reinforcing fiber. This study does not focus on this phenomenon.

In summary, process-related parameters such as pressure (ΔP) (varied by screw speed), temperature (changed to vary the viscosity (η)), and post-extrusion draw ratio; material-related parameters including fiber aspect ratio (e) and fiber volume fraction (V_f); and die geometry parameters such as die angle, ratio of entry to exit diameter, and land length can substantially influence the orientation of fiber during thermoplastic composite processing. Before reviewing previous studies in this area, an introduction to two major thermoplastic composite processing methods is presented below.

2.1.6 Injection Molding of Thermoplastics

Injection molding [38] is a rapid, robust production method in which small thermoplastic pellets are melted, mixed, and shaped into useful finished products. Figure 2.13 shows the principle components of an injection molding machine. First, solid pellets of thermoplastic material are fed through a hopper into the heated barrel of the injection molding machine. Inside the barrel is a rotating tapered screw. As the pellets travel down the increasingly thin flights of the screw, dissipative heating and external heating melt the pellets into a highly viscous liquid.

In addition to rotating, the screw also reciprocates within the barrel under the force of electric or hydraulic actuators. Due to the rotation and forward motion of the screw, the melted material is moved forward and forced through a nozzle into the mold cavity.

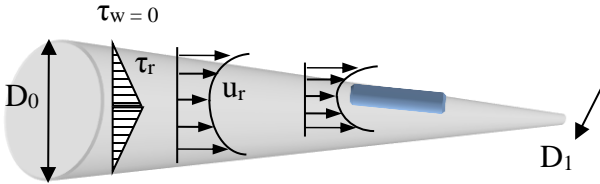


Figure. 2.12. Post processing of fibers.

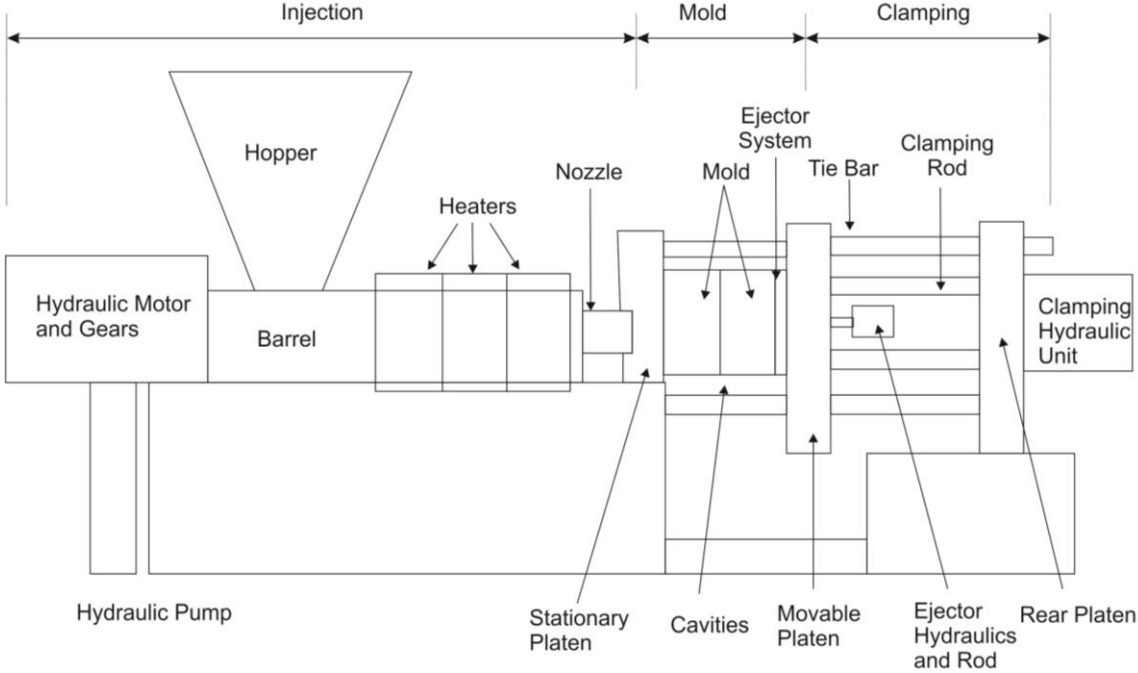


Figure 2.13. The principal components of an injection molding machine.

Immediately after exiting the barrel, the melt traverses through a series of narrow runners that may feature sharp corners and/or reductions in cross section. The runners which directly feed the mold are termed sprites, and the polymer melt traverses through a gate before entering the mold. The sprues and upstream runners are frequently circular in cross section, while the gates may be circular (a pin gate) or thin and rectangular (a film gate). The design of the sprues and gates are dictated by the mold geometry and the desired flow rate and pattern. In case of molded polymer composites, the orientation of fibers follows the flow pattern.

2.1.7 Extrusion of Thermoplastics

Unlike injection molding, extruders are used to manufacture shapes without molds. The molten polymer is extruded through a die with a hole of required shape. There are two basic extruder types, ram and screw (Brent [39]). The ram extruder uses a ram to push a molten polymer through the die. In a screw extruder, a rotating screw melts the polymer pellets fed through the feeder, homogenizes it and extrudes it through the die. The screw extruder has three zones as depicted in Figure 2.14. The conveying zone is that part of the barrel where solid particles are fed and compacted for melting. In the transition zone, the melting, mixing, and pressurization occur. In the metering zone, the melt is pumped up to full pressure to pass through the die. Heat is applied using heaters embedded within the walls of the barrel of the extruder; since a barrel is built by assembling individual sections, the temperature of the sections in the three zones as well as that of the die is controlled to impose a desired temperature profile on the melt. After passing through the shaping die, the polymer is cooled and used in that form, or it can be subjected to a secondary shaping step.

Next section identifies important micro-structural parameters for discontinuous fiber polymer composites and discusses their characterization techniques.

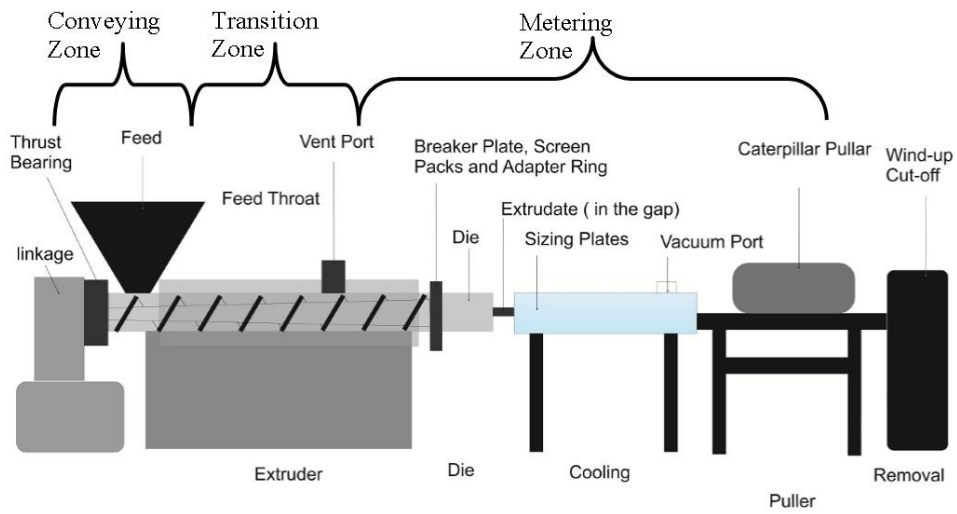


Figure 2.14. Typical extrusion line showing major equipment.

2.1.8 Composite Micro-Structural Parameters

There are three important micro-structural parameters that influence the mechanical properties of discontinuous fiber thermoplastic composites manufactured using extrusion or injection molding: Fiber Orientation Distribution (FOD), Fiber Length Distribution (FLD) and fiber content (i.e., fiber volume or weight fraction). Most studies on thermoplastic composite processing focus on these three parameters and relate them to the manufacturing variables. The most important of these three, namely FOD, is discussed below, while the other two do not require any introduction.

2.1.9 Fiber Orientation and Its Distribution

The orientation of an individual fiber can be defined by angle φ , with respect to the z -axis parallel to the extrusion direction, and angle θ , with respect to the y -axis perpendicular to the extrusion direction. The orientation can also be defined by Cartesian components of a vector \vec{p} , aligned parallel to the fiber in a system of axes. The two descriptions are related as shown in Figure 2.15, since

$$\vec{p} = (\cos \theta \sin \varphi, \sin \theta \sin \varphi, \cos \varphi) \quad (2.9)$$

If not all fibers are oriented in the same direction, then a distribution in fiber orientation (FOD) would exist. This FOD has been characterized in the literature by defining either an orientation tensor or an orientation factor.

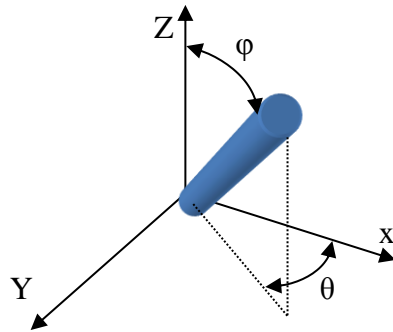


Figure 2.15. Coordinate system used in determination of fiber spatial orientation.

2.1.9.1 Orientation Tensor

For a collection of fibers as depicted in Figure 2.16, it is impossible to specify the orientation of each fiber, so an alternative is to use the probability distribution function, $\psi(\varphi, \theta)$, which evaluates the probability of finding fibers at (φ, θ) in the sample. The probability of fibers being oriented between θ and $\theta + d\theta$, and between φ and $\varphi + d\varphi$ is equal to:

$$P(\theta_1 \leq \theta \leq \theta_1 + d\theta, \varphi_1 \leq \varphi \leq \varphi_1 + d\varphi) = \psi(\varphi_1, \theta_1) \sin\varphi_1 d\theta d\varphi \quad (2.10)$$

Although the probability density functions provide a complete characterization of fiber orientation, any calculation based on these data are highly computationally intensive. Advani and Tucker [40] proposed a second-order orientation tensor $[a_{ij}]$ which is a compact, general, and short formulation of probability density orientation function used for fiber orientation characterization.

$$a_{ij} = \int p_i p_j (\psi(\varphi, \theta)) d\Omega \quad (2.11)$$

where $\psi(\varphi, \theta)$ denotes the orientation distribution function and Ω is the unit sphere, with $\int (\psi(\varphi, \theta)) d\Omega = 1$ and $d\Omega = \sin\varphi d\theta d\varphi$,

where $p(\varphi, \theta)$ is a unit vector parallel to a fiber direction, with components of $p_1 = \sin\varphi \cos\theta$, $p_2 = \sin\varphi \sin\theta$, $p_3 = \cos\varphi$

For a number of fiber “N”, the global orientation tensors for a composite are obtained by averaging all individual fiber orientations:

$$a_{3333} = \sum_{i=1}^N \frac{\cos^4\varphi_i}{N}$$

$$a_{1313} = \sum_{i=1}^N \frac{\cos^2\varphi_i \sin^2\theta_i \cos^2\theta_i}{N} \quad (2.12)$$

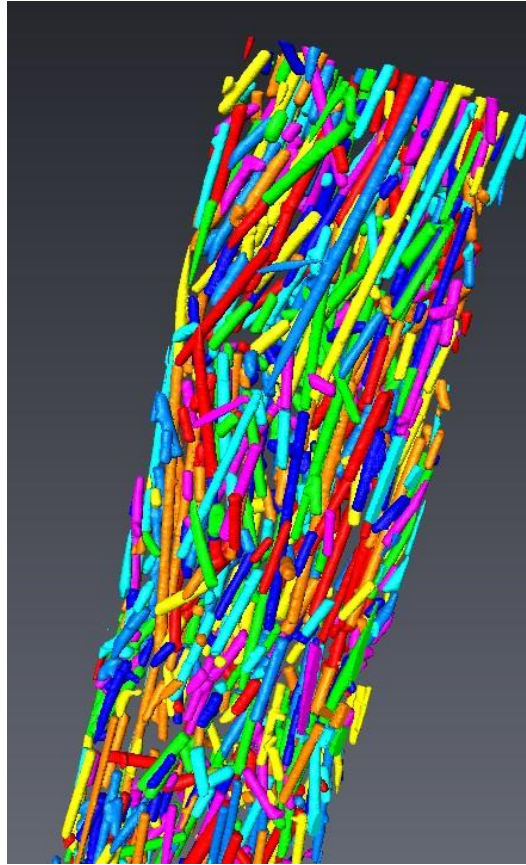


Figure 2.16. Collection of glass fibers in a polyethylene composite fiber.

Most micromechanical models use second or fourth order orientation tensors [41]. Alignment along the extrusion axis (Z) is determined by a_{3333} , and the in-plane orientation in the XY plane is determined through a_{1313} .

2.1.9.2 Orientation Factor

Since the most important feature of the internal structure of a discontinuous-fiber-reinforced composite is its state of fiber orientation, it is necessary to develop a metric which can describe the orientation state quantitatively. Pipes et.al [42] proposed an orientation parameter which provides a quantitative measure of the state of fiber orientation. The reference coordinate system, used to define the orientation of a reinforcement fiber within the composite fiber, is provided in Figure 2.15. Here a_{3333} is used as a measure of alignment along the extrusion direction. The a_{3333} varies from 0 to 1.0 as the glass fiber distribution varies from in-plane (XY) orientation to perfect alignment parallel to the longitudinal axis of the composite fiber (i.e. Z-axis extrusion direction). At the same time, a_{1313} also varies from 0 to 1.0 as the glass fiber orientation varies and the 1 value corresponds to the distribution where the fibers are aligned to the Z axis or extrusion direction. In this study, X-ray computed tomography along with Avizo Fire © software are used to measure the θ value for each fiber in the spun composite. Subsequently, θ is inserted in Equations (2.13) and (2.14) to calculate the orientation factor.

2.1.10 Measurement of FOD of Micro-Sized Fibers

One method widely reported in the literature is the method of sections, illustrated schematically in Figure 2.17. This method relies on the analysis of microscopic images of polished cross sections.

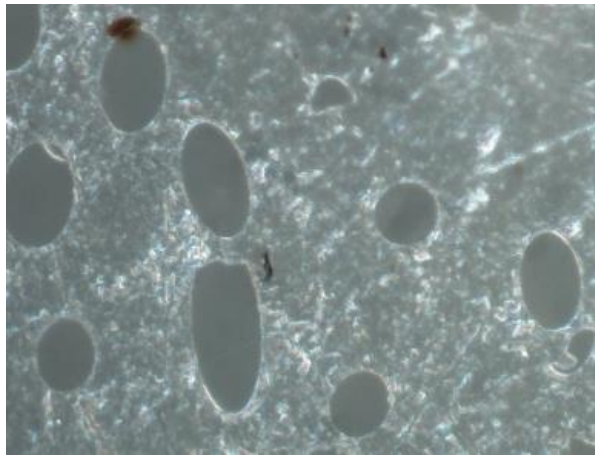


Figure 2.17. Cross section of extruded fiber.

Fibers are considered nearly cylindrical, so they appear as ellipses in a cross section if the orientation of that cross-section is not perpendicular to the fiber axis as depicted in Figure 2.17.

The cross section as illustrated in Figure 2.17 lies in the y-z plane; hence, the angle θ is determined from the orientation of the major axis of the ellipse by:

$$\cos \theta = a/d \quad (2.13)$$

where a is the minor diameter and d is the major diameter.

This method of orientation measurement has been implemented by many, including Hine et.al [43] and Eberhardt and Clarke [44]. A high-quality automated image analysis technique for measuring fiber orientation has been developed by Hine et al. [43]. Another method is Confocal microscopy [45], a technique in which multiple optical sections of the sample are made in order to construct 3D data. The fibers' geometric parameters are obtained through image analysis, while orientation tensors are used to define fiber orientation states. Blanc et al. [46] proposed an image processing approach to estimate fiber orientation distribution through image analysis of a single section of the composite. Their method was verified through characterization of carbon reinforcement of composite materials, and they also developed an algorithm to derive the orientation tensor and a probability distribution function based on the image analysis.

In the present research, the fiber orientation and its distribution have been characterized non-destructively using X-ray tomography. This method is explained in detail in chapter 4.

2.2 Processing-Microstructure Relationships

The micro structural parameters identified in the previous sections are influenced by the manufacturing variables. These variables can be categorized into following four groups:

- I. Processing parameters : Screw speed (SS), pressure P , temperature (T)

- II. Material parameters: Fiber Weight fraction in the feed (W_f) , Fiber Aspect ratio (AR)
- III. Die parameters: Entry Angle (EA) of die hole, Ratio of entry to exit diameters, Land length
- IV. Post processing parameter: Take up roll speed (TS) and temperature

Previous studies that have focused on the effect of one of more of these variables on FOD are reviewed below. These studies have been grouped under the following sections for clarity.

2.2.1 Micron-sized Fiber reinforced composites

2.2.1.1 Studies involving shear flow-induced fiber orientation

2.2.1.2 Studies involving elongational flow-induced fiber orientation

2.2.2 Nano-sized Fiber reinforced composites

2.2.2.1 Studies involving shear flow-induced nanofiber orientation

2.2.2.2 Studies involving elongational flow-induced nano-fiber orientation

2.2.1 Micron-Sized Fiber Reinforced Composites

2.2.1.1 Studies Involving Shear Flow-Induced Fiber Orientation

Barbosa and Kenny [1] investigated the effect of volume fraction and screw speed during manufacturing of glass fiber-reinforced polypropylene using a single screw extruder with a capillary die. They observed cross sections of specimens, obtained by fracturing extruded filaments in liquid nitrogen, using a Scanning Electron Microscope (SEM). Image analysis was performed on scanned SEM microphotographs. From the center of the sections six concentric annular regions of thickness of 100 μm were defined and analyzed. The fiber orientation factor was found to increase with increase in the shear rate and to decrease with the fiber concentration in the feed. The average fiber length decreased with an increasing fiber concentration and extrusion rate. The extruded filament surface showed reduced roughness when the shear rate was increased

or when the fiber concentration was decreased. A spun fiber with 5% weight fraction was smoother than the fiber with 30% weight fraction, which highlights the effect of fiber to fiber interaction.

Vaxman and Narkis [2] studied the influence of shear rate, fiber concentration, and temperature on fiber orientation. Polystyrene with short glass fibers was manufactured using an Instron capillary rheometer with a length to diameter ratio of 10, 20, 40, 60, and 90, and the measurements were carried out at temperatures of 180, 200, and 230°C. The orientation was measured by imaging the polished section using reflected-light microscopy and analyzing the cross section shape of fiber. For the same weight fraction, the higher the shear rate, the lower the in-plane orientation factor f_p , which is in contradiction to the findings of Barbosa and Kenny [1]. The effect of temperature on orientation was not conclusive.

Becraft et al. [3] studied the effect of shear rate on the alignment of glass fibers in injection molded high density polyethylene composites. They concluded that even a very low level of shear rate was sufficient for substantial fiber alignment in composites manufactured with a W_f of 40%. The fiber alignment measurement using tensor representation improved with increase in the shear rate.

Shogren and Selling [4] produced Polylactic acid (PLA)/starch fibers by twin screw extrusions of PLA with granular or gelatinized starch/glycerol followed by drawing both through a set of winders within the intermediate oven. At 30% starch, fibers were drawn to 2–5 times the original size. The tensile strength and the modulus increased with increase in the draw ratio but decreased with more starch content. The increase in modulus was related to the increase in the orientation of the starch fibers; however, there is no report of quantitative or qualitative measurement of FOD.

Hine et al. [5] used hydrostatic extrusion to orient short glass fibers within polyoxymethylene (POM). The starting material consisted of random glass fibers (25 wt% and average length 150 μm) in an isotropic POM matrix. Extrusion ratios of 1.77, 3.65, 5.31, and 6.91 were chosen, and the results show significant improvement in the orientation with increase in draw ratio.

Sanomura and Kawamura [6] studied FOD in the extruded short glass-fiber-reinforced polypropylene composites manufactured by ram extrusion. The draw ratio was 1.4, 1.7, 2, and 2.31, and alignment was measured using the orientation factor. The fiber orientation distribution improved from $f_a = 0$ to $f_a=0.197$ at higher draw rate.

Mor et al. [7] studied the effect of cylindrical solid walls and free surfaces on the orientation distributions of otherwise randomly oriented suspensions of poly(methyl-methacrylate) (PMMA) fibers with a length of 31.75 (mm) and a diameter of 1.587 (mm). The suspension fluid was 50% alkylaryl polyether alcohol, 36% polyalkylene glycol, and 14% tetrabromoethane. A suspension of 10% volume fraction flowed through the two cylinders with diameters of 1.5 and 10 times of the length of fiber, respectively. Two video cameras were placed in relative position to each other to obtain a three-dimensional image of system. The data recorded by the two cameras were digitally processed and converted to spatial and orientation is determined subsequently. Mont Carlo simulations were also done for a finite number of fiber in two cylinders mentioned previously and finding the orientation distribution function. The Mont Carlo simulation showed good agreement with the experimental results. Mor et al. found that for cylindrical channels containing extremely small concentrations, the orientation of the rods is not completely isotropic, in addition decrease in the cylindrical channel diameter results in better orientation .

Guo et al. [8] studied the effect of shear rate through simple static and dynamic injection molded samples of isotactic polypropylene reinforced with 5, 10 and 30 % weight fraction fiber glass. SEM and AFM images shows that because of higher shear the fibers in dynamic injection are more aligned across their thicknesses. However, SEM and AFM image analysis only provide qualitative orientation distribution data.

2.2.1.2 Studies Involving Elongational Flow-Induced Fiber Orientation

Shogren and Selling [4] produced Polylactic acid (PLA)/starch fibers by twin screw extrusion of PLA with granular or gelatinized starch/glycerol followed by drawing through a set of winders with an intermediate oven. At 30% starch, fibers were drawn to 2–5 times the original size. The tensile strength and the modulus increased with increase in the draw ratio but decreased with increase in the starch content. The increase in modulus was related to the increase in orientation of starch fibers, however there is no report of quantitatively or qualitative measurement of FOD.

Hine et al. [5] used hydrostatic extrusion to orient short glass fibers within polyoxymethylene (POM). The starting material was random glass fibers (25 wt% and average length 150 μm) in an isotropic POM matrix. Extrusion ratios of 1.77, 3.65, 5.31, and 6.91 were chosen, and the results show significant improvement in the orientation with increase in draw ratio.

Sanomura and Kawamura [6] studied FOD in the extruded short glass – fiber reinforced polypropylene composites manufactured by ram extrusion. The draw ratio was 1.4, 1.7, 2, and 2.31 and alignment was measured using orientation factor. Fiber orientation distribution changes from $f_a = 0$ to $f_a = 0.197$ for aligned distribution for higher draw rate.

Parsheh et al. [9] studied the orientation of rayon fibers in a high Reynolds contraction velocity field. High speed imaging was used to directly measure the orientation distribution function at various downstream locations along the contraction centerline. High speed imaging and laser Doppler velocimetry (LDV) were used to take images from flow and then analyzed to find the orientation and location of fibers along the channel. Subsequently having the orientation distribution for fiber in the flow the orientation tensor was calculated. The orthotropic orientation tensors obtained from experimental results were almost identical to those obtained using natural closure approximations. This study also found that the fiber orientation increased with increasing contraction, which translated to higher elongational strain.

Fras et al. [10] studied for various reinforcement weight fractions in the feed, the correlation among extrusion conditions, the draw ratio (elongation), the development of particle orientation (talc (00S)), and tensile properties of a plasticized polyvinylchloride. Their manufacturing method used a twin-screw extruder: Leistritz LSM 30. XRD analysis confirmed that weight fraction variation did not improve the orientation. The presence talc (00S) enhanced Young's modulus; however, the impact of reinforcement alignment on modulus was not clarified.

2.2.2 Nano-sized Fiber reinforced composites

2.2.2.1 Studies involving shear flow-induced nanofiber orientation

Sun et al. [11] studied the effect of shear rate on the orientation of needle-like hydroxyapatite (HA) nanoparticles combined with polycaprolactone (PCL). HA/PCL composites were prepared by compounding the surface-treated HA particles with PCL using an intermeshing co-rotating twin-screw extruder. The composite was subsequently subjected to shear stress in a rheometer while it was cooled; the HA needles were frozen in place as the matrix solidified. The particle orientation and its distribution were examined using electron micrographs, which showed

the HA nano-needles to be well dispersed in the PCL matrix and well aligned in the flow direction. However, no value for orientation was presented, and alignment was based on visual observation of the SEM image.

Sulong and Park [12] investigated the effect of shear rate on the alignment of Multi-walled Carbon Nanotubes (MWCNTs) in a polyethylene (PE) matrix, processed by a extrusion system constructed by the authors. The orientation of the MWCNTs in the PE matrix was analyzed through image analysis of a section using the SEM. They found the average degree of alignment to increase from 60° to 30° with increasing shear rates to $32,900\text{s}^{-1}$. It was also found that the mechanical properties of the CNT polymer composites improve with increasing shear rate.

Hobbie et al. [13] studied the orientation in semi-dilute dispersions of MWCNT in polybutadiene using a self-constructed shear light scattering photometer with an optical microscope. For a weakly elastic polymer melt, the data suggest that the semi-flexible tubes orient along the direction of flow at low shear stress, with a transition to vortices alignment above a critical shear stress, σ_c . In contrast, data for a highly elastic polymer solution suggest that the carbon nanotubes orient with the flow field at high shear rates. With increasing temperature, the transition from the flow alignment to the vortices alignment occurred at a higher shear rate, reflecting the effect of decrease in viscosity of the polybutadiene matrix with increase in temperature.

Kang and Ryu [14] investigated the correlation between shear stress and the orientation of single-walled carbon nanotubes (SWCNTs) in an SWCNT/polypropylene composite using a capillary rheometer. Polarized Raman Spectroscopy measurements were carried out at 0° and 90° orientations of the polarized laser beam with respect to the flow direction to investigate the orientation of the SWCNTs in polypropylenex. The relative intensity of the tangential mode (1578

cm-1) for polarization parallel to the fiber axis versus that for polarization perpendicular to the fiber axis was used to compare the degree of SWCNT orientation. The existence of a critical shear stress was observed for the orientation of the SWCNTs, and their orientation was found to occur more efficiently above this critical shear stress.

The effect of shear rate in compression (disk), injection (dog-bone), Micro-injection-compression (disk), Micro-injection (disk), and Micro-injection (dog-bone) molding on the nanotube alignment and on the properties of a Polycarbonate/MWCNT nanocomposite were investigated by Abbasi et al. [15]. The morphological analysis, using SEM, TEM and AFM, showed that the nanotubes were randomly oriented in the plane of the compression molded samples, which were subjected to the lowest shear value, while they were well aligned in the longitudinal flow direction in the microinjected dog-bone samples, which encountered very high shear values. Raman spectra were collected using a Renishaw spectrometer equipped with an Invia Raman microscope. Measurements were made when the fiber was 0° and 90° to the fiber axis to the flow direction. Raman spectroscopy results indicate Micro-injection molding (dog-bone) samples had the highest alignment among other injection molding processes. Interestingly, the nanotube alignment strongly affected the viscosity at a high shear rate which exhibited a shear thinning effect because of flow induced disentanglement and alignment.

Cooper et al. [16] studied composite fibers consisting of different quantities of carbon nanotubes and nanofibrils in a poly (methyl methacrylate) (PMMA) matrix, using a Brabender DSK 25 single-screw extruder with a 25 mm screw diameter, an L/D ratio of 22, and a temperature of 232° (C) . The orientation distribution of carbon fibrils and nanotubes in the composite was determined by image analysis and found to be maximized in the extrusion flow direction. Transmission electron microscopy (TEM) was used to determine the distribution and alignment of

the nanofibrils, and particularly nanotubes, in the PMMA matrix of the final composites. Orientation distribution was used to compare the alignment between different samples. The nanofibrils' concentration of 0.1 weight % achieved the best orientation in comparison with 4% and 10%; on the other hand, mechanical properties did not change with the addition of nano-reinforcement.

Cayla et al. [17] prepared polycaprolactone filled with 4 wt% of MWCNT by melt extrusion to obtain a conductive MWCNT-polycaprolactone composite. In a second stage, this conductive composite was mixed with polypropylene and melt spun again into multifilament yarns. Young's modulus of the yarns did not change for concentrations of MWCNT 0.4, 0.8, 1.2, 1.6, and 2 wt% Based on the changes in the electrical conductivity, the authors claimed an improved orientation of the MWCNT. FOD was not measured (Cayla et al. [17]).

2.2.2.2 Studies Involving Elongational Flow-Induced Nano Fiber Orientation

Miyazono et al. [18] studied the orientation of carbon nano-fiber (CNF) in polystyrene matrices which were compression molded. Composites containing 2, 5, and 10 wt% CNF were prepared and subsequently were stretched to a total strain of 0.1, 0.3, 1, or 3 at a constant extensional rate of 0.01, 0.1, or 1.0 s⁻¹. A strain-controlled rheometer from TA Instruments and an RME rheometer from Rheometrics Scientific were used to measure shear and extensional viscosity, respectively. A procedure to determine the value of angles θ for using a single 2D TEM image was developed based on the assumption that the angle θ for each fiber can be directly measured from the TEM image by measuring the angle the fiber makes with a reference axis and measuring the projected length of each fiber in the TEM image. From these measurements, it was

observed that CNFs were more aligned in the direction of flow during extensional flow compared with shear flow.

The orientation of the fibers in the direction of the applied strain was found to increase with the magnitude of the strain. Interestingly, there seems to be little relationship between strain rate and the amount of orientation achieved during flow for both shear and extensional flow; however, total strain appears to be important. During shear flow, the average value of the orientation tensor component a_{33} at steady state was ~ 0.5 , while for extensional flow that value was ~ 0.9 . In the case of extensional deformation, CNFs in the nanocomposite are readily oriented toward the direction of applied strain, however, in the case of the shear deformation, the shearing forces cause the CNFs to rotate and/or tumble, which prevents the formation of a highly oriented structure.

Potschke et al. [19] melt spun a conductive polycarbonate (PC) composite containing 2 wt% MWNT (Multi Wall Nano Tube) and pure PC using a Haake co-rotating, twin-screw extruder (L/D=10). Different take-up velocities were used up to 800 m/min, resulting in draw ratios up to 250. Draw ratio was defined as the ratio of the diameter of fiber at the die exit to the diameter of fiber after being collected on the wind up drum. The higher the take-up speed of the drum, the higher the draw ratio. The composite material of PC with MWNT was prepared by diluting a PC based master batch consisting of 15 wt% MWNT by melt mixing in an extruder. Raman spectroscopy along with TEM imaging showed an improvement in the alignment of the nanotubes within melt spun fibers with an increase in draw down ratio, which was also confirmed by the loss of the electrical conductivity of the fibers. The orientation measurement was done quantitatively.

Sulong et al. [20] optimized self-constructed melt spinning process parameters (spinning temperature, spinning distance, and the number of spinning revolutions) by Taguchi's method with

the objective of enhancing the mechanical properties of a composite fiber containing CNT. However, no alignment of CNT observed by SEM image analysis due to low shear rate and drawing ratio. Moreover, partially aligned CNT composites resulted in a higher mechanical strength than randomly oriented CNT composites.

Fischer et al. [21] applied transmission electron microscopy (TEM) and polarized Raman microscopy to quantify the orientation of the MWCNT as well as the crystallinity in the polycarbonate (PC). A Haake co-rotating, intermeshing twin-screw extruder (L/D=10) was used to manufacture a PC based composite with 2 wt% MWNT with draw ratio of 0, 50, and 100. Polarized Raman microscopy orientation analysis shows an improvement in orientation of the MWCNT with increasing take-up velocity during melt spinning. The authors did not provide any quantitative measure for orientation value.

Anand et al. [22] used melt spinning followed by drawing to manufacture poly (ethylene terephthalate)-single-walled carbon nanotube (PET-SWNT) nanocomposite fibers. When the draw ratio was increased, the tenacity and the modulus of the fibers increased, indicating that drawing induced orientation of the polymer molecules and SWNTs. Since the researchers compared neat drawn PET with PET-SWNT, the results showed that the increase in the modulus was also due to the orientation of the SWNT in addition to the orientation of the PET chains.

The effect of the orientation of carbon fillers with different aspect ratios on the resistivity and morphology of conductive polypropylene composites was investigated by Deng et al. [47]. MWCNTs and carbon black (CB) were used as conductive fillers to manufacture conductive polypropylene composites. The CPCs were made by melt compounding, hot pressing, and solid-state drawing. The alignment of the filler was observed after solid-state drawing by SEM

analysis, which was also confirmed by an increase in the electrical resistivity of the composites in the direction of drawing.

Chae et al. [23] spun Polyacrylonitrile (PAN)/single wall carbon nanotube (SWNT) composite fibers with 0, 0.5, and 1 wt% SWNT content using a draw ratio of 51. Herman's orientation factor based on WAXD (Wide Angle X-ray Diffraction) shows that as draw ratio increases from 3.2, 22, 32, and 51, the alignment of SWNTs increases. With the addition of 1 wt% SWNT to PAN and 51 draw ratio, the room temperature modulus increased by 6.6 GPa (from 22.1 to 28.7 GPa) in comparison to PAN.

Bhattacharyya et al. [24] melt-blended polypropylene (PP) with 0.8 wt% of SWCNT and spun them into a composite fiber with a draw ratio of 4.5. The polarized Raman spectra were determined using a Holoprobe Research 785 Raman Microscope made by Kaiser Optical System Inc. Herman's orientation factors calculated based on Raman scattering intensity of SWNT in PP/SWNT composite fibers were 0.81 and 0.95 for the as spun and the drawn fibers (draw ratio 4.5), respectively. This increase in Herman's orientation factors reflects the enhancement in alignment by draw ratio. However, no enhancement in mechanical properties was reported in this study.

Polyvinylalcohol-SWCNT composite fibers were gel spun using SWCNT volume fractions of 5, 10, 16, and 20% by Blighe et al. [25]. The modulus and the strength of the composite fibers increased linearly with the nanotube volume fraction reaching a plateau value beyond $V_f \sim 10\%$. An increase in draw ratio of 40% increased the modulus 2.7 times. Raman spectroscopy showed that the Herman's orientation factor increased from 0.5 for spun fiber without drawing to 0.7 for the highest drawing, indicating that significant nanotube alignment occurred due to drawing.

2.2.3 Effect of Die Parameters

Studies of die parameters are limited to pure polymer and are mainly focused on understating the pressure drop effect on flow through the die [48-50] and [30]. Below are the two studies which looked into die parameters. Silvia et al. [51] investigated polypropylene reinforced glass fibers with 5, 10, 20, 30 weight fraction and capillary dies with a diameter of 1.2 (mm) and lengths of 12, 24, 36, and 48 (mm). Samples were melt spun in a Haake single screw extruder with a rheometric capillary die. Orientations were calculated using the orientation factor. The results for 20% weight fraction show that as shear rate increased from 200 to 4500 (1/s) the orientation factor increased from 0.6 to 0.8. Then they studied the effect of die length on the extruded composite. According to the authors' findings, this did not have any correlation to fiber orientation.

Kim and Park [52] studied polystyrene-filled fiber glass of 20% extruded with a capillary rheometer. A sample of polystyrene/glass fiber was taken from inside the capillary die and observation with SEM indicated that there was not any difference among fiber orientations across the capillary diameter from wall to center. Also, shear rate variation from 25.4 to 3110 (1/s) did not change the orientation inside the capillary die. Neither orientation factors nor orientation tensor was considered for orientation comparison in their study.

2.3 Numerical Studies Prediction of Flow-Induced Orientation

There have been several studies to predict the fiber orientation and mechanical properties of injection molded composites. Fu and Lauke [53] studied effects of fiber orientation distributions and fiber length for predicting the tensile strength of short-fiber-reinforced polymers and compared these predictions with previously reported experiments. The results show that the strength of composites increases as the fiber orientation factor increases; however, composite fiber strength does not show any correlation with alignment of fiber. Experiments and predictions based on fiber

orientation distribution show good agreement. Jayaraman et al. [54] presented a model based on variable fiber orientation and fiber length to predict elastic modulus of short fiber composite. Vaxman et al. [55] investigated the effect of fiber orientation on rheological behavior of short glass fiber-reinforced thermoplastics. Their results shows that fiber orientation at low shear rates is shear-rate sensitive, while at the higher shear rates fibers are already highly oriented, so further increasing shear rates has only a little additional effect on the orientation level. The above studies highlight the significant importance of fiber orientation on structural and functional properties of short fiber-reinforced thermoplastics. Property prediction of composites based on orientation distribution has been reviewed further by Author [56-57], but this application is beyond the scope of this research.

Zhou and Lin [58] solved the orientation of a fiber in concentric, wedge, circular jet, and round pipe flow. The orientation tensors were predicted by solving Navier-Stoke equations. The predicted fiber orientation distribution for aspect ratios of 10 and 100 results indicated that in a simple homogeneous shear flow a higher aspect ratio shows higher alignment. Also, Zhou and Lin's [56] prediction indicates that extensional flow always aligns fibers in the direction of the flow.

Advani, SG. and Tucker [40] presented the orientation state of fibers in composite or suspension with a tensor's representation. The proposed tensor does not make any assumptions about the shape of the probability distribution function. The authors concluded that a fourth order orientation tensor can predict the mechanical property very well when compared with experimental results. A combination of second order and closure approximation can also predict mechanical properties with close agreement. As the orientation distribution function effects the property of the composite, flow can also alter the orientation of fibers. Closure approximation is a method to

examine the changes in the orientation tensor. Different closure approximations have been studied and developed to predict fiber orientation during flow [59-61].

Azaiez et al. [62] analyzed the developments in the numerical modeling of vinylon fibers in 65 wt% corn syrup/water solution suspensions in recirculating, circular contraction, and rectangular flow. Numerical and experimental approximations based on quadratic closure indicate that results for large aspect-ratio fibers confirm that all fibers align completely along the streamlines. However, for small aspect-ratio fibers, the computations predicted that complete alignment could be achieved, but the preferred angle was oblique to the streamlines.

Chung and Kwon [63] have reviewed and compared various closure approximation methods using Finite Element Analysis (FEA). Natural closure approximation was found to predict the flow results very well.

2.4 Analytical Studies on Flow Induced Orientation

The following studies looked into occurrence of fibers orientation in extrusion by existence analytical models. Hine et al. [64] studied polypropylene reinforced with short glass fiber at 20 and 30% weight fractions manufactured with melt extrusion through conical dies and slit dies with a semi-angle of 15 degrees. Fiber orientation after manufacturing was measured using their in-house developed image analysis facility. They concluded that extensional strain in both the conical and slit dies has a significant effect on the orientation of fibers. Also, fiber orientation prediction using the Pseudo-Affine deformation theory agreed well with experimental measurement. According to the Pseudo-Affine deformation theory, the orientation fiber after deformation can be predicted based on initial deformation and deformation strain.

Material travelling through a convergent flow zone will experience both elongation and shear deformations. Modlen [29] studied the effect of deformation work on fiber orientation, including both elongational and shear deformations, but concluded that particularly for uniaxial deformation, internal shearing becomes of decreasing importance as the extrusion ratio increases above four. He also manufactured Plasticine reinforced with copper wire at predetermined alignment to compare the predicted orientation with the distribution of copper wire after ram extrusion manufacturing.

A uniaxial elongational rheometer **was** used by Kobayashi et al. [65] to study the elongation viscosity of polystyrene-potassium titanate whisker composite melt. Wide-angle X-ray diffraction (WAXD) was used to measure the orientation of these fibers. Here the elongational viscosity was almost independent of the orientational change of the whiskers—the orientation of the whiskers was dependent on strain only. Their comparison of Jeffery theory orientation prediction with their experimental results shows close agreement.

2.5 Rheology of Polymer Composite

The effect of orientation distribution as well as volume fraction on rheology of polymer reinforced fibers has been studied by numerous researchers with capillary, cone and plate, parallel plate, creep, and injection molding. For example, the effects of volume fraction on shear viscosity as well as elongation viscosity were studied by Name [49] and Name [66]. Reviewing all the papers in this area is beyond the scope of this thesis; however, below are those studies that presented orientation distribution and volume fraction model to predict shear and elongation viscosity of polymer composite flow.

Using orientation tensor theory, Ausias et al. [67] proposed an anisotropic rheological constitutive model which characterizes the coupling between stress and fiber orientation. This model predicted the transient viscosity of polypropylene reinforced with 20 and 30% weight fraction glass fiber. Unfortunately, their results were not compared with experiment results.

Powell [68] presented a model considering the effect of volume fraction, fiber aspect ratio and fiber orientation distribution on the viscosity of a filled system. This model prediction was compared with previously reported experimental work. The proposed viscosity model considered hydrodynamic forces over a wide range of concentration models and showed close agreement with experimental data.

Shaqfeh and Fredrickson [69] proposed a model to predict the viscosity of polymer composites for isotropic and aligned fiber distribution for different volume fraction with high aspect ratio fibers.

2.6 Summary of Literature Review

Two important manufacturing processes for discontinuous fiber thermoplastic composites are injection molding and extrusion. While the polymer melt flow in the former is complex and predominantly shear, the polymer melt flow in the latter is relatively simple and can have both shear and extensional components. The relative advantages of shear and extensional components depend on the extrusion die design and process parameters. While some researchers have based their studies on the injection and extrusion equipment itself, a majority of studies have used a lab-scale capillary rheometer since it can generate typical shear rates ($\sim 1 - 2000 \text{ s}^{-1}$) encountered during extrusion or injection molding (lower end of the shear rates achievable). Few studies have used lab-scale cone and plate rheometers that can generate shear rates $< 1 \text{ s}^{-1}$, which are not in any case relevant to the two identified manufacturing processes; however, the steady-state viscosity

obtained from this equipment is combined with the results from the capillary rheometer to obtain the viscosity data over a wider shear rate range.

Studies based on capillary rheometers have mainly focused on the effect of fiber volume fraction and aspect ratio on shear viscosity. While experimental studies on the explicit relation between shear viscosity and fiber orientation are rare (except in numerical studies), the orientation of micron-sized fibers in shear flow has been studied, using capillary rheometer, by many researchers in the past. These studies have focused on a few of the variables identified in Table 2.3, but not all of them as identified in Table 2.1. While studies on injection molding involves complex flow pattern, the complexity makes interpretation of the effect of shear flow on fiber orientation difficult.

Studies on the orientation of micron-sized fibers in extensional flow have been limited to tensile drawing of composites heated beyond the melting point of the matrix, which mimics post-extrusion drawing but not what happens during extrusion. The interpretations from these studies are summarized in Table 2.2. Many studies using extruders have focused on rheological properties of composite (i.e., extensional and shear viscosity) rather than fiber orientation.

As mentioned before, the fiber orientation during extrusion is due to both shear and extensional flow. While studies mentioned above offer insight into fiber orientation in shear and extensional flows, additional research is required to understand the fiber orientation under combined extensional and shear flows encountered within an extrusion die. Since the various variables identified in Table 2.3 can alter the relative contributions from shear and extensional flow, knowledge on the combined effect of these variables on fiber orientation during extrusion is required but lacking.

In parallel, interest in orienting nanofibers within a polymer matrix has been steadily increasing during the past decade in order to achieve enhanced functional and structural properties in composites. As reviewed in the previous section, though many studies have identified the role of extensional viscosity on orientation of nano fibers through tensile drawing experiments, additional study is required to understand the orientation of nano fibers during extrusion (similar to micron-sized fibers).

Finally, the mechanical properties of composites depend on both the FOD and the fiber volume fraction in the processed composite. While the V_F in the processed composite is taken to be the same as that in the feed by previous studies, this may not be the case since V_F and FOD influence one another. This aspect and its dependence on extrusion variables have not been studied, but this knowledge is required for optimizing the extrusion variables. Additionally, a non-destructive characterization method is required to measure the FOD that is more representative of the composite volume than that measured by the sectioning method used by previous studies.

In summary, additional study is required to understand the combined effect of die design and processing variables on the micron-sized discontinuous fiber orientation in composites extruded using a twin screw extruder.

Table 2.1. Summary of Inference on the influence of parameters on FOD during extrusion of polymer composite with discontinuous reinforcement fibers in elongational flow.

| | Micro-meter reinforcement fibers | Nano-meter reinforcement fibers |
|--|----------------------------------|---------------------------------|
| | Elongational Flow | Elongational Flow |
| Manufacturing Variables | FOD | FOD |
| Die entry Angle (α) | N/S | N/S |
| Die land length to Die diameter (L/D) | N/S | N/S |
| Take up roll speed (Draw Ratio) | $\uparrow \rightarrow \uparrow$ | $\uparrow \rightarrow \uparrow$ |
| Reinforcement weight fraction (Wf) in feed | N/S | N/S |
| Reinforcement aspect ratio (AR) | N/S | N/S |

\uparrow means “increases”, \downarrow means “decreases”, and \rightarrow means “results in”, N/S means “ has not been studied”

Table 2.2. Summary of Inference on the influence of parameters on FOD during extrusion of polymer composite with discontinuous reinforcement fibers in shear flow.

| | Micro-meter reinforcement fibers | Nano-meter reinforcement fibers |
|--|-----------------------------------|---------------------------------|
| | Shear Flow | Shear Flow |
| Manufacturing Variables | FOD | FOD |
| Die entry Angle (α) | N/S | N/S |
| Shear rate (SR) | $\uparrow \rightarrow \uparrow$ | $\uparrow \rightarrow \uparrow$ |
| Die land length to Die diameter (L/D) | N/S | N/S |
| Reinforcement Weight fraction (Wf) in feed | $\uparrow \rightarrow \downarrow$ | N/S |
| Reinforcement aspect ratio (AR) | N/S | N/S |

\uparrow means “increases”, \downarrow means “decreases”, and \rightarrow means “results in”, N/S means “ has not been studied”

Table 2.3. Summary of Inference on influence of parameters on FOD during extrusion of polymer composite with discontinuous reinforcement fibers.

| | Micro-meter reinforcement fibers | Nano-meter reinforcement fibers |
|--|----------------------------------|---------------------------------|
| Manufacturing Variables | FOD | FOD |
| Screw speed (SS) | N/S | N/S |
| Pressure (P) | N/S | N/S |
| Temperature (T) | N/S | N/S |
| Shear rate (SR) | ↑→↑ | ↑→↑ |
| Die entry Angle (α) | N/S | N/S |
| Die land length to Die diameter (L/D) | N/S | N/S |
| Take up roll speed (Draw Ratio) | ↑→↑ | ↑→↑ |
| Reinforcement Weight fraction (Wf) in feed | N/S | N/S |
| Reinforcement aspect ratio (AR) | N/S | N/S |

↑ means “increases”, ↓ means “decreases”, and → means “results in”, N/S means “has not been studied”

CHAPTER 3. Experimental Details

3.1 Introduction

Details on the materials and experimental procedure used, to date, in realizing the objectives discussed in chapter one are provided and discussed in this chapter.

3.2 Materials

High Density Polyethylene (HDPE), milled fiber glass, Montmorillonite nanoclay, Multi-walled carbon nano-tubes (CNT), and Cellulose Acetate Butyrate (CAB) were purchased and used in this study. It should be noted that the CNT were purchased pre-mixed with Polyethylene (PE) as pellets. These were subsequently mixed with HDPE and CAB for further study. The suppliers and key material characteristic of these materials are tabulated in Table 3.1.

3.3 Fiber Spinning

3.3.1 Extruder

The HDPE fiber and the composite fibers were melt spun using Leistritz's ZSE18 co-rotating twin screw extruder located in civil engineering structural laboratory, shown in Figure 3.1. The composite fibers included HDPE -Glass, HDPE -Spherical Glass, HDPE-Nanoclay, HDPE-CAB-Nanoclay, HDPE-CNT, and HDPE-CAB-CNT. These included either HDPE or CAB as matrices. The reinforcements in these composite fibers included glass fibers, nanoclay, and multi-walled carbon nano-tubes.

The extruder was computer controlled. The material fed through the two feeders (the primary feeder at the beginning of the extruder and the secondary stuffer at the end of the extruder) as shown in Figure 3.2. The material was melt mixed and extruded through a die into composite

fibers. The material feed rate and the screw speed were controlled by the computer, and the temperature of the twelve barrel segments of the extruder as well as the die were programmed using the computer as well. As the polymer travels through the extruder barrel, it gets melt mixed because of the temperature profile imposed by barrel 1-12. The temperature profile used in this study was as per recommendations from the supplier of HDPE. The heating barrels temperature profile for HDPE manufactured fibers is tabulated in Table 3.2. The temperature profile varies because it depends on the polymer melting temperature and viscosity of melt as well as other rheological properties. A schematic of the heating barrel is depicted in Figure 3.2.

The pressure in the die was measured using a pressure transducer in the extruder and recorded by the computer. A typical barrel 12 temperature (barrel T profile) and die pressure profile as a function of five minutes of collecting the material recorded by the extruder is shown in Figure 3.3. The pressure fluctuation was ± 0.010 (MPa) and temperature fluctuation was ± 2 ($^{\circ}\text{C}$).

While HDPE-Glass composite fibers were spun, the HDPE was fed into the extruder barrel through the main feeder, and the discontinuous glass fibers were fed into the extruder barrel through the side stuffer. The HDPE was melted and homogenized before it arrived at the location of the side stuffer (through the rotational motion of the two co-rotation screws within the barrel), where it was mixed well with the glass fibers before extruded through the dies. The HDPE was gravimetrically fed using a main feeder at a rate of 0.3 kg/hr. The material feed rate for the side stuffer varied by 10 – 50% of the main feeder rate to achieve 10 - 50% weight fraction of glass fibers in the extruded composite fiber.

Table 3.1. List of materials and their suppliers.

| Material | Supplier | Product Name | Key Attributes** |
|-------------------------------|---|-------------------------|---|
| HDPE | Ashland Chemical, Covington, Kentucky, USA | M 6028 | Density of 958 kg/m ³ Modulus - 1050 MPa Melt Index-2.8 g/10 min |
| Fiber Glass | Fibertech, Bridgewater, Massachusetts, USA | 6608 | Fiber Diameter -16 μm Fiber Length -470 μm |
| Montmorillonite Nanoclay | Southern Clay Products, Inc., Gonzales, Texas, USA | Cloisite® 15 | Dry Particle Size < 10 μm d ₀₀₁ =3.63nm* |
| Cellulose Acetate Butyrate | Eastman Chemical Company, Kingsport, Tennessee, USA | CAB-381-0.5 | Butyryl Content 37 wt % Acetyl Content 13 wt % Molecular Weight |
| PE-CNT Pellets | Nanocyl s.a., Sambreville, Belgium | PLASTICYL ™HDPE 1501 | 15% MWCNT loading ⁺ |
| Solid Glass Microspheres | Potters, Valley Forge, PA | A-Glass 3000 | Density of 2500 kg/m ³ Modulus – 68.9 GPa |

* d₀₀₁ is basal spacing of montmorillonite

⁺ MWCNT stands for Multiwall Carbon Nano-Tube.

** Key attributes here is collated from each individual data sheet.

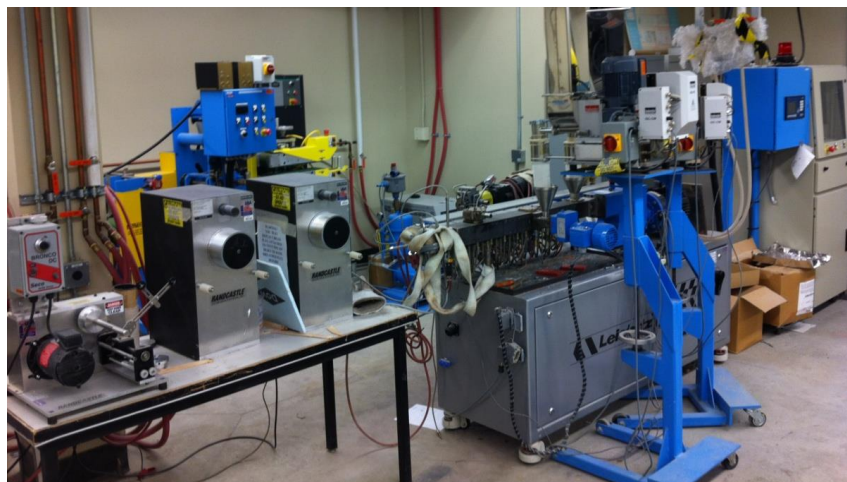


Figure 3.1. Leistriz Micro-18mm.

Table 3.2. Temperature profile of heating barrel for HDPE matrix.

| Heating Barrel number | 1 | 2 | 3 | 4 | 5 | 6 | 7 | 8 | 9 | 10 | 11 | 12 |
|-----------------------|-----|-----|-----|-----|-----|-----|-----|-----|-----|-----|-----|-----|
| Temperature (°C) | 232 | 232 | 232 | 235 | 235 | 240 | 240 | 242 | 242 | 242 | 242 | 242 |

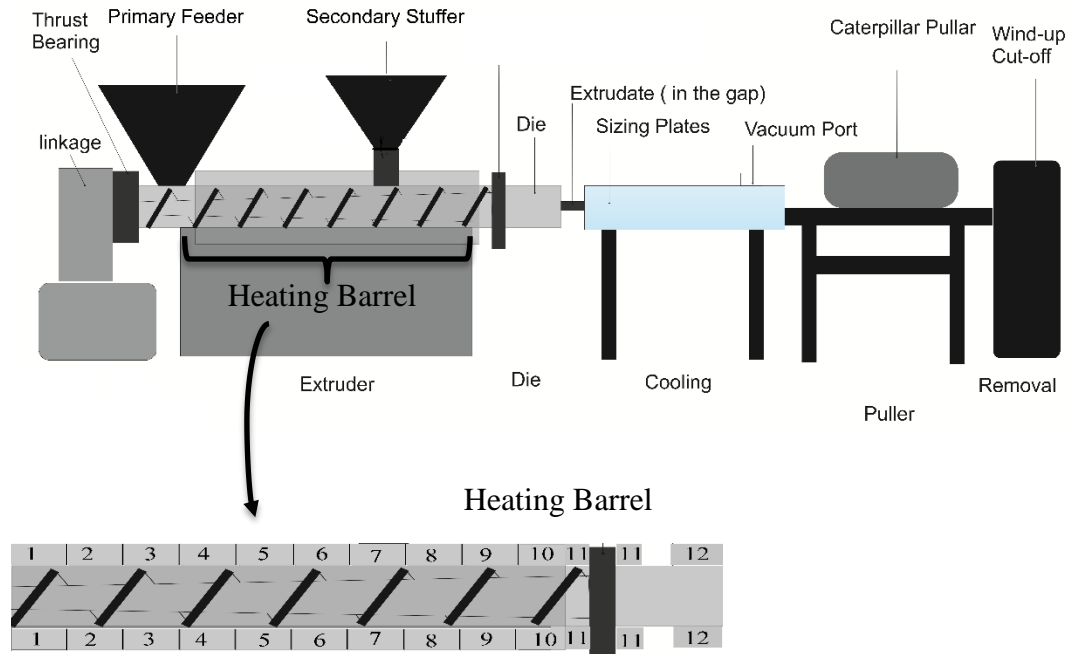


Figure 3.2. Schematic of Extruder.

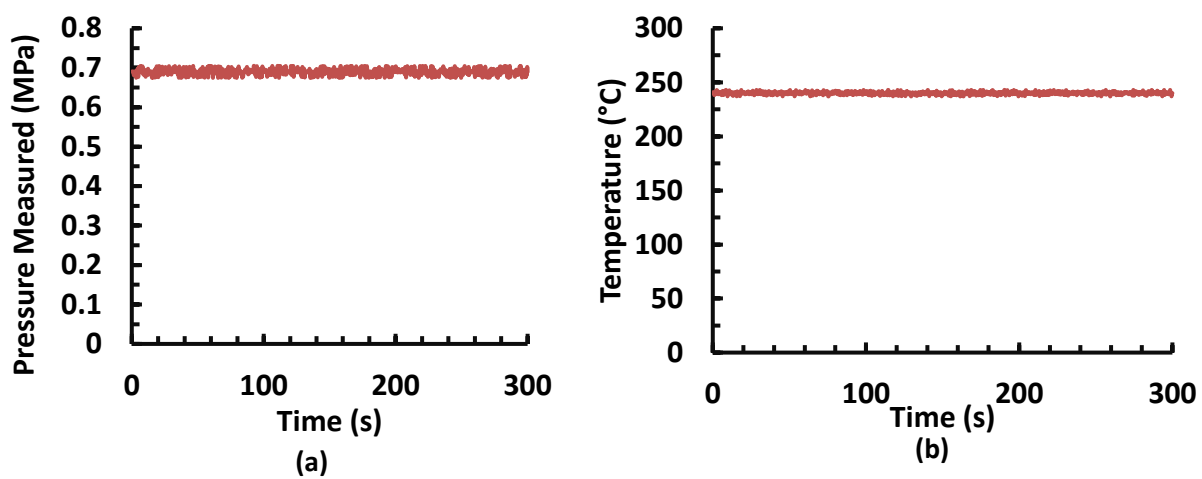


Figure 3.3. Pressure profile (a) and temperature profile (b) during collection of samples.

In the case of HDPE-CNT composite fibers, the purchased HDPE-CNT pellets were mixed with HDPE at desired weight fractions before being fed through the main feeder at a rate of 40 rpm.

The fibers were extruded through a die, which is an assembly of a die barrel and a die plate, shown in the schematic Figure 3.4 (a). The location of the pressure transducer used to measure the die pressure is also shown in Figure 3.4 (a). The die plate consisted of a number of die holes through which the fibers were extruded. The geometry of each die hole, shown in Figure 3.4 (b), consisted of a conical section and a capillary section (known as die-land). The geometry of the die hole (the diameter of the hole, the length of the conical and die-land sections, and the entry angle) were varied in this study (see next section).

The extruded fibers were air cooled and collected. The extruded fibers were of uniform diameter and of good quality without any defects such as orange peel skin and melt fracture effects as depicted in Figure 3.5.

For a given composition (i.e. weight fraction of reinforcement in the feed), the die pressure and the extrusion rate (i.e. weight of material extruded per unit of time) varied with screw speed. For each set of composition and screw speed, the die pressure and the extrusion rate were recorded.

The extrusion was continued for at least 30 minutes before the above two recorded parameters to allow a steady state of extrusion to develop. The extrusion rate was determined by collecting the extruded fiber for 5 minutes. The pressure and the extrusion rate were used in determining the viscosity of the composite material within the die, which was subsequently used to correlate with the development of the reinforcement orientation within the composite fiber during extrusion. The extruded composite fibers were tested for their density as well as for the orientation of the reinforcement. In addition, they were tested for mechanical properties.

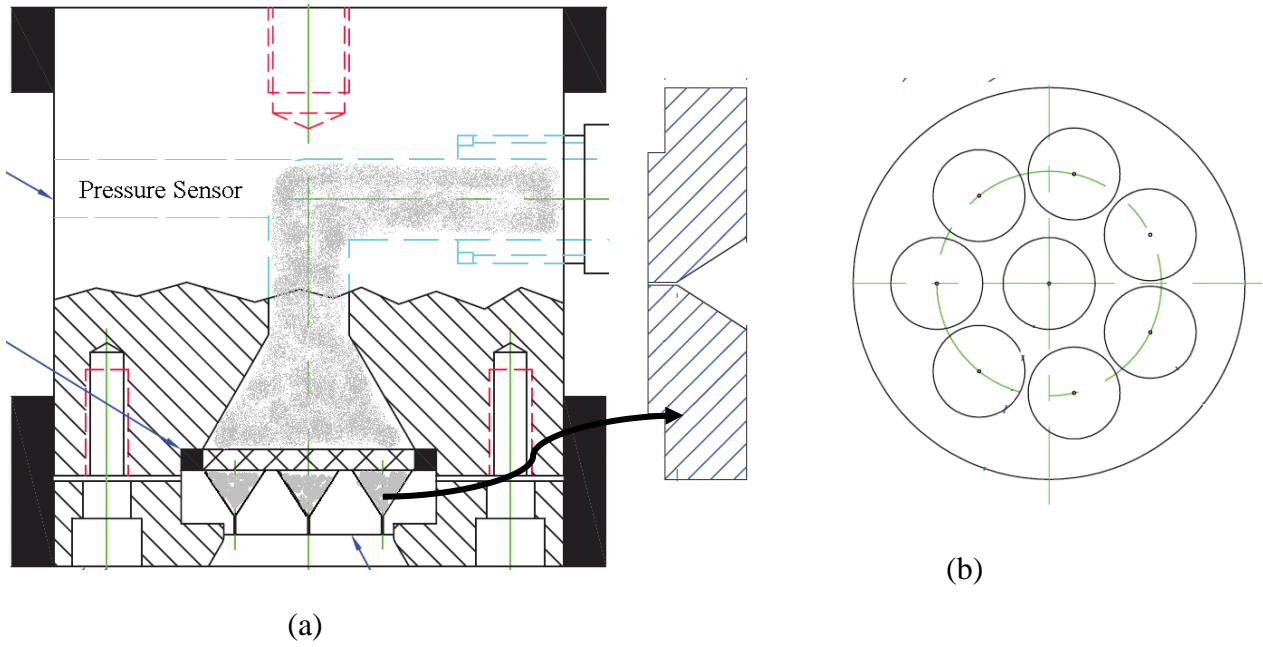


Figure 3.4. Die assembly (a) and die plate (b); grey area corresponds to polymer melt flow.

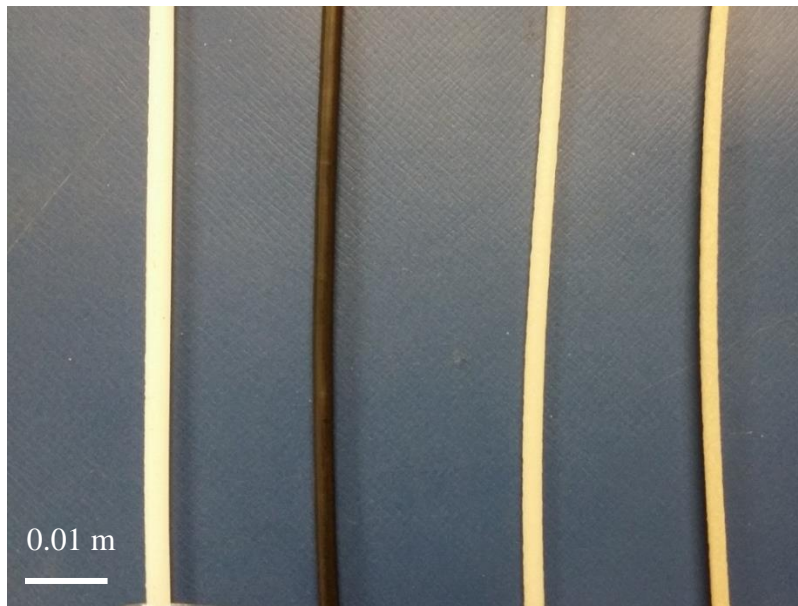


Figure 3.5. HDPE fiber, HDPE-CNT fiber, HDPE-glass fiber, HDPE-CAB-nanoclay fiber, from left to right respectively.

3.4 Experimental Design

The extrusion experiments were designed to study the effect of various materials, the die, and the process parameters on the orientation of the reinforcement within the extruded composite fibers. These are summarized in the tables 3.3-3.6 for each one of the extruded composite fibers.

3.4.1 HDPE Fibers

Fibers were extruded using HDPE to determine baseline mechanical properties for the matrix, which were subsequently used to analyze the mechanical properties of the composite fibers. In addition, HDPE fiber extrusion studies were carried out using a die hole with an entry angle of 180° and various land lengths, as tabulated in Table 3.3. Dimensional measurement of 180° die was conducted using CMM equipment at machine shop in mechanical engineering department. For each land length, the HDPE was extruded at different screw speeds, which were 40, 100, and 250 (rpm). The die pressure and the extrusion rate were measured for each screw speed. These data were used to determine the pressure drop across the conical section of the die hole as well as the die land, which were subsequently used to determine the extensional viscosity in the conical section and shear viscosity in the die land, respectively. Table 3.4 tabulates the design of this experiment for extruded HDPE fibers at different screw speeds and die land lengths.

3.4.2 HDPE-Glass Composite Fibers

The designed experiments are summarized in Table 3.5 - 3.8.

3.4.2.1 Material Parameters

The weight fraction of glass fibers in the feed was varied in the range of 0-50% with specific values at 0, 10, 20, 30, 40, and 50%.

Table 3.3. Die parameters used to manufacture Pure HDPE.

| Die number | Land Length (m) | Diameter (m) | Angle (Degree) |
|------------|-----------------|--------------|----------------|
| 1 | 0.0002 | 0.003 | 180 |
| 2 | 0.0050 | 0.003 | 180 |
| 3 | 0.0111 | 0.003 | 180 |

Table 3.4. Designed experiments of HDPE Fibers with screw speed of 40 (rpm), die entry angle of 180°, die diameter of 3 (mm), and with same temperature profile (Table 3.1) for all 9 specimens.

| Specimen number | Screw speed (rpm) | Die land length (mm) |
|-----------------|-------------------|----------------------|
| 1 | 40 | 0.2 |
| 2 | 40 | 5 |
| 3 | 40 | 11.1 |
| 4 | 100 | 0.2 |
| 5 | 100 | 5 |
| 6 | 100 | 11.1 |
| 7 | 250 | 0.2 |
| 8 | 250 | 5 |
| 9 | 250 | 11.1 |

The maximum value was chosen based on the experimentally determined limit of 52% for fiber weight fraction in the feed that allowed successful spinning of the composite fibers. This study was conducted for each die design discussed below. The fiber aspect ratio (L/D) was kept at 27. These were done for fiber weight fractions of 20, 30, 40, and 50% corresponding to the fiber volume fraction % in feeds of 7.87, 12.7, 18.57, and 25% respectively. Appendix A explains how to calculate the volume fraction based on the weight fraction.

3.4.2.2 Die Hole Geometry

The effect of the geometry of the die hole on the orientation of the glass fiber within the HDPE-glass composite fiber was studied by varying the entry angle and the hole diameter. The geometrical parameters of the die hole are tabulated in Table 3.5. A first set of experiments was carried out by varying the entry angle in the range of 30 – 180° while keeping the die hole exit diameter and land length constant at 3 mm and 2.7 mm respectively, as shown in table 3.6. A second set of experiments was carried out to understand the effect of the screw speed on pressure, flow rate, and volume fraction in final extruded fiber. The first and second sets of experiments were designed to study the changes in the extensional viscosity within the conical section of the die, with changes in the die hole parameters and their impact on reinforcement orientation.

3.4.2.3 Process Parameters

The screw speed was maintained at a constant 40 rpm (revolutions per minute) for the first and second set of experiments. However, it was varied in the range of 40 - 250 rpm for the last set of experiments, as tabulated in Table 3-7.

3.4.3 HDPE-Spherical-Glass Composite Fibers

Fiber aspect ratio has significant impact on the rheology of composite melt flow and the properties of the final extruded composite fiber. Here HDPE is extruded with spherical glass with a diameter of 50 (μm) at volume fractions of 4.6%, 5.9%, 17.4% using 60° and 90° dies, as tabulated in Table 3.8. The effect of the fiber aspect ratio on the viscosity of composite melt is determined by comparing HDPE-Spherical Glass with HDPE and HDPE-Glass extruded fibers.

3.4.4 HDPE-CNT fibers

3.4.4.1 Material and Extrusion Parameter

Nanocomposite fiber were extruded at 40 (rpm) using HDPE-HDPE-CNT at three CNT weight fraction of 3.75%, 7.5%, and 15% and a feed rate of 0.3 (kg/hr) with 30°, 60°, 90°, and 180° dies of 3 (mm) hole size to determine the effect of die angle on the orientation of the CNT. CNT was already purchased in premixed state from supplier, i.e. HDPE-CNT composite with a weight fraction of 15%. Designed experiments for HDPE-CNT are depicted in Table 3.9. Also, because the viscosity of HDPE-CNT is lower than that of pure HDPE, micron size micelles of HDPE-CNT micelles were deformed and elongated into ellipsoids. This process led to the CNT orienting inside the ellipsoids. The Spun HDPE-HDPE-CNT is be further characterized by electrical conductivity and tensile testing to determine the effect of die design on the orientation of the CNT.

3.4.4.2 Die Hole Geometry

The effect of the geometry of the die hole on the orientation of the CNT within the HDPE-CNT composite fiber was studied by varying the entry angle and the hole diameter. Experiments were carried out by varying the entry angle in the range of 30 – 180° while keeping the die hole exit diameter and land length constant at 3 mm and 2.7 mm respectively. The geometrical parameters of the die hole are tabulated in Table 3.10.

Table 3.5. Die-Hole Geometry.

| Die | Angle (Degree) | Cone length (m) | Land length (m) | Exit Diameter (m) | Entry diameter (m) | Number of Die Holes |
|-----|----------------|-----------------|-----------------|-------------------|--------------------|---------------------|
| 1 | 30 | 0.0116 | 0.0027 | 0.0030 | 0.0092 | 2 |
| 2 | 45 | 0.0075 | 0.0027 | 0.0030 | 0.0092 | 2 |
| 3 | 60 | 0.0053 | 0.0027 | 0.0030 | 0.0092 | 2 |
| 4 | 60 | 0.0053 | 0.0091 | 0.0030 | 0.0092 | 2 |
| 5 | 60 | 0.0071 | 0.0027 | 0.0010 | 0.0092 | 6 |
| 6 | 90 | 0.0113 | 0.0027 | 0.0030 | 0.0092 | 2 |
| 7 | 90 | 0.0045 | 0.0074 | 0.0015 | 0.0120 | 2 |
| 8 | 180 | 0.0058 | 0.0027 | 0.0030 | 0.0092 | 2 |
| 9 | 180 | 0.0058 | 0.0111 | 0.0030 | 0.0092 | 2 |

Figure 3.6 Fiber spinning dies.



Table 3.6. Designed second set of experiments to study the effect of the geometry of the die hole on the orientation of the glass fiber within HDPE-Glass composite fibers using a screw speed of 40 (rpm), a die land length of 2.7 (mm), a die diameter of 3 (mm), and the same temperature profile (Table 3.1) for all 18 specimens.

| Specimen Number | Fiber Volume fraction% | Die entry Angle |
|-----------------|------------------------|-----------------|
| 1 | 7.87 | 30° |
| 2 | 7.87 | 45° |
| 3 | 7.87 | 60° |
| 4 | 7.87 | 90° |
| 5 | 7.87 | 180° |
| 6 | 12.7 | 30° |
| 7 | 12.7 | 45° |
| 8 | 12.7 | 60° |
| 9 | 12.7 | 90° |
| 10 | 12.7 | 180° |
| 11 | 18.5 | 30° |
| 12 | 18.5 | 45° |
| 13 | 18.5 | 60° |

| Specimen number | Fiber Volume fraction% | Die entry Angle |
|-----------------|------------------------|-----------------|
| 14 | 25 | 30° |
| 15 | 25 | 45° |
| 16 | 25 | 60° |
| 17 | 25 | 90° |
| 18 | 25 | 180° |

Table 3.7. Designed experiments to study the effect of the geometry of the die hole on the flow rate at various screw speeds of the glass fibers within HDPE-Glass Composite Fibers, using a die angle of 60°, a die land length of 2.7 (mm), a die diameter of 3 (mm), and the same temperature profile (Table 3.1) for all 10 specimens.

| Specimen Number | Fiber Volume fraction% | Screw speed (rpm) | Specimen number | Fiber Volume fraction% | Screw speed (rpm) |
|-----------------|------------------------|-------------------|-----------------|------------------------|-------------------|
| 1 | 7.87 | 40 | 6 | 12.7 | 200 |
| 2 | 7.87 | 60 | 7 | 7.87 | 250 |
| 3 | 7.87 | 250 | 8 | 18.5 | 40 |
| 4 | 12.7 | 40 | 9 | 18.5 | 100 |
| 5 | 12.7 | 60 | 10 | 18.5 | 150 |

Table 3.8. Designed experiments of the HDPE-Spherical Glass Composite Fibers, using a die land length of 2.7 (mm), a die diameter of 3 (mm), and the same temperature profile (Table 3.1) for all 6 specimens.

| Specimen Number | Fiber Volume fraction% | Die entry Angle | Specimen number | Fiber Volume fraction% | Screw speed (rpm) |
|-----------------|------------------------|-----------------|-----------------|------------------------|-------------------|
| 1 | 7.8 | 60° | 4 | 7.8 | 90° |
| 2 | 12 | 60° | 5 | 12 | 90° |
| 3 | 25 | 60° | 6 | 25 | 90° |

Table 3.9. Designed experiments of the die hole geometry effect on the orientation of the CNT within HDPE-CNT Composite Fibers, using a die land length of 2.7 (mm), a die diameter of 3 (mm), and the same temperature profile (Table 3.1) for all 14 specimens.

| Specimen number | Weight Fraction (%) | Die Entry Angle (α) |
|-----------------|---------------------|------------------------------|
| 1 | 3.75 | 30° |
| 2 | 3.75 | 60° |
| 3 | 3.75 | 90° |
| 4 | 3.75 | 180° |
| 5 | 7.5 | 30° |
| 6 | 7.5 | 45° |
| 7 | 7.5 | 60° |
| 8 | 7.5 | 90° |
| 9 | 7.5 | 180° |
| 10 | 15 | 30° |
| 11 | 15 | 45° |
| 12 | 15 | 60° |
| 13 | 15 | 90° |
| 14 | 15 | 180° |

Table 3.10. Die-Hole Geometry for CNT spinning.

| Die | Angle | Cone Length (m) | Land Length (m) | Exit Diameter (m) | Entry Diameter (m) | Number of Die Holes |
|-----|-------|-----------------|-----------------|-------------------|--------------------|---------------------|
| 1 | 30° | 0.0116 | 0.0027 | 0.0030 | 0.0092 | 2 |
| 2 | 60° | 0.0053 | 0.0027 | 0.0030 | 0.0092 | 2 |
| 3 | 90° | 0.0113 | 0.0027 | 0.0030 | 0.0092 | 2 |
| 4 | 180° | 0.0058 | 0.0027 | 0.0030 | 0.0092 | 2 |

3.5 Characterization of Melt-Spun Fibers

3.5.1 Fiber Volume Fraction Measurement

The volume fraction of fibers (V_f) was calculated using

$$V_f = \frac{\rho_c - \rho_m}{\rho_f - \rho_m} \quad (3.1)$$

where ρ_f , ρ_m , and ρ_c are the density of the fiber, matrix, and composite respectively. These densities were measured as follows. The mass (m) of the test samples was measured to 0.1 mg accuracy using a balance. Subsequently, the volume of these samples was measured using an AccuPyc's 1330 helium pycnometer, as per ASTM D4892-89. The measurement cell size was 5 (cm³), and equipment was calibrated for measurement each time it was turned on. Using the mass and volume results, the density of the sample was determined. The densities of HDPE and glass fiber were 958 and 2800 kg/m³, respectively.

3.5.2 Reinforcement Fiber Orientation Distribution (FOD)

3.5.2.1 HDPE-Glass Composite Fiber

The composite fibers were non-destructively imaged by 3D tomography using X-Radia's Micro X-ray CT, shown in Figure 3.7. The reconstructed 3D images were subsequently analyzed using the commercial software AVIZO-Fire 7, developed by the VSG Company, to obtain the FOD. An objective lens with a magnification of 20X was used to maximize the quality of scan area on the cross-sections of fibers, resulting in a reconstructed 3D image of 420 × 440 × 940 μm. The smallest feature that could be resolved at this setting was 0.5 μm. The scanning was done by rotating the sample at 0.05° intervals from -90° to 90°, with an exposure time for each scan of 3 seconds. The reconstruction of the image was done by software that was linked to the acquisition software. One view of the 3D image of the composite is shown in Figure 3.8.

Reconstructed images were exported in the JPEG format and then imported to AVIZO Fire 7 and reconstructed for analysis, as shown in Figure 3.8-9. The diameter, length, volume, out-of-plane orientation (φ), and in-plane orientation (θ) were determined for each fiber in the image using AVIZO-Fire 7. Individual glass fiber volume is calculated using AVIZO-Fire 7 then volumes are added together and subsequently divided to the total volume of voxel size ($420 \times 440 \times 940 \mu\text{m}$.) to find volume fraction in extruded composite using image analysis.

Each image was then analyzed for the in-plane together and out-of-plane orientation of glass fibers in the melt-spun composite fiber, as follows. The reference coordinate system, used to define the orientation of a reinforcement fiber within the composite fiber, is provided in Figure 3.11. Note that the extrusion direction and the composite fiber's longitudinal axis are oriented along the z-axis. The orientation of the longitudinal axis of the glass fiber with respect to the longitudinal axis of the composite fiber (i.e. Z-axis) is φ .

Degree of fiber alignment is the extent to which the fibers in a composite are oriented parallel to a direction of interest. This can vary from perfect alignment (parallel to the direction of interest) to no alignment (perpendicular to the direction of interest). This is quantified by the second order tensor. Advani and Tucker [40] proposed using second-order orientation tensors $[a_{ij}]$, which are compact, general, and short formulation of probability density orientation functions used for fiber orientation characterization.

$$a_{ijkl} = \int p_i p_j p_k p_l (\psi(\varphi, \theta)) d\Omega \quad (3.2)$$

where $\psi(\varphi, \theta)$ denotes the orientation distribution function, and Ω is the unit sphere, with $\int (\psi(\varphi, \theta)) d\Omega = 1$ and $d\Omega = \sin\theta d\theta d\varphi$,

where $p(\varphi, \theta)$ is a unit vector parallel to a fiber direction, with components of $p_i = \sin \varphi \cos \theta$, $p_j = \sin \varphi \sin \theta$, $p_k = \cos \varphi$

For a number of fibers “N”, the global orientation tensors for a composite are obtained by averaging all individual fiber orientations:

$$a_{3333} = \sum_{i=1}^N \frac{\cos^4 \varphi_i}{N}$$

$$a_{1313} = \sum_{i=1}^N \frac{\cos^2 \varphi_i \sin^2 \theta_i \cos \theta_i^2}{N} \quad (3.3)$$

Most micromechanical models use second or fourth order orientation tensors [41]. Alignment along the extrusion axis (Z) is determined by a_{3333} and in plane orientation in XY plane is determined through a_{1313} .

The a_{3333} varies from 0 to 1.0 as the glass fiber distribution varies from in-plane (XY) orientation to perfect alignment parallel to the longitudinal axis of the composite fiber (i.e. Z-axis extrusion direction). On the same note, a_{1313} also varies from 0 to 1.0 as glass fiber orientation varies, and the 1 value corresponds to the distribution where the fibers are aligned to the Z axis, or extrusion direction.

Figure 3.9 depicts the cross section reconstructed image. The dark gray area is the HDPE matrix where its corresponding volume can be calculated with AVIZO Fire 7. Having the total volume of fibers as well as the matrix, the volume fraction of the composite can be calculated by dividing the volume of fibers by the sum of the volume of fibers and the volume of matrix.



Figure 3.7. X-radia's Micro X-ray CT.

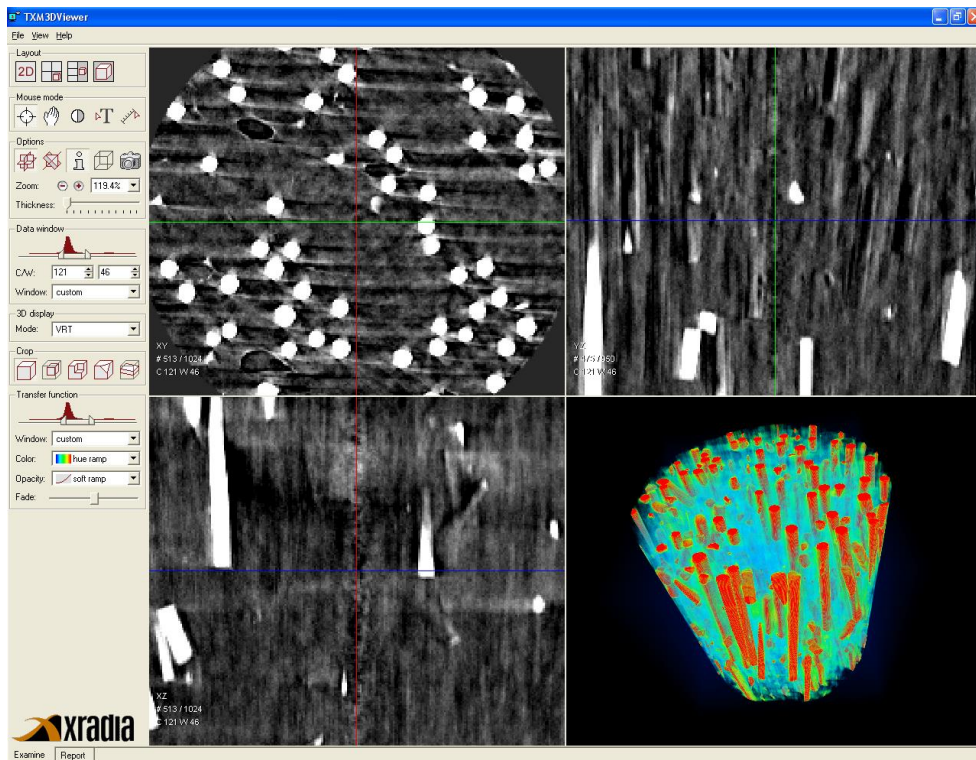


Figure 3.8. Computed tomography image of composite fibers.

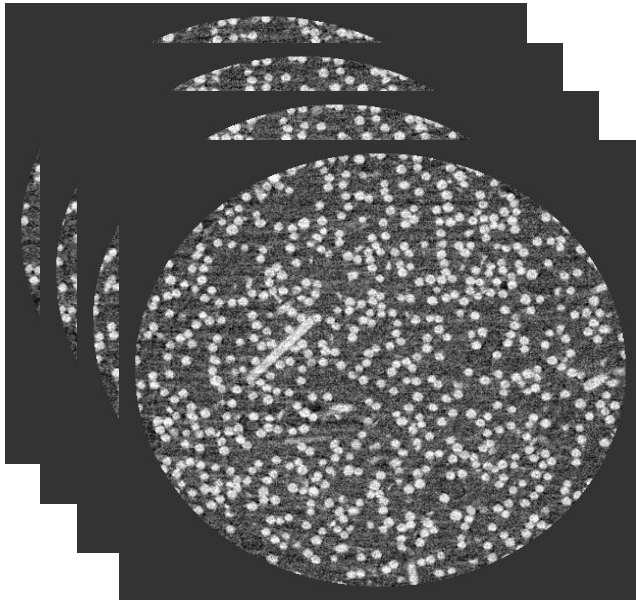


Figure 3.9. JPEG images exported by X-ray and ready to be analyzed by AVIZO Fire 7.

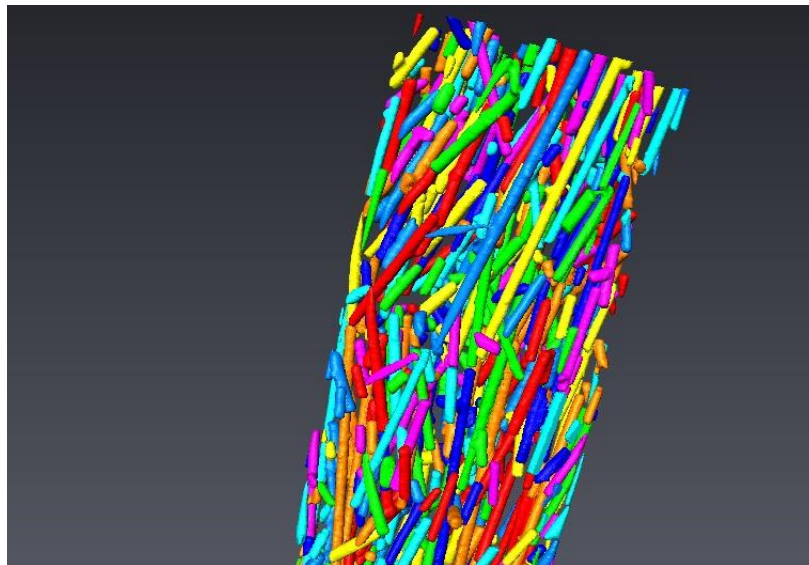


Figure 3.10. X-ray image reconstructed using Avizo Fire[®] software.

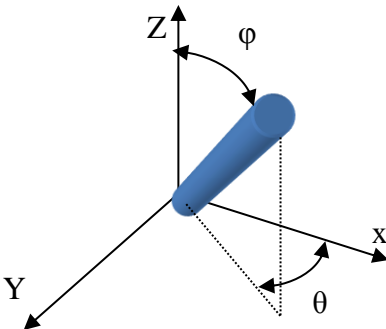


Figure 3.11. Coordinate reference system.

3.5.3 Repeatability and reproducibility

Mass flow rate and pressure are measured for all the fibers: HDPE, HDPE-Glass, HDPE-CNT fibers, and extruded fibers. Hence, to measure for repeatability and accuracy, the pressure was measured after 30 minutes of continuous run so the extruder could reach a steady state flow condition, as illustrated in Figure 3.12. For example, for the HDPE-Glass composite fiber extruded using a 90° angled die at 40 rpm with V_{IN} of 25%, fiber extrusion continued for 30 minutes to reach pressure, after which stabilization samples were collected for 5 minutes for image analysis, volume fraction analysis, and tensile testing.

In addition to pressure measurement, mass flow rate was also recorded after 30 minutes of continuous run and three trials were used and average values with standard deviation are reported. All these extruded fiber manufacturing processes were repeated to confirm repeatability for all extruded HDPE and HDPE-Glass fibers measured through 30°, 45°, 60°, 90°, and 180°, as tabulated in Table 3.11. Corresponding variance is reported in chapter 4.

3.5.4 Rheology measurement

Dynamic and steady shear rheological measurements were carried out on a TA AR 2000 as depicted in Figure 3.13. Afterwards, the measurements were run with 25 mm parallel plate geometry and a 1.5 mm sample gap. The viscoelastic properties were determined with frequencies from $7.5 \cdot 10^{-7}$ to 628 rad/s, and measurements were carried out at a temperature of 200°C.

Viscosity measurements were conducted on as received HDPE, HDPE-spherical glass fibers, and HDPE-glass composite fibers of $V_F=7.4\%$, 14%, and 19% which were extruded through 60° angle die. These measurements were conducted to understand the rheological properties of composite melt at different shear rates and volume fractions, as tabulated in Table 3.12.

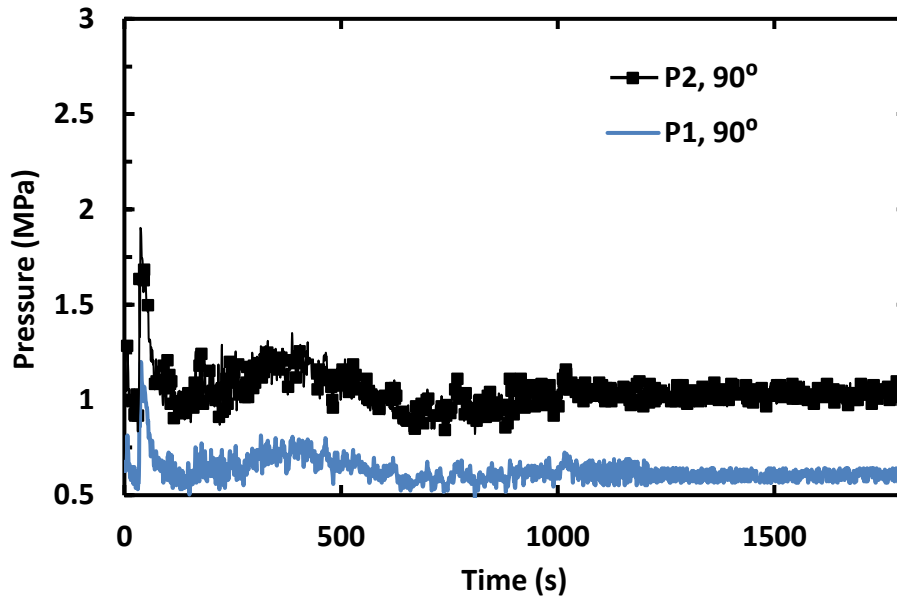


Figure 3.12. Pressure at the steady state condition for extruded composite with 90° die and

$$V_F=25\%$$

Table 3.11. Designed experiments of mass flow rate and pressure reparability.

| Specimen number | Fiber Volume fraction% | Die entry Angle | Pressure Mass flow Repeated | Specimen number | Fiber Volume fraction% | Die entry Angle | Pressure Mass flow Repeated |
|-----------------|------------------------|-----------------|-----------------------------|-----------------|------------------------|-----------------|-----------------------------|
| 1 | 3.66 | 30° | √ | 14 | 12.7 | 90° | √ |
| 2 | 3.66 | 45° | √ | 15 | 12.7 | 180° | √ |
| 3 | 3.66 | 60° | √ | 16 | 18.5 | 30° | √ |
| 4 | 3.66 | 90° | √ | 17 | 18.5 | 45° | √ |
| 5 | 3.66 | 180° | √ | 18 | 18.5 | 60° | √ |
| 6 | 7.87 | 30° | √ | 19 | 18.5 | 90° | √ |
| 7 | 7.87 | 45° | √ | 20 | 18.5 | 180° | √ |
| 8 | 7.87 | 60° | √ | 21 | 25 | 30° | √ |
| 9 | 7.87 | 90° | √ | 22 | 25 | 45° | √ |
| 10 | 7.87 | 180° | √ | 23 | 25 | 60° | √ |
| 11 | 12.7 | 30° | √ | 24 | 25 | 90° | √ |
| 12 | 12.7 | 45° | √ | 25 | 25 | 180° | √ |
| 13 | 12.7 | 60° | √ | | | | |

The parallel disks geometry is illustrated in Figure 3.14 with the following assumptions:

- 1-Steady, laminar, isothermal flow
- 2- $v_\theta(r, z)$ only; $v_r=v_z=0$
- 3-Negligible body forces
- 4-Cylindrical edge

Also, shear viscosity was calculated through the following procedure using the TA analysis software ©.

Equations of motion reduce to:

$$\begin{aligned} \theta: \frac{\partial \tau_{\theta z}}{\partial z} &= 0 \\ z: \frac{\partial \tau_{zz}}{\partial z} &= 0 \end{aligned} \quad (3.4)$$

$$\begin{aligned} r: \frac{1}{r} \frac{\partial}{\partial r} (r \tau_{rr}) - \frac{\tau_{\theta\theta}}{r} &= -\rho \frac{v^2 \theta}{r} \\ \text{Velocity: } v_\theta(r, z) &= \frac{r \Omega z}{h} \end{aligned} \quad (3.5)$$

$$\text{Shear rate: } \dot{\gamma}(r) = \frac{r \Omega z}{h} \quad (3.6)$$

$$\text{Shear: } \gamma = \frac{\theta r}{h} \quad (3.7)$$

$$\text{Torque: } M = 2\pi \int_0^R r \tau_{12}(r) r dr \quad (3.8)$$

$$\text{Change of Variables: } r = \frac{h}{\Omega} \dot{\gamma} = \frac{R \dot{\gamma}}{\dot{\gamma}_R} \quad \text{where } \dot{\gamma}_R = \frac{\Omega R}{h} \quad dr = \frac{R}{\dot{\gamma}_R} d\dot{\gamma} \quad (3.9)$$

$$M = 2\pi \int_0^{\dot{\gamma}_R} \left(\frac{R}{\dot{\gamma}_R} \right)^3 \dot{\gamma}^2 \tau_{12} d\dot{\gamma} \quad (3.10)$$

$$\tau_{12}(R) = \frac{M}{2\pi R^3} \left[3 + \frac{d \ln M}{d \ln \dot{\gamma}_R} \right]$$

$$\text{Normal Stress: } (N_1 - N_2) = \frac{F_z}{\pi R^2} \left[2 + \frac{d \ln F_z}{d \ln \dot{\gamma}_R} \right] \quad (3.11)$$

$$\eta(\tau_{12}) = \tau_{12} / \dot{\gamma}_R \quad (3.12)$$

Table 3.12. Designed experiments of the shear viscosity measurement of already extruded HDPE, HDPE-Spherical Glass, and HDPE-Glass fibers at a temperature of 200 (c) for all 7 specimens. Shear rate changes between 2.5×10^{-5} (s^{-1}) and 82 (s^{-1}) for specimen 1-4 and it was kept constant 0.1 (s^{-1}) for specimen 5-7.

| Specimen Number | Material | Fiber Volume Fraction (%) | Shear rate range (s^{-1}) |
|-----------------|----------------------|---------------------------|-------------------------------|
| 1 | HDPE | 0 | $[2.5 \times 10^{-5} - 82]$ |
| 2 | HDPE-Spherical Glass | 4.6 | $[2.5 \times 10^{-5} - 82]$ |
| 3 | HDPE-Spherical Glass | 5.9 | $[2.5 \times 10^{-5} - 82]$ |
| 4 | HDPE-Spherical Glass | 17.8 | $[2.5 \times 10^{-5} - 82]$ |
| 5 | HDPE-Glass Fiber | 7.4 | 0.1 |
| 6 | HDPE-Glass Fiber | 14 | 0.1 |
| 7 | HDPE-Glass Fiber | 19 | 0.1 |



Figure 3.13. AR2000 rheometer (TA Instruments).

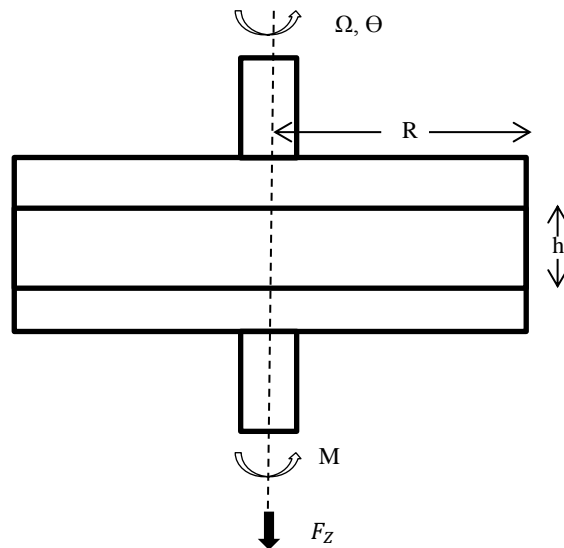


Figure 3.14. Parallel plate schematics.

3.5.5 *Electrical conductivity measurement*

Resistivity measurement can help to interpret the degree of alignment of CNT in HDPE-CNT fibers when compared at the same weight fraction but using a different die design, as explained in Table 3.9. For example, when the CNT alignment increases in a longitudinal direction, the conductivity increases because the CNT can establish a network to pass the current. At the same time, the transverse conductivity decreases because of loss of alignment in that direction. Therefore electrical conductivity can be a good indicator of CNT orientation. The bulk volume measurement was taken along CNT-HDPE fibers and perpendicular to the CNT-HDPE fiber axis.

An Agilent 4155c semiconductor parameter analyzer in a Suss MicroTec Standard semiconductor probe station was used for I-V measurement, as depicted in Figure 3.15. Conductivity was measured for HDPE-CNT manufactured using angles of 30°, 60°, 90°, and 180° with weight fractions of 3.75%, 7.5%, and 15%. Contact resistance is found to be insignificant by conducting prob spacing measurement, however is reported results contact resistance might be embedded in measurement. The design measurements of this experiment for longitudinal and transverse conductivity are tabulated in Tables 3.13 and 3.14 respectively. Bulk resistance for each HDPE-CNT along the 10 (cm) length of fiber and across the diameter was also considered in calculating the conductance of spun fiber under measurement

$$\rho = \frac{R}{l} A \quad (3.5)$$

where A is the cross section area, l is the fiber length, R is measured resistance, and ρ is the conductivity.



Figure 3.15. Probe station and semiconductor.

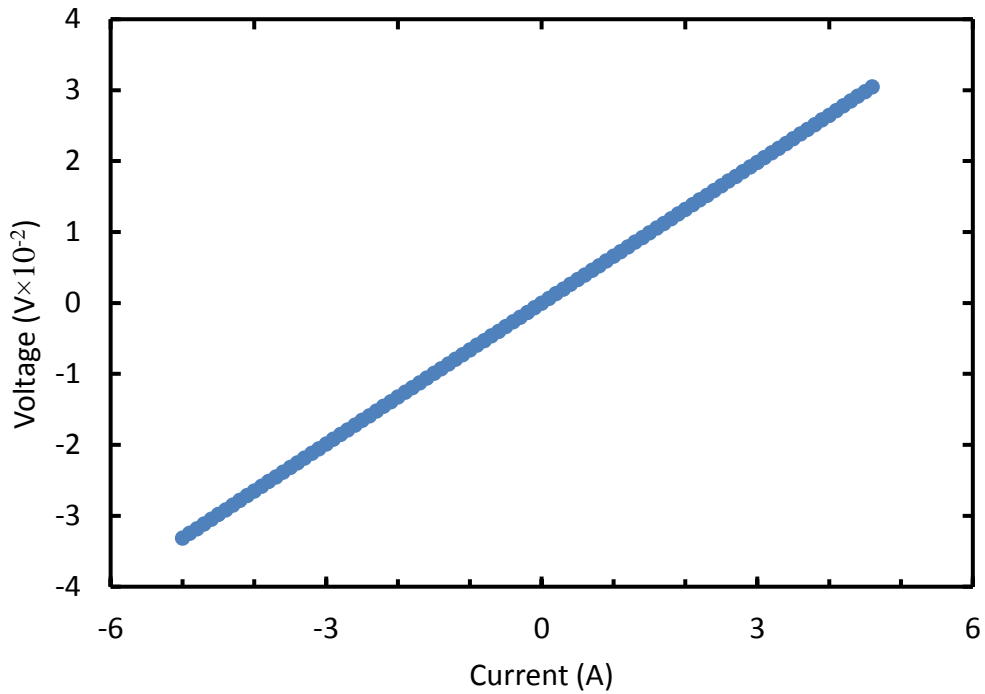


Figure 3.16. Current versus voltage measurement using semiconductor.

Table 3.13. Designed experiments of HDPE-CNT Composite Fibers' longitudinal conductivity measurement of already extruded fibers.

| Specimen number | CNT weight fraction (%) | Die entry Angle (α) |
|-----------------|-------------------------|------------------------------|
| 1 | 3.75 | 30° |
| 2 | 7.5 | 30° |
| 3 | 15 | 30° |
| 4 | 3.75 | 60° |
| 5 | 7.5 | 60° |
| 6 | 15 | 60° |
| 7 | 3.75 | 90° |
| 8 | 7.5 | 90° |
| 9 | 15 | 90° |
| 10 | 3.75 | 180° |
| 11 | 7.5 | 180° |
| 12 | 15 | 180° |

Table 3.14. Designed experiments of HDPE-CNT Composite Fibers' transverse conductivity measurement of already extruded fibers.

| Specimen number | CNT weight fraction (%) | Die entry Angle (α) |
|-----------------|-------------------------|------------------------------|
| 1 | 3.75 | 30° |
| 2 | 3.75 | 60° |
| 3 | 3.75 | 90° |
| 4 | 3.75 | 180° |

CHAPTER 4: RESULTS AND DISCUSSION

4.1 Introduction

In this chapter all the experiments to realize the thesis' objectives are presented, including fiber extrusion, x-ray tomography, and mechanical testing. The effects of pressure, flow rate, V_F , orientation, and mechanical properties on fiber orientation are reported here, and this chapter also discusses the accuracy of V_F and the orientation measurements, which were independently confirmed through pycnometer and mechanical testing. Subsequently, all the measurements are here used to calculate viscosity to understand the effects of pressure, flow rate, V_F and orientation on the microstructure of flow. Next, the evolution of fiber orientation through extrusion die is studied empirically using the Dinh-Armstrong [28] model to understand the impact of die assembly (cone and capillary sections). Also, nanocomposite extruded fibers are studied to understand the effect of manufacturing parameters on functional and structural properties of nanocomposites. Finally, in the discussion section of chapter 4 all earlier sections are connected to comprehend the effect of processing and die design parameters on fiber orientation in extruded fiber composites.

4.1.1 Experimental Results of Micron-Sized Fiber Reinforced HDPE Composite

The composite fiber consisting of the HDPE matrix and the micron-sized glass fiber was melt-spun under varying manufacturing conditions. Subsequently, fiber orientation distribution and fiber volume fraction were experimentally characterized. Fiber volume fraction was measured using pycnometer and X-ray Micro-CT. The fiber volume fraction was also determined using pycnometer and is compared in Figure 4.1 with the fiber volume fraction obtained non-destructively using X-ray Micro-CT. A very good correlation confirms the measurement accuracy. The mechanical properties, presented in section 4.1.2, corroborate the accuracy of the orientation

factor and thus the distribution obtained by non-destructive testing. In this chapter, V_{In} corresponds to fiber volume fraction in the feed, V_F corresponds to fiber volume fraction in the melt, and (V_{Out}) corresponds to fiber volume fraction in the extruded composite.

A representative plot of distribution in fiber orientation, obtained by non-destructive analysis of the image obtained using X-ray Micro-CT, is presented in Figure 4.2. The orientation of the fibers with respect to the extrusion axis varied between 0° and 90° with a peak close to 0° . Orientation tensors a_{3333} and a_{1313} are determined using fiber orientation distribution and are calculated by Equations (3.3) presented in chapter 3.

A representative plot of distribution in fiber length, determined by analysis of the image obtained using X-ray Micro-CT, is presented in Figure 4.3. As the screw inside the extruder mixes fiber glass with polymer, the mechanical forces from the screw as well as the shear force from the polymer resulted in reduction of the initial fiber aspect ratio. This process caused degradation of the fibers in melt spinning of the composite. Since this degradation happened inside the barrel of the extruder before reaching the die, there was no control over improving fiber length distribution. This distribution did not change with manufacturing variables, and hence is not focused on further in this chapter.

4.1.2 Confirmation of V_f and OF measurements through Mechanical Properties

The modulus of the extruded composite fibers, measured by tensile testing, was plotted as a function of experimentally measured V_{Out} in Figure 4.4. The tests were performed as per the ASTM standard D 4762-04 and three samples were tested for each data point. Data for various dies superposed, and the linear increase in modulus with V_{Out} was expected. The observed spread in the data is due to the difference in OF (a_{3333}).

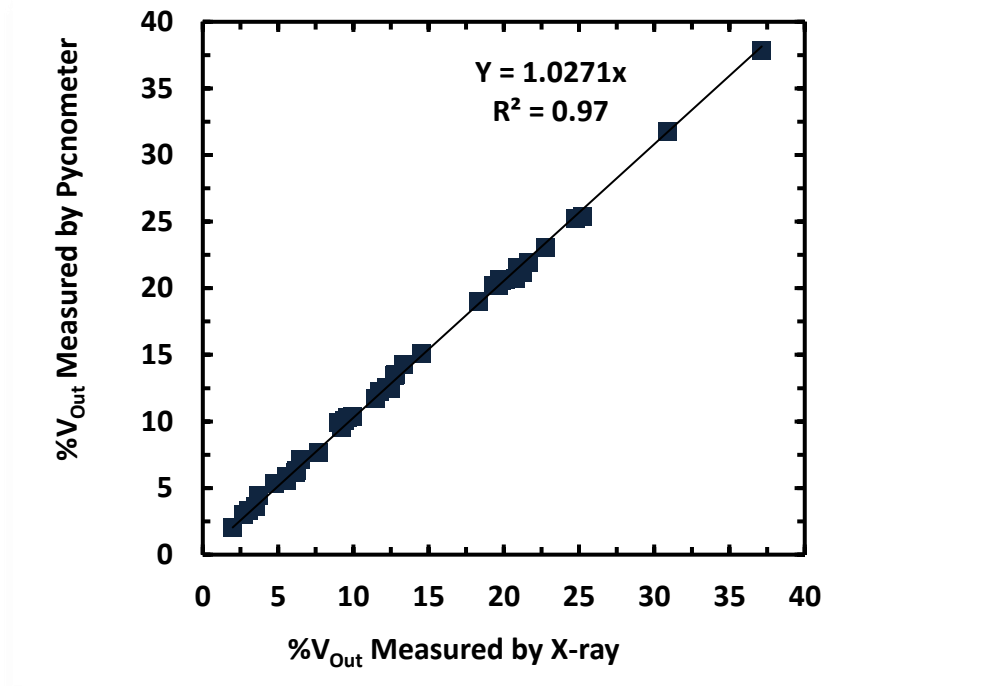


Figure 4.1. Volume fraction measurement verification with pycnometer and image analysis.

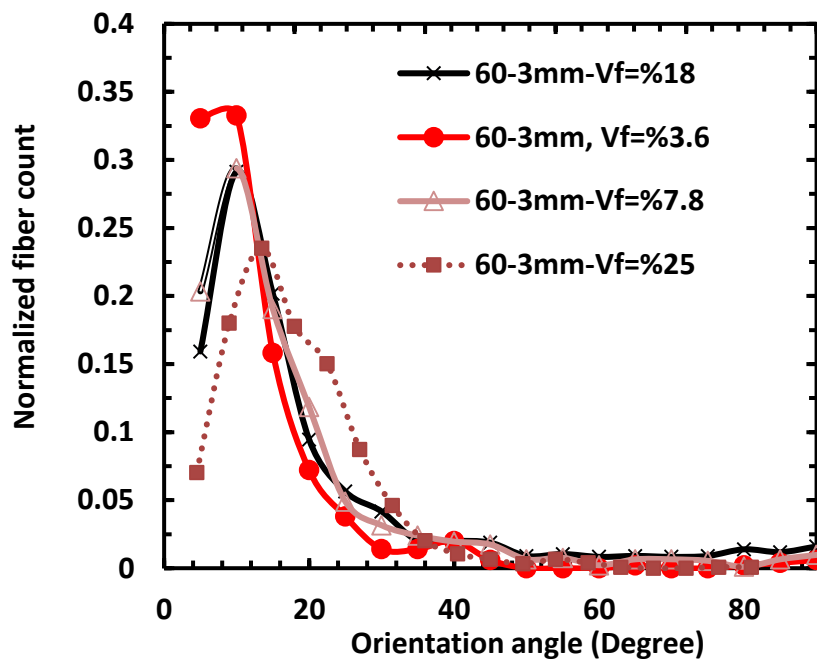


Figure 4.2. Fiber orientation distribution for 60-3mm die with volume fraction in feed from 3.6 to 25%.

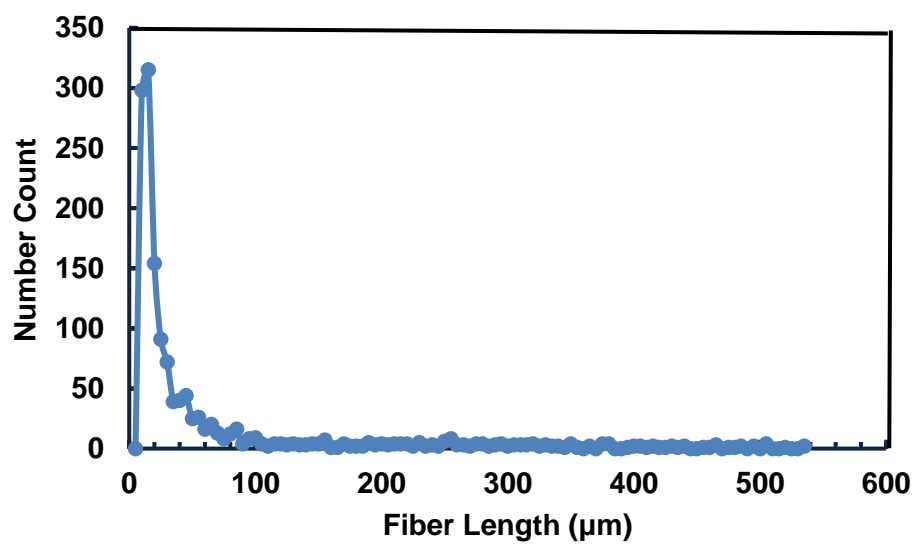


Figure 4.3. Fiber length distribution

In order to account for this, the modulus data in Figure 4.4 was replotted with respect to a product of V_F and a_{3333} in Figure 4.5. The reduction in spread confirms that the spread in data observed in Figure 4.5 is due to a_{3333} . Excellent superposition of modulus data for all composites manufactured using a wide range of manufacturing variables confirms the experimentally measured values for V_{Out} and a_{3333} . A simplistic model for the modulus of a discontinuous fiber composite, derived based on the rule of mixtures is, therefore, as follows:

$$E_C = \chi \xi E_f V_{Out} + E_m V_m \quad (\xi > 0) \quad (4.1)$$

where ξ is the orientation factor to account for the effect of orientation of fibers on modulus and χ is the effect of aspect ratio (reinforcing efficiency). The orientation factor is replaced in this thesis by a_{3333} since the load was applied only along the 3 direction during testing. Note that this equation cannot be used when load is applied perpendicular to the 3-direction and hence, this equation is valid only for $a_{3333} > 0$. The data in Figure 4.5 was fitted using the above equation.

The slope of the plot of E_C versus ξV_F yields $\chi E_f = 50.97$ GPa.

Using a glass fiber modulus of 70 GPa, the value of χ is 0.714 (i.e. a reinforcing efficiency of 71.4%). The low reinforcing efficiency could be due to high l_c (due to poor bonding between glass fiber and HDPE) and low l ($l < l_c$). This could be improved by optimizing the bonding between the glass fiber and the HDPE. Bonding between the PE and glass fiber was not focused in this study. The fiber was purchased from a commercial supplier and fibers has higher levels of surface treatment compatible with all thermoset and thermoplastic resins. Since the same fiber was used for all experiments in this thesis, any effect of bonding on the flow would have been same for all and hence, is believed to be not an issue.

The Y-intercept yields:

$$E_m V_m = 0.953$$

Since V_m is 1, $E_m = 0.953$ (GPa)

This modulus is comparable to the modulus of the HDHDPE, which is 1.050 (GPa).

In summary, the experimentally measured modulus provides an excellent confirmation of the V_{Out} and a_{3333} in the composite, validates the data from extrusion experiments, and adds credence to the analysis of the effect of manufacturing variables on V_{Out} and a_{3333} presented in the previous sections.

$50.97 = \chi E_f$, $E_f = 70$ GPa, therefor $\chi = 0.732$

4.2 Micron-Sized Fiber Reinforced HDPE Composite

Independent variables are V_{In} and screw speed, which can be varied independent of the other parameters. Control variables (such as die angle, die diameter, and die temperature) are kept constant while the independent variables vary. The dependent variables (V_{Out} , OF) are measured experimentally after extrusion. In this chapter OF is the orientation along the extrusion axis (a_{3333}). Melt flow variables include melt flow rate (which is also the extrusion rate), die pressure, and melt viscosity within the die. These are interdependent, and their magnitudes at steady state extrusion conditions are dictated by the independent and control variables. Figure 4.6 identifies the relationship among various variables schematically.

Measurements of V_{In} , V_F , V_{Out} , pressure, and OF were conducted along the extruder as illustrated in Figure 4.7. The effect of V_{In} in feed and screw speed on V_F and V_{Out} in the extruded composite was studied directly by varying the V_{In} and screw speed, as depicted in Tables 4.1 and 4.2 respectively. In response to the changes in V_{In} and screw speed, the die pressure and extrusion rate of the composite varied, as depicted in Table 4.3. Hence, the effects of flow rate and pressure on V_{Out} in the extruded composite was studied indirectly, as shown in Tables 4.4 and 4.5.

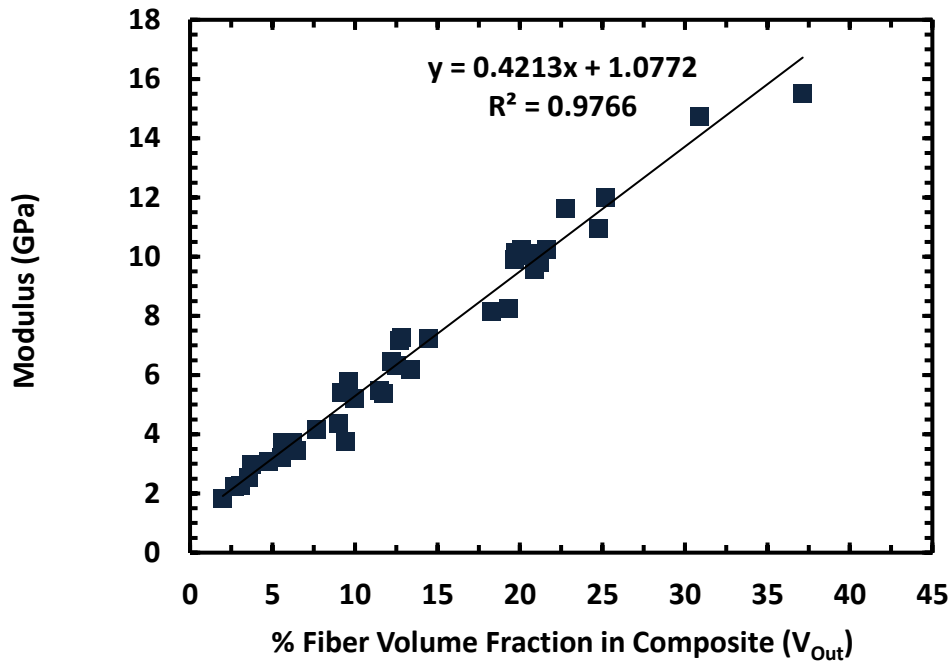


Figure 4.4. Composite Modulus versus experimental V_{Out}

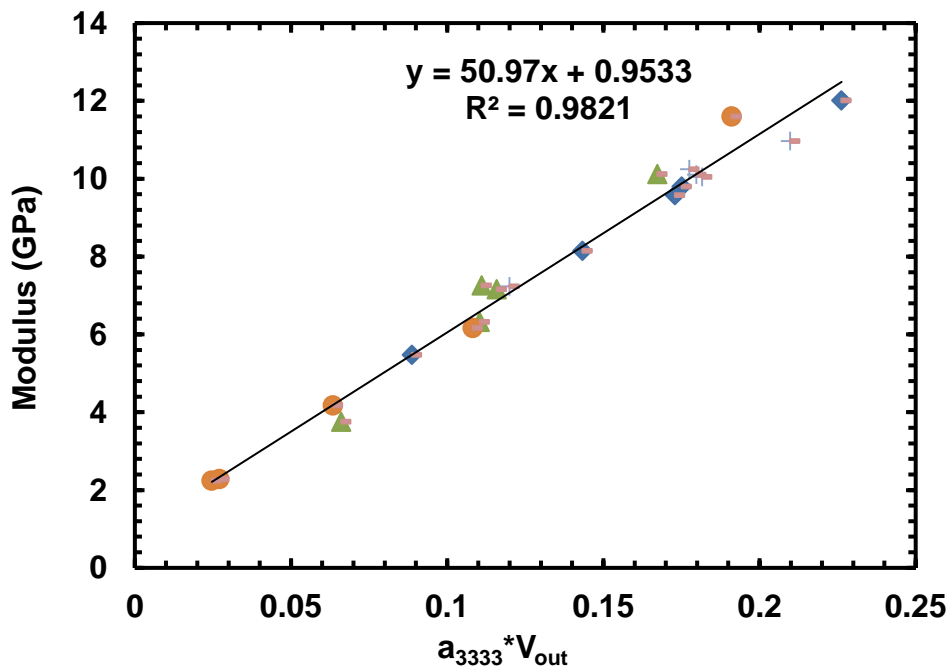


Figure 4.5. Composite Modulus versus experimental $V_{Out} * a_{3333}$

During extrusion of polymer composites, V_{In} and screw speed are changed while maintaining the die parameters and keeping the temperature constant to achieve a certain steady state extrusion rate. While assuming V_{Out} and V_{In} to be the same, many previous studies [4, 10, 11, 19, 21] attempted to correlate the V_{In} and screw speed with the reinforcement fiber orientation in the extruded composite. However, these studies are not conclusive, likely due to the limited scope of their studies.

If these factors influence the V_{Out} in the composite indirectly, then a clear relationship would emerge. However, if V_{Out} is a combined effect of all these variables, then a clear relationship between V_{Out} and each of these variables would not exist. The results of this study suggest the latter. Nevertheless, the individual effect of each variable is discussed first to highlight the case for a combined effect analysis, presented in section 4.2.4.

Figure 4.6 illustrates a flow chart of different variables. Melt flow variables including flow rate, pressure, and viscosity are constant in a steady state condition. All of aforementioned variables are function of independent and control variables. As discussed in chapter 1 and illustrated in Figure 4.6, data presented in this chapter are similar to those of previous publications in this area in which the direct correlation of independent variables, control variables, dependent variables, and viscosity have been studied on V_{Out} and OF.

In order to support the analysis, the combined effect of independent and control variables on melt flow variables was studied, and these data were subsequently correlated to V_{Out} and OF in extruded composite fiber. The independent and control variables were correlated to melt flow variables in order to understand the level of extensional and shear flow inside the dies, and this information subsequently aided in analyzing the combined effect on V_{Out} and OF.

All published literature have used the fiber volume fraction in the feed (V_{In}) to interpret the effect of various manufacturing variables, assuming the fiber volume fraction in the extruded composite (V_{Out}) to be same as in the feed (V_{In}). Therefore, no measurement has been done to measure V_{Out} . As composite melt (polymer/glass fiber) flows into the die cavity, depending on die temperature, die pressure, and fiber volume fraction in the feed (V_{In}), the exit velocity and hence the diameters of the spun composite vary. The fiber volume fraction in the extruded composite depends on its diameter and fiber orientation.

Hence, any one of these conditions; $V_{Out} = V_{In}$, $V_{Out} > V_{In}$, or $V_{Out} < V_{In}$ is possible, depending on the processing conditions. The current state of computational fluid dynamics does not yet have the capability to simulate the complexity of the extruder fiber spinning manufacturing process.

The results of this study, shown in Table 4.1, have proven the assumption of $V_{In} = V_{Out}$ to be incorrect. For any die angle, fiber volume fraction in the composite (V_{Out}) was not equal to that in the feed; it was less or more than the V_{In} in the feed in different cases. Plots of V_{In} versus V_{Out} for all 3mm dies are presented in Figure A.12 in Appendix A. For a given V_{In} in the feed, the V_{Out} in the composite varied with die angle even though the ratio of the entry to exit diameters was the same (See Table 4.1). Similarly, for a given V_{In} in the feed, the V_{Out} in the composite varied with the ratio of entry to exit diameter (L/D) ratio of 3 and 0.9 for two 60° dies in Table 4.6. Hence, the effect of die parameters on V_{Out} in the composite cannot be discerned from the results presented in Table 4.4, Table 4.5, and Table 4.6. For two die geometries in the same processing conditions, the manufacturing of extruded composite fiber was repeated in order to confirm the repeatability of results.

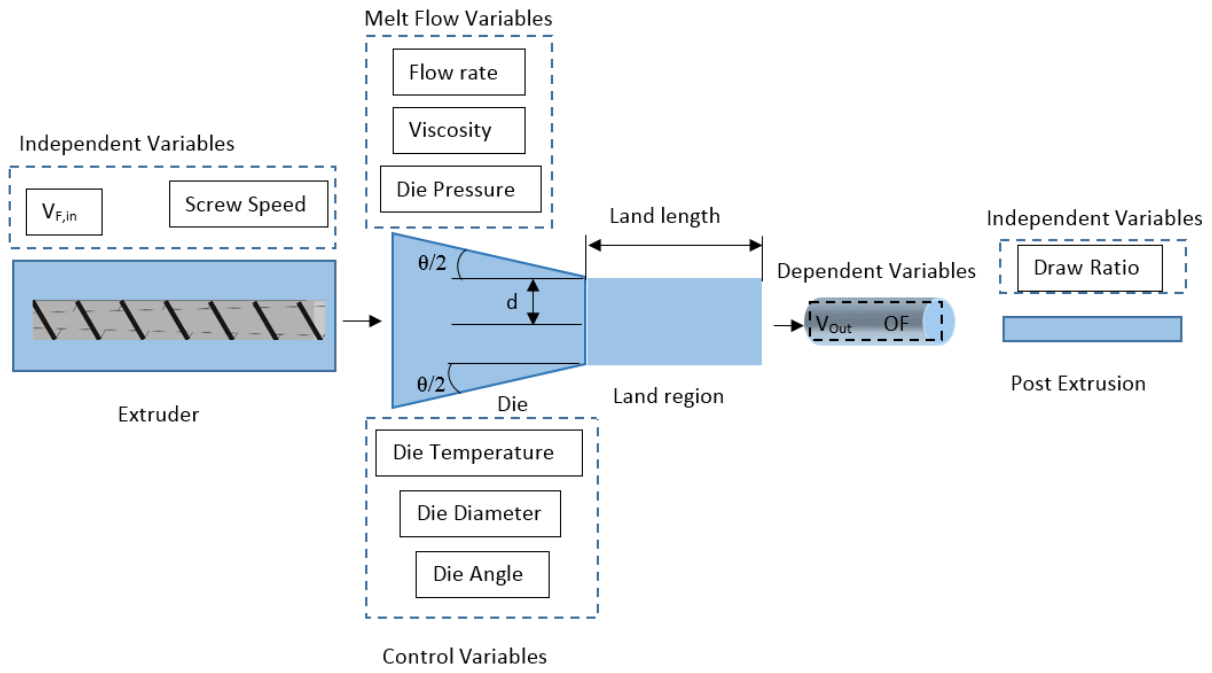


Figure 4.6. Flow chart of combined effect on V_{Out} and OF

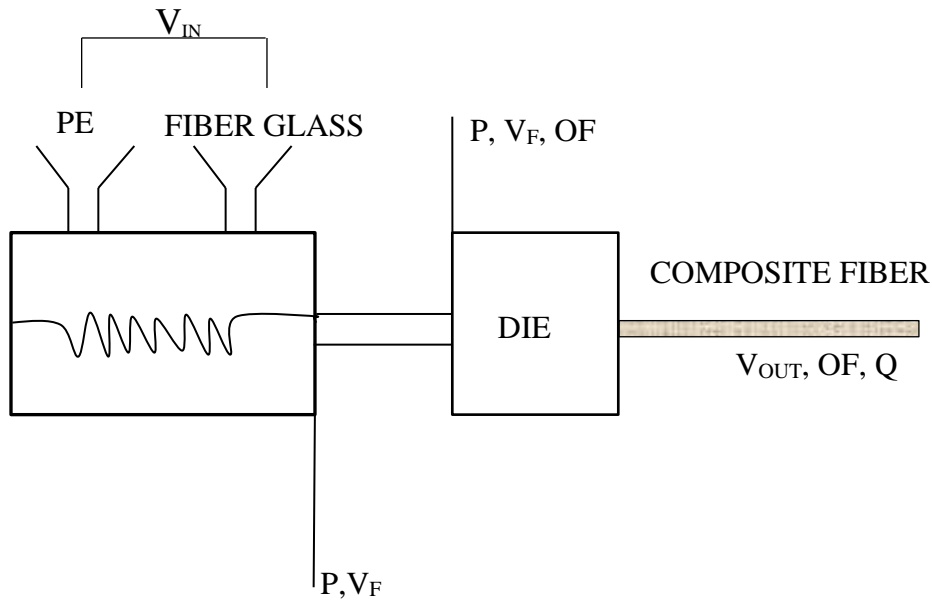


Figure 4.7. Measurements along extruder

Table 4.1. Changes in volume fraction along extruder at different location.

| Fixed parameters | Varied Parameter | Measured parameter | Measured parameter | Measured parameter |
|--|-----------------------------------|---|---|--------------------------------------|
| Die angle (degree) , Die Diameter (mm) , and Die land length (mm) | % V _{In} in Feed (±0.03) | % V _F measured without die (±0.05) | % V _F measured at die entrance (±0.04) | % V _{out} composite (±0.04) |
| 60, 3, 2.7 | 9.1 | 4.2 | 5.6 | 13 |
| 60, 3, 2.7 | 14 | 8.1 | 7.7 | 9.3 |
| 60, 3, 2.7 | 20 | 12 | 13 | 18 |
| 60, 3, 2.7 | 27 | 29 | 18 | 24 |
| 90, 3, 2.7 | 9.1 | 4.2 | 3.2 | 13 |
| 90, 3, 2.7 | 14 | 8.1 | 9.2 | 19 |
| 90, 3, 2.7 | 20 | 12 | 14 | 11 |
| 90, 3, 2.7 | 27 | 29 | 19 | 14 |
| 30, 3, 2.7 | 9.1 | 4.2 | 3.4 | 2.7 |
| 30, 3, 2.7 | 14 | 8.1 | 8.5 | 12 |
| 30, 3, 2.7 | 20 | 12 | 19 | 25 |
| 30, 3, 2.7 | 27 | 29 | 21 | 20 |

Table 4.2. Effect of V_{out} resulted from change in screw speed at constant feed rate.

| Fixed parameters | Varied Parameter | Measured parameter |
|--|-------------------|--------------------------------------|
| Die angle (degree) , Die Diameter (mm) , Die land length (mm), and % V _{In} in Feed | screw speed (rpm) | % V _{out} composite (±0.05) |
| 60, 3, 2.7, 7.8 | 40 | 13 |
| 60, 3, 2.7, 7.8 | 60 | 19 |
| 60, 3, 2.7, 7.8 | 250 | 19 |
| 60, 3, 2.7, 12 | 40 | 9.3 |
| 60, 3, 2.7, 12 | 60 | 11 |
| 60, 3, 2.7, 12 | 200 | 11 |
| 60, 3, 2.7, 12 | 250 | 13 |
| 60, 3, 2.7, 18 | 40 | 18 |
| 60, 3, 2.7, 18 | 100 | 23 |
| 60, 3, 2.7, 18 | 150 | 26 |

Table 4.3. Effect of pressure resulted from change in volume fraction in feed at 40 rpm screw speed.

| Fixed parameters | Varied Parameter | Measured parameter |
|---|-----------------------------------|--------------------------------|
| Die angle (degree) , Die Diameter (mm) , and Die land length (mm) | % V_{In} in Feed (± 0.03) | Pressure (MPa) (± 0.010) |
| 90, 1.5, 7.4 | 7.8 | 2.24 |
| 90, 1.5, 7.4 | 12 | 2.38 |
| 90, 1.5, 7.4 | 18 | 2.72 |
| 90, 1.5, 7.4 | 25 | 2.93 |
| 60, 1, 2.7 | 7.8 | 2.17 |
| 60, 1, 2.7 | 12 | 2.31 |
| 60, 1, 2.7 | 18 | 2.76 |
| 60, 1, 2.7 | 25 | 3.4 |
| 60, 3, 2.7 | 7.8 | 0.67 |
| 60, 3, 2.7 | 12 | 0.65 |
| 60, 3, 2.7 | 18 | 0.78 |
| 60, 3, 2.7 | 25 | 0.86 |
| 90, 3, 2.7 | 7.8 | 0.79 |
| 90, 3, 2.7 | 12 | 0.83 |
| 90, 3, 2.7 | 18 | 0.85 |
| 90, 3, 2.7 | 25 | 0.93 |
| 60, 3, 9.4 | 7.8 | 0.96 |
| 60, 3, 9.4 | 12 | 1.07 |
| 60, 3, 9.4 | 18 | 1.21 |
| 60, 3, 9.4 | 25 | 1.52 |
| 30, 3, 2.7 | 7.8 | 0.48 |
| 30, 3, 2.7 | 12 | 0.65 |
| 30, 3, 2.7 | 18 | 0.72 |
| 30, 3, 2.7 | 25 | 0.9 |
| 45, 3, 2.7 | 7.8 | 0.59 |
| 45, 3, 2.7 | 12 | 0.7 |
| 45, 3, 2.7 | 18 | 0.8 |
| 45, 3, 2.7 | 25 | 0.9 |
| 180, 3, 2.7 | 7.8 | 0.56 |
| 180, 3, 2.7 | 12 | 0.76 |
| 180, 3, 2.7 | 18 | 0.81 |
| 180, 3, 2.7 | 25 | 0.91 |

Table 4.4. Effect of pressure on %V_{Out} in composite at 40 rpm screw speed.

| Fixed parameters | Varied Parameter | Measured parameter | Measured parameter |
|---|----------------------------------|-------------------------------------|-------------------------|
| Die angle (degree) , Die Diameter (mm) , and Die land length (mm) | %V _{In} in Feed (±0.03) | %V _{out} composite (±0.05) | Pressure (MPa) (±0.010) |
| 90, 1.5, 7.4 | 7.8 | 3.5 | 2.24 |
| 90, 1.5, 7.4 | 12 | 11.7 | 2.38 |
| 90, 1.5, 7.4 | 18 | 37.1 | 2.72 |
| 90, 1.5, 7.4 | 25 | 30.8 | 2.93 |
| 60, 1, 2.7 | 7.8 | 12.1 | 2.17 |
| 60, 1, 2.7 | 12 | 6.4 | 2.31 |
| 60, 1, 2.7 | 18 | 19.6 | 2.76 |
| 60, 1, 2.7 | 25 | 21.6 | 3.4 |
| 60, 3, 2.7 | 7.8 | 22.7 | 0.67 |
| 60, 3, 2.7 | 12 | 9.3 | 0.65 |
| 60, 3, 2.7 | 18 | 18.3 | 0.78 |
| 60, 3, 2.7 | 25 | 24.7 | 0.86 |
| 90, 3, 2.7 | 7.8 | 13.3 | 0.79 |
| 90, 3, 2.7 | 12 | 19.7 | 0.83 |
| 90, 3, 2.7 | 18 | 11.4 | 0.85 |
| 90, 3, 2.7 | 25 | 14.4 | 0.93 |
| 60, 3, 9.4 | 7.8 | 6.1 | 0.96 |
| 60, 3, 9.4 | 12 | 9.1 | 1.07 |
| 60, 3, 9.4 | 18 | 19.3 | 1.21 |
| 60, 3, 9.4 | 25 | 9 | 1.52 |
| 30, 3, 2.7 | 7.8 | 2.7 | 0.48 |
| 30, 3, 2.7 | 12 | 12.7 | 0.65 |
| 30, 3, 2.7 | 18 | 25.2 | 0.72 |
| 30, 3, 2.7 | 25 | 20 | 0.9 |
| 45, 3, 2.7 | 7.8 | 7.6 | 0.59 |
| 45, 3, 2.7 | 12 | 12.4 | 0.7 |
| 45, 3, 2.7 | 18 | 21.2 | 0.8 |
| 45, 3, 2.7 | 25 | 20.7 | 0.9 |
| 180, 3, 2.7 | 7.8 | 3 | 0.56 |
| 180, 3, 2.7 | 12 | 12.8 | 0.76 |
| 180, 3, 2.7 | 18 | 20.8 | 0.81 |
| 180, 3, 2.7 | 25 | 19.8 | 0.91 |

Table 4.5. Effect of Flow rate (m^3/s) on $\%V_{\text{Out}}$ in composite at 40 rpm screw speed.

| Fixed parameters | Varied Parameter | Measured parameter | Measured parameter |
|---|--|---|---|
| Die angle (degree), Die Diameter (mm), and Die land length (mm) | $\%V_{\text{In}}$ in Feed (± 0.03) | $\%V_{\text{out}}$ composite (± 0.05) | Flow rate 10^{-8} (m^3/s) (± 0.7) |
| 90, 1.5, 7.4 | 7.8 | 3.5 | 8.69 |
| 90, 1.5, 7.4 | 12 | 11.7 | 8.82 |
| 90, 1.5, 7.4 | 18 | 37.1 | 6.57 |
| 90, 1.5, 7.4 | 25 | 30.8 | 7.20 |
| 60, 1, 2.7 | 7.8 | 12.1 | 8.06 |
| 60, 1, 2.7 | 12 | 6.4 | 10.0 |
| 60, 1, 2.7 | 18 | 19.6 | 9.95 |
| 60, 1, 2.7 | 25 | 21.6 | 9.62 |
| 60, 3, 2.7 | 7.8 | 22.7 | 9.02 |
| 60, 3, 2.7 | 12 | 9.3 | 10.5 |
| 60, 3, 2.7 | 18 | 18.3 | 10.8 |
| 60, 3, 2.7 | 25 | 24.7 | 6.97 |
| 90, 3, 2.7 | 7.8 | 13.3 | 8.69 |
| 90, 3, 2.7 | 12 | 19.7 | 10.0 |
| 90, 3, 2.7 | 18 | 11.4 | 9.90 |
| 90, 3, 2.7 | 25 | 14.4 | 9.86 |
| 30, 3, 2.7 | 7.8 | 2.7 | 9.42 |
| 30, 3, 2.7 | 12 | 12.7 | 11.5 |
| 30, 3, 2.7 | 18 | 25.2 | 10.6 |
| 30, 3, 2.7 | 25 | 20 | 10.8 |
| 45, 3, 2.7 | 7.8 | 7.6 | 9.13 |
| 45, 3, 2.7 | 12 | 12.4 | 9.98 |
| 45, 3, 2.7 | 18 | 21.2 | 10.4 |
| 45, 3, 2.7 | 25 | 20.7 | 10.6 |
| 180, 3, 2.7 | 7.8 | 3 | 9.33 |
| 180, 3, 2.7 | 12 | 12.8 | 10.6 |
| 180, 3, 2.7 | 18 | 20.8 | 10.7 |
| 180, 3, 2.7 | 25 | 19.8 | 11.0 |

Table 4.6. Effect of volume fraction in the feed on volume fraction in composite for die entry angles of 60°, die hole diameter of 3 mm, with two L/D ratios.

| Fixed parameters | Varied Parameter | Measured parameter |
|--|--------------------------------------|--|
| Die angle (degree), Die Diameter (mm), and Die land length (mm) | % V _{In} in Feed (±0.03) | % V _{Out} in Composite (±0.05) |
| 60, 3, 2.7 | 9.1 | 13 |
| 60, 3, 2.7 | 14 | 9.3 |
| 60, 3, 2.7 | 20 | 18 |
| 60, 3, 2.7 | 27 | 24 |
| 60, 3, 9 | 9.1 | 6.1 |
| 60, 3, 9 | 14 | 9.1 |
| 60, 3, 9 | 20 | 19 |
| 60, 3, 9 | 27 | 9 |

4.2.1 Effect of Manufacturing Variables on the Orientation Factor

A well-established approach to characterize the orientation distribution function is to consider the moments of the orientation distribution function. Even-order tensors give a concise description of orientation distribution function as explained in Chapter 3. Orientation factors a_{3333} and a_{1313} are determined using the orientation distribution as discussed in 3.5.2.

Table 4.7 shows the variation of the orientation factors at different locations on the extruder for various die entry angles. The effect of flow rate and pressure on orientation factors in the extruded composite was studied indirectly, as shown in Table 4.8 and Table 4.9.

The a_{3333} least value of 0.704 was obtained for a sample processed using a 60-3 mm value, while the maximum a_{3333} value of 0.912 was obtained for a sample processed using a 30-3 mm value. These data indicate a very high degree of alignment for composites processed using certain dies, which has been corroborated by independently measured mechanical properties as discussed in section 4.1.2.

It appears that a_{3333} decreases with an increase in V_{In} , while the trend is not a monotonic decrease. The a_{3333} varied the least for the 30° die, as depicted in Table 4.7, but it varied significantly with V_{In} in the feed for the 60° die. The observed variation in a_{3333} for other dies was between these two extremes.

The results in Tables 4.7 also suggest that, for dies with the same entry to exit diameter ratio, an increase in the die angle causes a decrease in the orientation along the fiber axis. Similarly, no trend was observed in the effect of die pressure and flow rate on a_{3333} in Tables 4.8 and 4.9, respectively.

Table 4.7. Changes in Orientation along the extruder at different locations.

| Fixed Parameters | Varied Parameter | Measured Parameter | Measured Parameter | Measured Parameter | Measured Parameter |
|---|-----------------------------------|---------------------------------------|---------------------------------------|------------------------------------|-------------------------------------|
| Die angle (degree), Die Diameter (mm), Die land length (mm), and % V_{In} in Feed | % V_{In} in Feed (± 0.03) | a_{3333} Inside Die (± 0.001) | a_{1313} Inside Die (± 0.001) | a_{3333} Die End (± 0.001) | a_{1313} Die End (± 0.0001) |
| 60, 3, 2.7 | 7.8 | 0.404 | 0.046 | 0.839 | 0.019 |
| 60, 3, 2.7 | 12 | 0.181 | 0.070 | 0.704 | 0.019 |
| 60, 3, 2.7 | 18 | 0.392 | 0.047 | 0.796 | 0.021 |
| 60, 3, 2.7 | 25 | 0.338 | 0.051 | 0.846 | 0.032 |
| 90, 3, 2.7 | 7.8 | 0.695 | 0.034 | 0.811 | 0.018 |
| 90, 3, 2.7 | 12 | 0.310 | 0.038 | 0.847 | 0.016 |
| 90, 3, 2.7 | 18 | 0.420 | 0.175 | 0.807 | 0.014 |
| 90, 3, 2.7 | 25 | 0.369 | 0.098 | 0.828 | 0.015 |
| 30, 3, 2.7 | 7.8 | 0.791 | 0.055 | 0.912 | 0.017 |
| 30, 3, 2.7 | 12 | 0.443 | 0.065 | 0.911 | 0.016 |
| 30, 3, 2.7 | 18 | 0.346 | 0.030 | 0.905 | 0.011 |
| 30, 3, 2.7 | 25 | 0.091 | 0.000 | 0.884 | 0.011 |

Table 4.8. Effect of orientation change resulted from change in pressure in feed at 40 rpm screw speed.

| Fixed Parameters | Varied Parameter | Measured Parameter | Measured Parameter | Measured Parameter |
|--|--------------------------------------|----------------------------|--|---|
| Die angle (degree), Die Diameter (mm), Die land length (mm), and % V _{In} in Feed | % V _{In} in Feed (±0.03) | Pressure (MPa) (±0.010) | a ₃₃₃₃ Die End (±0.001) | a ₁₃₁₃ Die End (±0.0001) |
| 60, 3, 2.7 | 7.8 | 0.67 | 0.839 | 0.019 |
| 60, 3, 2.7 | 12 | 0.65 | 0.704 | 0.019 |
| 60, 3, 2.7 | 18 | 0.78 | 0.796 | 0.021 |
| 60, 3, 2.7 | 25 | 0.86 | 0.846 | 0.032 |
| 90, 3, 2.7 | 7.8 | 0.79 | 0.811 | 0.018 |
| 90, 3, 2.7 | 12 | 0.83 | 0.847 | 0.016 |
| 90, 3, 2.7 | 18 | 0.85 | 0.807 | 0.014 |
| 90, 3, 2.7 | 25 | 0.93 | 0.828 | 0.015 |
| 30, 3, 2.7 | 7.8 | 0.48 | 0.912 | 0.017 |
| 30, 3, 2.7 | 12 | 0.65 | 0.911 | 0.016 |
| 30, 3, 2.7 | 18 | 0.72 | 0.905 | 0.011 |
| 30, 3, 2.7 | 25 | 0.90 | 0.884 | 0.011 |
| 45, 3, 2.7 | 7.8 | 0.59 | 0.897 | 0.019 |
| 45, 3, 2.7 | 12 | 0.70 | 0.884 | 0.019 |
| 45, 3, 2.7 | 18 | 0.80 | 0.875 | 0.021 |
| 45, 3, 2.7 | 25 | 0.90 | 0.864 | 0.032 |
| 180, 3, 2.7 | 7.8 | 0.56 | 0.884 | 0.019 |
| 180, 3, 2.7 | 12 | 0.76 | 0.867 | 0.016 |
| 180, 3, 2.7 | 18 | 0.81 | 0.864 | 0.011 |
| 180, 3, 2.7 | 25 | 0.91 | 0.914 | 0.012 |

Table 4.9. Effect of orientation change resulted from change in flow rate in feed at 40 rpm screw speed.

| Fixed Parameters | Varied Parameter | Measured Parameter | Measured Parameter | Measured Parameter |
|---|-----------------------------------|---|------------------------------------|-------------------------------------|
| Die angle (degree), Die Diameter (mm), Die land length (mm), and % V_{In} in Feed | % V_{In} in Feed (± 0.03) | Flow rate 10^{-8} (m^3/s) (± 0.7) | a_{3333} Die End (± 0.001) | a_{1313} Die End (± 0.0001) |
| 60, 3, 2.7 | 7.8 | 9.02 | 0.839 | 0.019 |
| 60, 3, 2.7 | 12 | 10.5 | 0.704 | 0.019 |
| 60, 3, 2.7 | 18 | 10.8 | 0.796 | 0.021 |
| 60, 3, 2.7 | 25 | 6.97 | 0.846 | 0.032 |
| 90, 3, 2.7 | 7.8 | 8.69 | 0.811 | 0.018 |
| 90, 3, 2.7 | 12 | 10.0 | 0.847 | 0.016 |
| 90, 3, 2.7 | 18 | 9.90 | 0.807 | 0.014 |
| 90, 3, 2.7 | 25 | 9.86 | 0.828 | 0.015 |
| 30, 3, 2.7 | 7.8 | 9.42 | 0.912 | 0.017 |
| 30, 3, 2.7 | 12 | 11.5 | 0.911 | 0.016 |
| 30, 3, 2.7 | 18 | 10.6 | 0.905 | 0.011 |
| 30, 3, 2.7 | 25 | 10.8 | 0.884 | 0.011 |
| 45, 3, 2.7 | 7.8 | 9.13 | 0.897 | 0.019 |
| 45, 3, 2.7 | 12 | 9.98 | 0.884 | 0.019 |
| 45, 3, 2.7 | 18 | 10.4 | 0.875 | 0.021 |
| 45, 3, 2.7 | 25 | 10.6 | 0.864 | 0.032 |
| 180, 3, 2.7 | 7.8 | 9.33 | 0.884 | 0.019 |
| 180, 3, 2.7 | 12 | 10.6 | 0.867 | 0.016 |
| 180, 3, 2.7 | 18 | 10.7 | 0.864 | 0.011 |
| 180, 3, 2.7 | 25 | 11.0 | 0.914 | 0.012 |

In order to understand the above trends or lack of trend for V_F and OF, everything is related to viscosity, which is related to structure change within the die. This is where packing comes into the picture. In a twin screw extruder, output does not depend on input, and the die acts as a reservoir with a buffer zone before the die assembly. Pressure, flow rate, V_F , and OF changes within the die all affect what is coming into the die. Previous research did not study [14, 51, 52] these changes, and capillary rheometer set ups were used without changing the die or V_F , nor was V_F measured in output. Hence viscosity, a function of the microstructure of melt, was studied next to understand the combined impact of pressure, flow rate, V_F , and OF on structural changes happening along the extruder.

4.2.2 Combined effect of OF and V_F microstructure of flow

Using the measured flow rate and pressure, the extensional and shear viscosity inside the cone and the land regions of the die were determined following the Cogswell approach [30]. Shear viscosity was independently measured using a rheometer and modeled to establish the effect of fiber aspect ratio, fiber volume fraction, and fiber orientation. Using this model and the measured fiber orientation and V_F in the land region, shear viscosity in the land region was simulated and compared with the values determined using the Cogswell approach. The viscosity results thus allowed this researcher to interpret the variation in the measured pressure and flow rate during various extrusions in terms of changing the FOD along the extrusion line. Viscosity model developed here are applicable to dilute composite solutions; however, these have been applied to concentrated composite solutions used in this thesis.

4.2.2.1 Viscosity measurement using rheometer

Dynamic and steady shear rheological measurements were carried out on a TA AR 2000, and measurements were run with 25 mm parallel plate geometry and a 1.5 mm sample gap. The viscoelastic properties were determined with frequencies from 0.1 to 500 rad/s, and measurements were carried out at a temperature of 200°C.

The combination of V_F , fiber aspect ratio, orientation, and density defines flow rate, with extruder viscosity being the combination of pressure, flow rate, and geometry. Flow rate and geometry at any location in the extruder defines the shear rate. The shear viscosity versus strain rate for neat High Density Polyethylene (HDPE) was measured for strain rate up to $80 \text{ (s}^{-1}\text{)}$. HDPE viscosity was used to determine shear behavior at different strain rates, which aids to calculate composite viscosity in the extruder process. In order to understand the viscosity in the extruder, the effects of fiber aspect ratio, orientation, and shear rate on viscosity of composite melt were studied using the rheometer as well.

Initially, the viscosity of the HDPE was measured at different shear rates to understand the behavior of the polymer matrix, as depicted in Figure 4.8. Subsequently, the HDPE-spherical glass fiber composite viscosity was measured at $V_F=4.6\%$, $V_F=5.9\%$, and $V_F=17.8\%$ as illustrated in Figure 4.9, Figure 4.10, and Figure 4.11 respectively. The effect of volume fraction and aspect ratio was determined for HDPE spherical glass fiber using equation 4.2 in which HDPE spherical glass viscosity compared with HDPE viscosity. The following viscosity model is used to determine volume fraction effect:

$$\eta = \eta_0(1+\alpha V_F) \quad (4.2)$$

Where η is the shear viscosity, η_0 is the neat HDPE shear viscosity, α is aspect ratio and volume fraction factor, and V_F is the volume fraction. As depicted in Figure 4.12, α is 9.3 for spherical glass. In order to determine α for an aspect ratio of greater than one, which is the case for extruded composite fiber through the die, samples were prepared with pre-existing orientation. Shear strain of 50 and shear rate of 0.1 (1/s) were applied to composite samples with volume fractions of 7.4%, 14%, 18%, and 19%, as depicted in Figure 4.13. Because these composite fibers already have pre-existing orientation, transient viscosity peaks at a strain of 0.001 with a value of about three times larger than that of steady state.

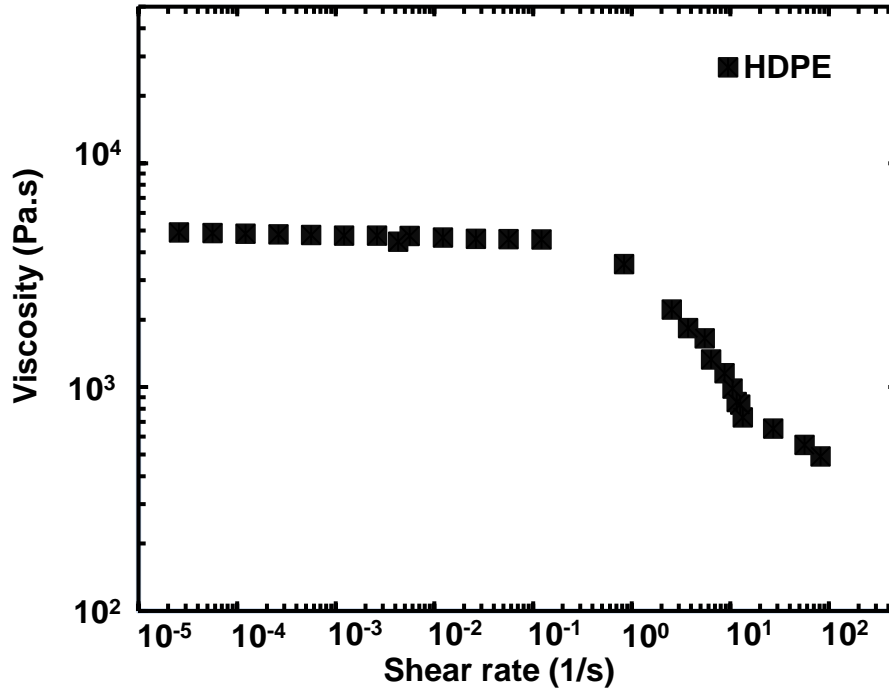


Figure 4.8. HDPE viscosity measured using Rheometer

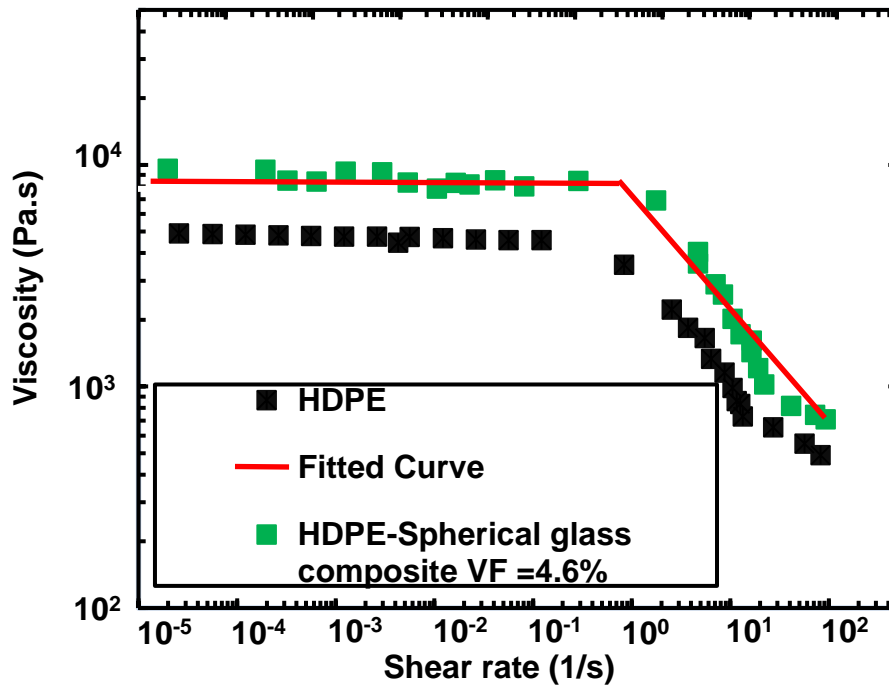


Figure 4.9. Experimental viscosity of HDPE-Spherical glass composite with a $V_F=4.6\%$

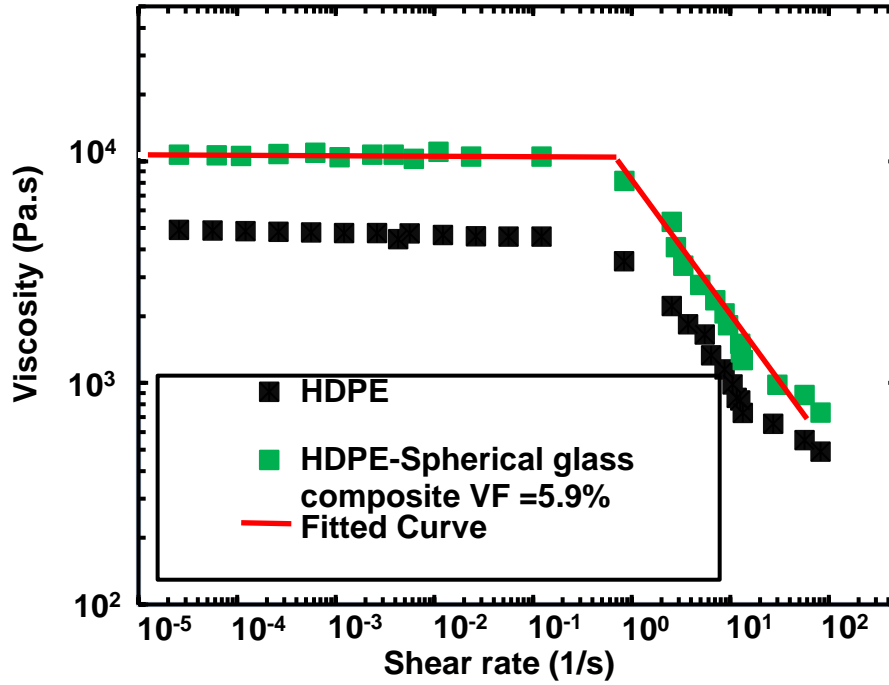


Figure 4.10. Experimental viscosity of HDPE-Spherical glass composite with a $V_F=5.9\%$.

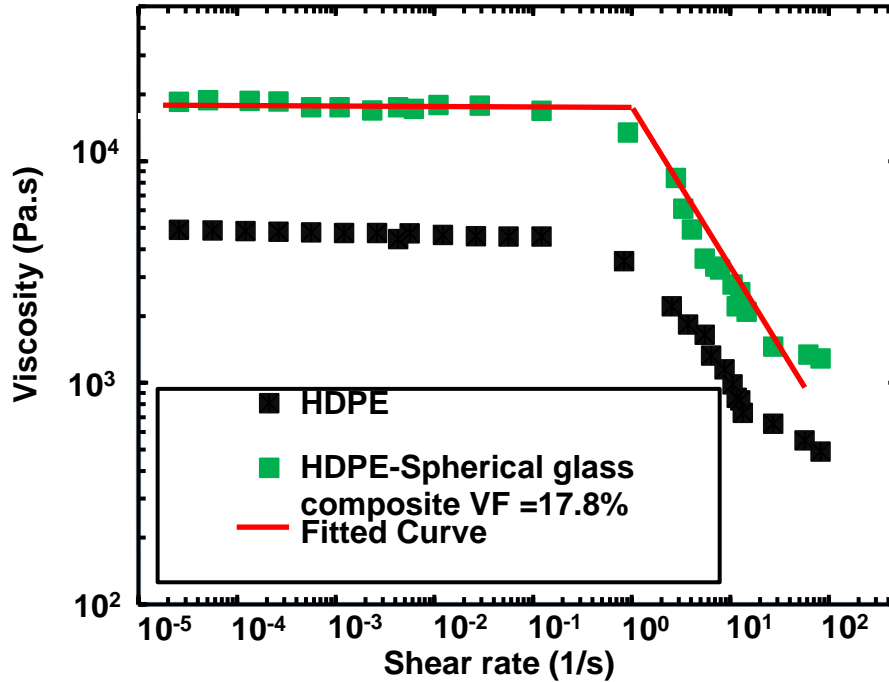


Figure 4.11. Experimental viscosity of HDPE-Spherical glass composite with a $V_F=17.8\%$

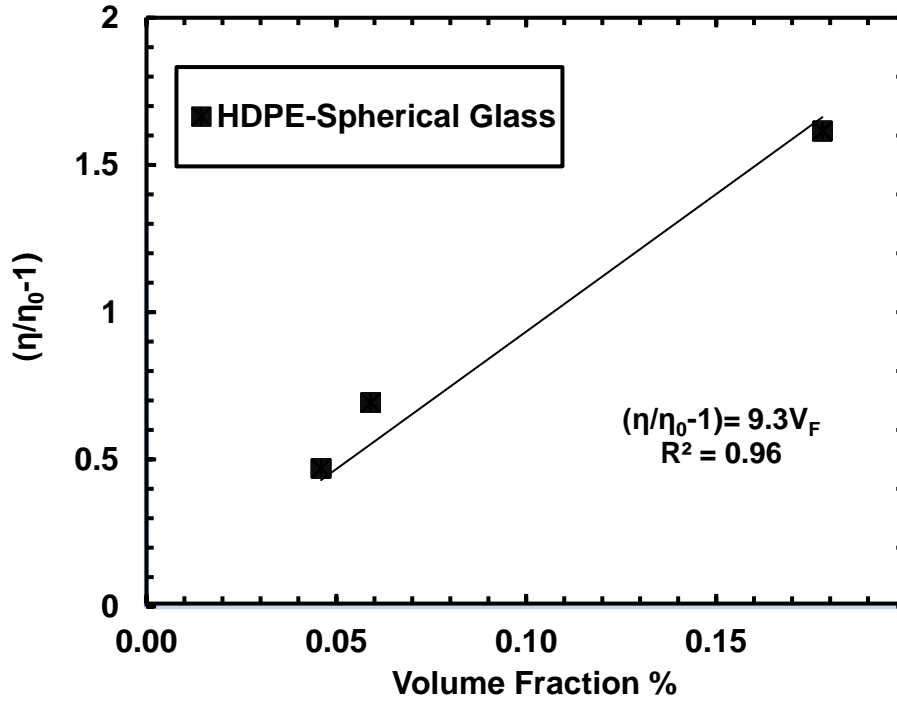


Figure 4.12. Volume fraction factor of HDPE-Spherical glass composite

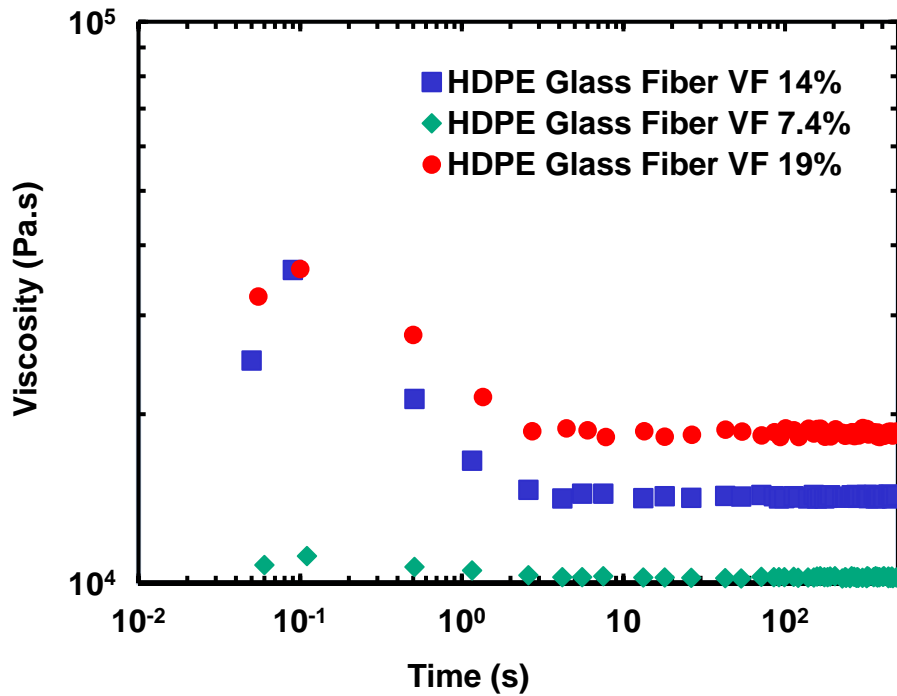


Figure 4.13. Experimental viscosity as function time of HDPE-fiber glass composite with V_F of

7.4%, 14%, and 19% at constant strain rate of 0.1 (1/s).

The difference between the shear viscosity plots in Figure 4.8-11 and Figure 4.13 is that first the viscosity of spherical glass fiber (aspect ratio of 1) was measured by varying the shear rate to understand the effect of volume fraction.

Next, the viscosity of glass fiber with an aspect ratio of 4 was measured at a constant shear rate of 0.1 (1/s) to understand the effect of preexisting orientation on viscosity.

Shear strain was carried out in order to reach a steady state orientation structure. In other words, all fibers were oriented along the shear direction at steady state viscosity. Equation (4.2) is used here to measure the effect of volume fraction and fiber aspect ratio at volume fractions of 7%, 14%, and 19% for HDPE glass fiber extruded composite fiber. η is the shear viscosity, η_0 is the neat HDPE shear viscosity, α is the aspect ratio and volume fraction factor, and V_F is the volume fraction. As depicted in Figure 4.14, α is 14.5 for glass fibers with an aspect ratio of 4.

In the start-up of shear flow ($\dot{\gamma}=0$), initial orientation will change with increasing shear strain γ and the fibers will be aligned in direction of shearing. Dinh Armstrong [28] developed a model which predicts that all of the fibers will eventually lie in shearing planes after enough bulk strain is applied. Ausias et al. [70] studied the transient viscosity at start-up. Their studies confirm the effect of aspect ratio and initial fiber orientation on maximum transient viscosity. Ausias et al. [70] developed a model that predicts shear viscosity based on neat polymer viscosity, volume fraction and in-plane orientation, as illustrated in Equation (4.3).

$$\eta = \eta_0 \{ 1 + V_F [2 + \xi \alpha_{1313}] \} \quad (4.3)$$

Here, the Ausias et al. [70] model was modified to capture the effect of the volume fraction/aspect ratio and orientation independently on shear viscosity, which is based on observed viscosity behavior.

$$\eta = \eta_0 \{ 1 + V_F \alpha + \xi \alpha_{1313} \} \quad (4.4)$$

The effects of volume fraction and aspect ratio are combined into α , and this factor already has been determined for the HDPE spherical glass composite with an aspect ratio of one, as well as for the HDPE fiber glass composite with an aspect ratio of four. In order to determine the orientation factor ξ , the transient viscosity (Figure 4.13 peak viscosity) along with pre-existing orientation a_{1313} of 0.019, 0.17, and 0.09 for volume fractions of 7%, 14%, and 19% are fitted into equation 4.4.

Xray-Tomography of samples tested after steady state confirms that the orientation of the fibers changed, with fibers aligning toward the direction of shear, as illustrated in table 4.10. a_{3333} close to 1 represents alignment toward the shear strain axis, and a low value of a_{1313} is accompanied with high a_{3333} value. Equation (4.4) is rearranged to determine the orientation factor ξ for the maximum transient viscosity of experimental data in Figure 4.15, and resultant data from Equation (4.5) is plotted in Figure 4.16.

$$\eta/\eta_0 - \{1 + V_F \alpha\} = \xi a_{1313} \quad (4.5)$$

Hence, a shear viscosity model to predict viscosity behavior is developed to understand composite melt behavior, which depends on volume fraction, aspect ratio, and the fiber orientation state.

$$\eta = \eta_0 \{1 + 14.3 V_F + 184 a_{1313}\} \quad (4.6)$$

The effect of fiber orientation a_{1313} on shear viscosity is illustrated empirically in Figure 4.17 at constant V_F of 5% and 50% for fiber with an aspect ratio of 4 using Equation (4.6). In addition, the effect of changes in V_F at constant orientation a_{1313} of 0.05 and 0.1 has been depicted in Figure 4.18. Increase in V_F and a_{1313} results in a monotonic increase of melt viscosity, and the effect of changes in a_{1313} is more profound on viscosity than is the effect of V_F , as illustrated in Figure 4.17.

Table 4.10. Fiber orientation before and after shear viscosity test using Rheometer.

| | Initial a_{3333} | X-ray measured a_{3333} after shear viscosity test | Initial a_{1313} | X-ray measured a_{1313} after shear viscosity test |
|------------------------------------|--------------------|--|--------------------|--|
| $V_F=7.4\%, \dot{\gamma}=0.1(1/s)$ | 0.89 | 0.92 | 0.019 | 0.015 |
| $V_F=14\%, \dot{\gamma}=0.1(1/s)$ | 0.42 | 0.89 | 0.175 | 0.011 |
| $V_F=19\%, \dot{\gamma}=0.1(1/s)$ | 0.36 | 0.84 | 0.098 | 0.018 |

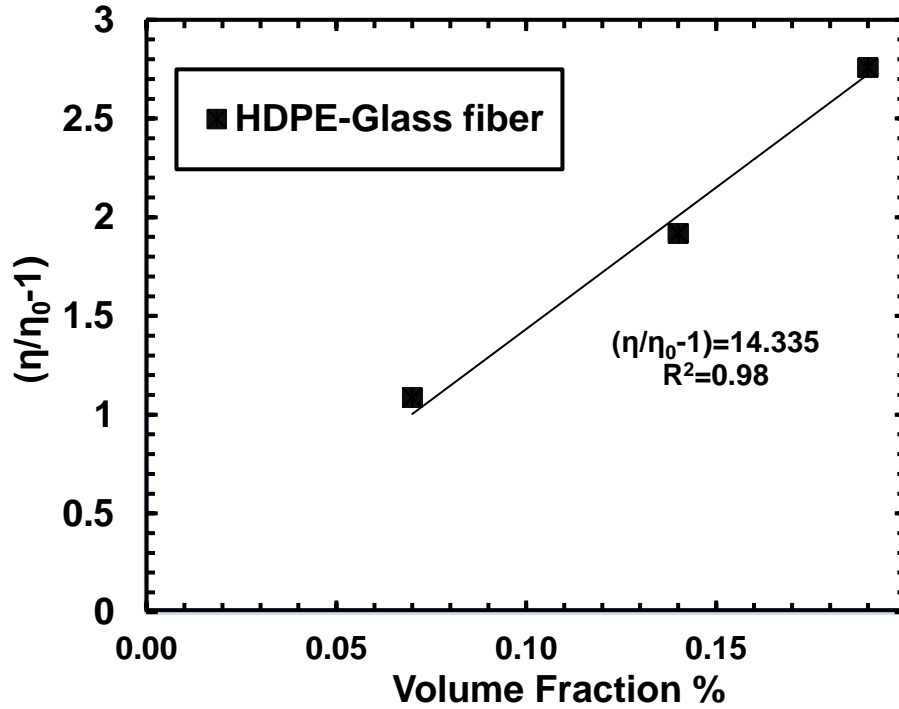


Figure 4.14. Volume fraction of factor of HDPE-fiber glass composite.

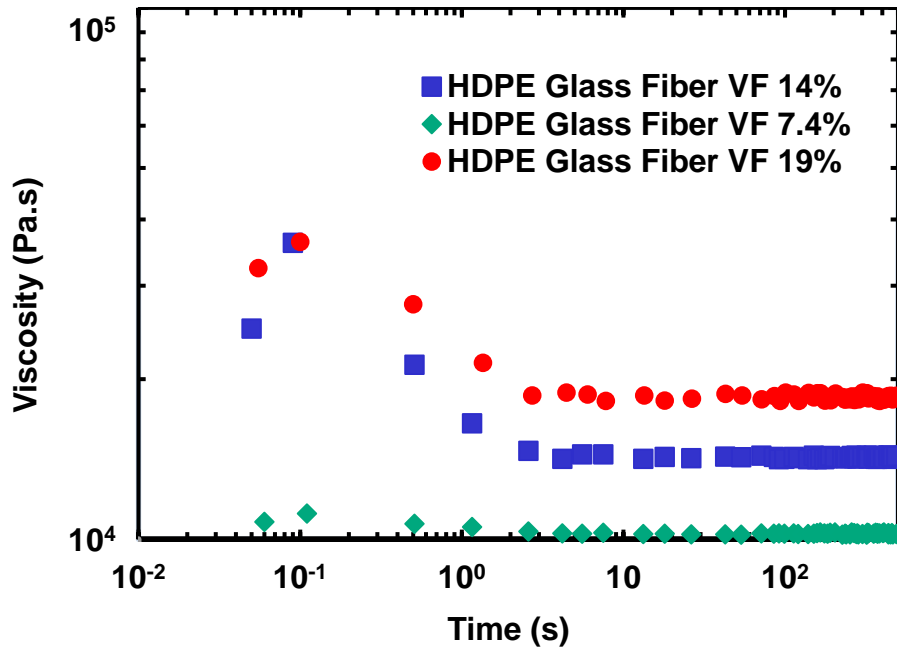


Figure 4.15. Experimental viscosity of HDPE-fiber glass composite as a function of time with V_F of 7.4%, 14%, and 19% at constant strain rate of 0.1 (1/s).

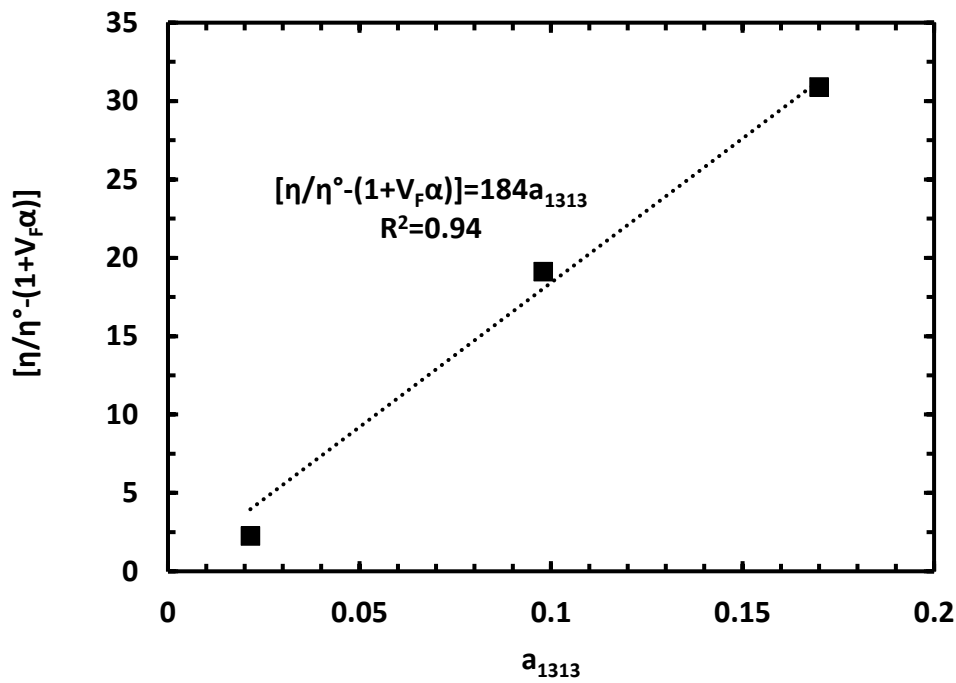


Figure 4.16. In plane orientation factor (a_{1313}) of HDPE-fiber glass composite

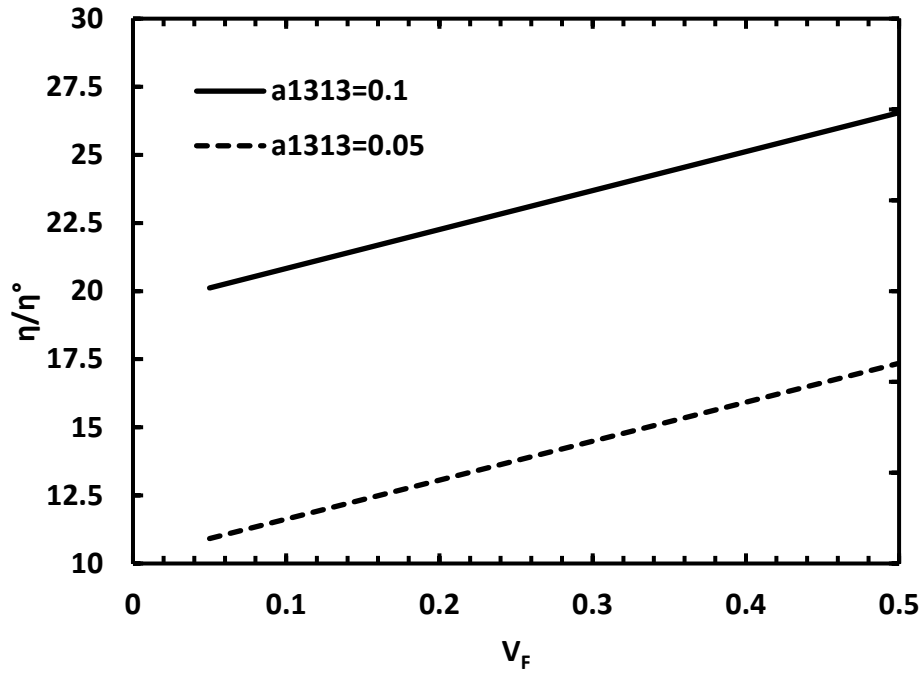


Figure 4.17. Effect of V_F on normalized viscosity at constant a_{1313} .

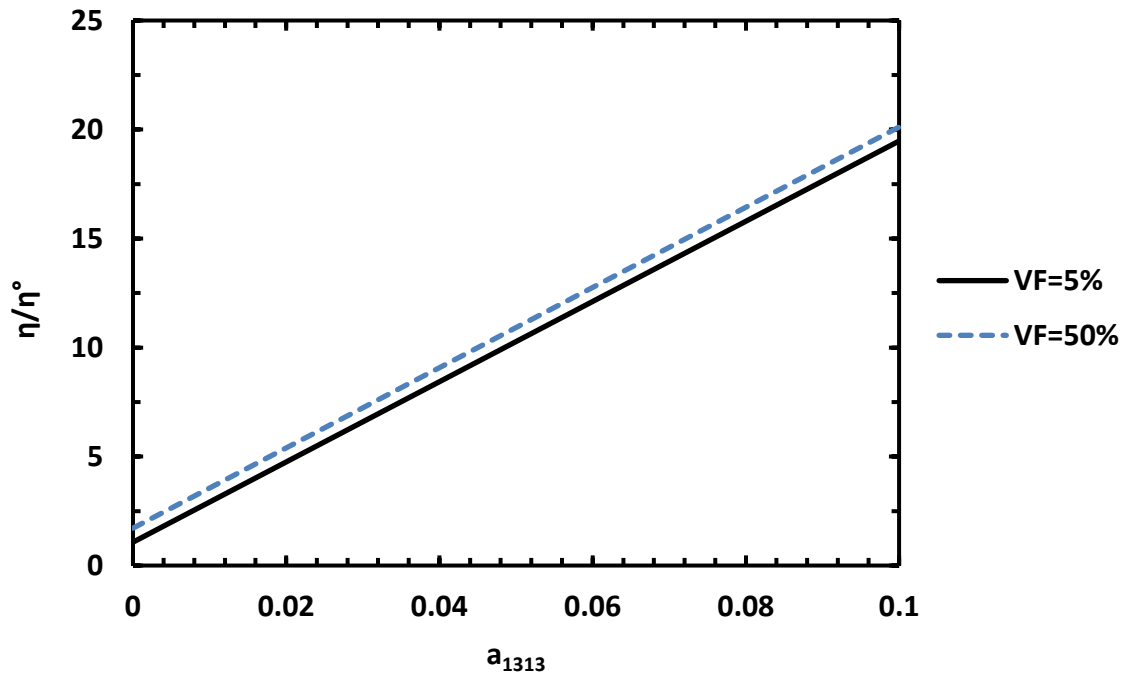


Figure 4.18. Effect of a_{1313} on normalized viscosity at constant V_F

Because of the significant impact of the fiber orientation on the viscosity, in the next section 4.2.3.3, a fiber orientation change was modeled as fibers are traveling inside the die section with imposed shear/elongation strain.

Next, viscosity in the extruder was determined based on pressure, flow rate and orientation at different locations in the extruder using the existing model. Subsequently, Equation (4.6) was applied in order to compare the existing viscosity model with the shear viscosity model developed using the rheometer.

4.2.2.2 Viscosity measurement inside extruder

Due to the interaction of the polymer melt with the die walls and the changes in the die diameter in the conical section, the melt pressure decreases as it travels from left to right in Figure 4.19. P_0 is the melt pressure at the entrance to the conical section of the die; it reduces along the length of the conical section to a value of P_1 at the end of the conical section. This pressure reduces further in the land section due to the interaction of the polymer melt with the die walls to P_2 at the end of the land section. While P_2 can be slightly higher than the atmospheric pressure, it is taken to be equal to atmospheric pressure. Based on the above, the following pressure drops can be defined:

$$\begin{aligned}
 P_0 - P_2 &= \Delta P_T \\
 P_0 - P_1 &= \Delta P_{\text{cone}} \\
 P_1 - P_2 &= \Delta P_{\text{Cap}} \\
 \Delta P_T &= \Delta P_{\text{Cone}} + \Delta P_{\text{Cap}}
 \end{aligned}
 \tag{4.7}$$

The pressure drop inside the cone consists of two components:

$$\Delta P_{\text{Cone}} = \Delta P_{\text{Cone,E}} + \Delta P_{\text{Cone,S}}
 \tag{4.8}$$

where $\Delta P_{\text{Cone,E}}$ is the pressure drop inside the cone due to the extensional flow of the melt, and

$\Delta P_{\text{Cone,S}}$ is the pressure drop inside the cone due to shear flow. It should be noted that the latter is different from the pressure drop within the land region due to shear flow (ΔP_{Cap}).

Cogswell et al. [30] derived equations relating these two pressure drops inside the cone to the extensional and shear viscosities of the melt within the cone assuming Newtonian viscosity and modified them for non-Newtonian viscosity. Using the following equation for extensional flow:

$$\sigma = \lambda \dot{\epsilon}^n \quad (4.9)$$

where σ is the applied normal stress, λ is the extensional viscosity, $\dot{\epsilon}$ is the extensional rate, and n is the power law constant obtained by mathematical fitting of the experimental data. Cogswell et al. [30] derived the following equation relating extensional viscosity within the cone with $\Delta P_{\text{Cone,E}}$.

$$\lambda = \frac{\Delta P_{\text{Cone,E}}}{\frac{2}{3n} \left(\frac{2Q \tan(\frac{\delta}{2})}{\pi r_1^3} \right)^n (1 - (\frac{r_1}{r_0})^{3n})} \quad (4.10)$$

where δ is the die angle, Q is the flow rate, r_0 is the entry diameter of the cone, and r_1 is the exit diameter of the cone.

Similarly, using the following equation for shear flow:

$$\tau = \eta \dot{\gamma}^n \quad (4.11)$$

where τ is the applied shear stress, η is the shear viscosity, $\dot{\gamma}$ is the shear rate, and n is the power law constant obtained by mathematical fitting of the experimental data. Cogswell et al. [30] derived the following equation relating shear viscosity within the cone with $\Delta P_{\text{Cone,S}}$:

$$\eta = \frac{P_S 3n \tan \delta}{2 \left(\frac{4Q}{\pi r_1^3} \right)^n (1 - (\frac{r_1}{r_0})^{3n})} \quad (4.12)$$

In this study, the above two Equations (4.10) and (4.12) were used to determine the extensional and shear viscosities within the cone. A procedure developed by Bagley [71] was used to determine ΔP_{cone} . The cone pressure drop required by these equations was derived experimentally and has been explained in detail in section A.2 in Appendix A.

Shear viscosity of both neat HDPE and HDPE spherical glass melts inside the extruder are calculated using Equation (4.12), and the results are compared with the rheometer-developed model in Equation (4.6). As depicted in Figure 4.20 and 4.21, the shear viscosity calculations by the Cogswell model and the rheometer-developed model are in close agreement. Extruded neat HDPE fiber is extruded without glass fiber reinforcement. The aspect ratio of spherical glass indicates that there is no fiber orientation as melt flows along the extruder for manufacturing the HDPE spherical glass extruded fibers. The HDPE spherical glass fiber flow rate is back calculated here using a rheometer viscosity model and then compared with an experimentally measured flow rate, as depicted in Figure 4.22, and the results are illustrated for the HDPE spherical glass fibers.

During extrusion, the molten composite with some initial orientation and V_F , determined by the V_{In} in the feed and by the mixing action of the screw of the extruder, leaves the extruder and enters the pipe section, as depicted in Figure 4.23, which corresponds to location 1. The composite flow enters the conical section of the die corresponding to location 1 in Figure 4.23. When the melt is forced through the die, extensional and shear forces are generated resulting in extensional and shear flow of the composite melt. The fibers within the melt would reorient in this shear and extensional flow and may compact, resulting in orientation and V_{Out} with values very different from the initial values. These as well as the die temperature would determine the viscosity of the melt within the conical section of the die hole.

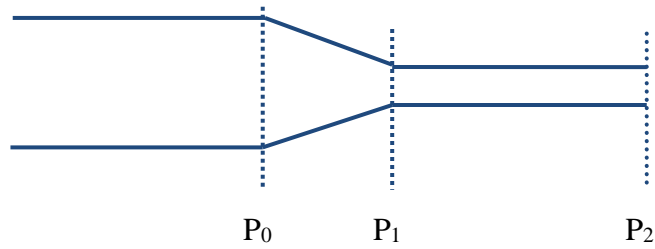


Figure 4-19. Pressure variation along the length of a die hole

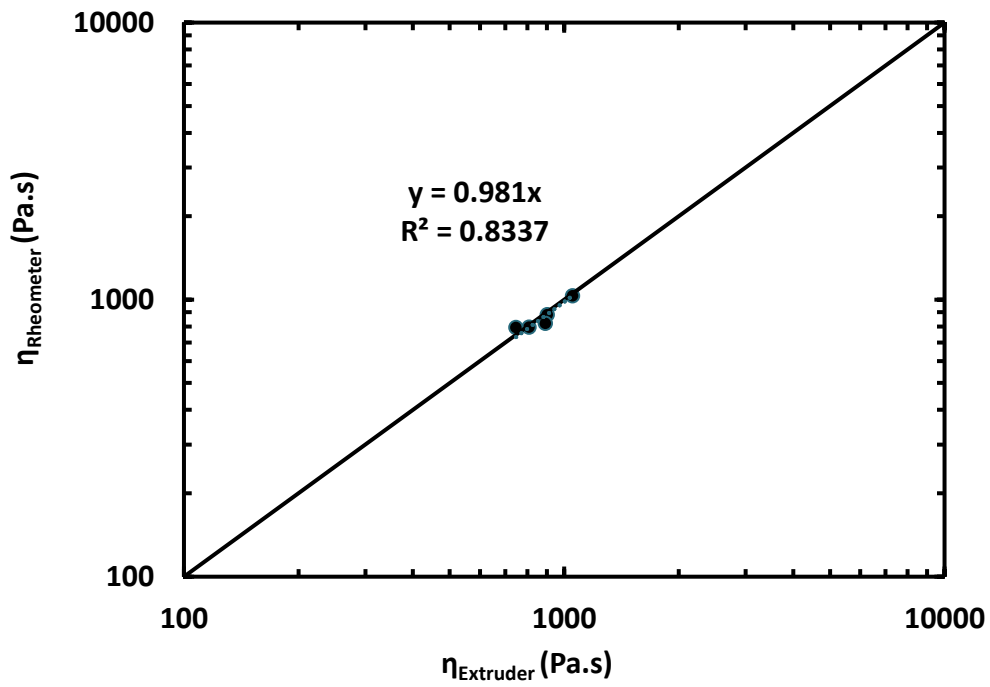


Figure 4.20. Comparison of shear viscosity measured using extruder with shear viscosity measured using Rheometer for HDPE.

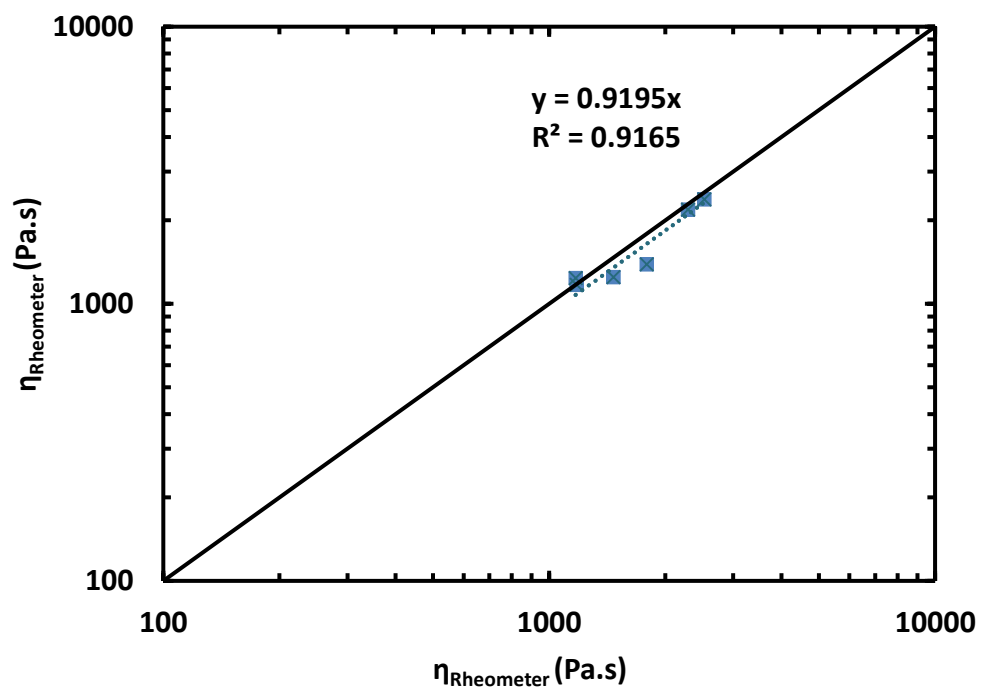


Figure 4.21. Comparison of shear viscosity measured using extruder with shear viscosity measured using Rheometer for HDPE Spherical glass.

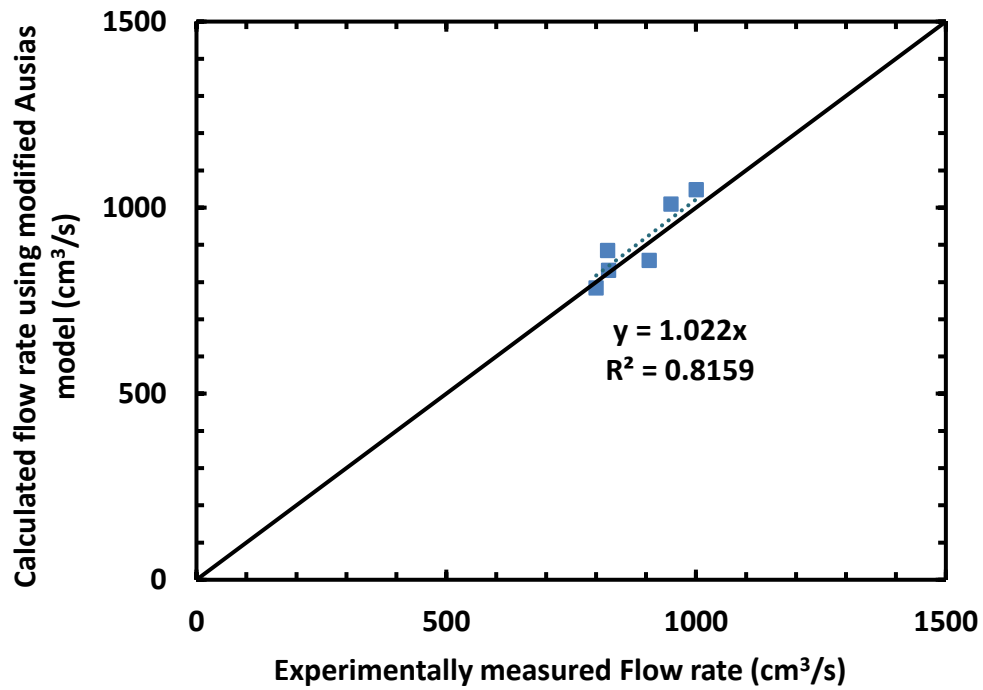


Figure 4.22. Comparison of experimental measured flow rate using extruder with that calculated using modified Ausias model for HDPE Spherical glass composite with $V_F = 4.6, 5.9,$ and 17.8% ..

The V_{Out} and orientation in the composite obtained experimentally correspond to the V_{Out} and orientation in the melt when the melt exits the conical section of the die hole. Afterwards, the melt flows through the land section (Capillary) of the die hole corresponding to location 3 in Figure 4.23. Viscosity is calculated using Cogswell et al. [30] as explained in section 4.2.4.1 used here to aid the analysis. Ideally, the volume fraction and orientation and hence the viscosity would continually change from the entry point to exit point of the conical section of the die hole. However, it is not possible to measure this variation.

The die pressure and melt viscosity within the die would determine the rate of flow of material out of the die. Hence, die pressure and melt viscosity can be considered as independent variables, while the flow rate can be considered as the dependent variable. Once the steady state flow condition is established, a unique combination of die pressure, melt viscosity, and flow rate characterizes the flow condition.

Shear viscosity in the pipe section was calculated according to pressure change across the pipe, flow rate, and pipe geometry, and results were compared with the developed model from Equation (4.6). The pipe viscosity calculation is reported in Appendix A. Since experimentally measuring orientation of fibers inside the pipe is not possible, the orientation values of inside the die (location 2) are used for the pipe section to calculate using the rheometer model. Hence, developed viscosity model prediction (which is based on volume fraction, orientation, and shear rate) is less than viscosity calculated, based on pressure change and flow rate as depicted in Figure 4.24. The reason for this difference is the assumption of using the orientation of inside the die for the pipe section. From inside the die at the entrance of location 2, samples were collected and analyzed through X-ray tomography, and fiber orientation was calculated for 30, 60, 90 degree

angles of die. Subsequently, these measured orientations along pressure data, flow rate, and die geometry used in the Cogswell model to calculate the viscosity for the cone section. Fiber orientation and volume fraction input into the rheometer model were compared with results from the Cogswell model, as illustrated in Figure 4.25. In addition, the flow rate was back calculated using the rheometer viscosity model and compared with experimental measured flow rate, as shown in Figure 4.26 and 4.27. There is a discrepancy between the Cogswell model and rheometer model results, and the source of the difference is because of the limited range of shear rate for extruder measurement which was from 25 (1/s) to 45 (1/s) as well as the assumption of constant fiber orientation as the composite melt flows through the cone.

The rheometer viscosity model and the Cogswell model are in close agreement for the capillary section (land section) of die as shown in Figure 4.27, and the same trend exists for flow rate as illustrated in Figure 4.28.

The elongation viscosity of the composite melt, determined using the procedure described in Appendix A, is plotted as a function of the extensional rate in Figure 4.29 for all dies. The extensional rate was determined using:

$$\dot{\epsilon} = \frac{4Q \tan \theta}{\pi r_1^3} \quad (4.13)$$

$\dot{\epsilon}$ is the extensional rate, Q is the flow rate, θ is cone angle, r_1 is the exit diameter, and n is the power law constant obtained by mathematical fitting of the experimental data.

Due to limitations on the screw speed (as discussed in previous paragraphs), the range of extensional rate achievable in each die is limited. However, the extensional rate achieved in various dies increased in this order: 30-3 < 45-3 < 60-3 (both L/D) < 90-3 < 180-3. This ordering is due to the combined effects of both the die angle and the cone exit diameter. The extensional viscosity of the composite melt within the conical section of the die also decreased in that order.

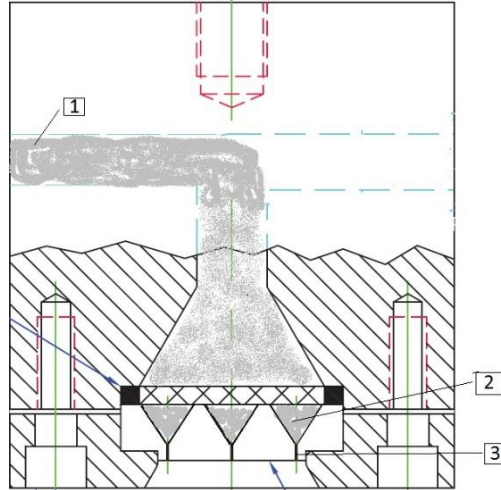


Figure 4.23. Location 1, 2, and 3 where viscosity was calculated with die assembly.

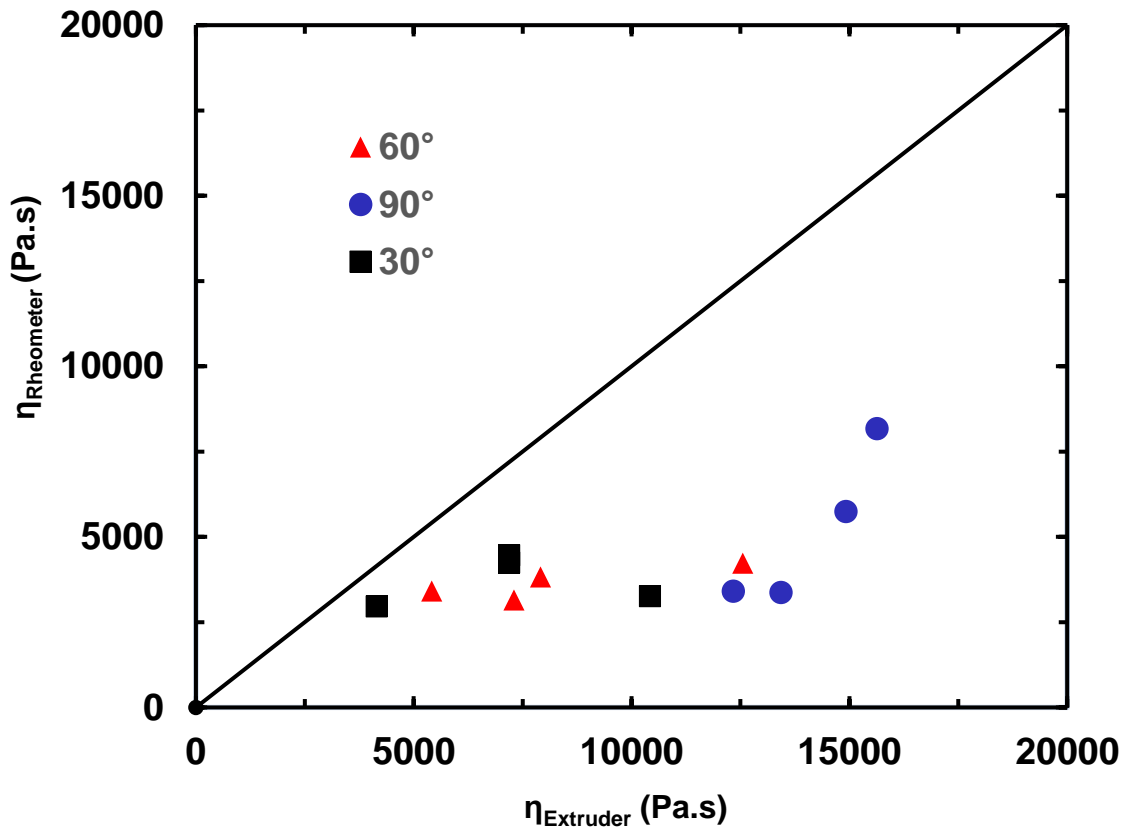


Figure 4.24. Comparison of shear viscosity measured using extruder is location 1 with shear viscosity calculated using modified Ausias Rheometer developed model for HDPE glass fiber composite with $V_F=9.1, 14, 20,$ and 27 .

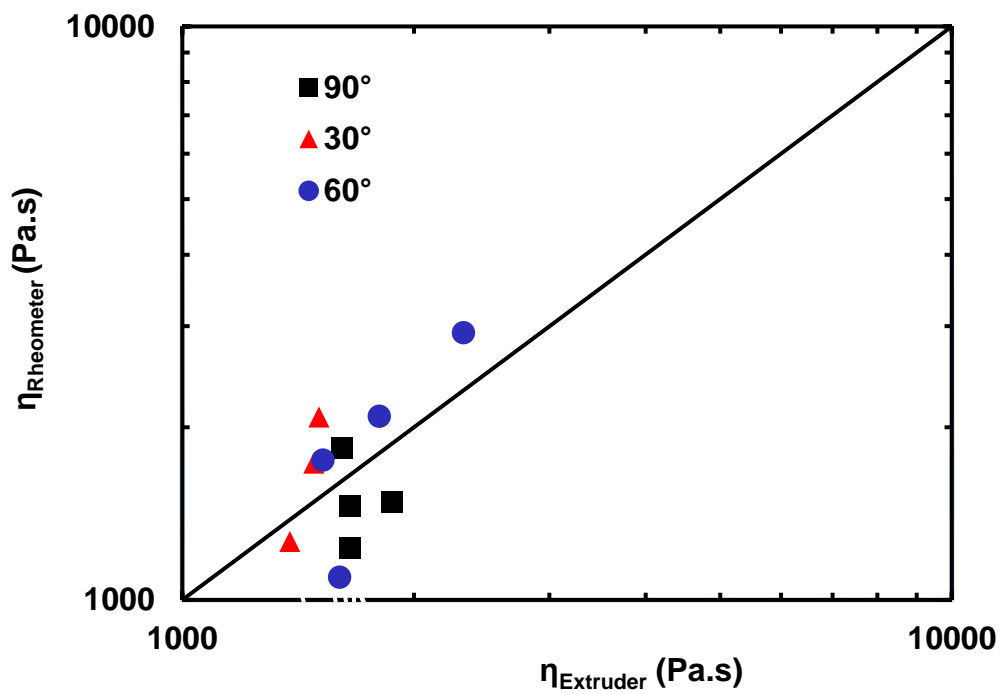


Figure 4.25. Comparison of shear viscosity measured using extruder is location 2 with shear viscosity calculated using modified Ausias Rheometer developed model for HDPE glass fiber composite with $V_F=9.1, 14, 20,$ and 27 .

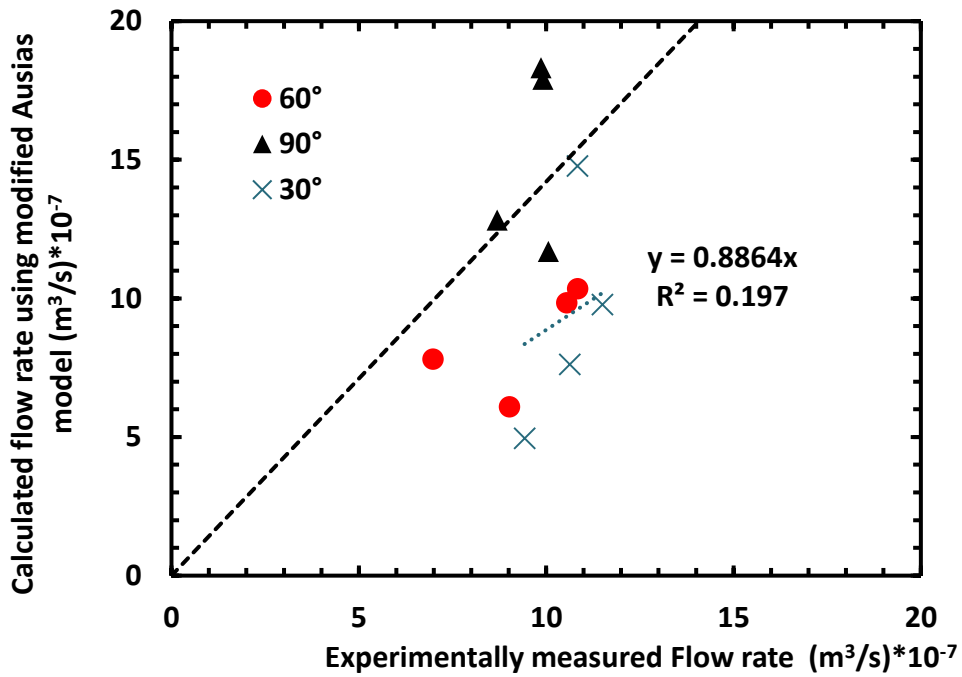


Figure 4.26. Comparison of experimental measured flow rate in location 2 with that flow rate calculated using modified Ausias model for HDPE fiber glass composite with $V_F=9.1\%$, 14% , 20% , and 27% .

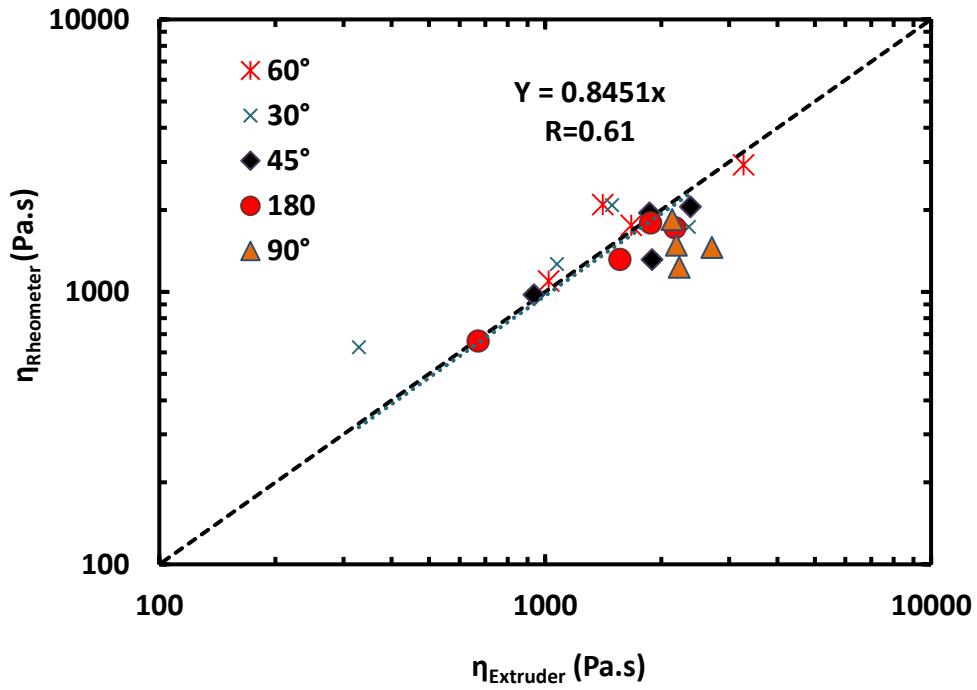


Figure 4.27. Comparison of shear viscosity measured using extruder in location 3 with shear viscosity calculated using modified Ausias Rheometer developed model for HDPE glass fiber composite with $V_F=9.1\%$, 14%, 20%, and 27%.

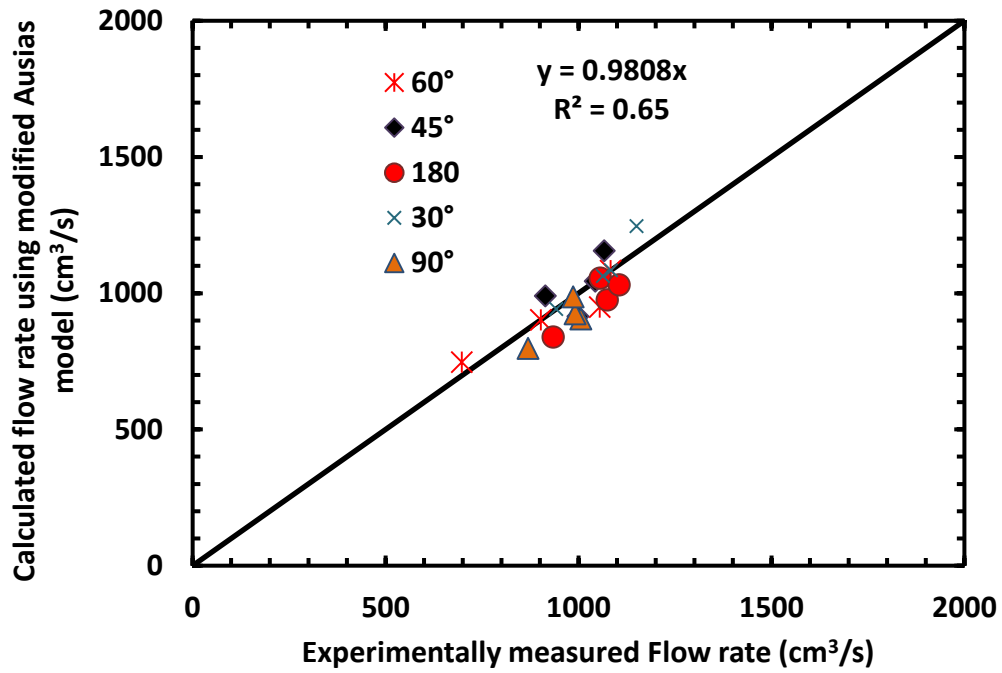


Figure 4.28. Comparison of experimental measured flow rate in location 3 with that flow rate calculated using modified Ausias model for HDPE fiber glass composite with $V_F=9.1\%$, 14% , 20% , and 27% .

The data in this plot clearly shows the effect of die geometry on the extensional viscosity of the melt within the die. The extensional viscosity also exhibits a non-Newtonian behavior; i.e., it decreases with an increase in the extensional rate.

In summary, viscosity is a result of the microstructure of melt, which is a function of orientation and volume fraction. As fibers rotate, the viscosity of melt changes within the die impacts pressure and subsequently the required flow rate. Next, fiber rotation inside the cone and capillary sections were studied through the Dinh-Armstrong model to predict fiber rotation due to shear and elongation strain imposed by die geometry.

4.2.2.3 Fiber orientation modeling

Shaqfeh and Fredrickson [69] modified Batchelor's [27] model to calculate the effect of fiber-fiber interaction on stress tensor and used viscosity as a function of particle concentration and its aspect ratio. Tucker [40] proposed a model to calculate stress tensor and the viscosity used in its calculation. Azaiez et al. [62] predicted fiber orientation in flow through different channels, and viscosity was one of the key parameters to calculate fiber orientation along the streamline. All the above models were used to predict flow in injection modelling; however, no previous study looked into fiber orientation changes in twin screw extruder usage and its impact on structural changes in viscosity within the twin screw extruder assembly.

Using FOD at the die entry, the extensional and shear strains imposed by the die design, and the Dinh-Armstrong model, the fiber rotation (and this changes in FOD) within the die was predicted and analyzed to delineate the combined effect of die design and extrusion variables on the fiber orientation in the extruded composite.

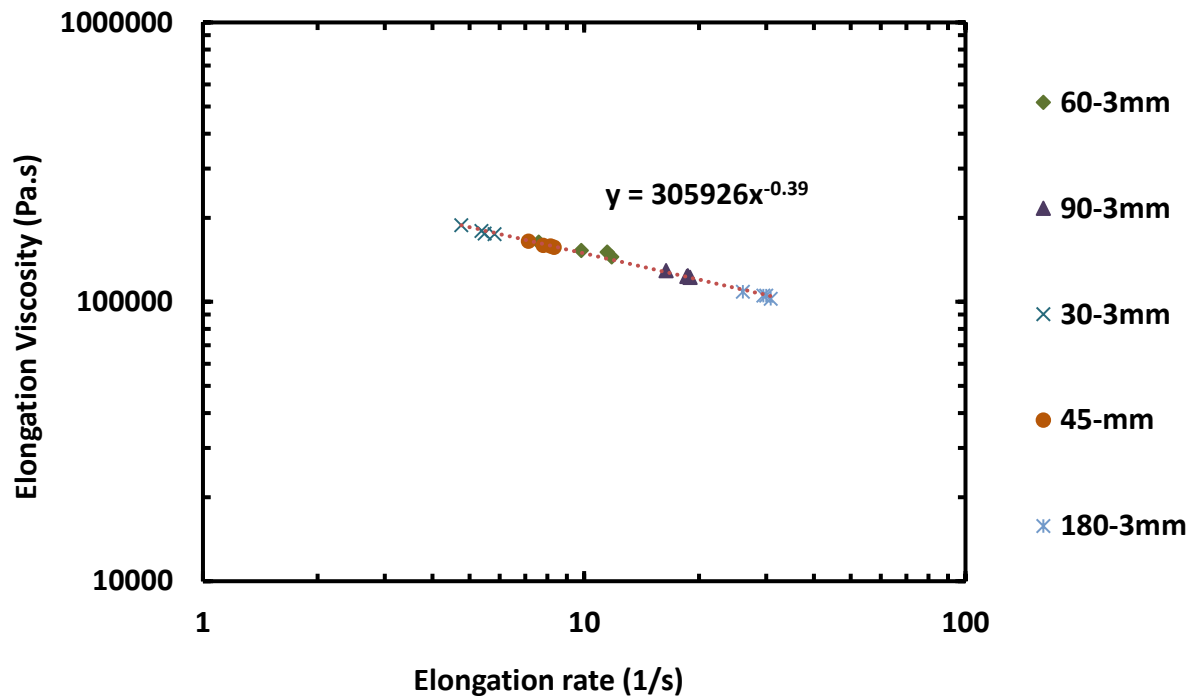


Figure 4.29. Elongation viscosity as function of elongation rate calculated using Cogswell model in location 2 for HDPE glass fiber composite with $V_F=9.1\%$, 14%, 20%, and 27%.

Dihn-Armstrong model are applicable to dilute composite solutions; however, these have been applied to concentrated composite solutions used in this thesis. Based on these results, recommendations are made on optimal die design.

The orientation of the fibers within the composite fiber is analyzed in this thesis in terms of θ (the angle between the fiber axis and z -axis extrusion axis) and φ (the angle between the x -axis and either the fiber axis or its projection onto the x - y plane, as shown in Figure 3.11. Orientation measurements were conducted inside the die and in the final fiber composite, as illustrated in Figure 4.30. Fiber orientation distribution (θ , φ) for 90° is depicted in Figures 4.31 (a) and 4.31 (b) and show here fiber orientation changes when the melt travels through the cone and capillary section. Hence, the Armstrong fiber rotation model is implemented here to understand the orientation changes in the die assembly.

Batchelor [27] was the first to develop a constitutive equation for Newtonian particle suspension at any concentration, and Dinh-Armstrong [28] modified the Batchelor [27] model for semi-concentrated suspensions and calculated drag force on neighboring particles. In order to calculate the rheological property of flow, Armstrong proposed a shear flow model which describes fiber rotation by Equation (4.14):

$$\theta = \arctan(\tan\theta_0 \left[\gamma^2 \sin^2\varphi_0 + 2\gamma \sin\varphi_0 \cos\varphi_0 + 1 \right]^{1/2})$$

$$\varphi = \arctan\left(\frac{1}{\cot\varphi_0 + \gamma}\right) \quad (4.14)$$

where γ is the total shear strain measured from the start of the flow. The initial fiber orientation is given by (θ_0, φ_0) . Fiber orientation with respect to the extrusion axis is θ , while the in-plane fiber orientation is φ . The Armstrong fiber rotation model for elongation flow on fibers with an initial orientation of (θ_0, φ_0) is given by Equation (4.15):

$$\theta = \text{arc tan} (e^{-\left(\frac{3}{2}\right)\epsilon} \tan\theta_0) \quad (4.15)$$

where ϵ is the elongation strain, and fiber rotation has exponential correlation to applied strain; therefore, fibers are expected to orient faster in elongation flow.

Hine et al. [5] used the Armstrong elongation flow model to predict fiber orientations in hydrostatically extruded glass-fiber polyoxymethylene through 15 degree converging die. Even though the Armstrong model was applied to a concentrated suspension of $V_F=14\%$, prediction and experimentally measured orientation are in close agreement.

Here, in order to determine initial fiber orientation before entering locations 2 and 3 in the die assembly (Figure 4.30), samples were collected from inside the die for 30, 60, and 90 degrees die for volume fraction of 9.1%, 14%, 20%, and 27%. These samples were x-rayed and further analyzed by image analysis software to find orientation of fibers.

As melt flows through the converging conical section of the die, fibers are subjected by elongation and shear strain because of die geometry. After fiber melt reaches the capillary section of the die, the only strain is shear. An algorithm developed here simulated the effect of shear and elongation strain on the fiber orientation change in the die using the Armstrong shear and elongation model, as depicted in Figure 4.32. As the flow chart shows in Figure 4.32, shear strain is first applied to the initial fiber orientation, and subsequently, elongation strain inside the cone is applied. Since shear and elongation strain are applied in steps, algorithm steps for cone strain continues until geometrical shear and elongation reach the cone section.

Following the cone section, there is the capillary section in which the only strain is shear strain. Shear strain is calculated based on melt residence time inside the capillary section along with the shear strain rate inside the capillary section. The converging criteria for the algorithm are a_{1313} and a_{3333} value corresponding to shear and elongation strain steps and their difference with

experimentally measured a_{1313} and a_{3333} for fibers extruded from 30, 60, and 90 die. As shown in Figure 4.33, the initial fiber orientation is different for 30°, 60°, and 90° die angles because of different die geometry, which in conjunction with viscosity requires different pressure to push the melt through the die.

The cone and capillary sections are identified in Figures 4.34-4.45, and changes in a_{3333} and a_{1313} illustrated that fiber orientation evolves beyond the cone section, while fiber alignment continues inside the capillary section. Cone section in Figures 4.34-4.45 is identified in which only shear strain up to 0.75 is applied on glass fibers and subsequently any shear strain beyond 0.75 is imposed in capillary section of the die, which is marked as capillary section on the Figures 4.34-4.4. In addition, the Armstrong model simulation results highlight that shear strain (the only type of strain inside the capillary section) has significant influence on fiber rotation since a_{3333} and a_{1313} continue to change inside the capillary section, as depicted in Figures 4.34-4.45. Transition happens in a_{3333} and a_{1313} predictions as fiber leaves the cone and enters the capillary section, as shown in Figure 4.30. These transition regions correspond to changes in cross section from cone to capillary section.

Also as depicted in Figures, 4.34-4.45 elongation strain (imposed only in the cone section) is not enough to reach the experimentally measured orientation, therefore the capillary section has a significant impact on orientation beyond the cone section. Another interesting observation is that for a lower volume fraction it takes less strain to reach the experimental value for a_{3333} , and it is important to understand this initial fiber orientation distribution plotted in Figure 4.46. For example, fibers extruded through a 30 degree die with a V_{In} of 9.1% have a_{3333} starting value of 0.79 and reach to the experimental measurement a_{3333} after an elongation strain of 1.70. In contrast, as depicted in Figure 4.36, for V_{In} of 25%, the a_{3333} starting value is 0.32 which does not

converge to the experimental measurement a_{3333} in the extruded fiber composite based on the developed model. Comparing Figures 4.34 and 4.43 shows that a_{3333} corresponding to $V_{In} = 9.1\%$ converges to experimental values faster than $V_{In} = 25\%$. As expected, it takes less shear strain for $V_{In} = 9.1\%$ to orient the fiber because of less fiber entanglement, or more room for fiber rotations.

Empirical modeling results indicate that fiber orientation changes continue to happen inside the capillary section of the dies assembly (the cone and capillary sections are identified in Figures 4.34-4.45). The conducted simulation confirmed experimental measurements that the least V_{In} exhibits a higher alignment (a_{3333}) to the extrusion axis, and an angle of 30° resulted in the best alignment, followed by 90° . A 60° die angle offers the least alignment among the three dies. The difference in alignment among the three dies is the result of different initial fiber orientations (Figure 4.46 depicts the initial orientation condition for 30°), which is effect of structural changes inside the die as a result of the melt viscosity.

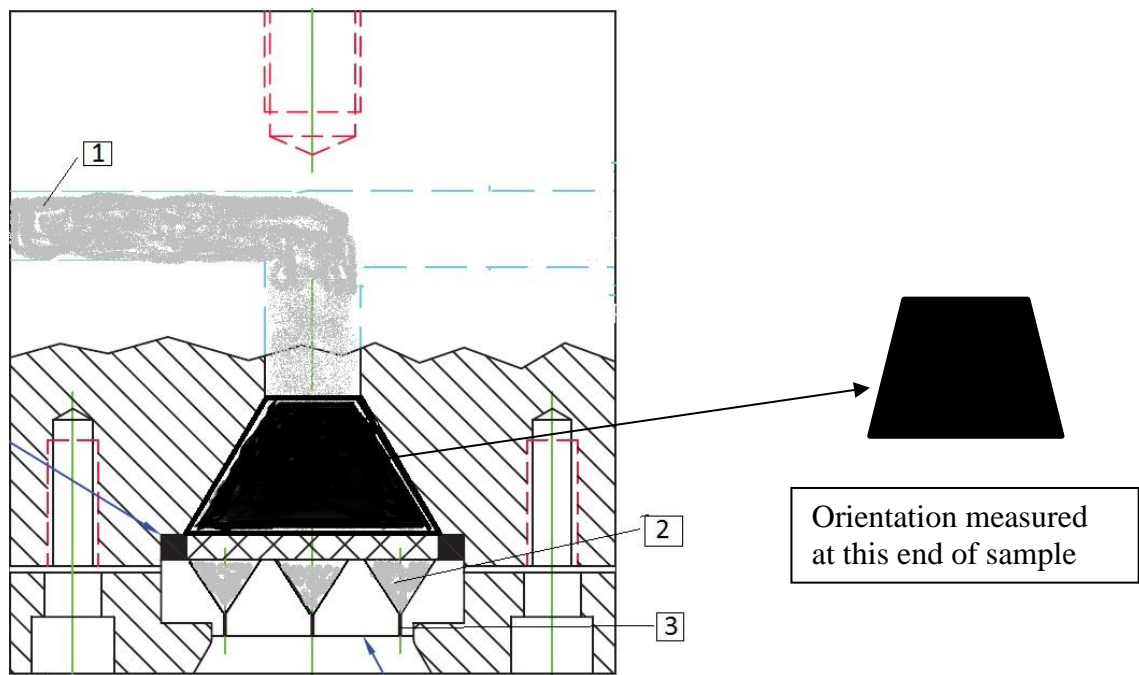


Figure 4.30. Location for measurement of initial fiber orientation

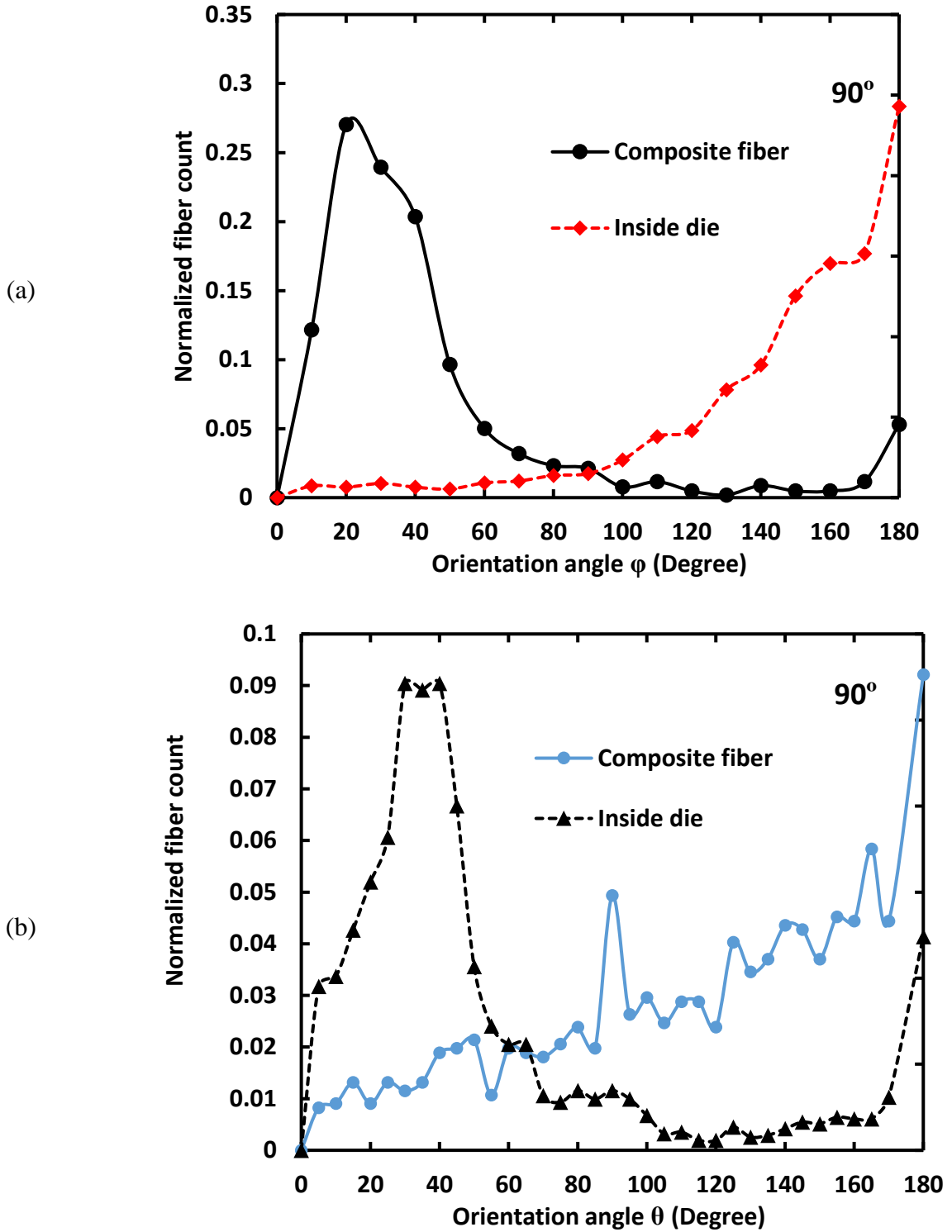


Figure 4.31. Comparison of fiber orientations inside the die and in the final fiber composite. (a) ϕ with respect to extrusion direction (Z) and (b) is in plane (XY) orientation angle of θ with respect to X axis.

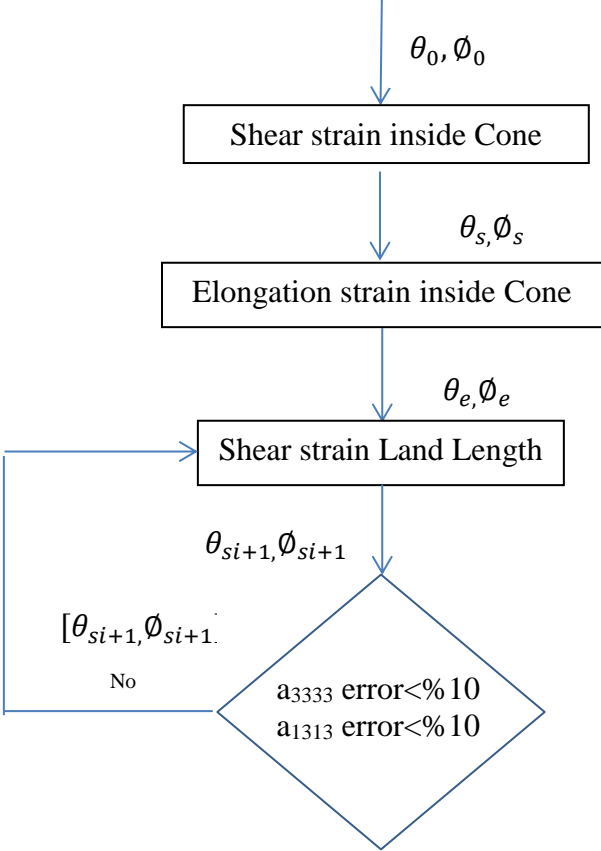


Figure 4.32. Fiber rotation model

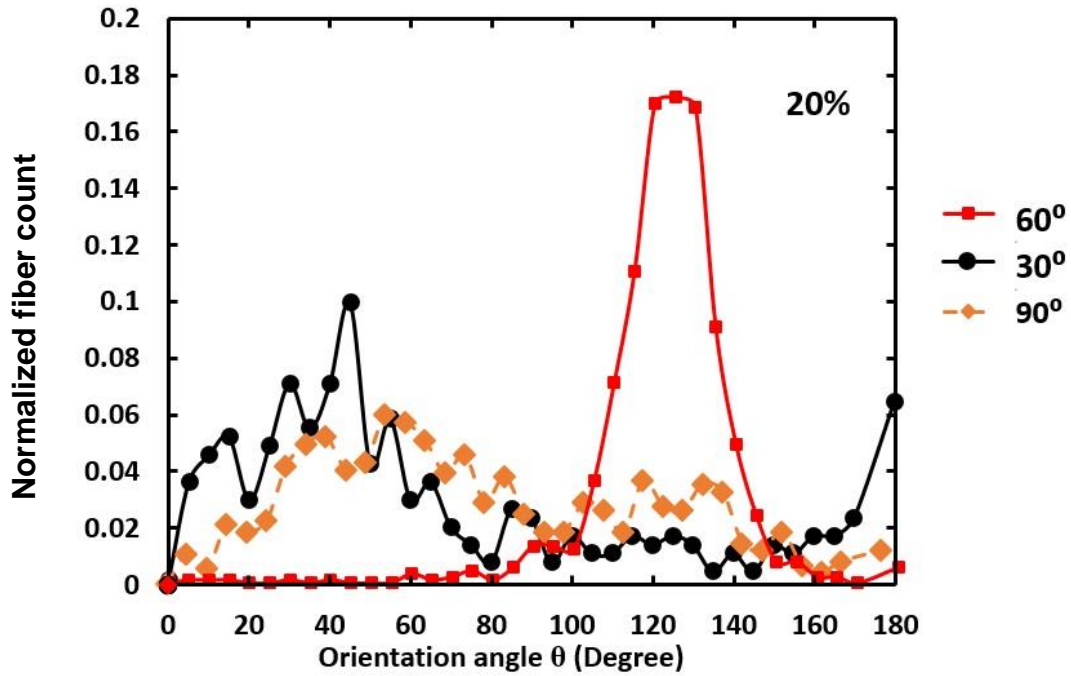


Figure 4.33. Initial fiber orientation distribution at die cone entry for 30°, 60°, and 90° die

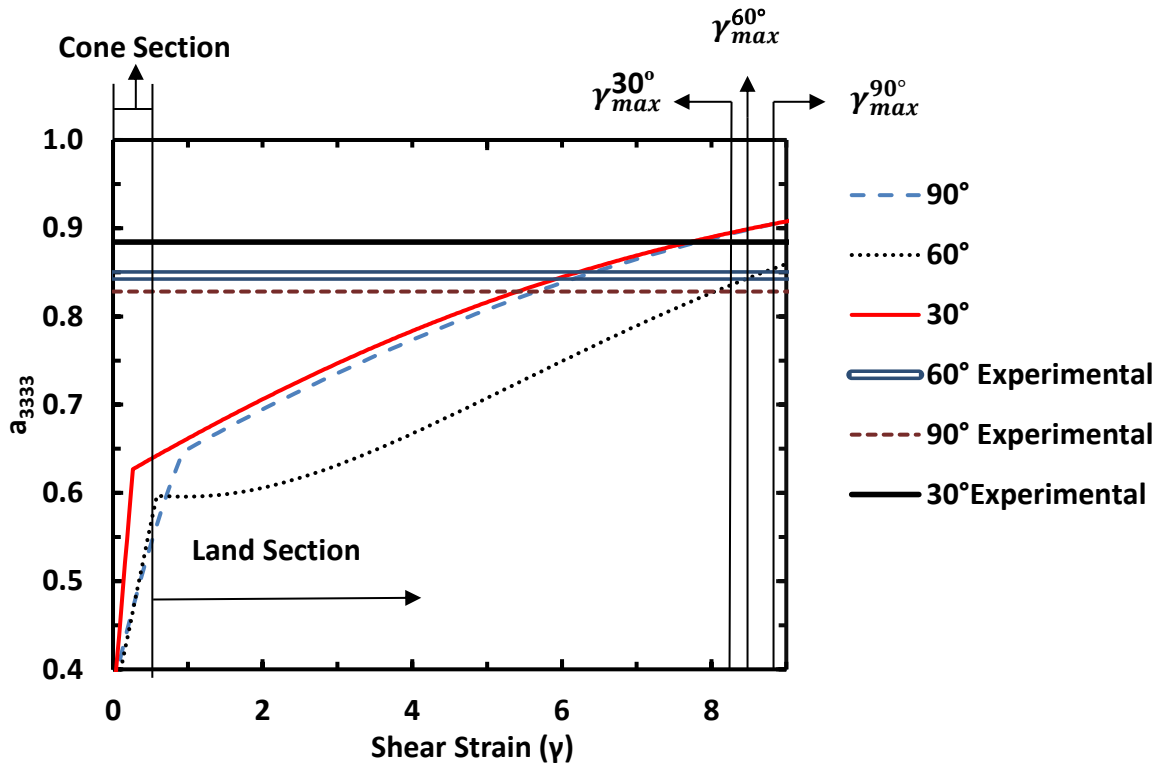


Figure 4.34. Armstrong model prediction of a_{3333} for composite ($V_{In}= 25\%$) manufactured using 30, 60, 90 degree die.

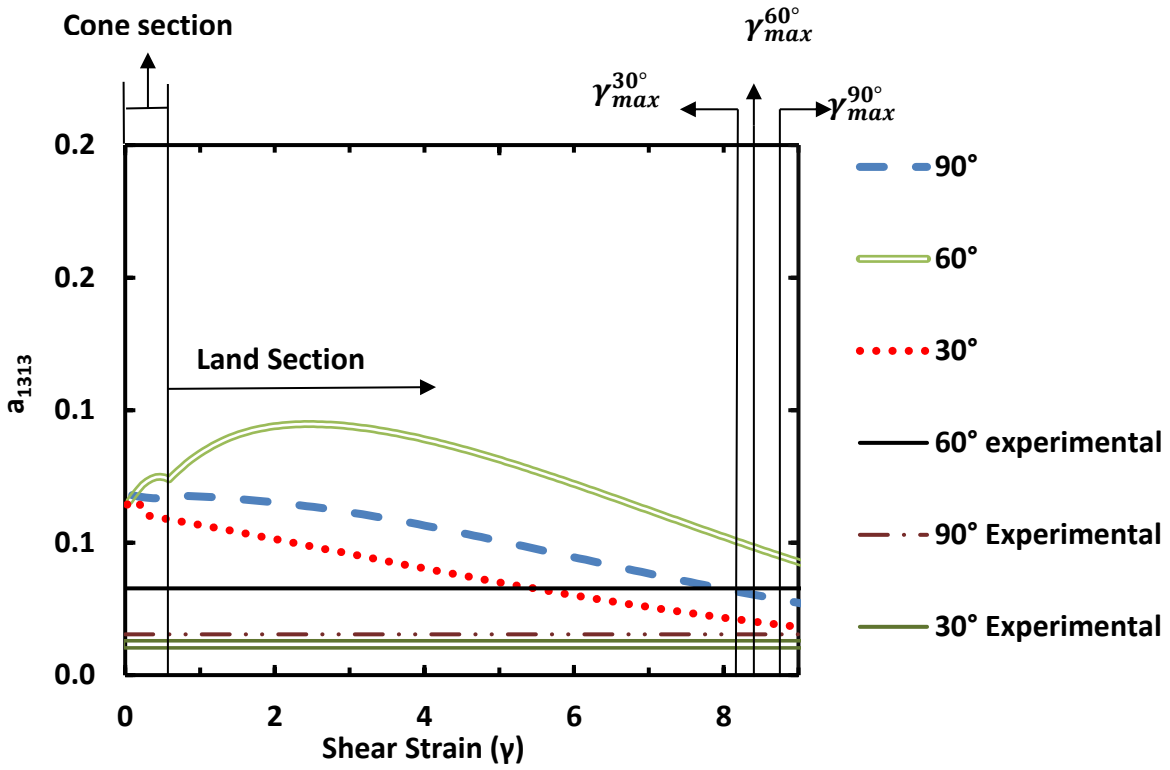


Figure 4.35. Armstrong model prediction of a_{1313} for composite ($V_{ln} = 25\%$) manufactured using 30, 60, 90 degree die.

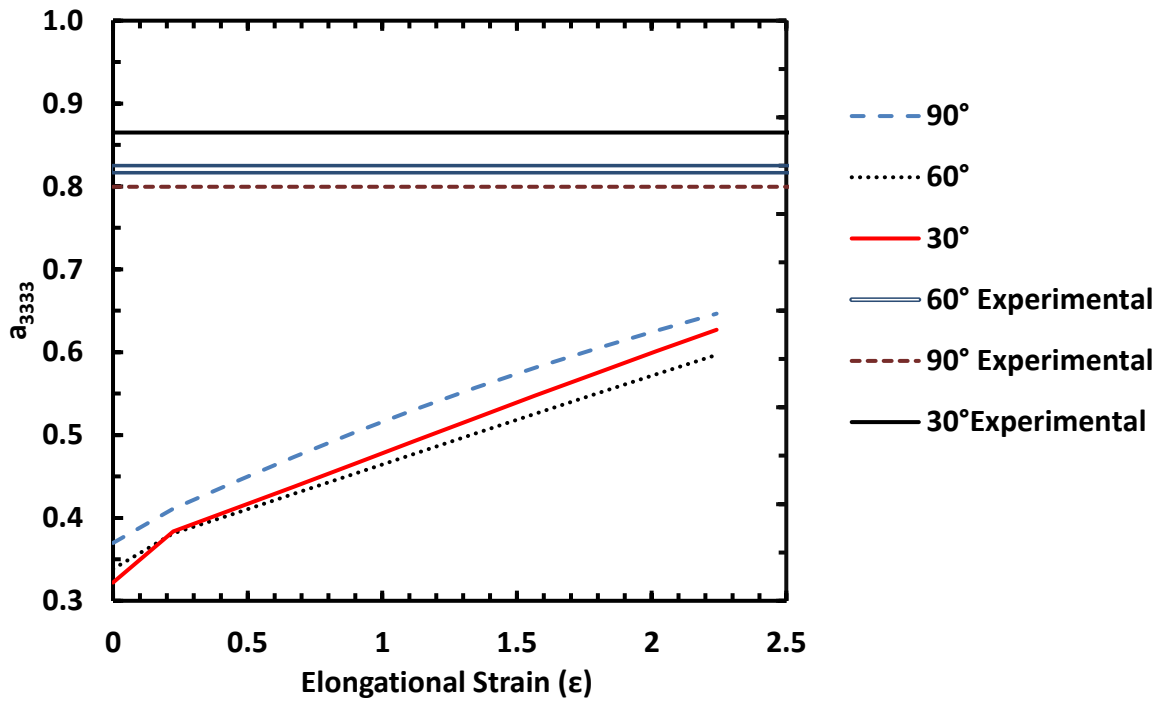


Figure 4.36. Armstrong model a_{3333} prediction vs changes in elongational strain for 30, 60, and 90 degree die at volume fraction of $V_{In} = 25\%$

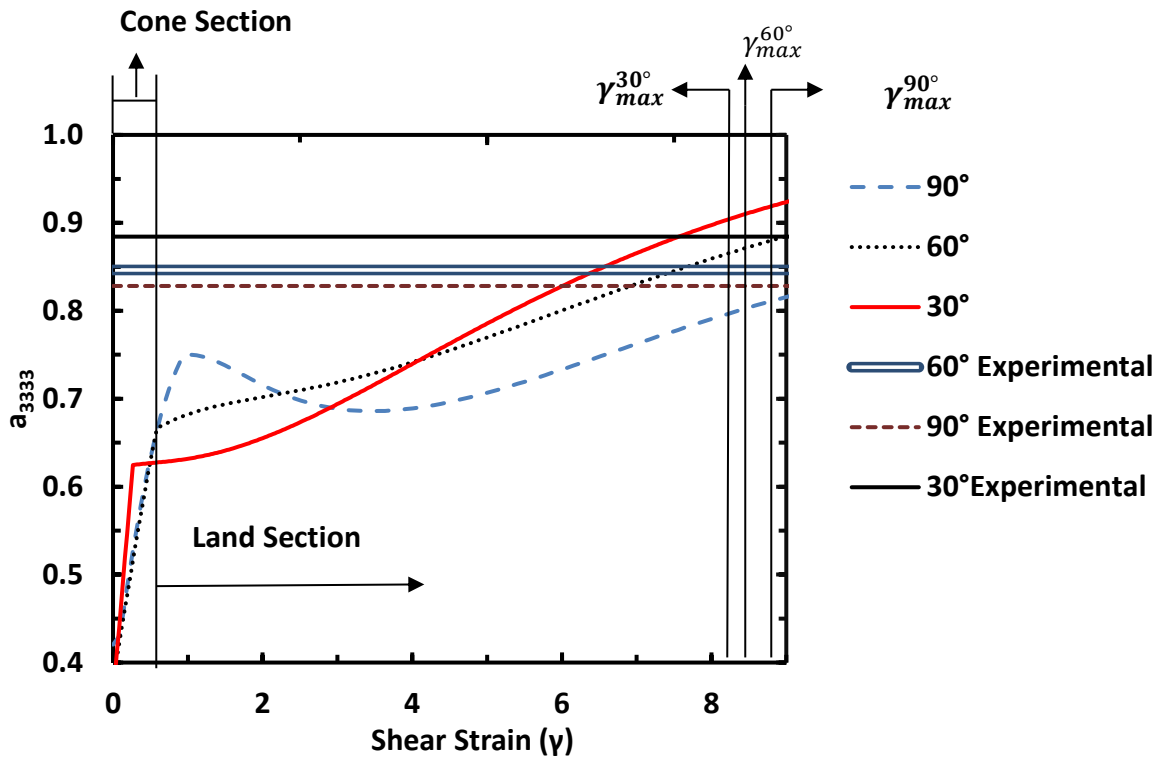


Figure 4.37. Armstrong model prediction of a_{3333} for composite ($V_{In}= 18\%$) manufactured using 30, 60, 90 degree die.

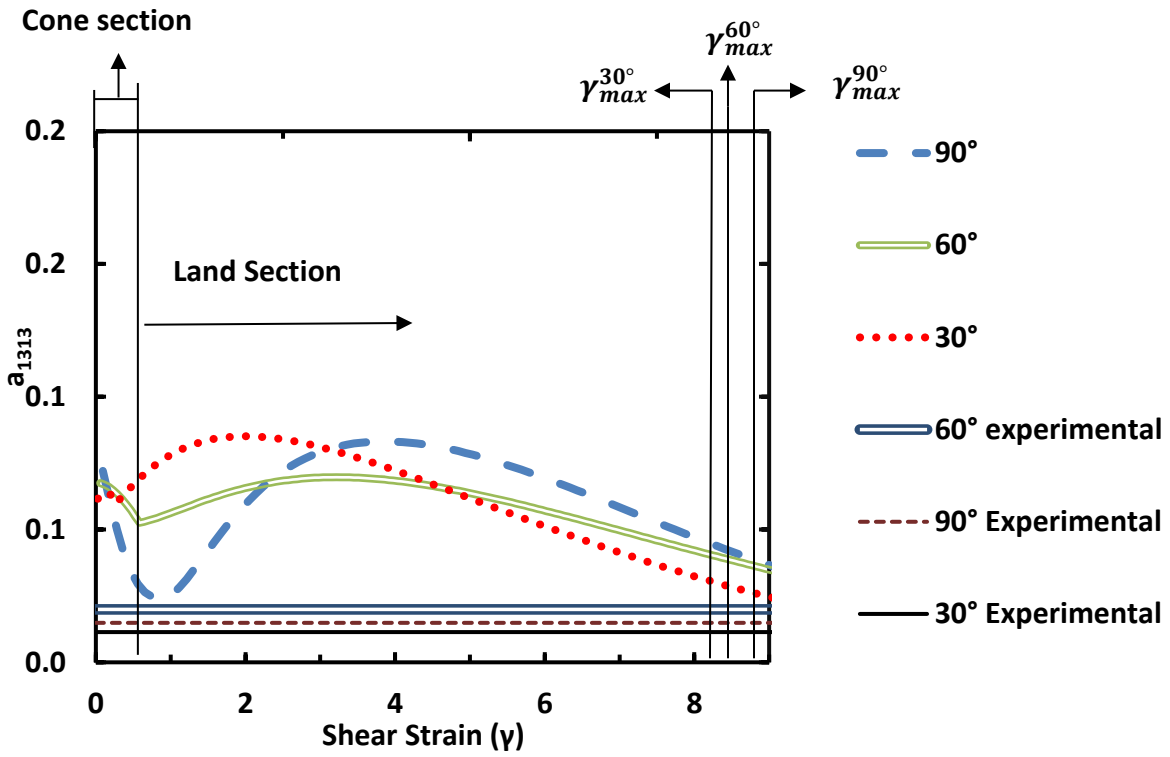


Figure 4.38. Armstrong model prediction of a_{1313} for composite ($V_{In}= 18\%$) manufactured using 30, 60, 90 degree die.

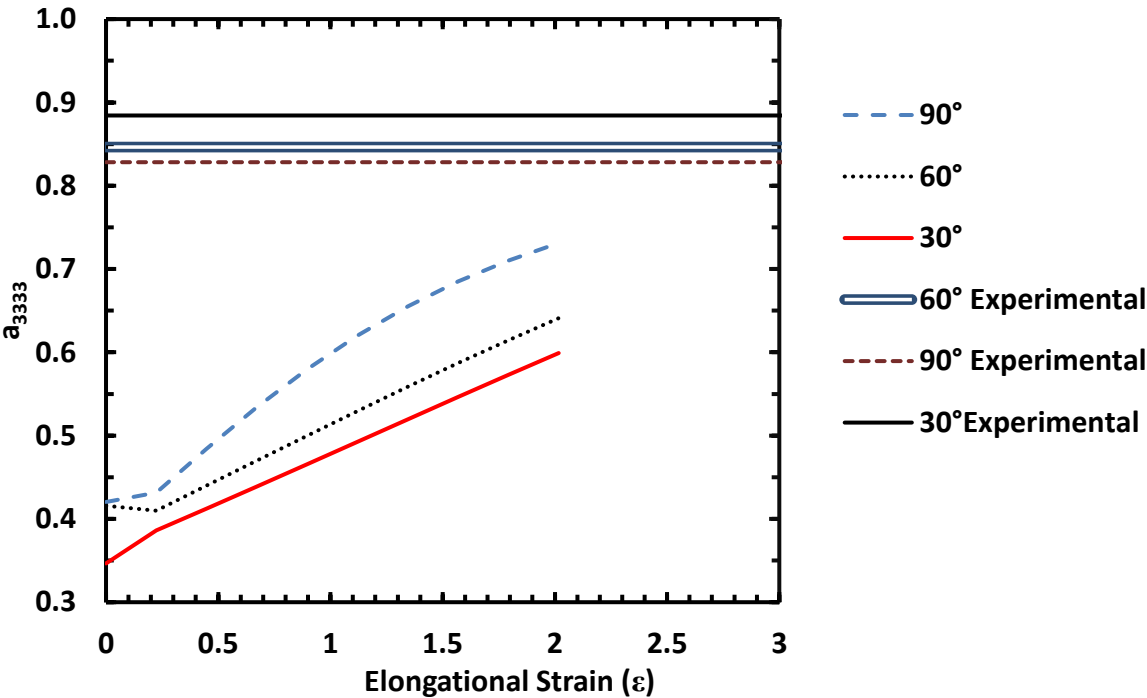


Figure 4.39. Armstrong model prediction of a_{3333} for composite ($V_{In} = 18\%$) manufactured using 30, 60, 90 degree die.

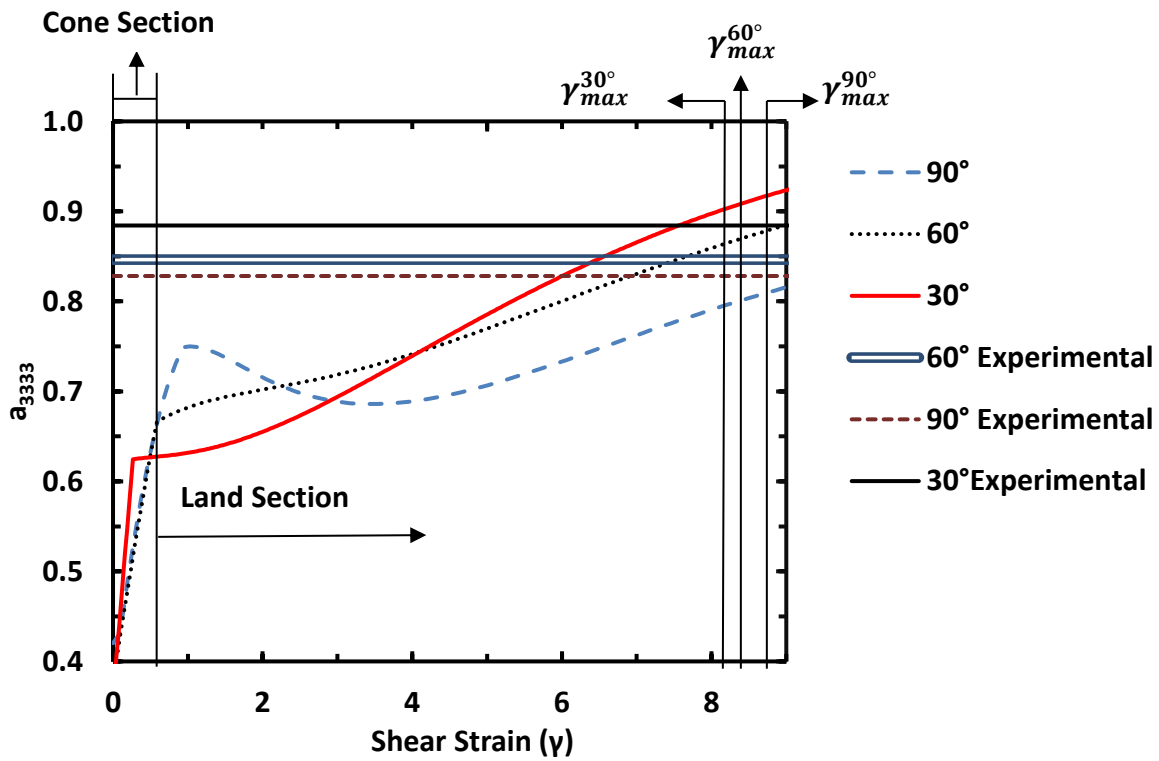


Figure 4.40. Armstrong model prediction of a_{3333} for composite ($V_{In}= 12\%$) manufactured using 30, 60, 90 degree die.

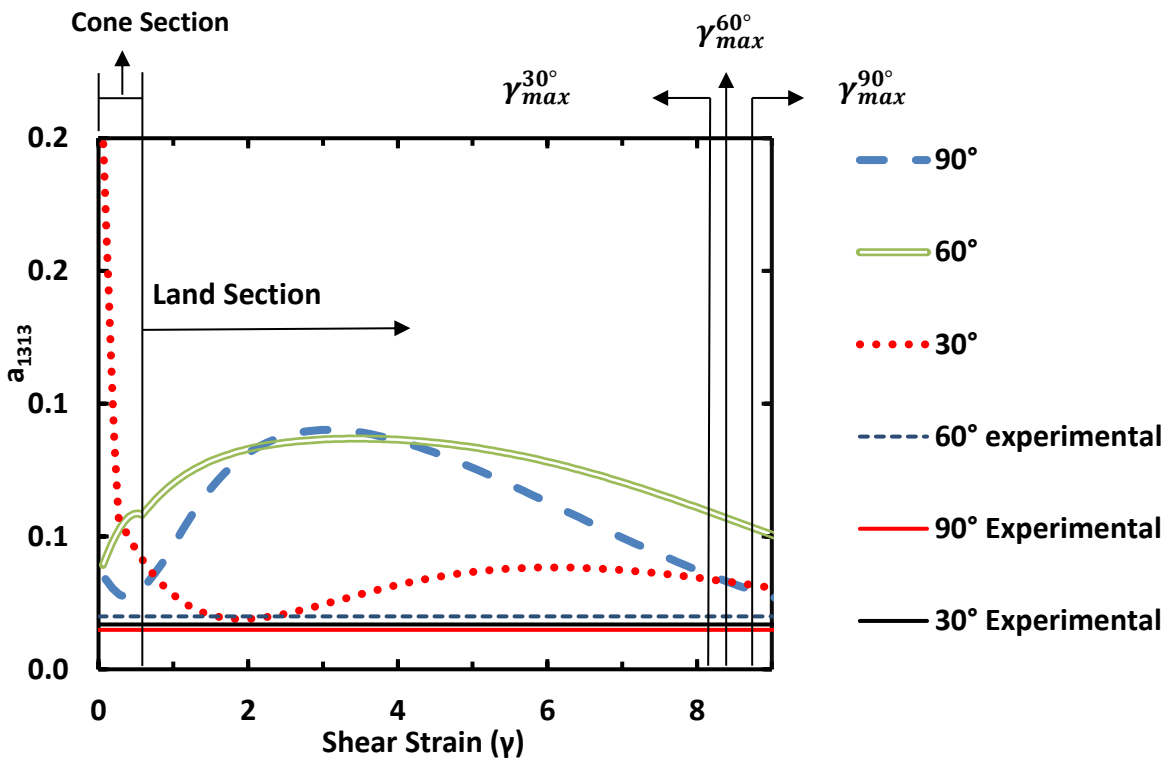


Figure 4.41. Armstrong model prediction of a_{1313} for composite ($V_{In}= 12\%$) manufactured using 30, 60, 90 degree die.

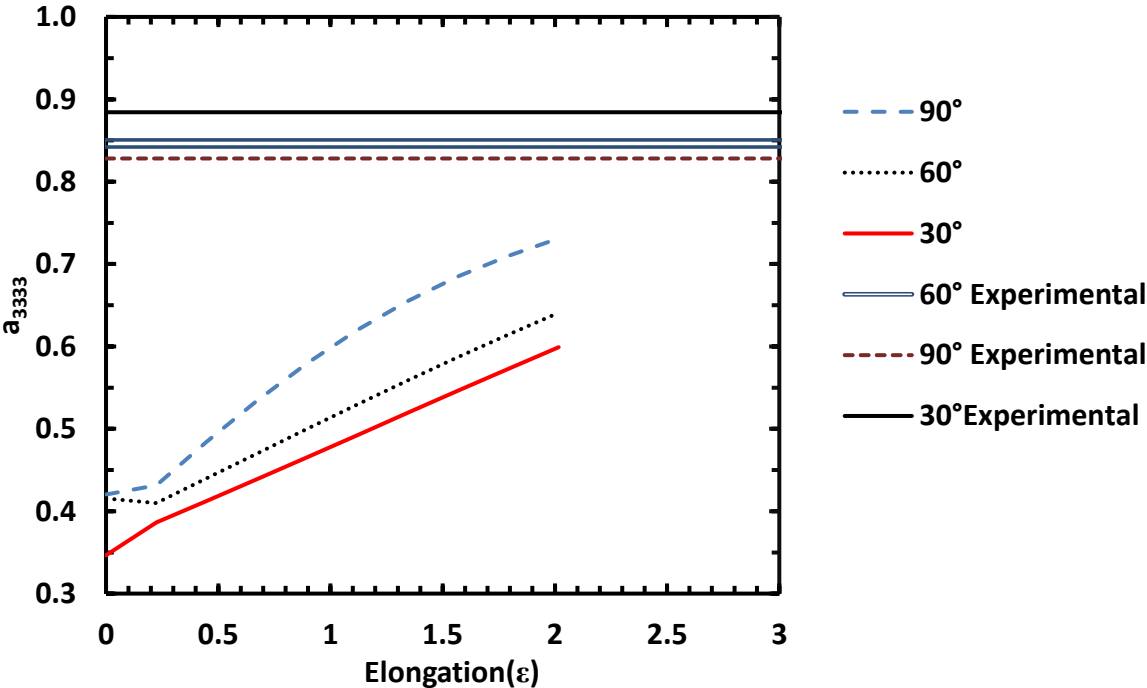


Figure 4.42. Armstrong model prediction of a_{3333} for composite ($V_{In} = 12\%$) manufactured using 30, 60, 90 degree die.

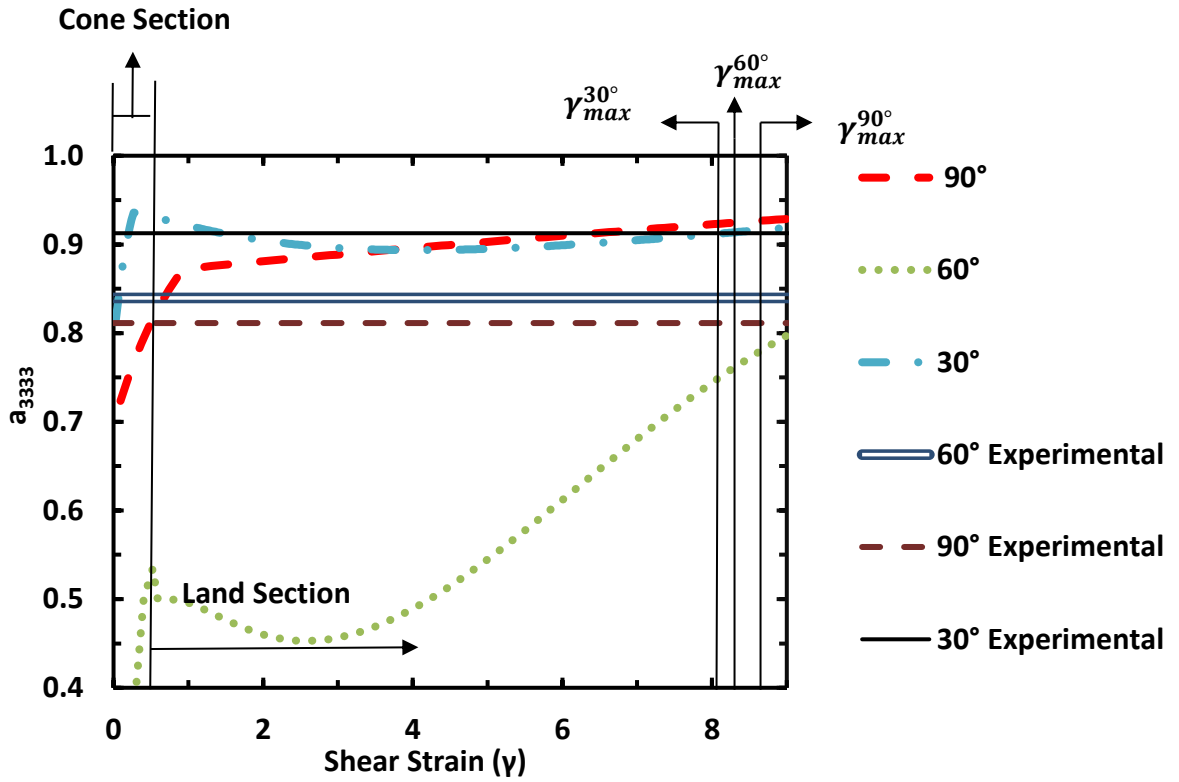


Figure 4.43. Armstrong model prediction of a_{3333} for composite ($V_{In} = 9.1\%$) manufactured using 30, 60, 90 degree die.

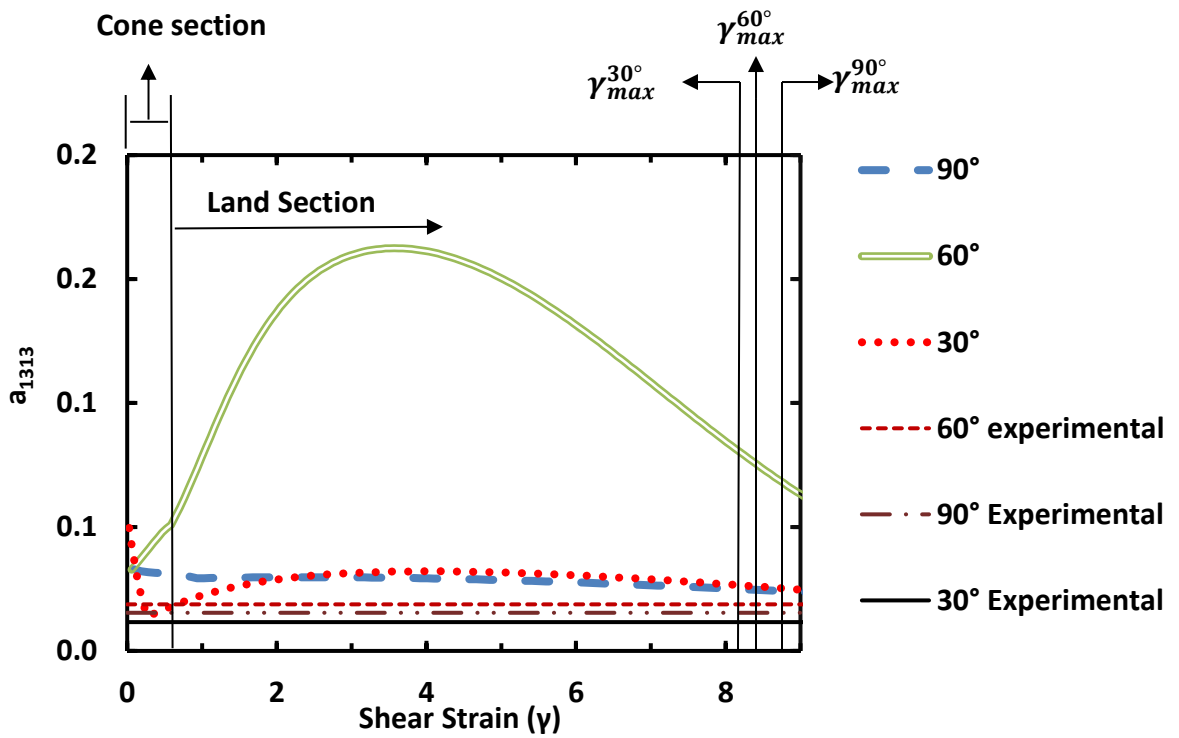


Figure 4.44. Armstrong model prediction of a_{1313} for composite ($V_{In}=9.1\%$) manufactured using 30, 60, 90 degree die.

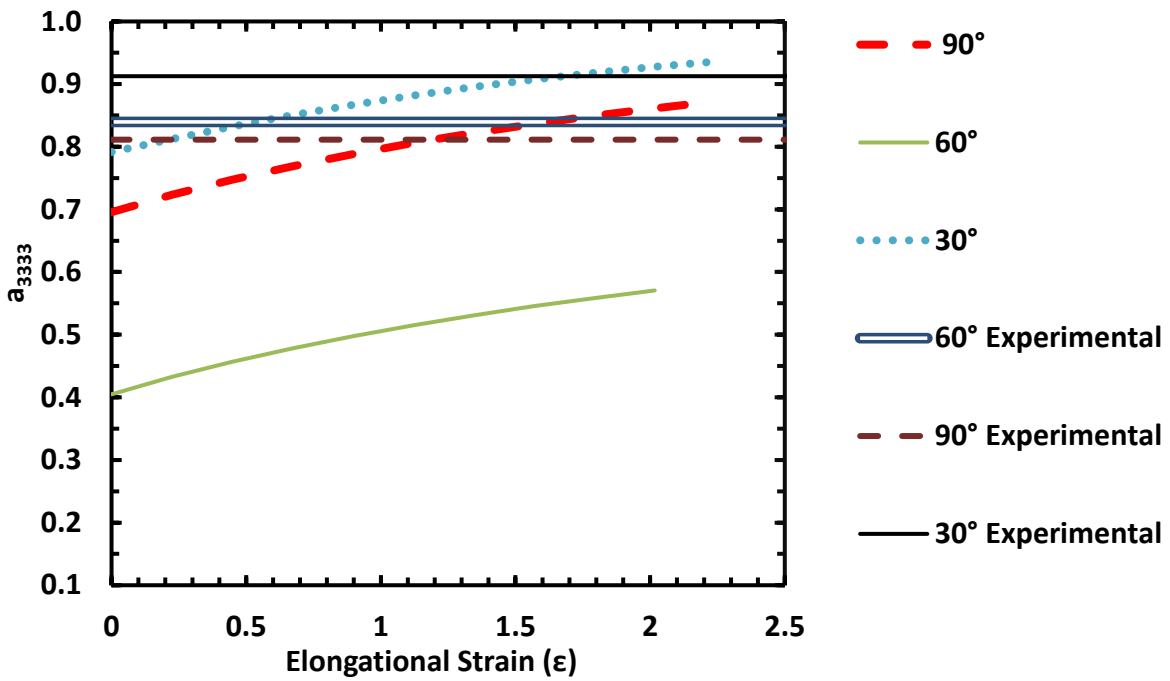


Figure 4.45. Armstrong model prediction of a_{3333} for composite ($V_{In}= 9\%$) manufactured using 30, 60, 90 degree die.

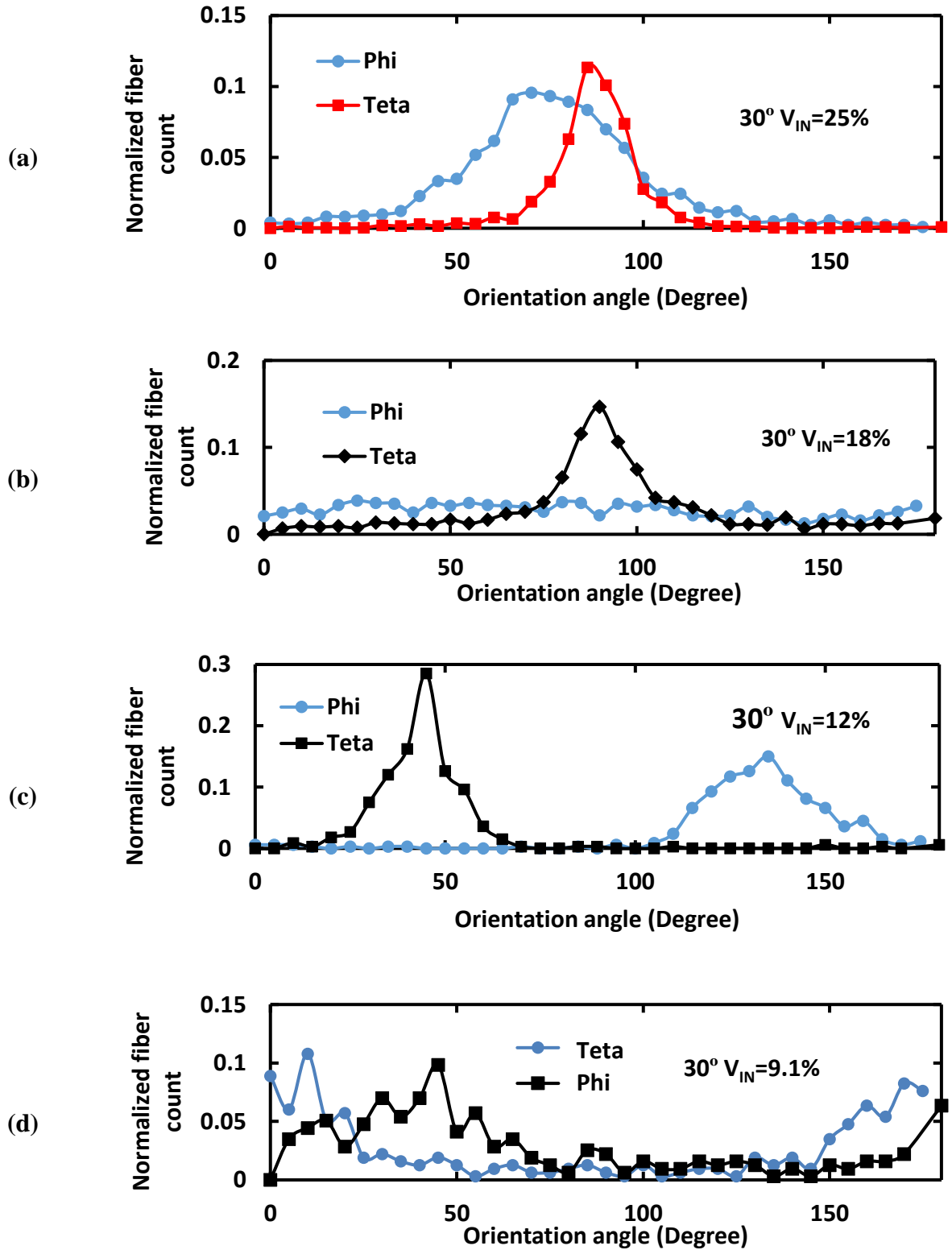


Figure 4.46. Initial fiber orientation distribution for fiber composite in the cone region of 30° die for various die.

The Dinh-Armstrong model is implemented to empirically study the effect of shear and elongation strain independently on orientation as the melt flows through the die. Under these conditions, both elongation and shear strain imposed by the die induce fiber rotation.

Shear strain alone has a substantial effect on orientation, and the higher the initial orientation (the solid line in Figure 4.47) along the extrusion direction, the lower the degree of fiber rotation. The actual measured a_{3333} (where the higher value of a_{3333} is indicative of a higher alignment toward the extrusion direction) thus reached the plateau value, as illustrated in Figure 4.48. In contrast, as the initial orientation (the dotted line in Figure 4.47) along the extrusion direction decreases, the shear strain induces a higher degree of fiber rotation toward the extrusion axis.

In case of elongation strain, only the fiber orientation changes monotonically from the initial to the final value, as illustrated in Figure 4.48. Regardless of the initial orientation value, the elongation strain has the same magnitude of increase on fiber orientation change. The higher the value of initial orientation, the less amount of strain is required to rotate the fiber so the die can be designed with a shortened land length and die angle.

As illustrated in Figure 4.48, elongation strain induces less fiber rotation compared to shear strain; therefore, to only rely on elongating strain to rotate fibers without shear strain, a larger die (higher $d_{\text{exit}}/d_{\text{inlet}}$) is required to generate enough elongation strain. This change requires higher pressure to push the material through the die. However, the objective for die design is to achieve maximum rotation through both shear and elongation with the smallest die possible because of manufacturing constraint and quality of final spun fiber. By increasing the die angle, shear increases will result in higher orientation values, provided that the initial orientation is random (the

least oriented along the extrusion direction). In the extrusion process initial orientation cannot be controlled.

The Dinh-Armstrong model was also verified by simulating known fiber orientation distribution undergoing shear strain in the rheometer. The final sample was tested in the rheometer, then analyzed in x-ray tomography to find out the final fiber orientation distribution. Subsequently, the x-ray tomography orientation measurements were compared with the Dinh-Armstrong model's predictions and tabulated in Tables 4.12 and 4.13. The a_{3333} and a_{1313} predictions are in close agreement with experimental data.

4.3 Nanocomposite fiber orientation

Conductive polymers have application in polymer based electronic and biosensors; however, controlling the mechanical properties and stability of these materials has been a challenge. Furthermore, they are expensive. In this research, nanocomposites were manufactured, and knowledge learned from experimenting with these micron sized fibers was extended to orient Carbon Nano Tubes (CNT) inside a polymer matrix. Manufactured nanocomposites here are conductive polymers which can be manufactured on an industrial scale with enhanced electrical as well as mechanical properties. Interest in orienting nanofibers within polymer matrices has been steadily increasing during the past decade to achieve enhanced functional and structural properties in composites. Many studies (as reviewed in chapter 2) have identified the role of extensional viscosity on the orientation of nano fibers through tensile drawing experiments.

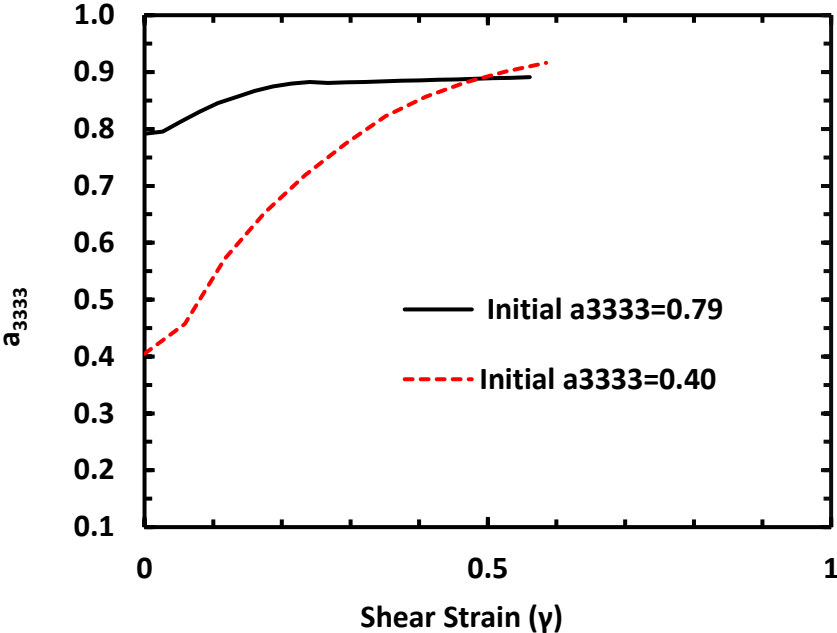


Figure 4.47. Effect of imposed shear strain of 0.5 imposed on fiber rotation in a composite with two different initial a_{3333} with V_{in} of 9.1%.

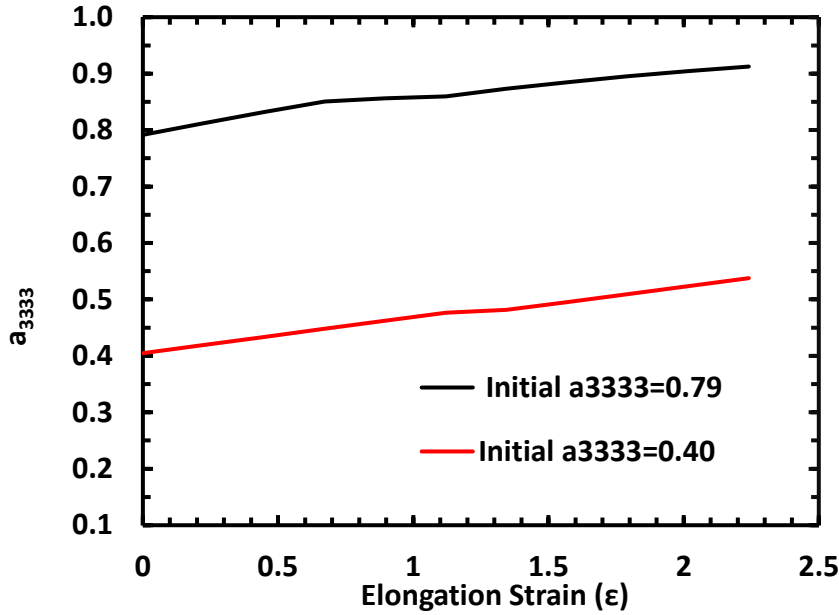


Figure 4.48. Effect of imposed elongation strain of 2.2 imposed on fiber rotation in a composite with two different initial a_{3333} with V_{in} of 9.1%.

Table 4.12. Comparison of experimental measured a_{3333} for samples tested for shear viscosity using Rheometer with a_{333} predicted using Dinh-Armstrong model.

| | Initial a_{3333} | x-ray measured a_{3333} after test | Dinh-Armstrong model prediction a_{3333} |
|------------------------------------|--------------------|--------------------------------------|--|
| $V_f=7.4\%, \dot{\gamma}=0.1(1/s)$ | 0.890 | 0.92 | 0.94 ($\gamma=0.491$) |
| $V_f=14\%, \dot{\gamma}=0.1(1/s)$ | 0.420 | 0.89 | 0.87($\gamma=0.259$) |
| $V_f=19\%, \dot{\gamma}=0.1(1/s)$ | 0.369 | 0.84 | 0.86 ($\gamma=0.273$) |

Table 4.13. Dinh-Armstrong model a_{1313} confirmation with rheometer

| | Initial a_{1313} | x-ray measured a_{1313} after test | Dinh-Armstrong model prediction a_{1313} |
|--------------------------------------|--------------------|--------------------------------------|--|
| $V_f=7.4\%, \dot{\gamma}=0.1(1/s)$, | 0.0195 | 0.0151 | 0.0135 ($\gamma=0.491$) |
| $V_f=14\%, \dot{\gamma}=0.1(1/s)$, | 0.1756 | 0.0113 | 0.0115 ($\gamma=0.259$) |
| $V_f=19\%, \dot{\gamma}=0.1(1/s)$, | 0.0988 | 0.0181 | 0.0191 ($\gamma=0.273$) |

Here, the knowledge gained by studying the orientation of HDPE/ Carbon Nano Tubes (CNT) extruded by a twin screw extruder, together with previous studies on micro-sized reinforcement, is extended to nanocomposites reinforced with CNT For micron size reinforced composite fibers, techniques such as X-ray tomography can be used to qualitatively and quantitatively determine reinforcement orientation.

However, due to the dimension scale of the nano-reinforcement process, there is no technique available to determine the orientation in bulk volume of nanocomposites. Small-Angle X-ray Scattering and Transmission Electron Microscopy was used to determine orientation; however, due to the limitation of these methods, results were not quantitative and cannot be used to compare different fibers extruded into HDPE-CNT composite fiber. Therefore, the orientation of CNT in HDPE-CNT composite fiber is determined indirectly by measuring electrical and mechanical properties. Potschke et al. [19], Sulong et al. [20], and Anand et al. [22] correlated the increase in orientation of nano-reinforcement to the increase in mechanical and electrical properties of nanocomposites. Hence, in the current study electrical and mechanical property measurements were used to quantitatively compare the orientation of nano-reinforcement fibers. Also, the effects of die geometry and V_F on electrical and mechanical properties were studied, and great correlation between the effects of die geometry on micron sized reinforcement orientation and nano-reinforcement functional properties was observed.

4.3.1 HDPE/CNT composite fiber

HDPE/CNT composites with various CNT weight fractions were manufactured by varying the entry angle in the range of $30^\circ - 180^\circ$ while keeping the die hole exit diameter and land length constant at 3 mm and 2.7 mm respectively, with weight fractions of 2%, 5%, 10%, and

15%, as depicted in Table 4.10. The geometrical parameters of the die hole are tabulated in Table 3.10.

The electrical conductivity characterization of the HDPE/CNT composite was achieved by using a 2 point probe station (Agilent 4156 C). Details of the conductivity measurement set up are explained in chapter 3. Figure 4.49 illustrates the longitudinal resistivity, measured along the length of the composite which was manufactured using 30° – 180° die angles. There is transition in conductivity at a weight fraction of 3.75%, but at weight fractions less than 3.75% CNT there is not enough CNT in the nanocomposite fiber to establish a network for electrons to flow in the longitudinal direction. Hence, the impact of die design on orientation is negligible, whereas weight fraction values make a difference. At weight fractions greater than 7.5, the effect of die geometry becomes more apparent on longitudinal conductivity, and at higher weight fractions fibers become conductive compared to the conductivity of HDPE, which is 1.6×10^{-6} (S/m). The effect of die geometry is more apparent at a weight fraction of 15% with the following order of increase in conductivity $60^\circ < 180^\circ < 90^\circ < 30^\circ$. As illustrated in Figure 4.50 (a), the higher the CNT orientation along the nano-composite fiber axis, the more connection between CNT, which results in a better route for electrons to travel from end to end. Figure 4.50 (b) shows a scenario where the same fiber content is poorly distributed, making it difficult for electrons to flow along the fiber axis. On other hand, a CNT distribution similar to Figure 4.50 (b) is expected to have higher transverse conductivity.

Using a polymer matrix of HDPE, previous studies reported conductivity of 125 (S/m) for a 15% weight fraction of CNT [41], 1 (S/m) for a 7% weight fraction of CNT [72], and 6.6 (S/m) for a 7.5 % weight fraction of CNT [73]. The electrical conductivity of manufactured

nanocomposite in this research (also using an HDPE matrix) resulted in higher conductivity for the nanocomposite.

Measurements made to determine the relationship between transverse and longitudinal conductivity are shown in Figure 4.51. In these measurements, a 60° angle die resulted in the highest transverse conductivity, thus confirming the inverse correlation between transverse and longitudinal conductivity.

Tensile testing results using a weight fraction of 15% validate these longitudinal conductivity measurements as the modulus is the highest for 30° and lowest for 60° angles. The same sequences of 60° < 18° < 90° < 30° exist for the modulus values as well. However, strength and strain to failure do not follow a pattern similar to that of the modulus.

4.4 Discussion

Viscosity is a result of microstructure of melt which is a function of orientation and volume fraction. Pressure required to push material through the die as well as viscosity determines how much flow rate is required. Flow rate, pressure, and viscosity are interrelated through Equations (4.10) and (4.12). Initial feed, screw speed, and die dimensions are controlled in all of measurements presented in previous section. Die dimensions set initial fiber orientation. As fiber rotates, viscosity of melt changes within the die which impacts pressure and subsequently the required flow rate.

When the experiments start, programmed feed rate pushes through certain flow rate which sets initial pressure oscillation in the extruder and after reaching to a steady state, pressure decreases to a plateau after 30 minutes as illustrated in Figure 4.52.

Table 4.14. Longitudinal conductivity tests

| Die Angle | 30° | 60° | 90° | 180° |
|-----------------|-------|-------|-------|-------|
| Weight fraction | 15% | 15% | 15% | 15% |
| | 7.5% | 7.5% | 7.5% | 7.5% |
| | 3.75% | 3.75% | 3.75% | 3.75% |

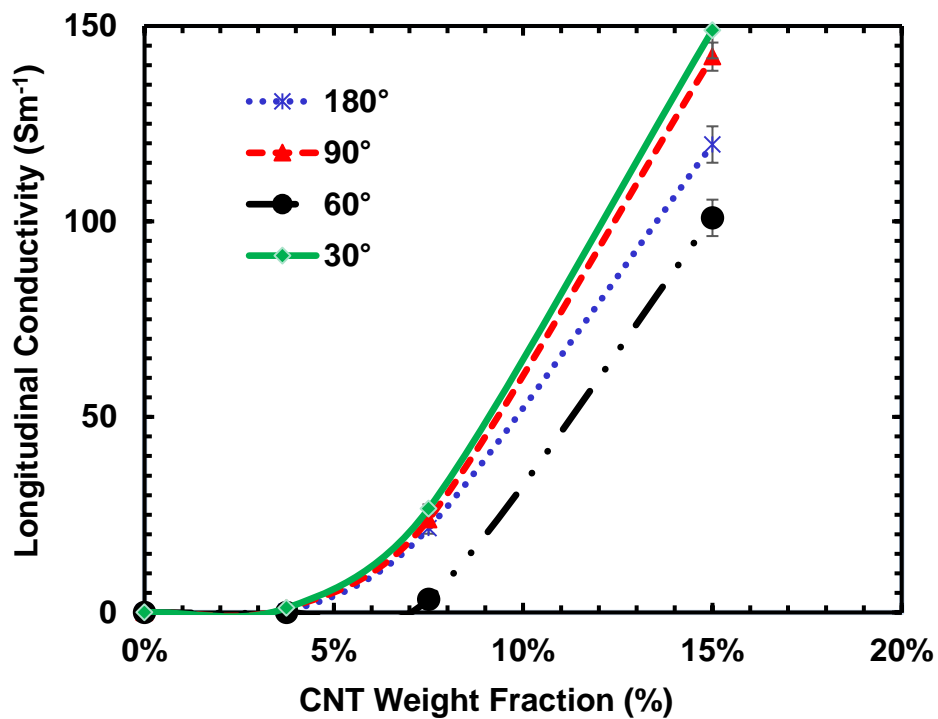


Figure 4.49. Measured longitudinal electrical conductivity for HDPE-CNT composite

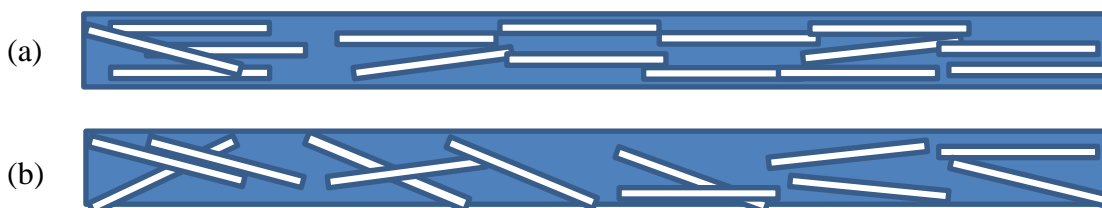


Figure 4.50. (a) Schematic of CNT longitudinal alignment in polymer matrix, (b) CNT random distribution within polymer matrix.

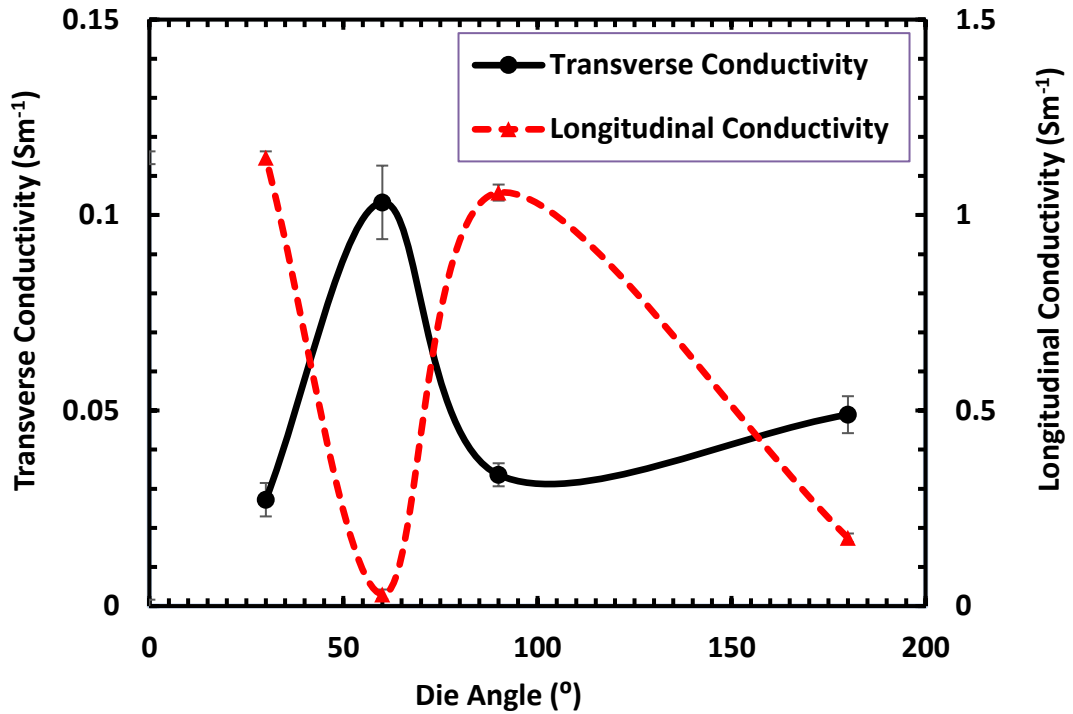


Figure 4.51. Transverse and longitudinal electrical conductivity (line between points are connected for illustration purpose and it is not fitted curve)

Table 4.15. Tensile testing of HDPE-CNT extruded composite with weight fraction of 15%.

| Angle | Modulus (MPa) | Strength (MPa) | Strain to failure |
|-------|---------------|----------------|-------------------|
| 30 ° | 1345±2.44 | 36.9±0.5 | 0.056±0.04 |
| 60 ° | 1272±4.54 | 35.3±0.6 | 0.065±0.06 |
| 90 ° | 1314±2.62 | 36.2±0.7 | 0.061±0.05 |
| 180 ° | 1282±1.69 | 36.6±0.8 | 0.064±0.06 |

As steady state the combination of flow rate, pressure, and viscosity is fixed/established which is defined by microstructure of the melt. In case of PE and PE-Spherical glass, flow rate was constant at the extruder end (without die assembly attached) and at the die end. As there is no fiber orientation happening (because of aspect ratio 1) within the die, viscosity is not changing. Extruder viscosity measurements and rheometer viscosity measurements confirm this phenomenon. In other words, the output is controlled by the input/feed as shown in Figure 4.52. Flow rate calculated from rheometer measurement is in close agreement with actual flow rate measured at the die end in the extruder. Ausias model for HDPE Spherical glass composite with $V_F = 4.6, 5.9, \text{ and } 17.8\%$.

In case of PE-Glass fiber with aspect ratio of four, die output flow rate is slightly different than extruder end (without die assembly attached). In some cases, the output is more and in some cases, the output is less. The reason for variation is because of reservoir after extruder end which acts as a buffer zone; when die demands more flow rate buffer zone supplies the flow rate and in other cases, it saves excess flow rate since die demands less flow rate. Comparison of buffer zone volume measurement and actual flow rate from die confirms that output coming out of die only fills up to 30% of buffer zone volume as tabulated in Table 4.16.

The mass flow rate $\dot{m} = \dot{Q}\rho$ where is \dot{Q} the volumetric flow rate and ρ is the density of the composite. The mass flow rate should be same at locations within the extrusion line. However, the volume metric flow rate and density can change maintaining the mass flow rate constant. Note that the change in density is due to change in fiber volume fraction, which was measured in this study. However, volumetric flow rate at various locations along the extrusion line could not be measured.

As shown in Figure 4.53, the extruder had a reservoir before the material travelled to the die. The mass flow rate out of the extruder end (measured just after the reservoir) without any attached die is different from the programmed mass flow rate as shown in Figure 4.54. This is possible since the twin screw extruder is starve fed (i.e. screws are not completely filled).

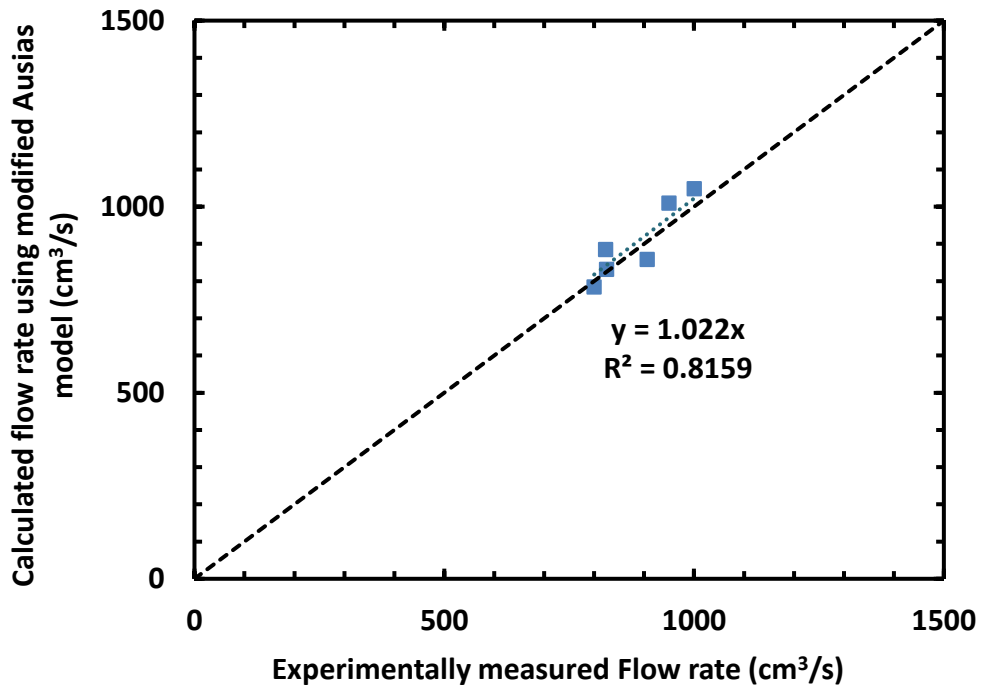


Figure 4.52. Comparison of experimental measured flow rate with that calculated using modified

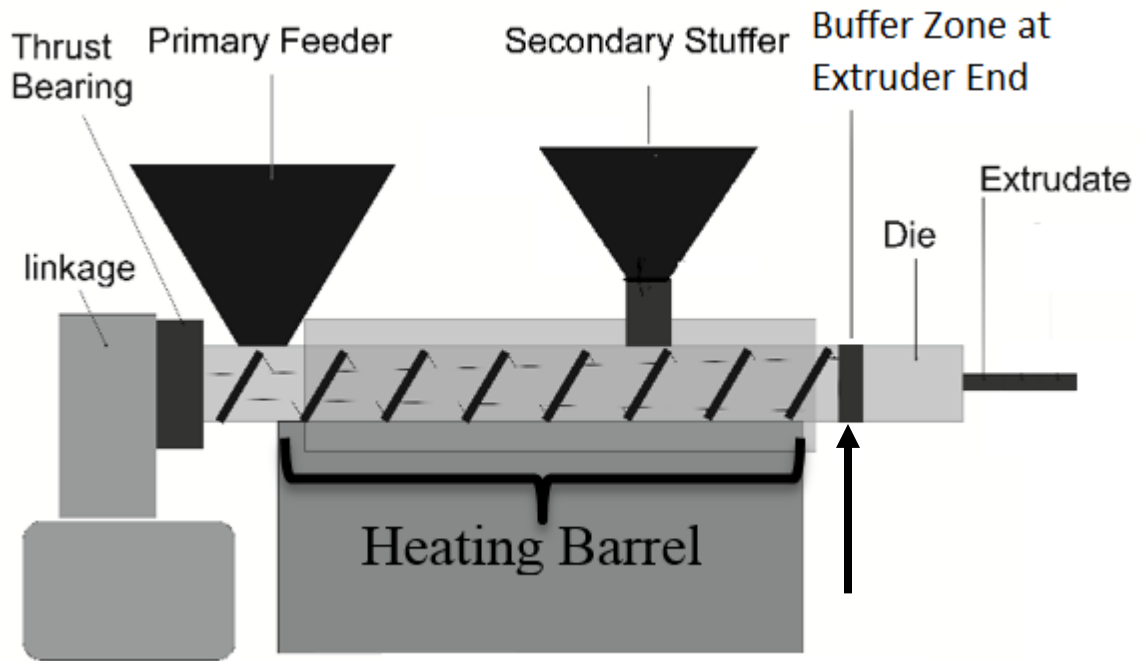


Figure 4.53 Buffer zone at extruder end identified by arrow.

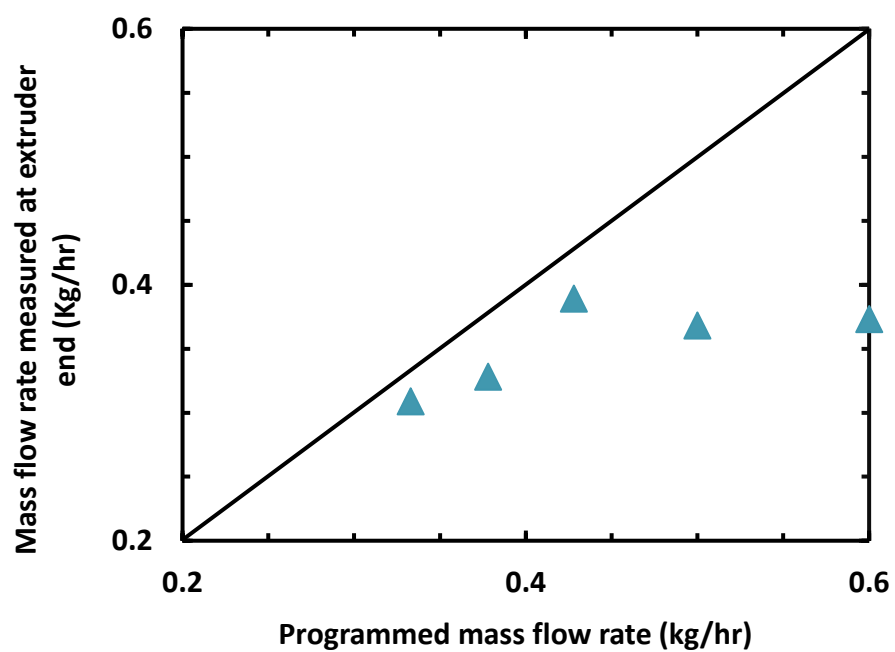


Figure 4.54 Comparison of experimental measured mass flow rate with programmed mass flow rate 90 degree die at constant screw speed of 40 rpm.

The mass flow rate out of the reservoir (identified as extruder end) reported in Figure 4.53 would change when the die is attached. When the die is attached, the viscosity of the melt in the die and the pressure difference across the die determines the mass flow rate out of the die. This has been suggested by White et al. [74] also. This demand on mass flow rate set by the die is met by the extruder by varying the amount of material coming out of the reservoir. In other words, although the rate at which the material coming out of the screws and into the reservoir is fixed, for a given programmed feed rate and screw speed, as shown in Figure 4.54, the rate at which the material goes out of the reservoir is dictated by the die. Thus, the % of reservoir filled with melt depends on the type of die attached although the programmed feed rate and the screw speed are kept constant. This is discussed further in detail next in this section.

Since the reservoir is before the die (cone and land sections of the die), the fiber orientation in the die cannot be altered by the reservoir. However, the initial fiber orientation in the melt coming out of the reservoir undergoes change while it travels from the reservoir to the die entrance. The fiber orientation at the die entrance is altered further as the melt progresses through the die. The amount of fiber rotation within the die depends on the shear and extensional strains imposed by the geometry of the die. Due to changes in fiber orientation the viscosity of the melt changes as it travels through the die. The viscosity of the melt within the die and pressure gradient across the die determine the mass flow rate out of the die. While the pressure gradient across the die determines the pressure gradient between the reservoir and the die entrance, and the mass flow rate out of the die determines the mass flow rate out of the reservoir.

It should be noted the changes in fiber orientation and viscosity of the melt within the die, development of pressure gradient across the die, and mass flow rate out of the die are coupled (i.e. they don't change independently). At the start of extrusion, the screw melts and pushes the material

through the empty extrusion line and the flow of melt through the die is in non-steady state. All of these coupled variables change spatially and temporally. As an example, the changes in pressure, P_1 (just after the reservoir) and P_2 (at the die entrance), with time is shown in Figure 4.55.

Once the steady state is reached (after 1800 s when the samples were collected), none of these variables change with time. Coupled changes in these variables, within the die dictate mass flow rate of the die, which in turn decides the mass flow rate out of the reservoir.

Mass flow rate at extruder end (out of reservoir) = Mass flow rate at die entrance = mass flow rate at die exit (i.e flow rate of composite out of the die)

$$\begin{aligned} \dot{m}_1 &= \dot{m}_2 = \dot{m}_3 \\ \dot{Q}_1 \rho_1 &= \dot{Q}_2 \rho_2 = \dot{Q}_3 \rho_3 \end{aligned} \tag{4.16}$$

Since the fiber volume fractions (and hence the density of the composite) at these three locations differ, the volumetric flow rate would also differ. However, the mass flow rate would not differ, thus experimental observation of fiber volume fraction changing with position would not violate the condition of continuity.

The viscosity model developed in this research highlights significant impacts of orientation and volume fraction as well as aspect ratio on viscosity. Viscosity within the die changes due to changes in orientation caused by shear and elongation strain imposed by the die as predicted by Dinh-Armstrong model [28]. Results presented in previous section showed that fiber rotation occurred in both cone and land sections (as illustrated in Figure 4.56) of the die. While majority of rotation in cone section was due to elongation strain, the fiber rotation in land section was due to shear strain.

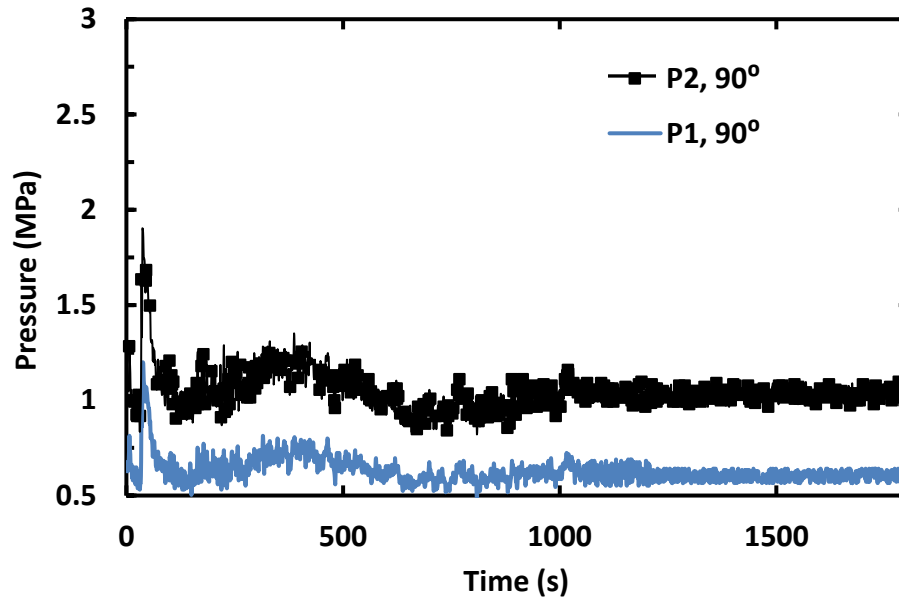


Figure 4.55. Pressure at the steady state condition for extruded composite with 90° die and $V_F=25\%$

The required level of orientation can be achieved through die design. The die can be designed so it only induces elongation through elongational strain or it can be designed so it only induces shear through shear strain induced orientation.

In die design, both extension and shear strain can result in very high orientation subject to the following conditions:

- 1- If only applying elongation strain alone with low initial orientation (i.e. $a_{3333} < 0.4$) then larger elongation strain is required to orient fibers. Hence, a large die is required to achieve the desired orientation.
- 2- If only applying shear strain for rotation, simulation shows that if initial orientation distribution is low (i.e. $a_{3333} < 0.4$) very high orientation can be achieved with shear strain only.
- 3- If neither of conditions 1 and 2 are applicable in other word combination of both shear and elongation strain exists, then dies in this research can be used which provide both shear and elongation strain for fiber rotation in small volume of die.

In die design, cone angle does not matter as long as elongation strain is kept constant between all die angles. However, experiments in this research showed that die angle affects pressure which subsequently affects initial orientation. Hence, if die design includes both shear and elongation strain, the lower angle results in better orientation.

Nanocomposite fiber manufactured by 30°, 60°, 90°, and 180° die also confirms the observation of micron-sized fiber. In a nanocomposite, higher conductivity is correlated to a better orientation along the direction of measuring conductivity. It is observed that 30° die resulted in the highest electrical conductivity and mechanical property.

Table 4.16. Reservoir degree of fill for $V_{IN}=25\%$ for different dies.

| $V_{IN}=25\%$ | ΔP (MPa) | Volumetric flow rate (m^3/s) $\times 10^{-8}$ | Buffer zone volume (m^3) $\times 10^{-8}$ | Degree of Fill |
|---------------|------------------|--|--|----------------|
| 30° | 1.1134 | 10.8 | 37 | 29% |
| 45° | 1.1134 | 10.6 | 37 | 29% |
| 60° | 1.0721 | 6.97 | 37 | 19% |
| 90° | 1.1410 | 9.86 | 37 | 27% |
| 180° | 1.1134 | 11.0 | 37 | 30% |

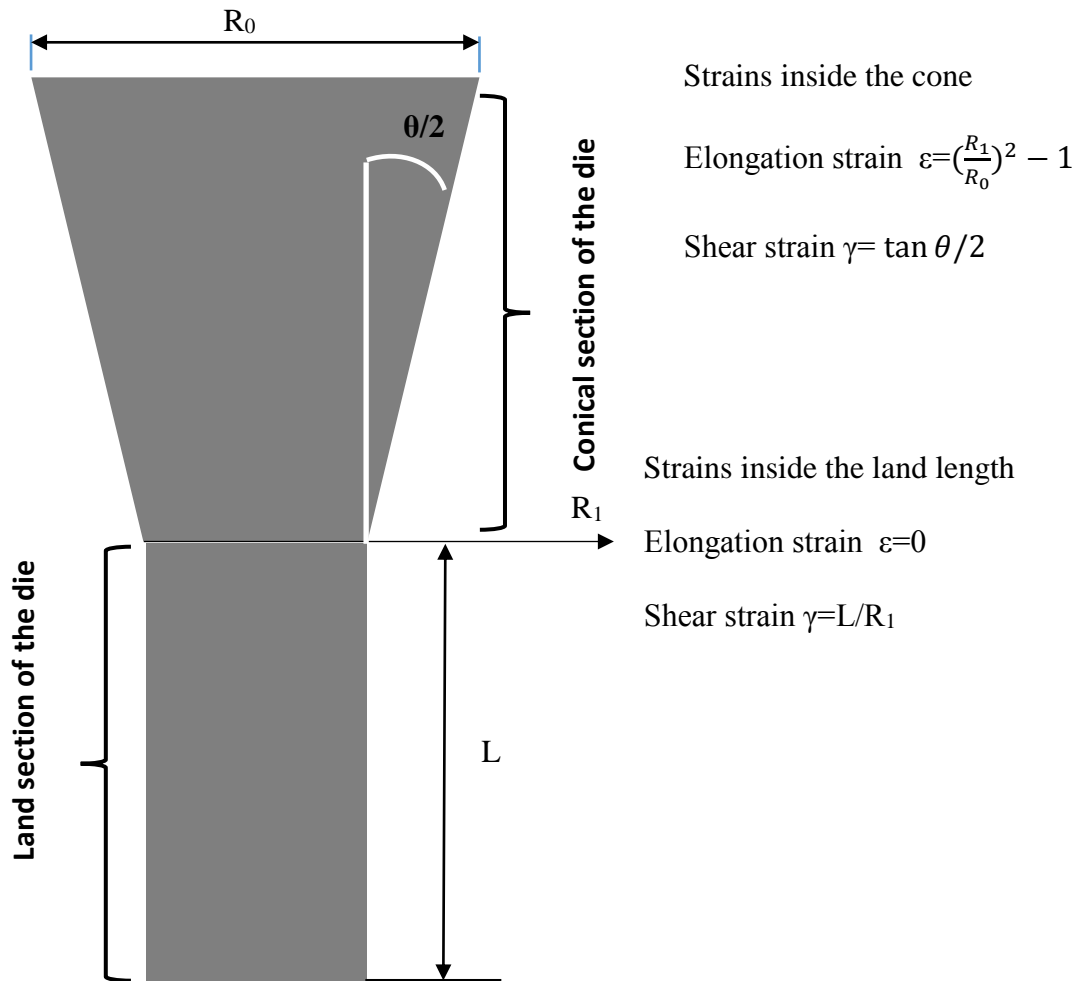


Figure 4.56. Shear and elongation strain in die

CHAPTER 5. CONCLUSION

Flow induced orientation of discontinuous fibers results in higher mechanical and functional properties. Previous studies on flow-induced orientation is limited only to injection molding, capillary and parallel plate rheometers. Knowledge on the combined effect of die design and process variables (such as feed rate, fiber volume fraction in feed and screw speed) on fiber orientation during extrusion of composites using a twin screw extruder is currently not available and addressing this knowledge gap was the goal of this thesis. Hence, this thesis set out to address this knowledge gaps through three specific objectives identified in 1.2.

5.1 Summary of Tasks and Results

These three objectives and the goal of this thesis have been successfully realized through the following tasks.

- (a) Nine conical dies with angles of 30° , 45° , 60° , 90° , 180° were designed and used.

These dies were designed to impose same extensional strain and varying shear strain within the conical section of the die. The length of the land region was kept constant for all dies and hence, the shear strain imposed was constant for all dies. However, the shear strain imposed in the land region was more than that imposed in the conical section.

- (b) Composite fibers, made up of HDPE and micron-sized glass fibers (aspect ratio of 27), were extruded using each of these nine dies. For each die, extrusion was done at a screw speed of 40 RPM while varying the weigh fraction from 10 – 50%. During each run the pressure was measured at two locations, at the extruder end (after reservoir) and at die entry, after steady state is reached. The composites specimens, were collected, after reaching the steady state, at three locations, extruder end, die entry, and die exit. Fiber

- orientation distribution (FOD) and the fiber volume fraction (V_f) in these specimens were determined non-destructively using x-ray tomography. The mass flow rate out of the reservoir (without attached die) as well as out of the die were measured.
- (c) In addition, pure HDPE and HDPE filled with glass spheres (aspect ratio of 1) were extruded using 60° and 90° dies, in order to help with modeling the effect of aspect ratio and volume fraction on viscosity.
 - (d) In order to study the effect of screw speed, additional experiments were completed using the 60° die at 40, 60, 100, 150, and 250 (rpms). All extrusions were completed at a constant die temperature of 200 (c) with 7.87, 12.7 18.5% volume fraction.
 - (e) The V_f in composites with glass spheres and fibers, determined non-destructively using x-ray tomography, was independently confirmed using helium pycnometer. Modulus of composites measured by tensile testing was used to confirm the orientation determined by X-ray tomography.
 - (f) Using the measured mass flow rate and pressure, the extensional and shear viscosity inside the cone and the land regions of the die were determined following the Cogswell approach.
 - (g) Shear viscosity was independently measured using a rheometer and modeled to establish its effects on fiber aspect ratio, fiber volume fraction, and fiber orientation. Using this model and the measured fiber orientation and V_f in the land region, shear viscosity in the land region was simulated and compared with the values determined using the Cogswell approach, to confirm the V_f and fiber orientation with the land region. Similar comparisons were made for the cone region of the die and region at the die entry.

- (h) Composite specimens with known fiber orientation and V_f were subjected to a known shear strain in a rheometer. The fiber orientation in the sheared composite was measured using X-ray tomography and compared with predictions using Dinh-Armstrong model to validate the model.
- (i) Finally, using the FOD at the die entry, the extensional and shear strains imposed by the die design, and the Dinh-Armstrong model, the fiber rotation (which changes in the FOD) within the composite melt as it travelled through the die was simulated.
- (j) In addition, the fiber rotation inside the die was analyzed to understand the combined effect of die design and extrusion variables on the fiber orientation in the extruded composites. These results were used to make recommendations on optimal die design.
- (k) HDPE/CNT composites with CNT weight fractions of 2%, 5%, 10%, and 15 were manufactured using the six dies. Electrical conductivity and modulus were measured and used to interpret the effect of die design on CNT orientation indirectly.

Results from these tasks, have been presented and discussed in Chapter 4.

5.2 Conclusions

Based on the results from these tasks, the following can be concluded:

- a) The viscosity of the composite used in this study changed with fiber orientation, fiber aspect ratio, and fiber volume fraction, according to the following equation:

$$\eta = \eta_0 \{ 1 + 14.3V_F + 184 a_{1313} \} \quad (5.1)$$

- (b) The fiber orientation distribution (FOD) and the fiber orientation tensors, a_{3333} and a_{1313} calculated using this FOD, changed as the composite melt traveled from the extruder end to the die exit. Hence, the viscosity of the melt also changed along the extrusion line.

(c) The change in the viscosity of the melt within the die due to changes in FOD together with pressure gradient across the die, which develops concurrently with the change in the viscosity, determined the mass flow rate (i.e volumetric flow rate) of composite melt out of the die, according to equation below:

$$Q = 0.41 \sqrt{\frac{P_S \tan \delta^{1.23}}{2 \left(\frac{4Q}{\pi r_1^3} \right)^{0.41} \left(1 - \left(\frac{r_1}{r_0} \right)^{1.23} \right) \eta}} \quad (5.2)$$

(d) This demand on mass flow rate imposed by the die is met by the extruder by varying the amount of melt coming out of the reservoir (at the end of the screws). Thus, although the mass flow rate out of the die is different from the programmed mass flow rate into the extruder (at the feed), it is believed to be same as that coming out of the reservoir, thus satisfying the conservation of mass requirement. The measured mass flow rate out of the reservoir (when no die was attached) was different than the programmed mass flow rate into the extruder, which is to be expected in the starve-fed (i.e. space between the screws and the barrels are not completely filled) twin screw extruder used in this study.

(e) The negative pressure gradient across the die (i.e. between die entry and exit) was matched (i.e. change in pressure was same) by a positive pressure gradient between the reservoir and the die entry. Since this varied with die design, the change in FOD as the melt travelled from the reservoir towards the die and the FOD / fiber orientation tensor values at the die entry were found to be vary with the die design. Hence, although the extensional strains did not vary with die design (shear strain in the cone region varied slightly but was less than the constant shear strain imposed in the land region for all dies), the magnitude change in FOD within the

die varied with die design. Thus, the magnitude change in viscosity within the die and the concurrent change in pressure gradient across the die varied with die design. Hence, the composite melt's mass flow rate out for the die varied with die design despite a constant feed rate and screw speed. Due to coupled effect of many variables, a simple correlation between input and output variables (for example output mass flow rate versus die design variable such as angle or FOD in the extruded composite versus FOD in the melt coming out of the reservoir, etc.) could not be observed.

(e) Dinh-Armstrong model, developed for predicting change in FOD in dilute composite solutions, has been found to predict successfully the change in FOD in concentrated composite solution used in this study.

(f) Simulation results suggest that shear strain results in better orientation than extensional strain. However, the effect of shear strain on the initial FOD. More random the FOD, better the fiber alignment induced by shear strain. However, the magnitude change in FOD by extensional strain does not depend on the initial FOD.

(g) The smallest die angle of 30° used in this study resulted in maximum fiber orientation in the extruded composite.

(h) The fiber volume fraction (and hence, the density of the composite melt) was found to vary along the extrusion line. Hence, volumetric flow rate would have varied along the extrusion line to maintain a constant mass flow rate.

(i) The effect of die design on CNT orientation was similar to the trend observed for micron-size glass fibers.

5.3 Guidelines for Die Design

An ideal die should result in maximum fiber orientation and output mass flow rate at least die pressure and should be small enough not to cause temperature variation of the melt within the die.

Based on the above conclusions, the following tentative guidelines are suggested for the die design.

- If die length is not the primary concern (when compared to maximum fiber orientation and output mass flow rate at least die pressure), then low angle dies (similar to 30°) used in this study would be better than large angle dies.
- If die length is a primary concern, then high angle dies are suggested with the caveat that the fiber orientation, output mass flow rate, and die pressure may be less than optimal.
- In this study, the high amount of fiber rotation through shear was achieved in the land region of the die than the conical section of the die due to limitation of constant extensional strain imposed during die design. Relaxing this constrain in future studies as suggested in 5.5 and optimizing both extensional and shear strain in the cone region may result in a single optimal die instead of two dies suggested above.

5.4 Original Contributions

To the best knowledge of the author, the following contributions are the first in this area:

- Comprehensive study of the effect of processing parameters and die design on discontinuous fiber orientation within composites extruded using a twin screw extruder;
- Quantitative measurement of changes in V_F and fiber orientation distribution along the extrusion line using X-ray tomography
- Validation of modified Ausias viscosity model using a set of data, which is more comprehensive than what is available in the literature.

- Delineation of the effect of both shear and elongation strain imposed by the die on fiber rotation as well as the on the changes in the fiber orientation distribution within the composite melt as it travels through the die, aiding in the development of guidelines for die design.
- Delineating the effect of die design on the orientation of CNTs within the composite extruded using a twin screw extruder.

5.5 Limitation of This Work and Recommendations for the Future Work

- a) The current die design maintained the extensional strain imposed by the die while allowing the shear strain imposed by the die to vary slightly. New design, varying the extensional strain while maintaining the shear strain constant, would help confirm the observations made in this thesis on die design over a wider range of extensional strains.
- b) Dinh-Armstrong model used in this thesis for modeling fiber rotation assumes that there is no fiber-fiber interaction. Changes in fiber volume fraction observed along the extrusion line suggests that there may be a coupling between changes in fiber volume fraction and fiber orientation, which imply fiber-fiber interaction. Hence, further study in this area is recommended.
- c) In this thesis, the orientation of CNT in 3-D volume of the composite was studied and qualitative results were obtained. Direct quantitative study of CNT orientation (using TEM) would be easy if the composite volume is restricted to 2-D such as thin films. Hence, future study involving extrusion of composite thin films containing CNT is recommended. The design of wedge dies used in such studies can be designed based on the results of this study.

REFERENCES

- [1] Barbosa, S.E. and Kenny, J.M., "Processing of short-fiber reinforced polypropylene. I. Influence of processing conditions on the morphology of extruded filaments", *J. of Polymer Engineering and Science*, Vol. 40, no. 1, pp. 11-22 (2000).
- [2] Vaxman, A., Narkis, M., Siegmann, A. and Kenig, S., "Short fiber reinforced thermoplastics. II. Interrelation between fiber orientation and rheological properties of glass fiber-reinforced noryl", *J. of Polymer Composites*, Vol. 10, no. 2, pp. 84-91 (1989).
- [3] Becraft M. L. and Metzner A. B., "The rheology, fiber orientation, and processing behavior of fiber-filled fluids" *J. of Rheology*, Vol. 36, no. 1, pp.143-170 (1992).
- [4] Shogren, R.L., Selling, G. and Willett, J.L., "Effect of Orientation on the Morphology and Mechanical Properties of PLA/Starch Composite Filaments", *J. of Polymers and the Environment*, Vol. 19, no. 2, pp. 329-334 (2011).
- [5] Hine, P.J., Davidson, N., Duckett, R.A., Clarke, A.R. and Ward, I.M., "Hydrostatically extruded glass-fiber-reinforced polyoxymethylene. I: The development of fiber and matrix orientation", *J. of Polymer Composites*, Vol. 17, no. 5, pp. 720-729 (1996).
- [6] Sanomura, Y. and Kawamura, M., "Fiber Orientation Control of Short-Fiber Reinforced Thermoplastics by Ram Extrusion", *J. of Polymer Composites*, Vol. 24, no. 5, pp. 587-596 (2003).
- [7] Mor, R., M. Gottlieb, L. A. Mondy, and A. L. Graham., "Effect of Surfaces on the Static Distribution of Orientations in Suspensions of Rod-Like Particles." *J. of Rheology*, Vol. 47, pp. 19-35 (2003).

- [8] Guo, M., Yang, H., Hong, T., Wang, W., Zhang, Q., and Du, R., Fu, Q., "Shear Enhanced Fiber Orientation and Adhesion in PP/Glass Fiber Composites", *J. of Macromolecular Materials and Engineering*, Vol. 291, no. 3, pp. 2339-246 (2006).
- [9] Parsheh, M., Brown, M.L. and Aidun, C.K., "Investigation of closure approximations for fiber orientation distribution in contracting turbulent flow", *J. of Non-Newtonian Fluid Mechanics*, Vol. 136, no. 1, pp. 38-49 (2006).
- [10] Fras, I., Boudeulle, M., Cassagnau, P. and Michel, A., "Mechanical properties of plasticized poly(vinylchloride): Effect of drawing and filler orientation", *J. of Polymer*, Vol. 39, no. 20, pp. 4773-4783 (1998).
- [11] Sun, S.-., Wei, M., Olson, J.R. and Shaw, M.T., "Rheological behavior of needle-like hydroxyapatite nano-particle suspensions", *J. of Rheologica Acta*, Vol. 50, no. 1, pp. 65-74 (2011).
- [12] Sulong, A.B. and Park, J., "Alignment of multi-walled carbon nanotubes in a polyethylene matrix by extrusion shear flow: Mechanical properties enhancement", *J. of Composite Materials*, Vol. 45, no. 8, pp. 931-941 (2011).
- [13] Hobbie, E.K., Wang, H., Kim, H., Lin-Gibson, S. and Grulke, E.A., "Orientation of carbon nanotubes in a sheared polymer melt", *J. of Physics of Fluids*, Vol. 15, no. 5, pp. 1196-1202 (2003).
- [14] Kang, D.W. and Ryu, S.H., "Orientation of carbon nanotubes in polypropylene melt", *J. of Polymer International*, Article in press (2012).
- [15] Abbasi, S., Carreau, P.J. and Derdouri, A., "Flow induced orientation of multiwalled carbon nanotubes in polycarbonate nanocomposites: Rheology, conductivity and mechanical properties", *J. of Polymer*, Vol. 51, no. 4, pp. 922-935 (2010).

- [16] Cooper, C.A., Ravich, D., Lips, D., Mayer, J.J. and Wagner, H.D., "Distribution and alignment of carbon nanotubes and nanofibrils in a polymer matrix", *J. of Composites Science and Technology*, Vol. 62, no. 7-8, pp. 1105-1112 (2002).
- [17] Cayla, A., Campagne, C., Rochery, M. and Devaux, E., "Melt spun multifilament yarns of carbon nanotubes-based polymeric blends: Electrical, mechanical and thermal properties", *J. of Synthetic Metals*, Vol. 162, no. 9-10, pp. 759-767 (2012).
- [18] Miyazono, K., Kagarise, C.D., Koelling, K.W., Mahboob, M. and Bechtel, S.E. , "Shear and extensional rheology and flow-induced orientation of carbon nanofiber/polystyrene melt composites", *J. of Applied Polymer Science*, Vol. 119, no. 4, pp. 1940-1951 (2011).
- [19] Pötschke, P., Brünig, H., Janke, A., Fischer, D. and Jehnichen, D., "Orientation of multiwalled carbon nanotubes in composites with polycarbonate by melt spinning", *J. of Polymer*, Vol. 46, no. 23, pp. 355-363 (2005).
- [20] Sulong, A.B., Park, J., Azhari, C.H. and Jusoff, K., "Process optimization of melt spinning and mechanical strength enhancement of functionalized multi-walled carbon nanotubes reinforcing polyethylene fibers", *J. of Composites Part B: Engineering*, Vol. 42, no. 1, pp. 11-17 (2011).
- [21] Fischer, D., Pötschke, P., Brünig, H. and Janke, A., "Investigation of the orientation in composite fibers of polycarbonate with multiwalled carbon nanotubes by raman microscopy", *Macromolecular Symposia*, Vol. 230, pp. 167-172 (2005).
- [22] Anand, K.A., Jose, T.S., Agarwal, U.S., Sreekumar, T.V., Banwari, B. and Joseph, R., "PET-SWNT nanocomposite fibers through melt spinning", *J. of Polymeric Materials*, vol. 59, no. 6, pp. 438-449 (2010).

- [23] Chae, H.G., Minus, M.L. and Kumar, S., "Oriented and exfoliated single wall carbon nanotubes in polyacrylonitrile", *J. of Polymer*, Vol. 47, no. 10, pp. 3494-3504 (2006).
- [24] Bhattacharyya, A.R., Sreekumar, T.V., Liu, T., Kumar, S., Ericson, L.M., Hauge, R.H. and Smalley, R.E., "Crystallization and orientation studies in polypropylene/single wall carbon nanotube composite", *J. of Polymer*, Vol. 44, no. 8, pp. 2373-2377 (2003).
- [25] Blighe, F.M., Young, K., Vilatela, J.J., Windle, A.H., Kinloch, I.A., Deng, L., Young, R.J. and Coleman, J.N., "The effect of nanotube content and orientation on the mechanical properties of polymer-nanotube composite fibers: Separating intrinsic reinforcement from orientational effects", *J. of Advanced Functional Materials*, Vol. 21, no. 2, pp. 364-371 (2011).
- [26] Jeffery, G. B. "The motion of ellipsoidal particles immersed in a viscous fluid" *Proceedings of the Royal Society of London*. Vol. 102, pp.161–179 (1922).
- [27] Batchelor G. K., "Slender-body theory for particles of arbitrary cross-section in Stokes flow", *Journal of Fluid Mechanics*, Vol.44, Issue 3, pp.419-440 (1970).
- [28] Dinh, S.M. and Armstrong, R.C., "A Rheological Equation of State for Semi-Concentrated Fiber Suspensions". *J. of Rheology.*, Vol. 28, p207-227 (1984).
- [29] Molden, G.F., "Re-orientation of fibers during mechanical working", *J. of Material Science*, Vol. 4, pp. 283-289 (1969).
- [30] Cogswell, F.N., "Converging flow of polymer melts in extrusion dies", *J. of Polymer Engineering & Science*, Vol. 12, no. 1, pp. 64–73 (1972).
- [31] Petrie, C.J.S. , "The rheology of fiber suspensions", *J. of Non-Newtonian Fluid Mechanics*, Vol. 87, no. 2-3, pp. 369-402 (1999).
- [32] Tate, Kenneth Roy. "Extrusion and orientation of higher molecular weight polyethylenes", PhD Thesis. Toronto, ON, Canada, University of Toronto, (1992).

- [32] Reasy, T. S. and Y. S. Kim., "Equal-Channel Angular Extrusion of Thermoplastic Matrix Composites for Sheet Forming and Recycling," Technical Paper - Society of Manufacturing Engineers, Vol.42, pp.356-362 (2005).
- [33] Lin, C. -M and C. -I Weng. "Simulation of Compression Molding for Sheet Molding Compound Considering the Anisotropic Effect." J. of Polymer Composites, Vol 20, no 1, pp. 98-113 (1999).
- [34] Han, S.P. and Yang, S., "Orientation distribution and electrophoretic motions of rod-like particles in a capillary", J. of colloid and interface science, Vol. 177, no. 1, pp. 132-142 (1996).
- [35] Sturman, P.C. and McCullough, R.L., "Static field electrical conductivity of dilute fiber suspensions", J. of Applied Physics, Vol. 72, no. 7, pp. 2883-2888 (1992).
- [36] Brenner, H., "Rheology of a dilute suspension of axisymmetric brownian particles", Int. J of Multiphase Flow, Vol. 1, no. 2, pp. 195-341 (1974).
- [37] Binding, D.M. "An approximate analysis for contraction and converging flows", Vol. 27, no. 2, pp. 173-189 (1988).
- [38] Phelps, Jay H. "Processing-Microstructure models for short and long fiber thermoplastic composites", PhD Thesis. Urbana, IL, USA, University of Illinois at Urbana-Champaign, (2009).
- [39] A. Brent Strong. *Plastics: Materials and Processing* (3rd Edition). NY, Prentice Hall; pp. 173 (2005).
- [40] Advani, SG. and Tucker, CL, "The use of tensors to describe and predict fiber orientations in short fiber composites" J. of Rheology , Vol. 31, pp. 751 (1987).

- [41] Ping Tang, Rong Zhang, Ran Shi, Yuezhen Bin, "Synergetic effects of carbon nanotubes and carbon fibers on electrical and self-heating properties of high-density polyethylene composites", *Journal of materials science*, Vol.50(4), pp.1565-1574 (2015).
- [42] Pipes, R.B., McCullough, R.L. & Taggart, D.G. "Behavior of discontinuous fiber composites: fiber orientation", *J. of Polymer Composites*, Vol. 3, no. 1, pp. 34-39 (1982).
- [43] Hine, P.J., Duckett, R.A., Davidson, N. and Clarke, A.R., "Modelling of the elastic properties of fiber reinforced composites. I: Orientation measurement", *J. of Composites Science and Technology*, Vol. 47, no. 1. pp. 65 (1993).
- [44] Eberhardt, C. and Clarke, A., "Fibre-orientation measurements in short-glass-fibre composites. Part I: Automated, high-angular-resolution measurement by confocal microscopy", *J. of Composites Science and Technology*, Vol. 61, no. 10, pp. 1389-1400 (2001).
- [45] Lee, K.S., Lee, S.W., Youn, J.R., Kang, T.J. and Chung, K., "Confocal microscopy measurement of the fiber orientation in short fiber reinforced plastics", *J. of Fibers and Polymers*, Vol. 2, no. 1, pp. 41-50 (2001).
- [46] Blanc, R., Germain, C., Da Costa, J.P., Baylou, P. and Cataldi, M., "Fiber orientation measurements in composite materials", *J. of Composites Part A: Applied Science and Manufacturing*, Vol. 37, no. 2, pp. 197-206 (2006).
- [47] Deng, H., Zhang, R., Bilotti, E., Loos, J. and Peijs, T., "Conductive polymer tape containing highly oriented carbon nanofillers", *J. of Applied Polymer Science*, Vol. 113, no. 2, pp. 742-751 (2009).
- [48] Thomassetta, J., Carreaua, P.J., Sanschagrina, B., and Ausias, G., "Rheological properties of long glass fiber filled polypropylene", *J. of Non-Newtonian Fluid Mech*, Vol.125, no.1, pp. 25-34 (2005).

- [49] Mobuchon, C., Carreau, P. J., Heuzey, M.C., Sepehr, M., “Shear and Extensional Properties of Short Glass Fiber Reinforced Polypropylene”, *J. of Polymer Composites*, Vol. 26, no 3, pp 247–264 (2005).
- [50] Gibson A. G. and Williamson, G. A. , “Shear and extensional flow of reinforced plastics in injection molding. II. Effects of die angle and bore diameter on entry pressure with bulk molding compound”, *J. of Polymer Engineering & Science*, Vol. 25, no. 15, pp. 980–985 (1985).
- [51] Silvia, E. B, Jose, M. K, “Processing of Short-Fiber Reinforced Polypropylene. I. Influence of Processing Conditions on the Morphology of Extruded Filaments.”, *J. of Polymer Engineering and Science*, Vol. 40, pp.11-22 (2000).
- [52] Kim, J.K., and Park, S.H., “Fiber orientation and rheological properties of short fiber-reinforced plastics at higher shear rates”, *J. of Materials Science*, Vol. 35, no. 5, pp. 1069-1078 (2000).
- [53] Fu, S.-. and Lauke, B., "Effects of fiber length and fiber orientation distributions on the tensile strength of short-fiber-reinforced polymers", *J. of Composites Science and Technology*, Vol. 56, no. 10, pp. 1179-1190 (1996).
- [54] Jayaraman, K. and Kortschot, M.T., "Correction to the Fukuda-Kawata Young's modulus theory and the Fukuda-Chou strength theory for short fibre-reinforced composite materials", *J. of Materials Science*, Vol. 31, no. 8, pp. 2059-2064 (1996).
- [55] Vaxman, A., Narkis, M., Siegmann, A. and Kenig, S., "Fibre orientation and rheology in short fibre reinforced thermoplastics", *J. of Materials Science Letters*, Vol. 7, no. 1, pp. 25-30 (1988).

- [56] Zainudin, E.S., Sapuan, S.M., Sulaiman, S. and Ahmad, M.M.H.M., "Fiber orientation of short fiber reinforced injection molded thermoplastic composites: A review", *J. of Injection Molding Technology*, Vol. 6, no. 1, pp. 1-10 (2002).
- [57] Fu, S.-., Hu, X. and Yue, C.-., "Effects of fiber length and orientation distributions on the mechanical properties of short-fiber-reinforced polymers - a review", *Materials Science Research International*, Vol. 5, no. 2, pp. 74-83 (1999).
- [58] Zhou, K. and Lin, J., "Three dimensional fiber orientation distribution in two dimensional flows", *J. of Fibers and Polymers*, Vol. 9, no. 1, pp. 39-47 (2008).
- [59] Advani S.G. and C.L. Tucker III, "Closure approximations for three-dimensional structure tensors", *J. of Rheology*, Vol. 34, no. 3, pp. 367-386 (1990).
- [60] Cintra J.S. and C.L. Tucker III, "Orthotropic Closure Approximations for Flow-Induced Fiber Orientation", *J. of Rheology*, Vol. 39, no. 10, pp. 1095-1122 (1995).
- [61] Verleye, V., Coumiot, A. and Dupret, F., "Prediction of fiber orientation in complex injection molded parts", *Materials Division, Proceedings of the ASME Annual Meeting, New Orleans*, pp. 265-270 (1993).
- [62] Azaiez, J., Chiba, K., Chinesta, F. and Poitou, A., "State-of-the-art on numerical simulation of fiber-reinforced thermoplastic forming processes", *Archives of Computational Methods in Engineering*, Vol. 9, no. 2, pp. 141-198 (2002).
- [63] Chung D.H. and Kwon T.H., "Fiber orientation in the processing of polymer composites" *J. of Korea-Australia Rheology*, Vol. 14, no. 4, pp. 175-188 (2002).
- [64] P.J Hine, S.-W Tsuib, P.D Coatesb, I.M Warda, R.A Ducketta, "Measuring the development of fibre orientation during the melt extrusion of short glass fibre reinforced

polypropylene”, *J of Composites Part A: Applied Science and Manufacturing*, Vol. 28, no. 11, pp. 949-958 (1997).

[65] Kobayashi, M., Takahashi, T., Takimoto, J. Koyama, K., “Flow-induced whisker orientation and viscosity for molten composite systems in a uniaxial elongational flow field” *Vol.36, no.20, pp. 3927–3933 (1995).*

[66] Sepehr, M., Carreau, P. J., Moan, M., and Ausias, G., “Rheological properties of short fiber model suspensions”, *J. of Rheology*, Vol. 48, no. 5, pp.1023 (2004).

[67] Ausias, G., “A modified viscosity for short fiber reinforced polymer flow”, 12th International rheology congress, pp. 594-595 (1996).

[68] Powell, R.L., “Rheology of suspensions of rodlike particles”, *J. of Statistical Physics*, Vol.62, no. 5, pp. 1073-1094 (1991).

[69] Shaqfeh, E. S. G., and Fredrickson, G.H., “The hydrodynamic stress in a suspension of rods”, *J. of Physics of Fluids A: Fluid Dynamics*, Vol. 2, no. 1, pp. 7 (1990).

[70] Ausias G., Agassant J. F., Vincent M., Lafleur P. G., Lavoie P. A. and Carreau P. J. “Rheology of short glass fiber reinforced polypropylene”, *Journal of Rheology* Vol.36, pp. 525 (1992)

[71] Bagley EB, “End corrections in the capillary flow of polyethylene”, *J of Applied Physics* Vol. 28, pp. 193–209 (1957).

[72] Olga Valentino, Maria Sarno, Nicola G Rainone, Maria Rossella, Nobile Paolo, Ciambelli Heinz, C Neitzert, George P Simon, “Influence of the polymer structure and nanotube concentration on the conductivity and rheological properties of polyethylene/CNT composites”, *Physica* , Vol.40, no.7, pp.2440-2445 (2008)

- [73] Dray Delphine, Gilormini Pierre, Régnier Gilles, “Comparison of several closure approximations for evaluating the thermoelastic properties of an injection molded short-fiber composite”, *Composites Science and Technology*, Vol.67, no. 7, pp.1601-1610 (2007)
- [74] Kim, P.J. and White, J.L., “Flow visualization and residence time distributions in a modular co-rotating twin-screw extruder”, *Intern. Polymer Process journal*, Vol. 9, pp.108, (1994).

APPENDIX A

Introduction

In this appendix formulations for various calculation in thesis are presented respectively.

A.1 Volume Fraction

Calculation of input volume fraction in the feed (V_{In}) based on weight fraction:

$$W_{matrix} + W_{fiber} = W_{composite} \quad (A.1)$$

$$W_{composite} = V_{composite} \times \rho_{composite} \quad (A.2)$$

$$V_{matrix} = W_{matrix} / \rho_{matrix} \quad (A.3)$$

$$V_{fiber} = W_{fiber} / \rho_{fiber} \quad (A.4)$$

W , V , and ρ stands for weight, volume, and density respectively.

$$V_{fiber} = V_{fiber} / V_{composite} = (W_{fiber} \times \rho_{composite}) / (W_{composite} \times \rho_{fiber}) \quad (A.5)$$

$$V_{matrix} = V_{matrix} / V_{composite} = (W_{matrix} \times \rho_{composite}) / (W_{composite} \times \rho_{matrix}) \quad (A.6)$$

$$V_{fiber} + V_{matrix} = 1$$

$$\rho_{composite} = 1 / [(W_{fiber} / W_{composite}) \times 1 / \rho_{fiber} + (W_{matrix} / W_{composite}) \times 1 / \rho_{matrix}] \quad (A.7)$$

$W_{fiber} / W_{composite}$ changes from 10% -50% and also ρ_{fiber} and ρ_{matrix} is given therefore $\rho_{composite}$ can be calculated.

Equation A.5 can be calculate by $\rho_{composite}$ value from equation A.7.

A.2 Rheology of Composite Melt within the Die

All manufacturing variables affect the viscosity of the composite melt within the die. Since the viscosity is also affected by the OF and the V_F in the die, the OF and the V_F in the extruded composite is likely to be influenced by the viscosity in the die. Hence, the latter was characterized using the extruder.

Due to interaction of the polymer melt with the die walls and change in diameter of the die in the conical section, the melt pressure decreases as it traverse from left to right in Figure A.1. P_o is the melt pressure at the entrance to the conical section of the die and it reduces along the

length of the conical section to a value of P_1 at the end of the conical section. This pressure reduces further in the land section due to interaction of the polymer melt with the die walls to P_2 at the end of the land section. While P_2 can be slightly higher than the atmospheric pressure, it is taken to be equal to atmospheric pressure. Based on these, the following pressure drops can be defined.

$$\begin{aligned}
 P_0 - P_2 &= \Delta P_T \\
 P_0 - P_1 &= \Delta P_{\text{cone}} \\
 P_1 - P_2 &= \Delta P_{\text{cap}} \\
 \Delta P_T &= \Delta P_{\text{Cone}} + \Delta P_{\text{Cap}}
 \end{aligned}
 \tag{A.8}$$

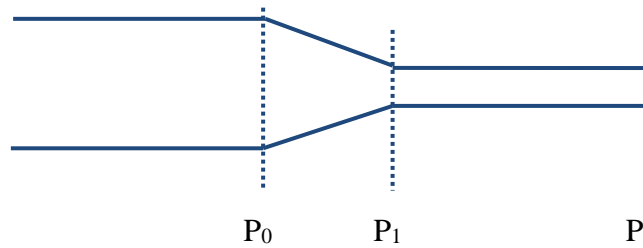


Figure A.1 Pressure variation along the length of a die hole

The pressure drop inside the cone consists of two components,

$$\Delta P_{\text{Cone}} = \Delta P_{\text{Cone,E}} + \Delta P_{\text{Cone,S}}
 \tag{A.9}$$

where $\Delta P_{\text{Cone,E}}$ is the pressure drop inside the cone due to extensional flow of the melt and $\Delta P_{\text{Cone,S}}$ is the pressure drop inside the cone due to shear flow. It should be noted that the latter is different from the pressure drop within the land region due to shear flow (ΔP_{Cap}).

Cogswell [10] derived equations relating these two pressure drops inside the cone to the extensional and shear viscosities of the melt within the cone assuming Newtonian viscosity. Gibson et al. [69] modified them for non-Newtonian viscosity. Using the following equation for extensional flow

$$\sigma = \lambda \dot{\epsilon}^n
 \tag{A.10}$$

where σ is the applied normal stress, λ is the extensional viscosity, $\dot{\epsilon}$ is the extensional rate, and n is the power law constant obtained by mathematical fitting of the experimental data, Gibson et al. [69] derived the following equation relating extensional viscosity within the cone with $\Delta P_{Cone,E}$.

$$\lambda = \frac{\Delta P_{Cone,E}}{\frac{2}{3n} \left(\frac{2Q \tan(\frac{\theta}{2})}{\pi r_1^3} \right)^n (1 - (\frac{r_1}{r_0})^{3n})} \quad (A.11)$$

where θ is die angle, Q is flow rate, r_0 is entry diameter of the cone and r_1 is the exit diameter of the cone.

Similarly, using the following equation for shear flow

$$\tau = \eta \dot{\gamma}^n \quad (A.12)$$

where τ is the applied shear stress, η is the shear viscosity, $\dot{\gamma}$ is the shear rate, and n is the power law constant obtained by mathematical fitting of the experimental data, Gibson et al. [69] derived the following equation relating shear viscosity within the cone with $\Delta P_{Cone,s}$

$$\eta = \frac{P_S 3n \tan\theta}{2 \left(\frac{4Q}{\pi r_1^3} \right)^n (1 - (\frac{r_1}{r_0})^{3n})} \quad (A.13)$$

In this study, the above two equations A.11 and A.12 were used to determine the extensional and shear viscosities within the cone. The cone pressure drop required by these equations were derived experimentally as follows.

A procedure developed by Bagley [70] was used to determine ΔP_{cone} . The principle behind the procedure is as follows. The total pressure drop during extrusion is measured using a series of dies with various land length but same cone angle. At a constant shear rate, the total pressure drop would increase with aspect ratio (L/D) as shown in the schematic in Figure A.2 (known as Bagley Plot), which can be fitted to

$$\Delta P_T = \Delta P_{Cone}(\dot{\gamma}) + \beta \left(\frac{L}{D} \right) \quad (A.14)$$

where ΔP_{Cone} is the cone pressure drop, L is the land length, D is the exit diameter of the cone of the die hole and β is the slope of the curve.

The Y-intercept for zero L/D would yield the cone pressure drop

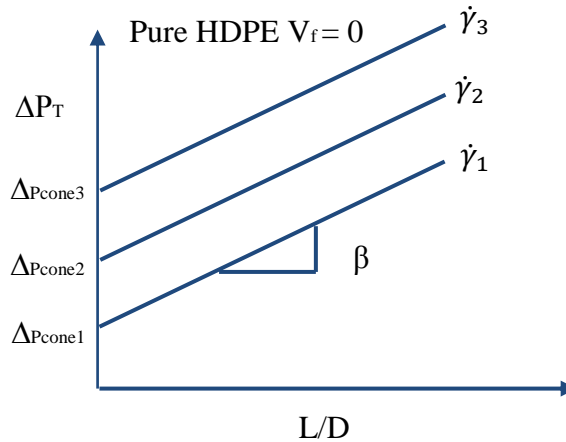


Figure A.2 Total pressure versus different L/D for various shear rate

In this study, three 180° dies with land lengths of 0.0255, 5.082, and 11.184 mm length and cone exit diameter of 3 mm were used to measure the cone pressure drop. Pure HDPE was melt spun using each of these dies at three different flow rates and the total pressure drop across the die hole was measured. The flow rates were varied by varying the screw speed. The total pressure drop is plotted as a function of maximum shear rate in the land region in Figure A.3.

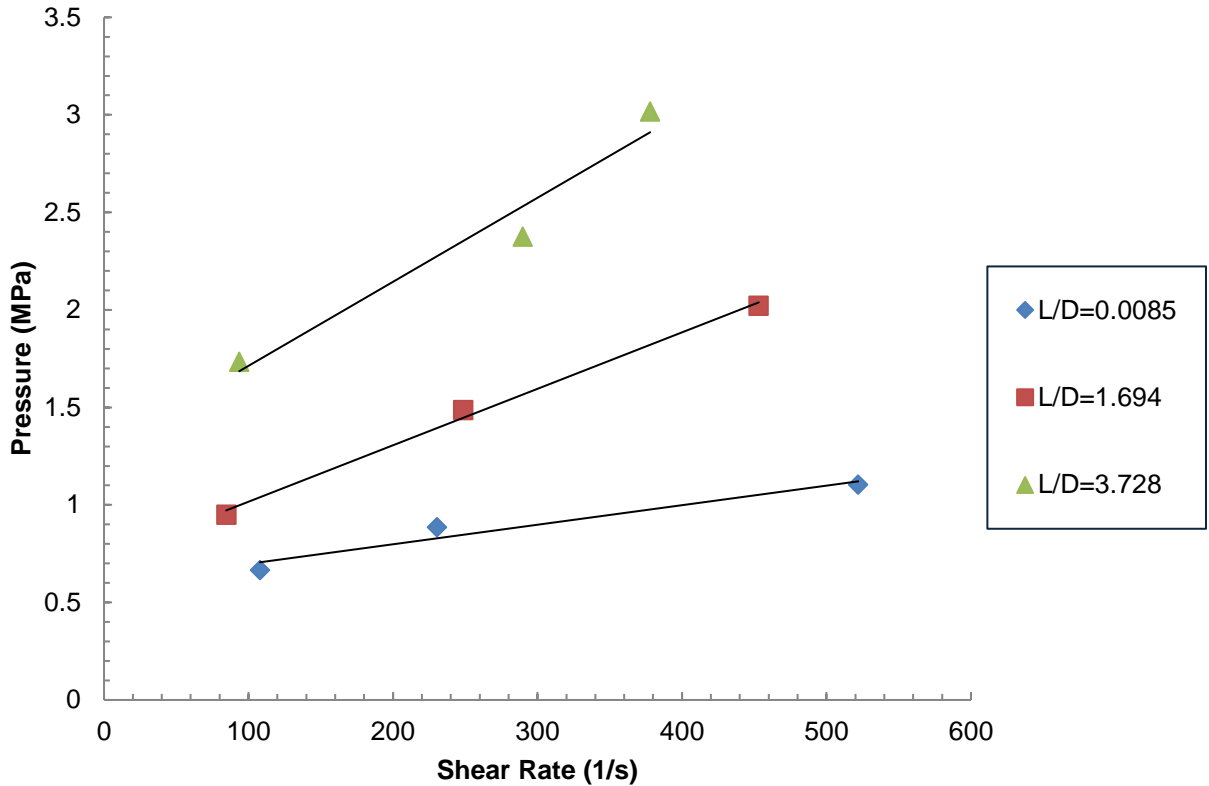


Figure A.3 Pressure versus shear rate for Bagley pressure drop measurement

The maximum shear rate in the land region is obtained using the experimentally determined flow rates using

$$\dot{\gamma} = \frac{Q}{\pi r_1^3} \left[3 + \frac{1}{n} \right] \quad (\text{A.15})$$

$\dot{\gamma}$ is the shear rate Q is flow rate, and r_1 is the exit diameter of n is the power law constant obtained by mathematical fitting of the experimental data.

These results are replotted as Bagley plot in Figure A.4. The data in this figure was fitted using linear regression and the fitted values are also shown in the Figure A.4. The cone pressure is a function of shear rate as shown in Figure A.5, which is fitted using linear regression.

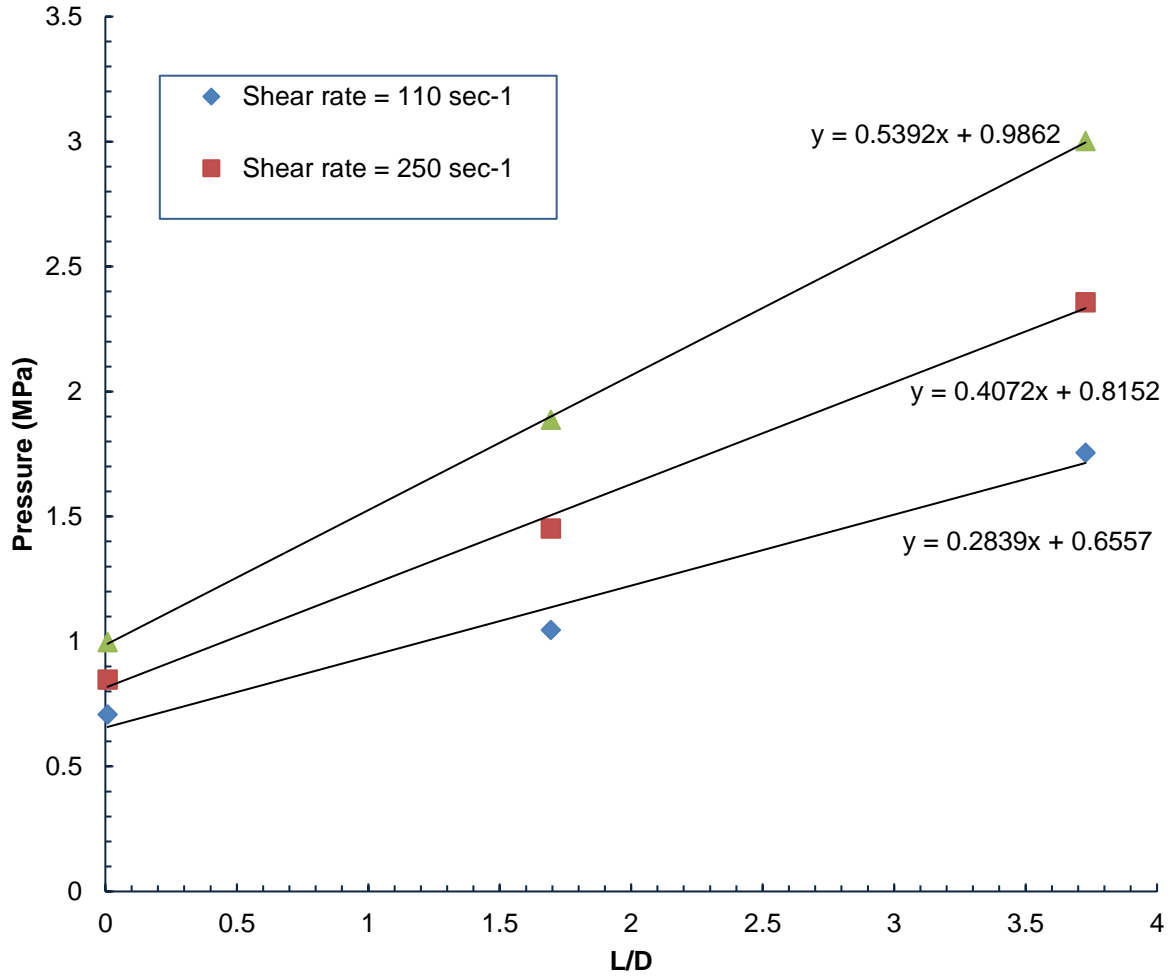
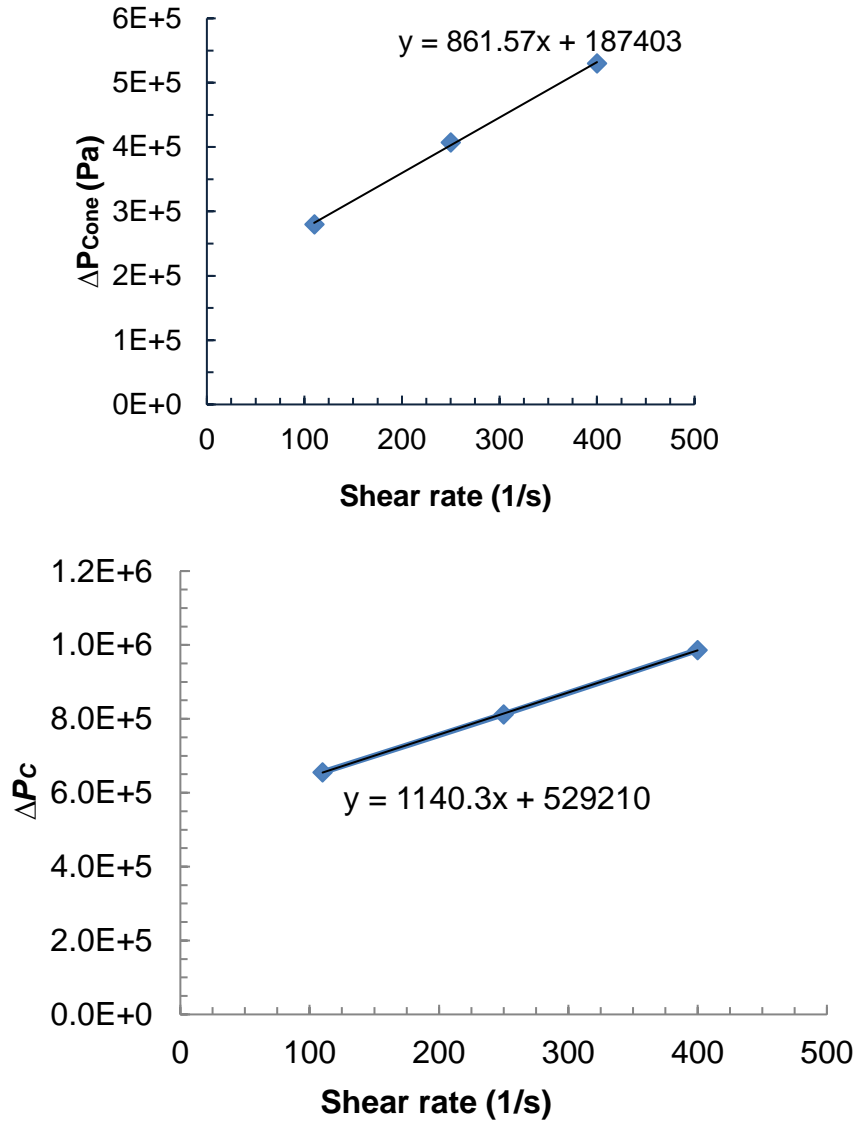


Figure A.4 Experimentally measured total pressure drop versus L/D

$$\Delta P_{Cone}(\dot{\gamma}) = \Delta P_{Cone}^0 + A\dot{\gamma} \quad (5-9)$$

where ΔP_{Cone}^0 is the cone pressure drop at zero shear rate and $A = 861.57$ (Pa.s) is the slope of the curve in Figure A.5.

Figure A.5 ΔP_{Cone} versus shear rate

The data in Figure A.5 is for a die angle of 180° . One previous study Ansari et al [71] has found that the pressure drop, for PE melt flow through a conical die hole, reduces with increase in die angle in the range of 0 to 30° and reaches a plateau value for die angles $> 30^\circ$. Hence, the data in Figure A.5 was assumed to be applicable to dies with various entry angles used in this study.

However calculated cone pressure drop corresponds to pure HDPE and does not account for the effect of fiber volume fraction and orientation factor for the extruded composite.

In order to determine these effects on cone pressure drop, similar experiments were repeated using composite melt with V_F in the feed of 3.66 and 18.5%. The corresponding V_F in the extruded composite were 3.7 and 20 % respectively. The dies used had a cone angle of 180° and 90° , cone exit diameter of 3 (mm) and land lengths of 2.7 (mm). The Bagley plot for two composites and HDPE is shown in Figure 4.26 for a shear rate of 37 (1/s). As expected, the total pressure drop at L/D as well as the cone pressure drop increased with increase in fiber volume fraction in the composite. Here, it is assumed that the fiber volume fraction in the melt within the cone is same that measured using the extruded composite. It is interesting to note that the slope of the curve does not change with fiber content. As shown in Figure A.3, this slope is a function of shear rate only.

The variation of cone pressure drop with fiber volume fraction in the melt is shown in Figure A.7. The data in this figure is fitted using linear regression.

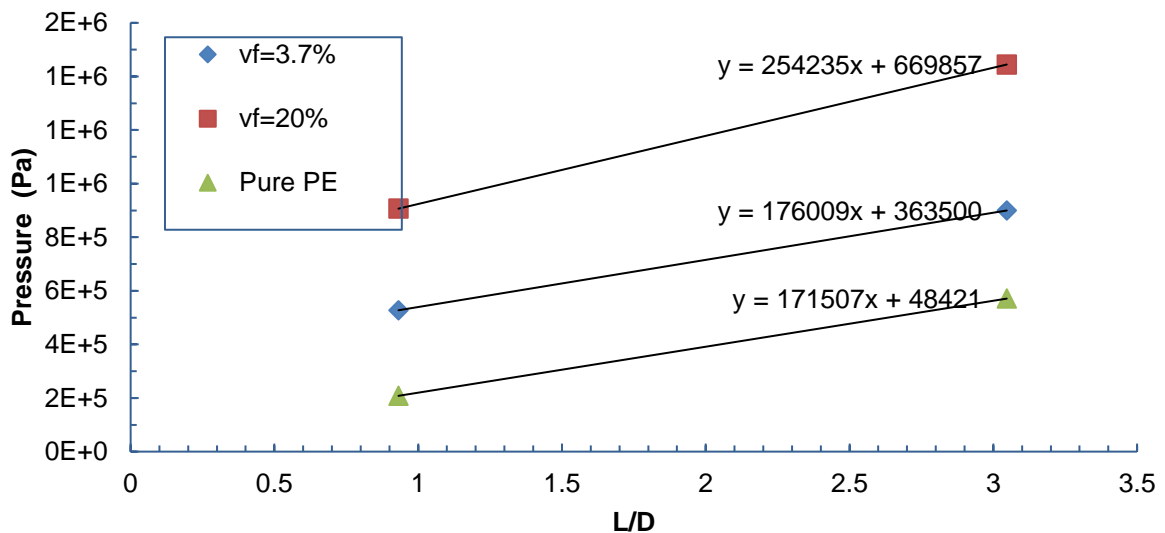


Figure A.6 Effect of fiber volume fraction on Total pressure drop for various L/D ratio

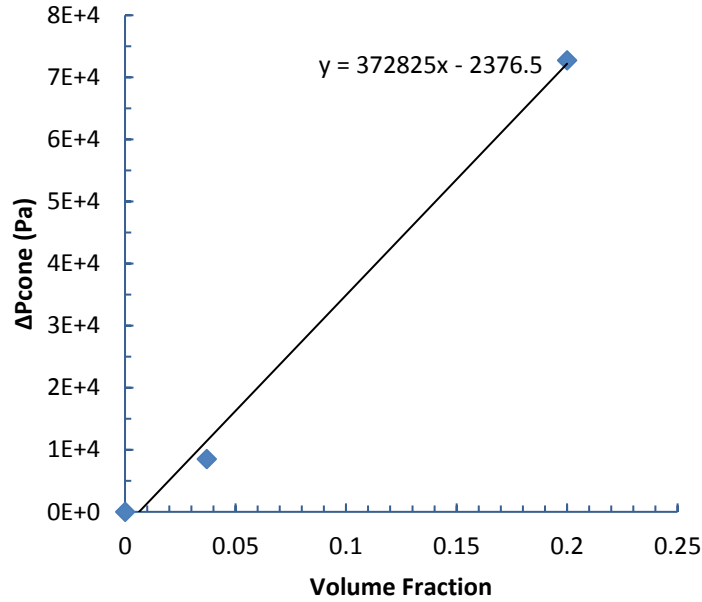


Figure A.7 Cone pressure drop versus Fiber volume fraction

$$\Delta P_{Cone}(V_F) = \Delta P_{cone}(\dot{\gamma}) + C V_F \quad (A.17)$$

Where $C = 372525$ (Pa) is the slope of the curve in Figure 5-27.

Using equation (A.16)

$$\Delta P_{Cone}(V_F) = \Delta P_{cone}^o(\dot{\gamma}) + 861.57 \dot{\gamma} + 372525 V_F \quad (A.18)$$

Equation A.14 can be modified as

$$\Delta P_T = \Delta P_{Cone}(V_F) + 119272 \left(\frac{L}{D}\right) \quad (A.19)$$

Finally, in order to determine the effect of fiber orientation on cone pressure drop, similar experiments were repeated using composite melt with V_F in the feed of 18%. The corresponding V_F in the extruded composite was 20%. The dies used had a cone angle of 30°, 90° and 180°, cone exit diameter of 3 (mm) and land lengths of 0.9 and 3.0. An increase in OF reduced the total pressure drop as shown in Figure A.8. The cone pressure drop decreased with increase in orientation factor as shown in Figure A.9, which is fitted using linear regression.

$$\Delta P_c(\text{OF}) = \Delta P_c(V_F) + D(\text{OF}) \quad (\text{A.20})$$

where $D = -535150$ (Pa) is the slope of the plot in Figure A.9. (A.21)

$$\Delta P_c(\text{OF}) = \Delta P_c^0(\dot{\gamma}) + A\dot{\gamma} + C V_F + D(\text{OF}) \quad (\text{A.22})$$

Hence, the total pressure drop can be written as

$$\begin{aligned}
 P_T &= \Delta P_c(\text{OF}) + \beta \left(\frac{L}{D}\right) = \\
 &= \underbrace{\Delta P_c^0(\dot{\gamma}) + A\dot{\gamma}}_{[\text{Effect of } \dot{\gamma}]} + \underbrace{C V_F}_{[\text{Effect of } V_f]} + \underbrace{D(\text{OF})}_{[\text{Effect of OF}]} + \underbrace{\beta \left(\frac{L}{D}\right)}_{[\text{Effect of } L/D]} \quad (\text{A.23})
 \end{aligned}$$

Therefore for a composite extruded using a given die, the cone pressure drop was determined using

$$\Delta P_c = P_T - \beta \left(\frac{L}{D}\right) = \Delta P_c(\dot{\gamma}) + A\dot{\gamma} + C V_F + D(\text{OF}) \quad (\text{A.24})$$

The $\beta \left(\frac{L}{D}\right)$ for the die was determined and subtracted from the experimentally measured total pressure drop to determine the cone pressure drop. Although the knowledge of A , C , and D is not required, the above analysis to determine them is presented to highlight the effect of various factors on cone pressure drop. The effect of V_F and OF has not been studied before.

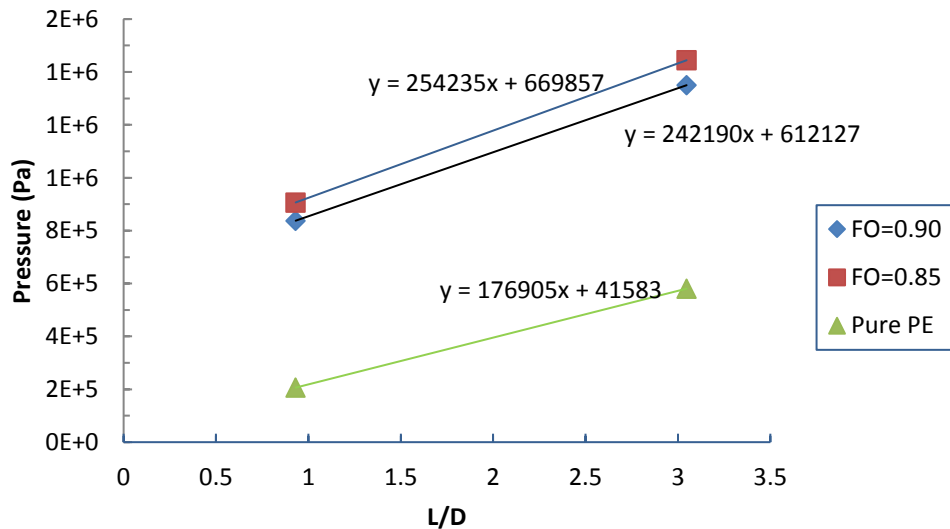


Figure A.8 Total pressure drop versus L/D for various orientation factors.

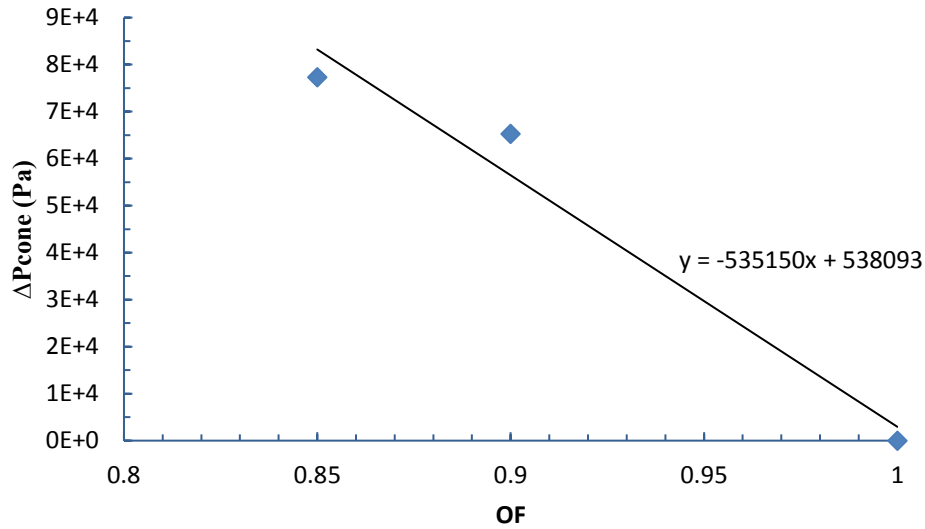


Figure A.9 ΔP_{Cone} versus Orientation factor

The following procedure was used to determine the extensional and the shear components of the total pressure drop since these components cannot be measured directly. The shear viscosity was first determined using the pressure drop across the land section. Since the die hole exit diameter is same the diameter of the land section, the maximum shear rate is the same for both sections and is given by

$$\dot{\gamma} = \frac{Q}{\pi r_1^3} \left[3 + \frac{1}{n} \right] \quad (\text{A.25})$$

$\dot{\gamma}$ is the shear rate Q is flow rate, and r_1 is the exit diameter of n is the power law constant obtained by mathematical fitting of the experimental data.

Assuming that the melt flow velocity distribution remains the same from the cone exit (where P1 is measured) to the end of the land section (where P2 is measured), the maximum shear stress at the die wall of the land section can be determined using

$$\tau_w = \frac{r_1 \Delta P_{Cap}}{L} \quad (\text{A.26})$$

τ_w is the shear stress at wall, and r_1 is the exit diameter of L is the length of land section and ΔP_{cap} is pressure drop across land section of die.

Hence, the maximum shear viscosity in the capillary and cone section will be same and calculated using the above two equations

$$\eta = \frac{\tau_w}{\dot{\gamma}_w} = \frac{\mu r_1^4 \Delta P_{cap}}{2QL} \left(\frac{n}{n+1} \right) \quad (\text{A.27})$$

The shear viscosity is plugged into equation (A.13) to determine the cone pressure drop due to shear flow ($\Delta P_{Cone,S}$) within the conical section of the die hole.

Using this and the cone pressure drop determined using the Bagley Plot, the cone pressure drop due to extension flow was determined as per the following equation.

$$\Delta P_{Cone,E} = \Delta P_{Cone} - \Delta P_{Cone,S} \quad (\text{A.28})$$

Using $\Delta P_{Cone,E}$ and equation (A.11), elongation viscosity was calculated.

The maximum shear viscosity of the HDPE melt within the conical section of the die hole, determined using the procedure discussed above, is plotted in Figure A.10 as a function of maximum shear rate. The experimentally derived values are fitted with a power law. The fitted values for the HDPE shear viscosity derived from two dies with different L/D ratios compare very well confirming the validity of the procedure used in obtaining these values. The shear viscosity exhibits a non-Newtonian behavior, i.e. the shear viscosity decrease with increase in shear rate (shear thinning behavior) and it reaches a plateau value at shear rates below $\sim 20 \text{ s}^{-1}$. The value for this plateau value (known as steady state or zero shear rate viscosity) is about 683-717 (Pa.s) and this is comparable to the values published in the literature. It should be noted that the data in this corresponds to a die temperature of 242 ($^{\circ}\text{C}$). The maximum shear rate was inversely proportional to the cone exit diameter; hence, 60-1 mm die encountered a higher shear rate than 90-1.5 mm die, which in turn encountered a higher shear rate than all 3 mm dies. Because of this, the $\eta_{60-1} < \eta_{90-1.5}$.

$1.5 < \eta_{0-3}$. Due to the limitation posed by the maximum allowable die pressure, the screw speeds that could be used were limited and hence, the shear rates for each were limited to a very small range. Hence, the composite shear viscosity for 3 mm dies are limited to the shear rate range of $30 - 50 \text{ s}^{-1}$ and hence, all data points are bunched together. However, the shear viscosity for composites, derived from all dies, was higher than that for HDPE by a factor in the range of 1.3 – 5.7, depending on the V_F . For 30-mm die, the OF varied the least and the V_F in the melt varied in the range of 5 – 23%. Hence, the range of shear viscosities observed in Figure A.10 for 30-mm die is mainly due to change in V_F . However, the same could not be concluded for other dies that showed simultaneous variation in both V_F and OF. Hence, lines could not be drawn for a constant V_F or a constant OF. The data in this plot clearly shows the effect of die geometry (specifically exit diameter) and V_F /OF on the shear viscosity of the melt within the die

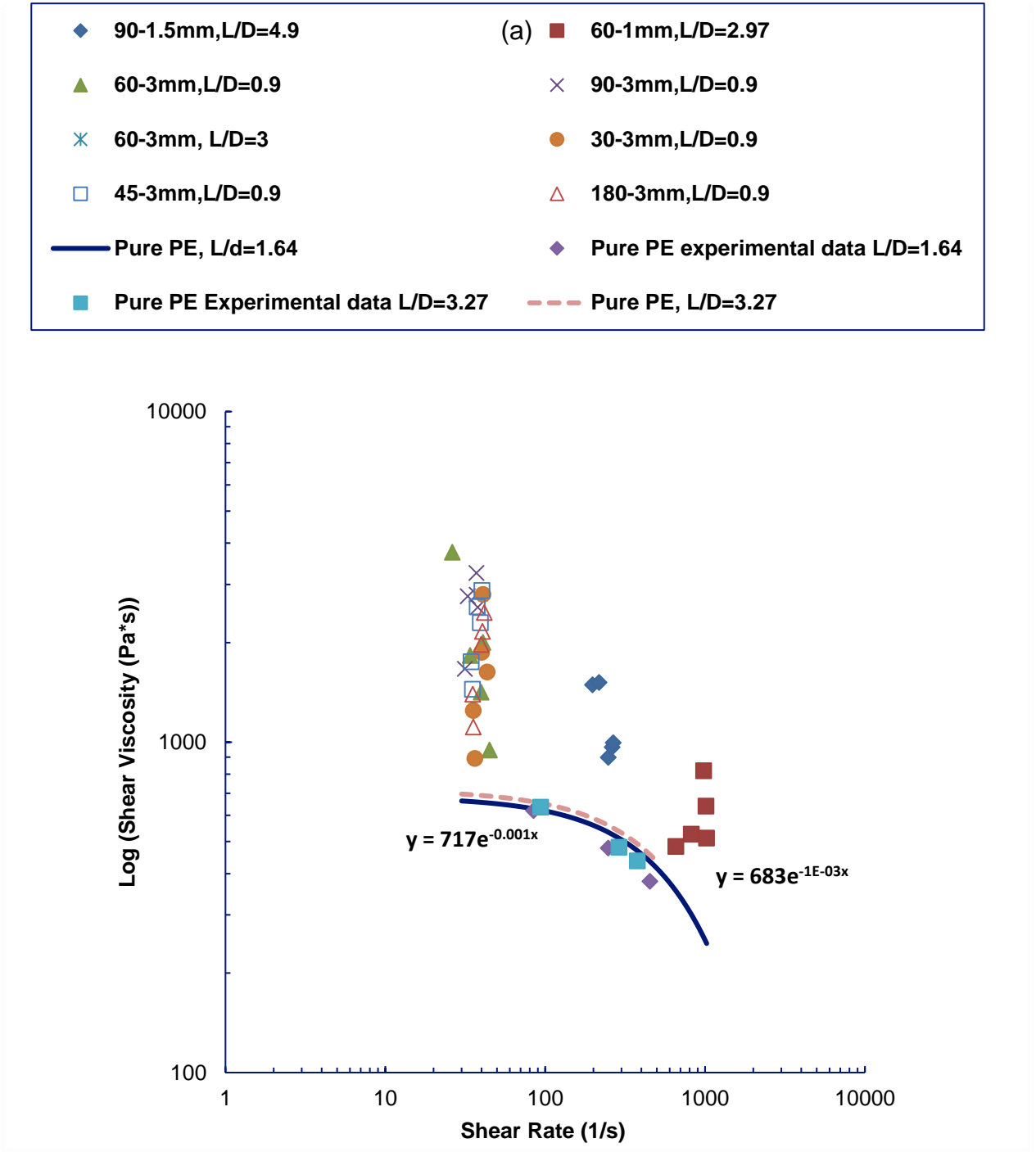


Figure A.10 Maximum Shear viscosity within the conical portion of the die as a function of maximum shear rate.

The elongation viscosity of the composite melt, determined using the procedure described above, is plotted as a function of extensional rate in Figure 5-31 for all dies. The extensional rate was determined using

$$\dot{\epsilon} = \frac{4Q \tan \theta}{\pi r_1^3} \quad (\text{A.31})$$

$\dot{\epsilon}$ is the extensional rate Q is flow rate, θ is cone angle, r_1 is the exit diameter of n is the power law constant obtained by mathematical fitting of the experimental data.

Due to limitations on screw speed (as discussed in previous paragraphs), the range of extensional rate achievable in each die is limited. However, the extensional rate achieved in various dies increased in this order: 30-3 < 45-3 < 60-3 (both L/D) < 90-3 < 180-3 < 90-1.5 < 60-1. This ordering is due to the combined effect of both the die angle and the cone exit diameter. The extensional viscosity of the composite melt within the conical section of the die also decreased in that order. The data in this plot clearly shows the effect of die geometry on the extensional viscosity of the melt within the die. All experimentally derived data were fitted using a power law equation, as shown in Figure A.11. The extensional viscosity also exhibits a non-Newtonian behavior, i.e. it decreases with increase in extensional rate. The extensional viscosity appears to approach a constant value at lower extensional rates. The ratio of this value to zero shear viscosity is in the range of $\sim 45 - 200$ depending on the V_F . This ratio known as Trouton ratio is 3 for Newtonian fluids and greater than 3 for non-Newtonian fluids.

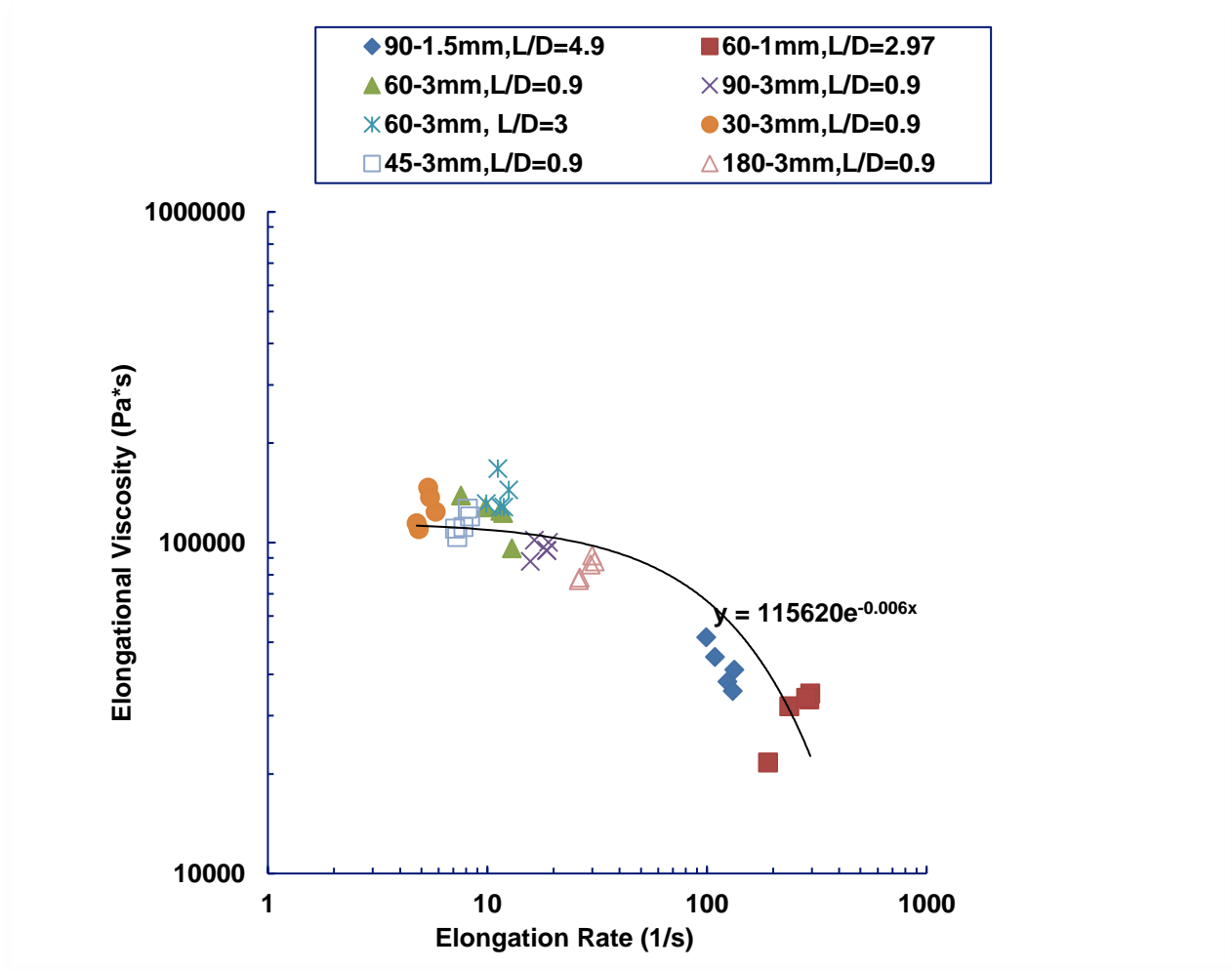


Figure A.11 Elongation Viscosity versus elongation rate

APPENDIX B***A.1 Manufacturing of Sub-micron sized HDPE/CNT composite fiber***

Results from micron-sized glass fiber extrudates suggest that reducing the exit diameter of the conical section of the die hole results in better orientation of the glass fibers. However, due to practical considerations, this diameter could not be reduced below 0.5 mm and this may be still relatively larger when compared to the size of the CNT and may not result in CNT orientation. Hence, the purpose of this task is to develop an alternate way of reducing the extrudate size and examine if reducing the diameter of the extrudate to sub-micron size would improve CNT orientation.

Figure A.12 shows the schematic of sub-micron HDPE/CNT composite fiber manufacturing process. The HDPE/CNT pellets are melt mixed with HDPE with a different viscosity, resulting in micron-sized molten globules of HDPE/CNT within molten HDPE. When this is extruded through the conical die hole, the globules would extrude within the HDPE matrix resulting in a sub-micron sized HDPE/CNT composite fiber within a matrix of HDPE resulting in HDPE- HDPE/CNT composite. The mechanical properties and SAXS characterization of this composite is envisaged to be undertaken to verify the V_F and OF within this composite and correlate it to manufacturing variables.

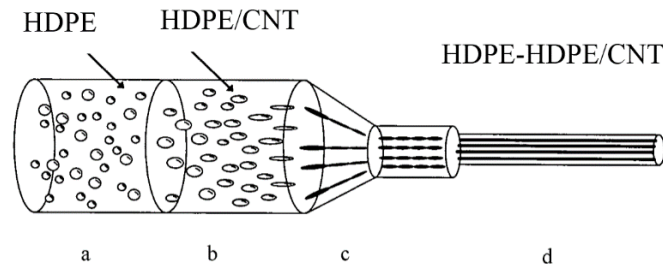


Figure A.12 HDPE-HDPE/CNT submicron manufacturing process

Prior to embarking on the manufacturing of the above-mentioned composite, two preliminary steps were undertaken to validate the concept.

A.1.1 Step 1: Confirmation of the ability to manufacture sub-micron polymer fiber

The HDPE (identified to be used with CNT) was melt blended with Cellulose Acetate Butyrate (CAB) and extruded into a composite fiber using 80% CAB and 20% HDPE weight fraction and melt spun using die angle of 60° with 3mm exit hole diameter. CAB was chosen because it could be dissolved in acetone to extract the HDPE fibers for further examination as shown in the schematic in Figure A.13. The CAB/HDPE composite fiber was also subjected to post-extrusion drawing before the extraction of the sub-micron HDPE fiber.

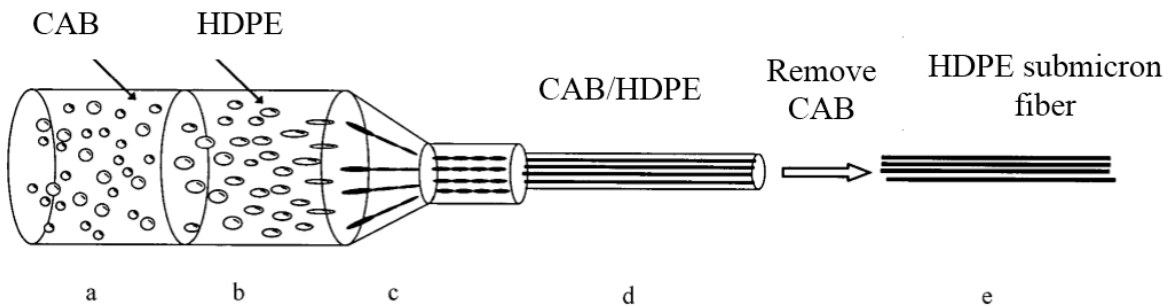


Figure A.13 A schematic of the manufacturing process for sub-micron HDPE fiber.

SEM image of the extracted HDPE fiber is shown in Figure A.14. The diameter of this fiber without any post-extrusion drawing was 4 microns, which reduced drastically to sub-micron size with post-extrusion drawing as shown in Table A.1.

Table A.1 Measured diameter of extracted HDPE for various post-extrusion draw ratios

| | DR=0 | DR=2.6 | DR=8.3 |
|------------------------------------|---------------------|------------------------|------------------------|
| Average diameter of extracted HDPE | 4 (μm) | 0.65 (μm) | 0.59 (μm) |



Figure A.14 SEM image of extracted HDPE

A.1.2 Step 2: Confirmation of the ability to manufacture sub-micron composite fiber

Instead of using costly CNT, cheaper nano-clay was chosen as the nano-reinforcement for this preliminary study. HDPE/Nano clay composite was initially manufactured using die angle of 60° die hole with exit diameter and land length constant at 3 mm and 2.7 mm respectively. Wide-angle X-ray diffraction results are shown in Figure A.15.

These millimeter sized HDPE/Nanoclay fibers were pelletized and mixed with CAB and extruded again. After extrusion, the diameter of extracted HDPE/Nano-clay fibers were $2.5\ (\mu\text{m})$ as depicted in Figure A.15. These extracted fibers were tested under Wide-angle X-ray diffraction to confirm the presence of nano-clay within the HDPE. The X-ray results presented in Figure A.16 are similar to that for HDPE/nano-clay presented in step 1. Presence of peaks corresponding to both nano-clay and HDPE in the HDPE/Nanoclay confirm the presence of nano-clay within HDPE. The dissolved CAB was precipitated by evaporating by acetone and subjected to X-ray diffraction to confirm that no HDPE/Nano-clay fibers were left behind. A comparison of X-ray results for

precipitated CAB with as received CAB in Figure A.16 along with the result for as received HDPE confirms that no HDPE/nanoclay is left behind in the precipitated CAB.

These two steps confirmed the ability to manufacture sub-micron composite fiber. Subsequently, CAB – HDPE/CNT composite was extruded using die angle of 30° with CNT weight fraction loading of 3%.

Wide angle X-ray diffraction confirmed the presence of HDPE in the extracted fibers. However, it could not identify CNT due to their size. Further characterization using SAXS is underway.

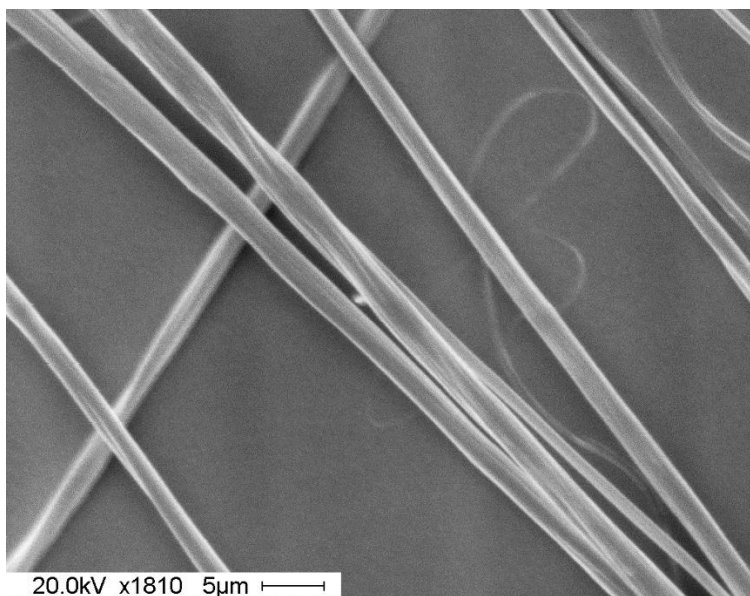


Figure A.15 SEM image of PE-nanoclay after removing CAB with average diameter of 2.5 (μm).

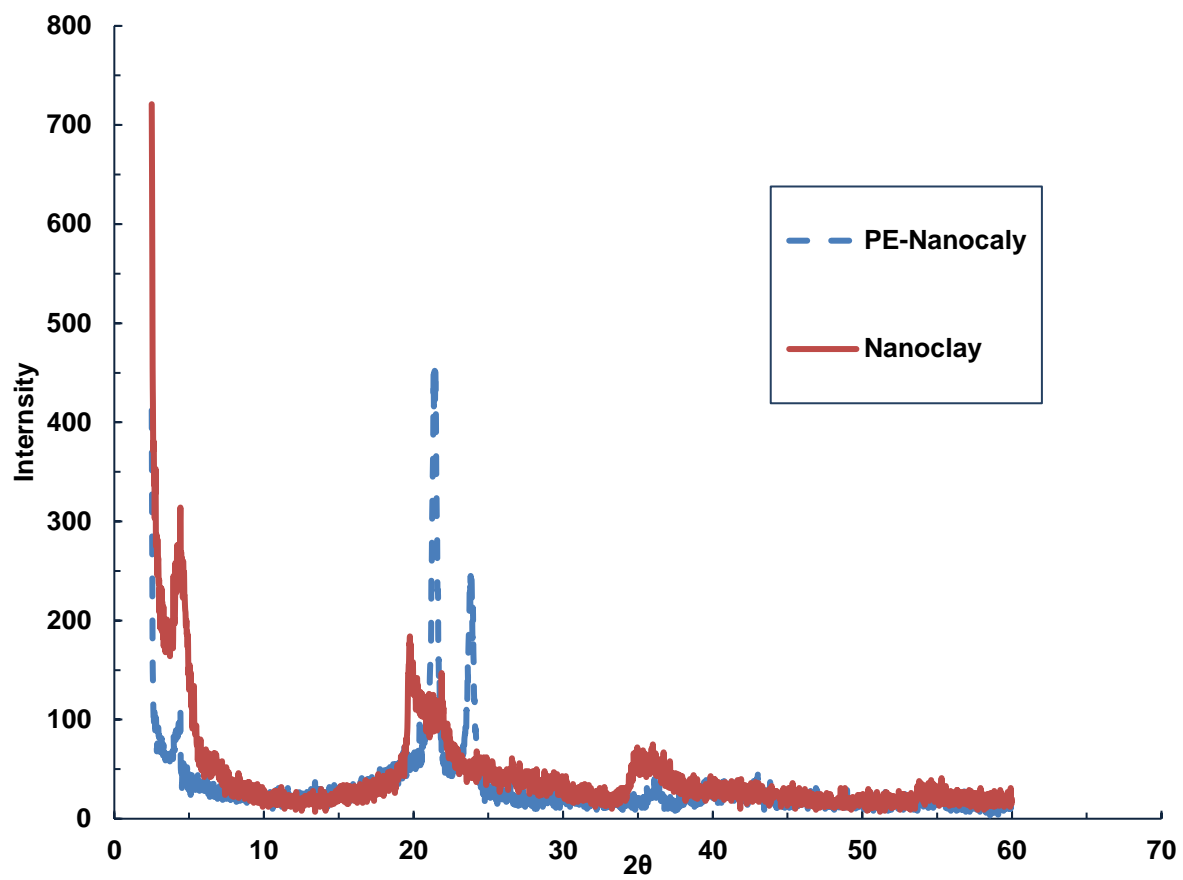


Figure A.16 X-ray diffraction of PE-nanoclay compared with as received nanoclay.

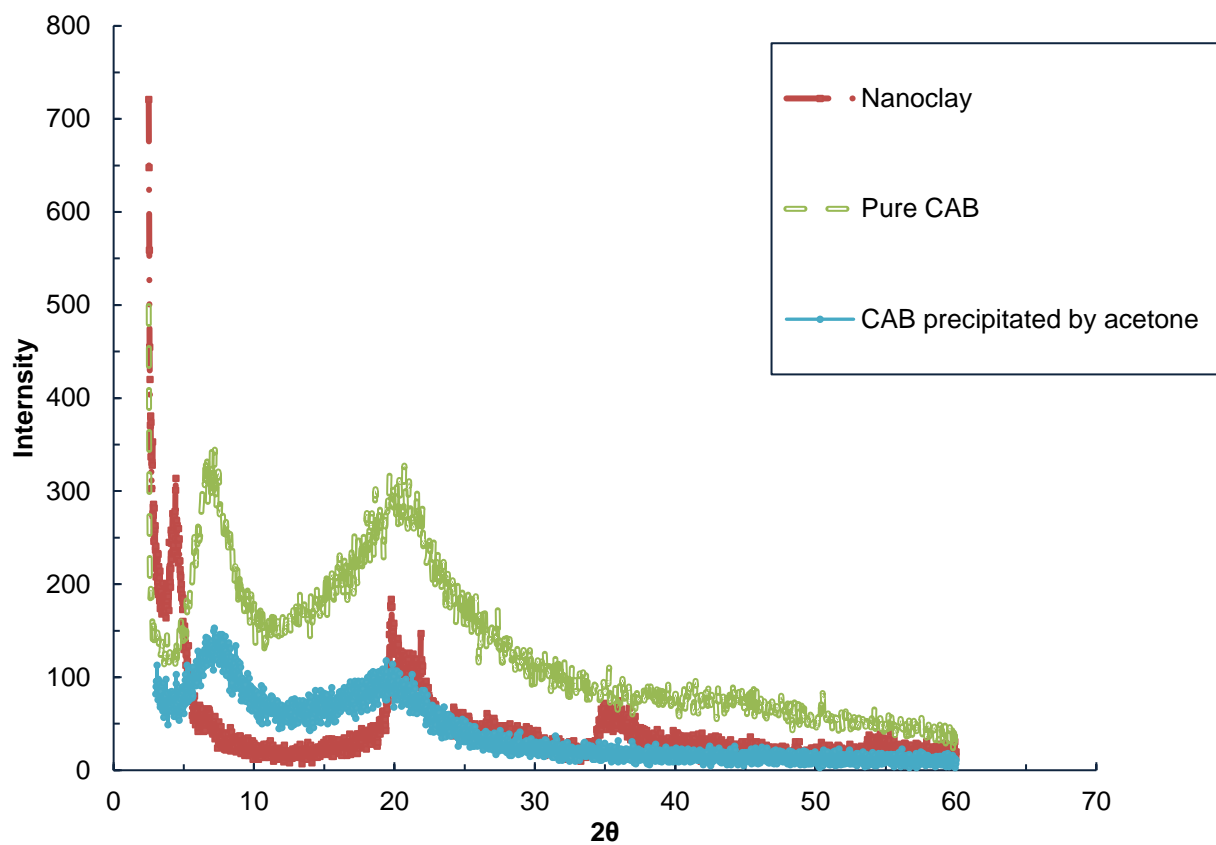


Figure A.17 X-ray diffraction of CAB precipitated by acetone compared with pure CAB.

APPENDIX C***A.c.1 Micron-Sized Fiber Reinforced HDPE Composite***

For two die geometries and same processing condition, the manufacturing of extruded composite fiber is repeated in order to confirm the repeatability of results. Computational fluid dynamic has not yet have the capability to simulate the complexity of extruder fiber spinning manufacturing process. The results of this study shown in Figures A.18 and A.19, have proven the assumption of $V_{In} = V_{Out}$ to be incorrect. For any die angle fiber volume fraction in the composite (V_{Out}) was not equal to that in the feed, while it was less or more than the V_{In} in the feed in different cases. For a given V_{In} in the feed, the V_{Out} in the composite varied with die angle even though the ratio of the entry to exit diameters was the same (See Figure A.19).

Similarly, for a given V_{In} in the feed, the V_{Out} in the composite varied with the ratio of entry to exit diameter (L/D) ratio of 3 and 0.9 for two 60° dies in Figure A.19.

The effect of screw speed on V_{Out} for constant V_{In} of 20% and 30% is depicted in Figure A.20 which illustrates there is no correlation between screw speed and V_{Out} . The effect of changing the screw speed is to change the die pressure (measured before die hole entry) and flow rate (i.e., extrusion rate); an increase in the former is expected to cause an decrease in the latter. Such a trend is observed in Figure A.21, where in, the flow rate is plotted as a function of die pressure for 60-3 mm die and a constant $V_{In} = 12.7\%$ in the feed. The pressure was changed by changing the screw speed in the range of 40 rpm to 250 rpm.

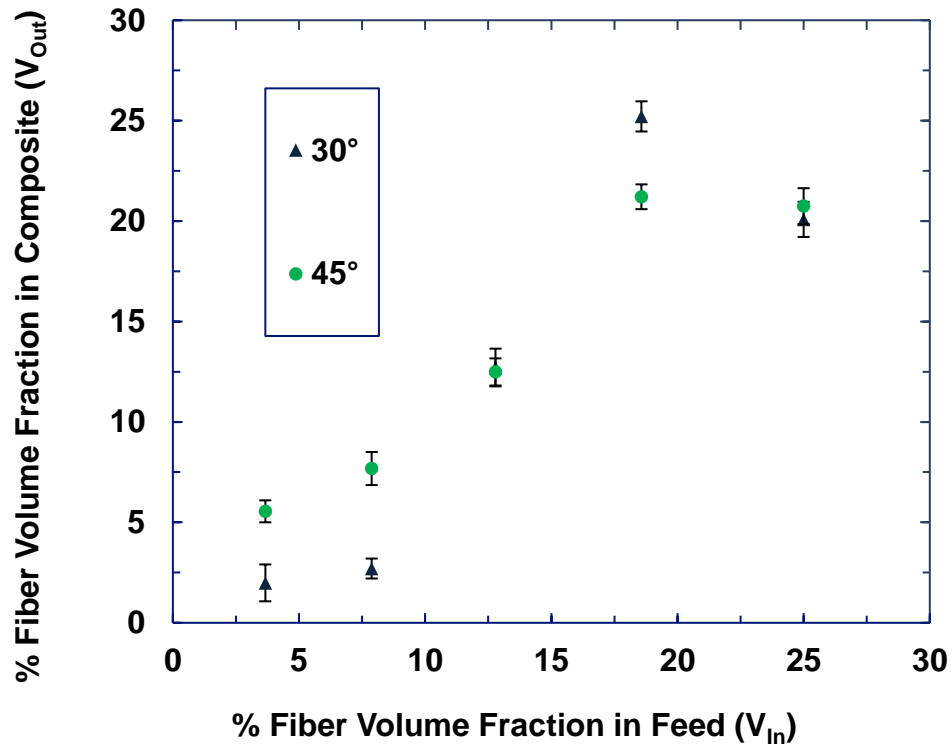


Figure A.18 Effect of Fiber volume fraction in the feed (V_{in}) on the fiber volume fraction in the composite (V_{out}) for various die entry angles with 3 mm die diameter.

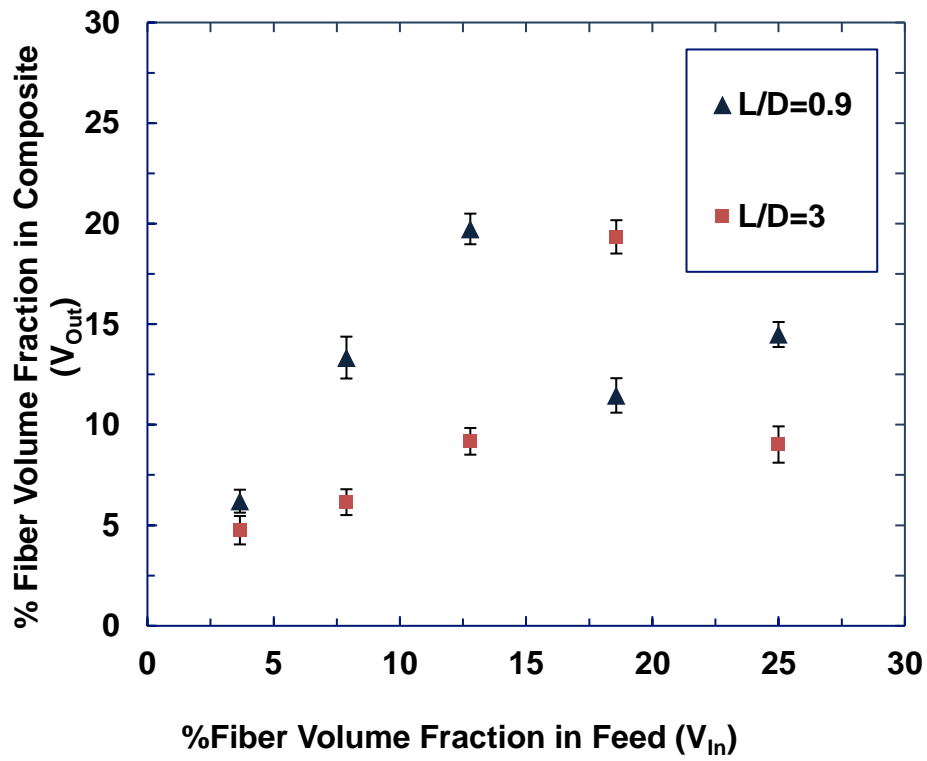


Figure A.19 Effect of volume fraction in the feed on volume fraction in composite for die entry angles of 60° , die hole diameter of 3 mm, with two L/D ratios.

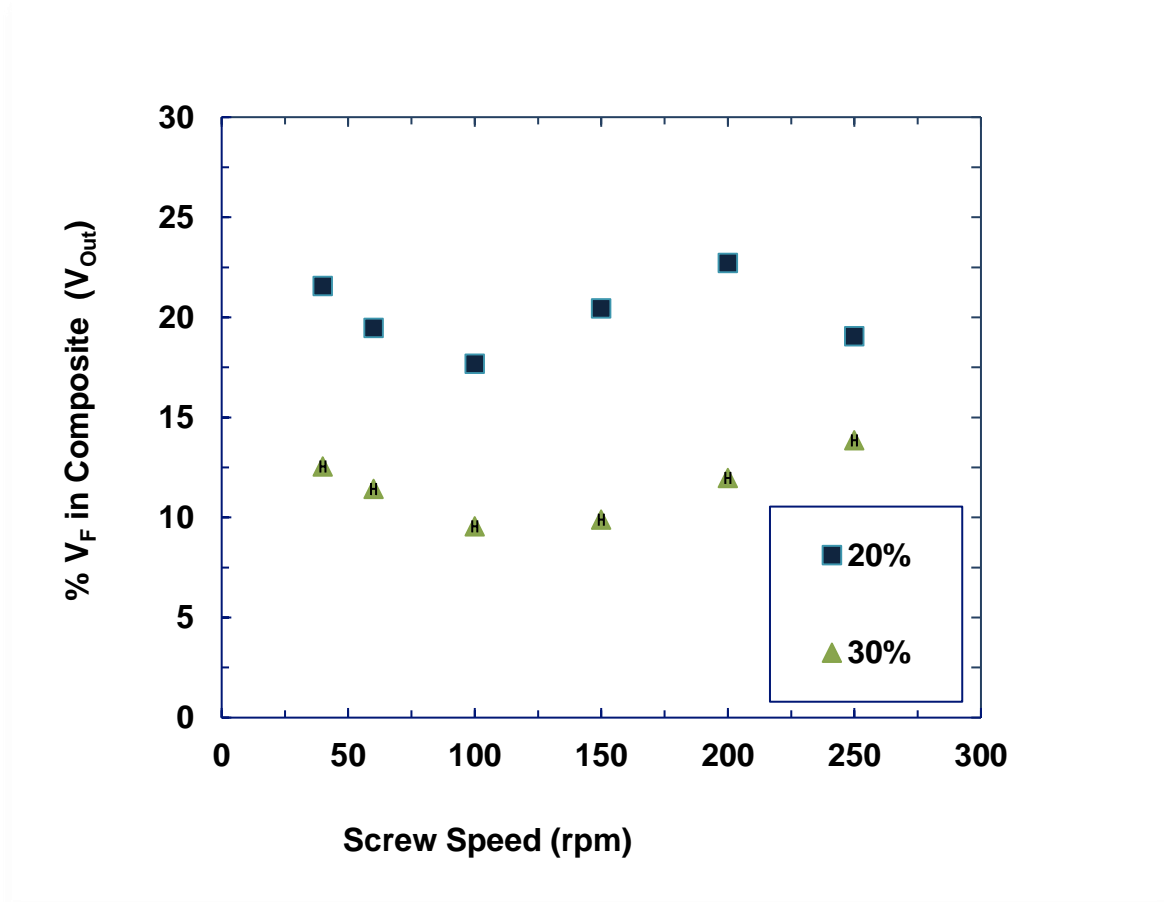


Figure A. 20 Effect of screw speed on V_{Out} in composite for constant V_{In} in feed for die entry angles of 60° , die hole diameter of 3 mm.

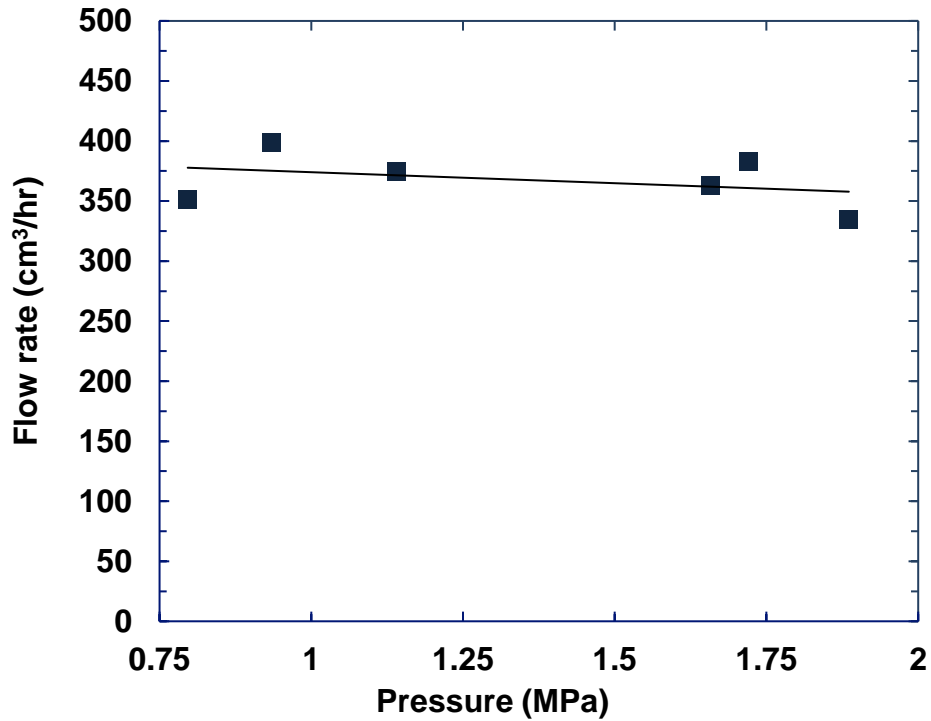


Figure A.21 Effect of pressure resulted from increasing screw speed from 40-250 rpm.

The die pressure also increased with an increase in V_{in} in the feed at a constant screw speed of 40 rpm. In other words the flow rate shows a monotonic increase with die pressure as observed in Figure A.22 for 60° and 45° when the V_{in} was varied from 3.6% to 25% .

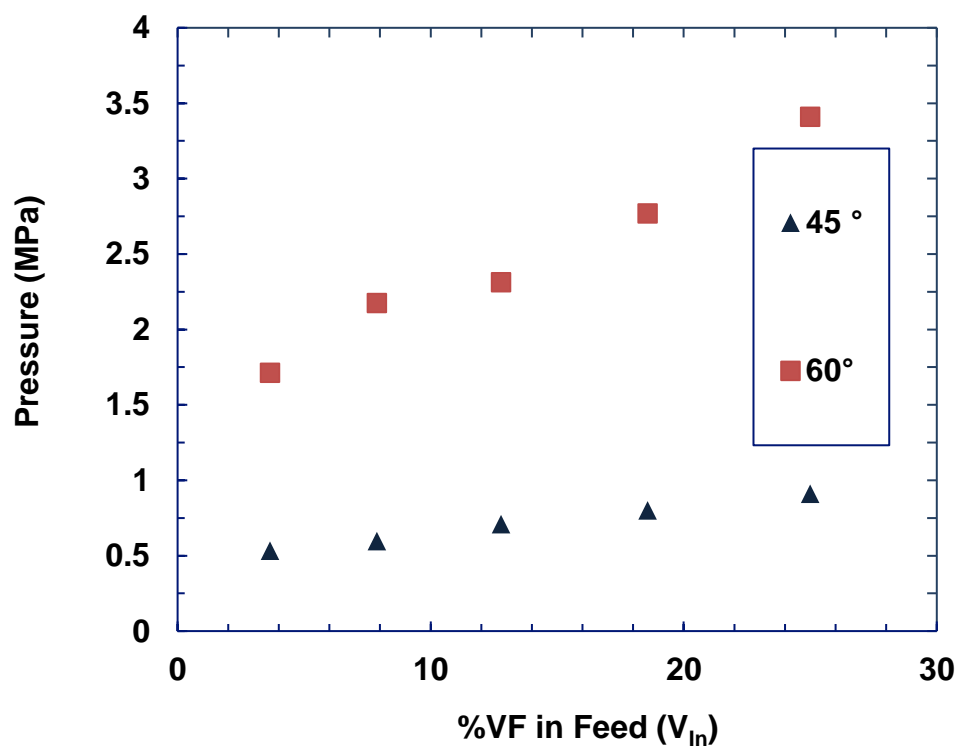


Figure A.22 Effect of pressure resulted from change in volume fraction in feed (V_{in}) at 40 rpm

APPENDIX D

Dinh-Armstrong model Matlab code is reported below:

```

shear=0.284;
elongation=0.1 ;
steps=10;
shearstrain=1*shear/steps;
elonstrain=1*elongation/steps;
tetashear=[];
phishear=[];
steps1=steps*1;
delta111=[];

a=a1;
b=a;
bb=[];
a33=[];
a13=[];
jj=[];
ii=[];
ffff=0;
dddd=0;
for j=1:steps1
    a3333=0;
    a1313=0;
    if j==1
        a=a1;
    else
        a=bb;
    end
    bb=[];
    tetashear=[];
    phishear=[];
    if j<=10
        for i=1:length
            tetashear=atan(tan(a(i,1))*((shearstrain)^2*(sin(a(i,2)))^2+2*(shearstrain)*s
            in(a(i,2))*cos(a(i,2))+1)^0.5);
                phishear=atan(1/(cot(a(i,2))+(shearstrain)));
                tetaelongation=abs(atan(exp(-0.5*elonstrain)*tan(tetashear))-
                pi()/2);
                teta=[teta;tetaelongation];
                a3333=a3333+cos(tetaelongation)^4/length;

            a1313=a1313+((cos(phishear))^2*(sin(tetaelongation))^2*(cos(tetaelongation))^
            2)/length;
                phi=[phi;phishear];
                a1313factor=1;
                a3333factor=1;
            end
        elseif j>10
            elongationfactor=input(1,1);

```

Appendix

```
shearfactor=input(1,2);
for i=1:length

tetashear=atan(tan(a(i,1))*((shearstrain*shearfactor)^2*(sin(a(i,2)))^2+2*(shearstrain*shearfactor)*sin(a(i,2))*cos(a(i,2))+1)^0.5);
    phishear=atan(1/(cot(a(i,2))+(shearstrain*shearfactor)));
    tetaelongation=atan(exp(-
0.5*elonstrain*elongationfactor)*tan(tetashear));
    teta=[teta;tetaelongation];
    a3333=a3333+cos(tetaelongation)^4/length;

a1313=a1313+((cos(phishear))^2*(sin(tetaelongation))^2*(cos(tetaelongation))^2)/length;
    phi=[phi;phishear];
end
end

a33=[a33;a3333];
a13=[a13;a1313];
if j<=10
    aaaa=j*elonstrain;
    bbbb=j*shearstrain;
    a1313factor=(1-input1(1,1))*(j-10)/9+1;
    a3333factor=(1-input1(1,2))*(j-10)/9+1;
    a1313=a1313*a1313factor;
    a3333=a3333*a3333factor;
else
    aaaa=0*elonstrain;
    bbbb=j*shearstrain;
    a1313=a1313*a1313factor;
    a3333=a3333*a3333factor;
end
    delta3333=abs(a3333-expa3333)/expa3333 ;
    delta1313=abs(a1313-expa1313)/expa1313;

    ii=[ii;j,a3333,a1313,aaaa,bbbb,delta3333,delta1313];
end

end
plot(a1(:,1),teta(:,1))
```

)